University of Liège - Faculty of Applied Sciences
Urban & Environmental Engineering Research Unit
Hydraulics in Environmental and Civil Engineering Research Group

Experimental Study of Nappe Oscillations on Free Overfall Structures

Thesis submitted in partial fulfillment of the requirements
for the degree of
Doctor of Philosophy in Applied Sciences by

Maurine Lodomez

January 2019

Members of the Doctoral Jury

Prof. Tom DE MULDER
Dept. of Civil Engineering
Ghent University

Prof. Benjamin DEWALS (Co-Advisor)
Hydraulics in Environmental and Civil Engineering
University of Liège

Prof. Grigorios DIMITRIADIS (President)
Dept. of Aerospace & Mechanical Engineering
University of Liège

Prof. Sébastien ERPICUM (Advisor)
Hydraulics in Environmental and Civil Engineering
University of Liège

Prof. Blake TULLIS
Utah Water Research Laboratory
Utah State University

Acknowledgments

I would like to express my sincere gratitude to my advisor Sébastien Erpicum for his continuous support, encouragement, scientific expertise and skillful guidance along the whole thesis.

I wish to thank my co-advisor Benjamin Dewals for sharing his knowledge, following my advances and providing valuable comments.

I want also to express my deepest appreciation to Michel Pirotton and Pierre Archambeau for their warm welcome in the research group and for their scientific advices that contributed to raising the quality of this work.

I wish to thank the President of the Jury committee Grigorios Dimitriadis and the members of the committee Blake Tullis and Tom De Mulder for the review of my work.

In addition, thanks to Brian Crookston for all the stimulating discussions and constructive critiques that you gave me and that definitely contributed to the success of this work.

I would like to express my deepest appreciation to Blake Tullis for his support, insightful comments and interesting feedback during the whole thesis.

Didier Bousmar and Thibaut Mouzelard, thank you for the interest you have shown in this research and your help that made in situ measurements possible.

I want to thank those at the Hydraulic Laboratory of University of Liège who provided help and assistance in a variety of ways: Max, Claude, Denis et Alain. Special thanks go to my colleagues, Diana, Martin, Louis, Fred, Yann, Ismael, Xhuefang and Thomas. You have been a great source of energy, passion and friendship that helped me come through the rough road of this PhD thesis. Mohammad, thank you for your support and your good mood: I first met you as a colleague and quickly discovered a friend.

Thanks to Blake, Brenda and their family for their welcome during my research stay at the Utah Water Research Laboratory. Thank you for your hospitality and friendship.

Most of all, I am thankful for the support of my family and friends, in particular Hélène, David and my loving boyfriend, Bruno, for their everyday support. Thank you also to Marita for her contribution to the review of this manuscript.

Finally, this PhD thesis was performed thanks to the support of the HECE research group and the University of Liège, thanks to both. I am also grateful for the financial support of the Féderation Wallonie-Bruxelles for my research stay in Utah.

Abstract

Free overfall structures such as weirs and crest gates are commonly used as control structures for a variety of applications including irrigation, water treatment and dam safety. The gravity-driven free-falling jet on the downstream side of these structures, called the nappe, may display a variety of behaviors and instabilities among which, under relatively low heads/discharges, nappe oscillations, also known as nappe vibrations. This oscillating phenomenon is characterized by oscillations of the thin flow nappe cascading downstream of the crest and results in a significant disturbing noise production that increases negatively the environmental and societal impacts of the hydraulic structure.

Given the lack of quantitative information reported in literature and the inchoate understanding of the dominant processes underpinning nappe oscillations occurrence and development, the global objective of this PhD thesis was to improve the knowledge of the nappe oscillations phenomenon. To that end, experimental modeling was seen as the best way to analyze the problem.

First, a prototype scale model of a linear weir has been specifically designed and made flexible with respect to the main parameters of the weir. Then, two original characterization methods of the nappe oscillations properties have been developed based on the distinct audio and visual features of the phenomenon. The application of these methods allowed the determination of the occurrence and development of the oscillations and their associated frequencies. Both were used systematically to assess the influence of various hydraulic and geometric parameters on the nappe oscillations phenomenon.

Secondly, given the importance of scale physical modeling for hydraulic structure design, the possible scale effects affecting nappe oscillations were studied by considering a 1/3 scale model of the aforementioned prototype scale facility. The operation of this second model showed that nappe oscillations cannot be scaled according to the traditional similitude for weirs (Froude similitude). Instead, they always occur within the same unit discharge range independent of size scale, although they are prone to hysteretic behavior and are less stable over time for smaller weir dimensions.

Thirdly, considering the data collected from the study of 52 geometric configurations and the expertise gained from hours of nappe oscillations observations and analysis, necessary conditions for nappe oscillations occurrence have been defined. Along with geometric criteria regarding the fall height and width of the structure, these conditions, although not sufficient, allow to predict the occurrence of the oscillations in many cases.

Finally, original mitigation techniques have been developed with the help of

practicing engineers and contractors. Identified with respect to constructability, durability, performance and maintenance, these solutions were tested and proved to be effective regarding disturbing noise reduction without impacting the hydraulic efficiency of the structure.

Besides these extensive experimental works, in situ measurements at two Belgian dams proved the applicability and robustness of the measurement methodologies developed in the framework of this thesis and the utility of the results to solve real world problems.

Résumé

Les ouvrages de déversement à surface libre tels que les seuils et les vannes sont couramment employés dans le domaine de l'irrigation, du traitement des eaux et de la sûreté des barrages afin de contrôler les débits évacués. Le jet généré par la chute libre de l'eau en aval de ces structures est appelé nappe. Cette nappe est sujette à divers comportements et instabilités dont le phénomène d'oscillations, également appelées vibrations, qui apparait dans une gamme de faibles charges amont/faibles débits. Le phénomène est caractérisé par des oscillations de la nappe déversante qui génèrent des nuisances sonores importantes. Ces nuisances affectent l'impact environnemental et sociétal de la structure hydraulique.

Compte tenu du peu d'information quantitative disponible dans la littérature et de la compréhension incomplète des processus sous-jacents à l'apparition et au développement des oscillations de nappe, l'objectif principal de cette thèse de doctorat était d'améliorer la connaissance générale du phénomène. A cette fin, la modélisation physique a été considérée comme la meilleure technique d'analyse.

Dans un premier temps, un modèle à taille réelle d'un déversoir linéaire a été spécifiquement conçu et réalisé en vue de tester divers paramètres géométriques tels que la hauteur de chute, la largeur de seuil, la forme de la crête ou encore le confinement de la nappe. Ensuite, deux méthodes originales de caractérisations des oscillations de la nappe ont été développées. Elles sont basées sur les caractéristiques audio et visuelles spécifiques du phénomène. L'application de ces méthodes a permis de déterminer l'occurrence et le développement du phénomène ainsi que les fréquences associées. Ces méthodes ont systématiquement été appliquées au travers de 52 configurations du déversoir pour évaluer l'influence de divers paramètres hydrauliques et géométriques.

Dans un deuxième temps, au vu de l'importance accordée à l'exploitation de modèles réduits pour la conception de structures hydrauliques, les effets d'échelle qui pourraient affecter le phénomène des oscillations de nappe ont été appréhendés par l'exploitation d'un modèle réduit au $1/3^e$ du modèle à taille réelle mentionné plus haut. Cette analyse a montré que les oscillations ne peuvent être mises à l'échelle selon la loi de similitude traditionnelle en écoulement de surface (similitude de Froude) mais, au contraire, se produisent toujours dans la même plage de débits spécifiques. Il apparait néanmoins que, sur un ouvrage de petite taille, le phénomène présente un hystérésis et est moins stable temporellement.

En troisième lieu, les données récoltées sur 52 configurations de seuil et l'expertise acquise au fil de nombreuses heures d'observation et d'analyse du

phénomène ont permis de définir des conditions nécessaires à l'apparition des oscillations de nappe. Complétées par des critères relatifs à la hauteur de chute et à la largeur du seuil, ces conditions bien que non suffisantes, permettent de prédire l'occurrence du phénomène dans de nombreux cas.

Finalement, des contre-mesures originales ont été développées avec l'aide d'ingénieurs et entrepreneurs. Définies en vue de satisfaire des critères de constructibilité, durabilité et maintenance, ces solutions ont été testées et optimisées en terme de réduction des nuisances sonores tout en préservant l'efficacité hydraulique de la structure.

A côté de ces travaux expérimentaux, des mesures in situ sur deux barrages belges ont prouvé l'applicabilité et la robustesse des méthodes de caractérisation développées dans le cadre de cette thèse ainsi que l'utilité des résultats obtenus pour résoudre des problèmes réels.

Contents

Chapter I

Introduction and research objectives

I.1 Context

"The Earth is a watery place" (USGS, 2016). Although seventy percent of the Earth's surface is water covered, the majority of the water is saline water. Therefore, the control of freshwater resources which are limited and unevenly distributed, is an everyday goal. Today, one of the water control means is wielded by dams. The International Commission on Large Dams (ICOLD) recorded, all over the world, 59 071 large dams i.e., with a height of 15 m or greater from lowest foundation to crest or a dam between 5 and 15 m containing more than 3 million m^3, as reported in the present edition of the Register (ICOLD, 2018). Among the main roles of dams, irrigation is by far the most common. The others are hydropower, flood control and water supply for domestic and industrial use.

As a critical component of human civilization, these hydraulic structures have to be safe. Indeed, the failure of a dam may have disastrous consequences with a massive destruction of civilian population and its environment. Although the overall 1% failure rate of dams through the world seems low, a dam failure can generate immense damage and loss of life when it occurs. The worst dam failure event ever recorded is the simultaneous failures of 62 dams including two large dams in the Heran Province (China) in August 1975. This event, usually referred to as the Banqio Dam failure, happened after extreme storms and killed 171 000 people including those that perished following the famine and disease that followed the flooding (Reclamation, 2014).

To prevent dams from overtopping, in particular during floods, a specific work, called spillway, is integrated into the dam. This infrastructure is usually part of the dam body and ensures the evacuation of excess water entering the reservoir due to a flood. Usually two types of spillways are identified: the ones operating under pressure, called gates, and the ones with free surface flows, called free weirs or weirs. The first are mechanically managed to limit the discharge released and therefore to control the water level in the reservoir. The main drawback of the gates is their need for an effective operating system and regular maintenance. In contrast, free weirs are passive control spillways as they start to evacuate water once the water level exceeds the top of the structure. The discharge released in that case depends on the geometry of the structure and the reservoir water level. Although the main inconvenient of free weirs is their technical impossibility of water level management, they are usually preferred to gates in terms ofsafety and cost. In addition, a hybrid structure, called crest gate, exists and consists of a gate operating as a free overfall structure.

Classically, a weir is made of a linear wall, perpendicular to the flow direction, of which the crest is shaped to optimize the flow pressure distribution and the weir's hydraulic efficiency. Besides the crest shape, the wall length is the most influential factor to efficiency, but it is constrained by the structure width. Today, considering the infrastructure ages, the actual knowledge on climate change,

the better knowledge of dam failures and, additional or longer climatic data surveys, the safety criteria of spillways are upgraded (Xlyang and Cederström, 2007; Peltier et al., 2018; Millet et al., 1988). This leads to the definition of imaginative solutions, i.e., non-linear weirs, which ensure the required safety and the maximum storage capacity of the dam for new structures as well as in case of rehabilitations. Laybrinths weirs (Crookston and Tullis, 2012) and piano-key weirs (Lempérière and Ouamane, 2003) are common types of non-linear weirs. These hydraulic structures are linear weirs that are folded in plan-view to increase the crest length for a given width.

Despite a significant increase of dam safety in terms of maximum discharge capacity, the non-linear structures, and labyrinth weirs in particular, experienced specific problems due to more frequent operations under low heads. This problem, called nappe oscillations or nappe vibrations, is an instability phenomenon of the gravity-driven free-falling jet on the downstream side of the weir. This oscillating instability phenomenon induces a disturbing noise production and potential technical and operational issues, critical to the sustainability of the structures. Although these oscillations do not endanger the safety of the dam, this phenomenon affects the societal and political acceptance of the work.

In the past, nappe oscillations have been also observed to occur, under low head/discharge conditions, with other free overfall structures like linear weirs and crest gates. Solutions to avoid this phenomenon have been proposed and are today good practice, for instance, in gates design. However, the nappe oscillations problem is not fully understood to date. From a scientific point of view, the physical processes of this complex flow behavior are still unclear and a lack of consensus exists on the cause(s) of the oscillations while, from a practical point of view, more appropriate mitigation techniques are still required.

Currently the study of nappe oscillations is a hot topic. Indeed, many non-linear structures, which operate more frequently under low head than linear ones and therefore may be subject more often to a nappe oscillations phenomenon, were built in recent years. A better understanding of this oscillating instability phenomenon is thus required to face its potential occurrences and consequences.

I.2 Literature review

I.2.1 Introduction

As mentioned previously, free overfall structures (such as weirs and crest gates) are commonly used as flow control structures for a variety of open channel/free surface flow applications including irrigation, water treatment, and dam safety. The gravity-driven free-falling jet on the downstream side of these structures, called the nappe, may display a variety of behaviors and instabilities (Crookston and Tullis, 2012). In particular, nappe oscillations, otherwise known as nappe vi-

brations, can occur under relatively low-head discharges and have been observed on a variety of weirs (linear, labyrinth), crest gates and fountains (Casperson, 1993a,b, 1994, 1996; Crookston et al., 2014; Mori et al., 2012; Nishikawa, 1977; Partenscky and Khloeung, 1967; Reclamation, 1964). Frequently identified as undesirable and potentially dangerous, the most recognizable characteristics of this phenomenon are the horizontal banding on the nappe and the unmistakable acoustic energy resulting in low frequency noise that can be heard and felt in close proximity of the structure and affects negatively people living nearby (Casperson, 1993b; Crookston et al., 2014; Knisely, 1989). Moreover, nappe oscillations may merit structural consideration if one of the dominant nappe oscillations frequencies is close to the natural frequency of the structure (Guha and Luthra, 1963). In case of crest gates, the oscillations may cause vibration of the gates and jacks which could lead to malfunctioning.

For example, nappe oscillations were observed at the newly completed flat-topped linear weirs at Upper and Lower Rockyford Lake Dams (South Carolina, USA). Nappe oscillations were also detected at the labyrinth weirs at Martins Landing Dam [Fig.I.1(a)], North Fork Smith River Dam, Avon Dam and Linville Land Harbor Dam [Fig.I.1(b)]. The overflow gates of Coon Rapids Dam, Nisramont Dam and Papignies Dam [Fig.I.1(c-d)] also displayed nappe oscillations (Crookston et al., 2014; Bousmar and Libert, 2015, 2017; MWSB, 1980). In addition, weirs at dams being sometimes remotely located or flowing infrequently, nappe oscillations at these hydraulic structures may not be well documented (occurrence, operating conditions, etc.) and this suggests that other hydraulic structures subject to nappe oscillations may exist.

I.2.2 Fundamental researches

A review of the scientific literature shows that nappe oscillations have been subject to various theoretical and experimental modelings over the last 80 years. Squire (1953) investigated the breakup of thin falling liquid films of constant thickness due to the growth of the oscillations. He showed that the surface tension is a dominant factor in the stability analysis of the liquid film and in the determination of the wavelength of the oscillations that cause its breakup.

Schwartz (1966a) discussed the similarities between edgetones and nappe oscillations phenomena. The sensitivity of nappe oscillations to the crest weir roughness led the author to suggest the stability of the boundary layer on the weir crest as a significant nappe oscillations parameter. He also supported the integer-plus-one-quarter criterion (Schwartz, 1964a, 1966b), equivalent to the one proposed by Curle (1953) for the jet-edge system. This criterion considers that the pressure changes generated in the surrounding air by the nappe come into phase with the pressures exerted on individual nappe elements when the number of wavelengths contained in the length of the nappe is an integer-plus-one-

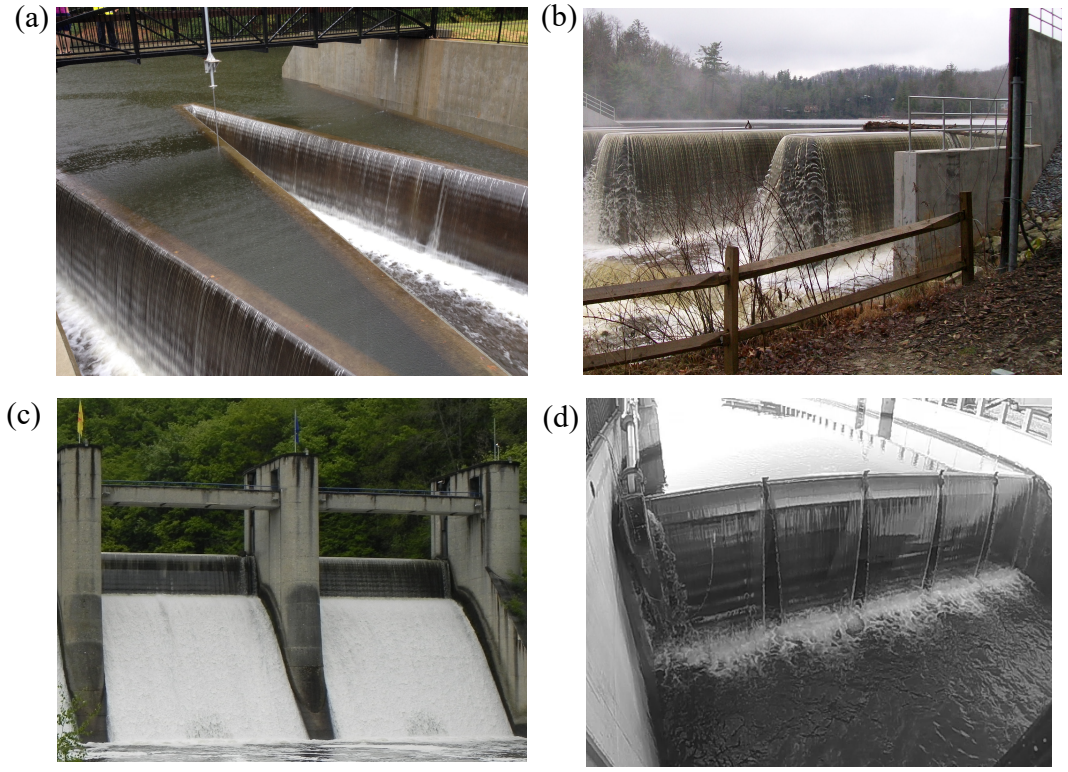

Figure I.1: Hydraulic structures experiencing nappe oscillations (a) Martin's Landing Dam (USA- Courtesy of Schnabel Engineering), (b) Linville Land Harbor Dam (USA-Courtesy of Schnabel Engineering), (c) Nisramont Dam (Belgium) and (d) Papignies Dam (Belgium)

quarter. Recently, further to the nappe oscillations problems experienced after the rehabilitation of the Linville Land Harbor Dam, new experimental investigations were undertaken at the Utah Water Research Laboratory on large scale free surface weirs (Anderson, 2014; Anderson and Tullis, 2018; Crookston et al., 2014). These tests suggested that the origin of the instability was most likely located at the weir crest. Indeed, the waves resulting in oscillations were observed directly after the flow separation from the weir crest (even for unconfined nappe [1]) and roughness modifications of the weir affected the oscillations occurrence. These findings support the theory of Schwartz (1966a) that the initiation of the instability occurs at the detachment of the nappe from the crest.

[1]The unconfined nappe conditions refer to the conditions when the nappe is not confined by downstream channel sidewalls; atmospheric pressure surrounded the nappe on all sides. By opposition the confined nappe conditions refer to a nappe confined between downstream channel sidewalls creating a trapped air pocket behind the nappe.

Binnie (1972) studied experimentally thin sheets of water flowing vertically along a 0.305 to 0.61 m high chute from 0.2 to 1.6 mm wide slots created in a pressurized tube. The desintegration of this vertical sheet falling at atmospheric pressure on both sides was examined and related to the Weber number at the breakup while, in case of an air pocket trapped on one side of the sheet, oscillations frequencies were evaluated. The frequency was measured with a microphone connected to an oscilloscope and was found to vary from 2 to 33 Hz. Based on these experimental results, Binnie (1974) theoretically investigated the instability of a vertically falling water sheet with disturbances due to resonance with the confined air pocket. Although this theory can explain some characteristics of the phenomenon, it does not specify which of an infinite number of modes and frequencies, theoretically defined, is likely to occur.

Casperson (1993a) examined experimentally the nappe oscillations occurring on Dunedin's fountains (New Zealand) and theoretically established integro-differential equations of the sheet waveforms and oscillations frequency of which the solutions are in agreement with the experimentally observed behavior. The experiments were performed for a nearly vertical flow with fall heights varying from 0.41 to 0.80 m and frequency in the range of 5 to 12 Hz. In a later study, Casperson (1994) derived a stability criterion based on this set of equations by exploring the dependence on the flow rate from the fountain height for various depths of air chamber, initial velocities and air velocities. In addition, this author validate for the case of the Dunedin's fountains the equation of the oscillations frequency proposed by Schwartz (1964a). He also recognized that the confined air pocket behind the water sheet plays a central role in providing a feedback mechanism as suggested in Naudascher (1965); Petrikat (1958); Schwartz (1964b). In addition to this feedback, he attributed the mechanism of amplification required to initiate the instability to shear forces that occur at the interface between the falling water and air, to a Kelvin-Helmholtz mechanism (Von Helmholtz, 1868).

Chanson (1996) suggested a pressure discontinuity at the weir crest as the cause of the phenomenon, with an origin of the oscillations at the crest. Indeed, when the nappe detaches itself from the weir crest, the nappe experiences a sudden pressure discontinuity as the pressure initially created by the water weight reduces to atmospheric pressure. Naudascher and Rockwell (1994) theorized that pressure fluctuations in the air pocket behind the water sheet are a driving force behind the nappe oscillations growth. However, the air pressure fluctuations can be considered as an instability amplifier (Naudascher, 1965; Petrikat, 1958; Schwartz, 1964a) since several studies (Anderson and Tullis, 2018; Binnie, 1972; Crookston et al., 2014; Sato et al., 2007) that included unconfined or vented nappe conditions displayed nappe oscillations.

Schmid and Henningson (2002) investigated theoretically the stability of a vertically falling water sheet enclosing an air pocket by applying a multimodal approach. The developed multimodal stability analysis demonstrated a strong

amplification of the total energy and the pressure difference in the air pocket for integers of the fall time. These results were in agreement with experimental data with a fall height and slot width varying respectively between 0.31 and 0.7 m and 1.5 and 2 mm. The frequencies experimentally reported were between 4 and 9.85 Hz. This study suggests that the nappe oscillations phenomenon is governed not by a single mode but by a linear interaction of several modes. In the same way, Sato et al. (2007) concluded that the nappe oscillations occur under conditions where the work done by the water sheet on the air pocket reaches a maximum when the product of the frequency and the falling time is an integer-plus-one quarter. In addition, Sato et al. (2007) found experimentally that the pressure fluctuations frequency is identical to the frequency of the confined water sheet oscillations, initiated through a slot of 1.3 or 3.1 mm. The falling height of the experimental apparatus varied from 0.47 to 0.62 m and the frequencies were recorded between 5.3 and 17.4 Hz.

Kyotoh et al. (2002) studied theoretically and experimentally the stability of falling water sheet from a weir. He developed a model describing the motion of the sheet in the longitudinal and normal directions. Experimentally, Kyotoh et al. (2002) investigated the trajectory and breakup of a 40-cm wide and 3-m high free fall sheet of water for discharges of 2.2×10^{-3} and 3.15×10^{-3} m^3/s. He also showed that the confinement of the sheet causes a modulation of the sheet amplitude. Finally, he pointed out three physical factors affecting the motion of a falling water sheet: the propagation of pressure fluctuations under the influence of confined air, the shear wave instability of the air flow induced by the falling water and the surface tension effects on the water sheet.

De Rosa et al. (2014) investigated theoretically the mutual influence of the air pocket behind the nappe with the nappe interface that generates self-induced forces by recasting the nappe global behavior as a driven damped spring-mass oscillator of which the mass is that of the liquid sheet and the equivalent stiffness of the spring is that of the air inside the enclosure. Through a modal and a non-modal linear approach, this unsteady global analysis examined both the dynamics and the energy aspect. The modal analysis indicated that the system is characterized by low-frequency, related to the quasi-constant spacing of the imaginary part of the eigenvalues (Schmid and Henningson, 2002) and high-frequency oscillations, related to a global spring-mass oscillator model. Finally, a substantial result of this study was a stability criterion "based on the ansatz that the system is stable if the crossing time of a perturbation over the whole length of the domain is shorter than the period of the spring mass oscillator". Recently, Girfoglio et al. (2017) further studied the global dynamic behavior of nappe oscillations of a vertical thin sheet interaction with an air pocket in the presence of surface tension effects. Key findings of the global dynamics analysis were the agreement with experimental data of the literature and the definition of the two characteristic frequencies, that of the spring-mass behavior and that

of the capillarity wave travelling over the sheet.

I.2.3 Mitigation techniques for free surface weirs

In addition to fundamental research on nappe oscillations, some studies have focused on mitigation techniques. Since nappe oscillations may be able to induce structural problems like movements and vibration of gates and jacks, early investigations were performed for crest gates. In 1939, the US Bureau of Reclamation (Reclamation) assessed the effectiveness of a nappe splitter at the Black Canyon Dam (Reclamation, 1964). The splitter was held in place against the downstream edge of the gate to aerate the overfalling jets. Tests showed that depending on the position of the splitter along the width (one third to one half), nappe oscillations vanished on both nappe sections (splitter at the midpoint) or only on the narrower nappe section. This study contributed to the use of splitters as a common mitigation technique for nappe oscillations in gates design. However, this technique requires special attention on the spacing of splitters (Pariset, 1955; Schwartz, 1966b). As an example, nappe oscillations were observed in Papignies dam, a new water level regulating structure in Belgium, despite of the nappe aeration by splitters 1.65-m spaced. Finally, experiments on site showed that low spaced splitters (less than 1 m) are effective in mitigating nappe oscillations(Bousmar and Libert, 2017).

In spite of its effectiveness in case of crest gates, the use of splitters is not recommended on free surface spillways as it reduces the discharge capacity, favours floating debris collection and also requires repair or replacement due to damage caused by floating debris and ice. Besides the use of splitters, others atypical mitigations for gates were developed and showed some effectiveness as, for example, the addition of rubber strips suspended on the downstream side of the gate at regularly spaced intervals across the gate (Knisely, 1989) or the setting of an inclined board at the lower end of the falling sheet to modify the impact conditions (Nagamine et al., 2011).

In case of a weir, nappe oscillations has not been idebtified as the cause of noticeable structural problems at dams but can negatively impact people, homes and structures nearby, which justifies the use of mitigation techniques. Thus, the effectiveness of several nappe oscillations countermeasures at a weir was investigated further to the nappe oscillations occurrence at the labyrinth spillway at Avon Dam in Australia (MWSB, 1980). Experiments were conducted on a full-scale model (4.27-m long and 3.05-m high) featuring flow splitters distributed along the crest. Nappe oscillations were effectively eliminated when the splitter spacing was $\tilde{<}$ 610 mm. In addition, the increase of the crest roughness through the addition of stones glued on the crest fully avoided noise disturbance generation and appeared to be the best solution. Finally, although complicated to install, the reshaping of the crest profile to keep the flow attached to the down-

stream weir face at disturbing low-head discharges was another effective countermeasure identified in laboratory testing. Coincidentally, the nearby Woronora labyrinth spillway crest was in poor condition with exposed aggregate; no oscillations had been observed at this structure. Therefore, due to field observations and the laboratory investigation, the selected mitigation approach was the crest roughening.

Sumi and Nakajima (1990) studied experimentally the impact of width reduction with the help of spoilers for restricting the oscillations and in particular the disturbing noise.

More recently, Anderson and Tullis (2018) further investigated the influence of surface roughness on nappe oscillations for a quarter-round crest profile. The investigation included smooth, partially roughened, and fully roughened weir crest configurations in confined and/or unconfined nappe conditions. The partially roughened configuration consisted of covering the curved portion of the quarter-round crest with stones (20 to 40 mm in diameter). The entire profile was covered with stones for the fully roughened tests. For unconfined nappe conditions, the partially roughened configuration proved sufficient to modify the flow structure and eliminate the nappe oscillations. For the confined nappe, oscillations were still observed but the affected unit discharge range was reduced. In contrast, both the fully roughened weir crest and a single row of stones at the downstream end on the weir crest (at detachment point) eliminated nappe oscillations. These findings confirmed the theory according to which nappe instability initiates at the point where flow separation occurs at the downstream end of the crest.

Even though the solutions presented above for weirs may be efficient to prevent nappe oscillations, they are however not optimal regarding durability, ease of installation, discharge capacity and debris collection.

I.2.4 Physical modeling of nappe oscillations for free surface weirs

To design hydraulic structures and to understand their behavior, two modeling methods exist: the numerical and the physical modelings. Nevertheless, to the knowledge of the author, only the physical modeling provided to date a faithful reproduction of the nappe oscillations. Indeed, despite the development of more and more accurate numerical models, no Computational Fluid Dynamics (CFD) model appeared able to model the nappe oscillations through the resolution of the classical equations of the fluid mechanics, i.e., the Navier-Stokes equations.

Furthermore, physical modeling remains challenging in that full model - prototype similarity and requires that geometric, kinematic and dynamic similitude be achieved. Using a common fluid (i.e., water) for both prototype and model scales makes full similarity impossible (Ettema et al., 2000), but, in many cases,

there is a single dominant force, along with inertia, which justifies neglecting the other minor forces that cannot be accounted for accurately. Particular laws of similitude have been developed based on the ratio of the inertia and other dominant forces [e.g., Froude (gravity), Reynolds (viscosity), Weber (surface tension), etc.]. Froude similitude is most appropriate, typically, for free surface flows as gravity and inertia represent the most relevant forces. In free surface flow, under certain circumstances, the minor influence of the other forces (e.g., viscosity and surface tension) can increase to the point where they are no longer negligible and Froude scaling results in discrepancies between the model and prototype hydraulic behavior. This phenomenon is referred to as scale effects. Thus, a main challenge of laboratory-scale physical modeling lies in the identification and understanding of the resulting scale effects (Heller, 2011).

The physical scaling of the nappe oscillations phenomenon is thus a key issue. Indeed, in the light of the importance attached to physical modeling regarding the hydraulic structure design, the detection of nappe oscillations occurrence on a scale model would indeed be valuable for designers and contractors.

From a literature review, the nappe oscillations for free surface weirs were studied experimentally on a prototype model (MWSB, 1980) or on a large scale model (Anderson, 2014; Anderson and Tullis, 2018; Crookston et al., 2014; Sumi and Nakajima, 1990). Besides these studies on large scale models, only one study addressing nappe oscillations on a fixed weir on a small scale model and, discussing the scale effect was found. Anderson and Tullis (2018) showed that smaller scale linear weir models exhibited more temporal variability and irregularity as well as hysteresis, relative to larger (non-geometrically similar) linear weir models. This study also implied that nappe oscillations may not scale with Froude similarity as nappe oscillations occurred for a common range of discharge at both model scales.

I.2.5 Conclusions

It can be concluded from literature that nappe oscillations are a complex hydraulic process in which more than one mechanism may initiate, provide feedback, and/or sustain the oscillations. On the one hand, the instability of a vertically falling water sheet generated through a thin slot and moving through air has been subject to many theoretical studies (Binnie, 1972; Casperson, 1993a,b, 1994; De Luca and Costa, 1997; De Rosa et al., 2014; Girfoglio et al., 2017; Kyotoh et al., 2002; Sato et al., 2007; Schmid and Henningson, 2002). These studies investigate the potential growth of an initial disturbance generated at the exit of the slot and developing along the path of the falling water sheet. From a theoretical perspective, the models presented in the literature require the presence of an air pocket behind the nappe to explain the oscillations development. In contrast, it is known and reported by some authors (Anderson, 2014; Anderson

and Tullis, 2018; Crookston et al., 2014; Falvey, 1980; Sato et al., 2007; Schwartz, 1964b, 1966b) that nappe oscillations can occur on free surface weirs (i.e., for nappe originating horizontally from a crest), even if the nappe is fully vented. In addition, the location of the initiation of the instability varies across several studies and a number of theories regarding the cause of nappe oscillations have been put forward: Kelvin-Helmoltz instabilities, pressure discontinuity at the weir crest and instability of the boundary layer.

On the other hand, nappe oscillations were studied experimentally. The majority of the experimental studies performed to date considered thin vertically falling sheets of water originating from a thin slot in a pressurized tube with limited fall heights (lower than one meter) and an air pocket trapped behind the nappe. For free surface weirs, experiments were all performed on a large scale model or a prototype size. Nonetheless, the range of tested geometric parameters (i.e., width, fall height, crest profile) was limited. For all research the oscillations frequency is the main parameter used to characterize the phenomenon. In addition, only one experimental research (Anderson and Tullis, 2018) investigated the scale effects that affect the nappe oscillations phenomenon.

Finally, studies of mitigation techniques have been undertaken and focused mainly on two aspects: the modification of the crest roughness and the reduction of the nappe width through splitters. These solutions, even though efficient to prevent nappe oscillations, may however induce problems in terms of ease of installation, durability and debris collection.

I.3 Research objectives

In view of the state of the art, the global objective of this research was to improve the understanding of the nappe oscillations phenomenon. To that end and in view of the inchoate understanding of the dominant processes underpinning nappe oscillation occurrence and development, the probable inability of existing CFD models to reproduce the phenomenon and the current lack of systematic quantitative information reported in the literature, experimental modeling was seen as the best way to analyze the problem.

A prototype scale model was thus specifically designed and made flexible with respect to the main parameters of the weir (Chapter II). The choice of a prototype scale model was justified by the will to avoid potential scale effects. Then, to collect relevant quantitative data, systematic methods and analyses were developed to characterize the nappe oscillations in terms of sound intensity and frequency over a large range of discharges (Chapters II and III). Both developed methods, a sound and an image analyses, were applied systematically to assess the influence of varied hydraulic and geometric parameters on the nappe oscillations phenomenon (Chapter V).

Then, in the light of the importance attached to physical modeling regarding

the hydraulic structure design, the nappe oscillations phenomenon was studied for a smaller scale model, geometrically similar to the prototype scale facility with a geometric scale factor of 3 regarding the fall height and the crest profile. This second model was developed to assess the potential scale effects (Chapter IV).

Besides these considerations related to the characterization of the phenomenon, new mitigation techniques have been developed. In view of the mitigation techniques already tested in the past which may not be optimal for fixed weirs, alternative mitigation techniques were tested using the large scale physical model and optimized regarding disturbing noise reduction without impacting the hydraulic efficiency of the weir. To satisfy practical and hydraulic requirements, the evaluated mitigation techniques were selected in collaboration with engineering consultants and contractors (Chapter VI). Finally, the nappe oscillations phenomenon was observed and characterized for two Belgian dams. In situ measurements proved the robustness of the measurement methodology developed in the framework of this thesis and the applicability of results gained on the model to prototype (Chapter VII).

I.4 Personal contributions

The main contributions of this PhD thesis are the following:

- Development of two methods for the characterization of nappe oscillations
  Two original characterization methods of the nappe oscillations properties have been developed based on the distinct audio and visual traits of the phenomenon. The application of these methods allows the determination of the occurrence of the phenomenon and its associated frequencies. These unique methods are complementary and provided information never noted before.

- Description of nappe oscillations development
  For the first time, this thesis provides a quantitative description of a nappe oscillations development on a free surface weir and its evolution depending on the discharge and key geometric parameters.

- Acquisition of a large data base
  The design of a flexible prototype scale model allowed testing various geometric parameters of the model such as the fall height, the weir width, the crest profile and the confinement. Thanks to the characterization methods, a large amount of nappe characteristics, in terms ofdischarge range of occurrence, noise production and oscillations frequency, as well as associated geometric and hydraulic parameters, were collected. This data base is presumed valuable as little data are available in the literature and only few

of them provide sufficient quantitative data in terms ofgeometry, hydraulic feature or even discharge range of occurrence and associated frequencies.

- Study of size scale effects
  Experiments have been performed on two identical models with different scale factors (prototype model and 1/3 scale model) to investigate the potential size scale effects on nappe oscillations. These experiments showed that nappe oscillations cannot be scaled according to the traditional similitude for weirs (Froude similitude) and always occurred in the same unit discharge range. This study confirms and completes the findings of the single similar study performed to date in the context of nappe oscillations.

- Identification of conditions for nappe oscillations
  Based on the expertise gained from hours of nappe oscillations observations and analysis, necessary conditions for nappe oscillations occurrence have been defined. Along with geometric criteria regarding the fall height and width of the structure, these conditions, although not sufficient, allow to predict the possible occurrence of the oscillations in many cases. The conditions for nappe oscillations were presented in the form of a questionnaire which is a practical and valuable tool for designers.

- Identification of possible causes of nappe oscillations
  To date, definitive proof as to the origin of instability was not found. However, based on all experiments, some observations that support theories were gained. A set of observations related mainly to two theories already exposed in the literature, i.e., the boundary layer and turbulence development and, the pressure discontinuity at the crest, were highlighted.

- Identification of new effective mitigation techniques for weirs
  With the help of practicing engineers and contractors, three innovative mitigation techniques were identified with respect to constructability, durability, performance, maintenance. These solutions were tested and proved effective regarding the noise reduction. These mitigations differ from the classical splitters presented in the literature and included crest roughening via projecting elements, the fragmentation of the nappe through deflectors, and a boundary layer and nappe trajectory modification through a small downstream step.

This PhD thesis contains excerpts of several papers published or accepted for publication in peer-reviewed journals, as well as communications at scientific conferences (Table I.1). At the beginning of each chapter, we clearly state the corresponding sources.

Table I.1: Outline of the thesis and references on which the chapters are (partly) based

Thesis chapter		Reference
I.	Introduction and research objectives	Lodomez et al. (2018c,b, 2019)
II.	Experimental setup	Lodomez et al. (2018c, 2019)
III.	Characterization of nappe oscillations	Lodomez et al. (2018c, 2019)
IV.	Nappe oscillations on scale model and size scale effects	Lodomez et al. (2019)
V.	Occurrence and frequencies of nappe oscillations	
VI.	Mitigation techniques for weirs	Lodomez et al. (2018b)
VII.	In situ measurements	Lodomez et al. (2018a)
VIII.	General conclusions	

Chapter II

Experimental setup

This Chapter is based on the following articles:

Lodomez, M., Pirotton, M., Dewals, B., Archambeau, P., Erpicum, S., 2018c. Nappe oscillations on free-overfall structures: Experimental analysis. Journal of Hydraulic Engineering 144 (3), 04018001.

Lodomez, M., Tullis, B., Dewals, B., Archambeau, P., Pirotton, M., Erpicum, S., 2019. Nappe oscillation on free-overfall structures : Size scale effects. Journal of Hydraulic Engineering 145(6), 040119022.

II.1 Introduction

To fulfill the objectives presented in Chapter I and thus improve the understanding of the nappe oscillations phenomenon through an experimental study, the first task conducted within the framework of this research was to define and design the experimental facilities. These weir models are presented in Section II.2. Then, the measuring tools adapted to collect hydraulic and oscillations characteristics are described (Section II.3). Finally, both methods specifically developed to analyze the data from the measurement devices, and then characterize the nappe oscillations in terms of affected discharge range and frequencies are presented in detail (Section II.4).

II.2 Weir models

Two experimental setups were specifically designed for this research. The first facility was a prototype scale model of a linear weir built at the Engineering Hydraulics Laboratory of the University of Liège (ULiège). The second facility, was a small scale model located at the Utah Water Research Laboratory (UWRL) of the Utah State University. It was a geometric similitude of the first facility with a 1/3 geometric scale regarding the fall height and the crest profile.

II.2.1 Prototype scale model – Model 1

The first facility, called Model 1 in the following manuscript, was a prototype-scale linear weir (Fig.II.1, Fig.II.2, Fig.II.3). It included an elevated headbox that provided flow to two identical weirs installed in parallel. These weirs had a maximum crest length of 3.45 m and a maximum fall height of 3.0 m. The weirs could be isolated so as to only operate one at a time as illustrated in Fig.II.2. The headbox was supplied by two pumps delivering up to 0.25 m^3/s through two perforated pipes parallel to the crest and located on the bottom of the reservoir. The discharge was measured with an electromagnetic flow meter installed on the supply pipes. Inflows passed through a metal grid and a synthetic membrane to establish uniform approach flows to either weir.

As illustrated in Fig.II.3, the weir located on the right side of the reservoir was confined downstream with two lateral walls and a back wall, to investigate a confined nappe and a non-vented air cavity behind the nappe. One lateral wall was made of Plexiglas for observation and the others of black multiplex panels. The weir on the left side only included one sidewall and was used for unconfined testing. Although the existence of the sidewall, the nappe was never in contact with the latter as the dividing wall is thicker (Fig.II.3). Therefore, experiments with confined or unconfined air behind the nappe were performed and referred to confined (C) or unconfined (UC) configurations.

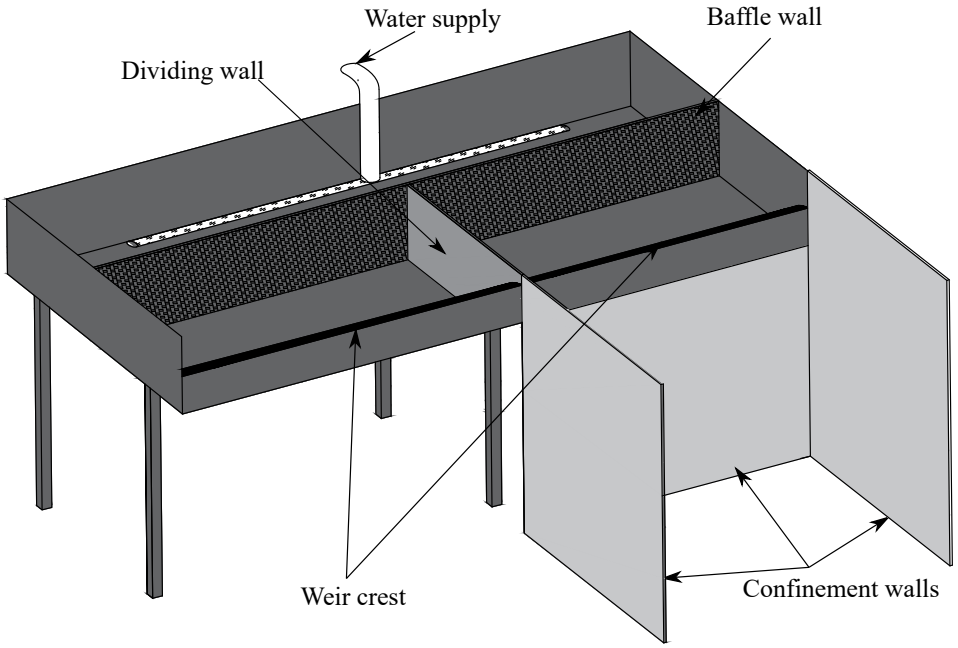

Figure II.1: Schematic view of the prototype scale model – Model 1

Figure II.2: View of the prototype scale model – Model 1 with flow over the unconfined weir

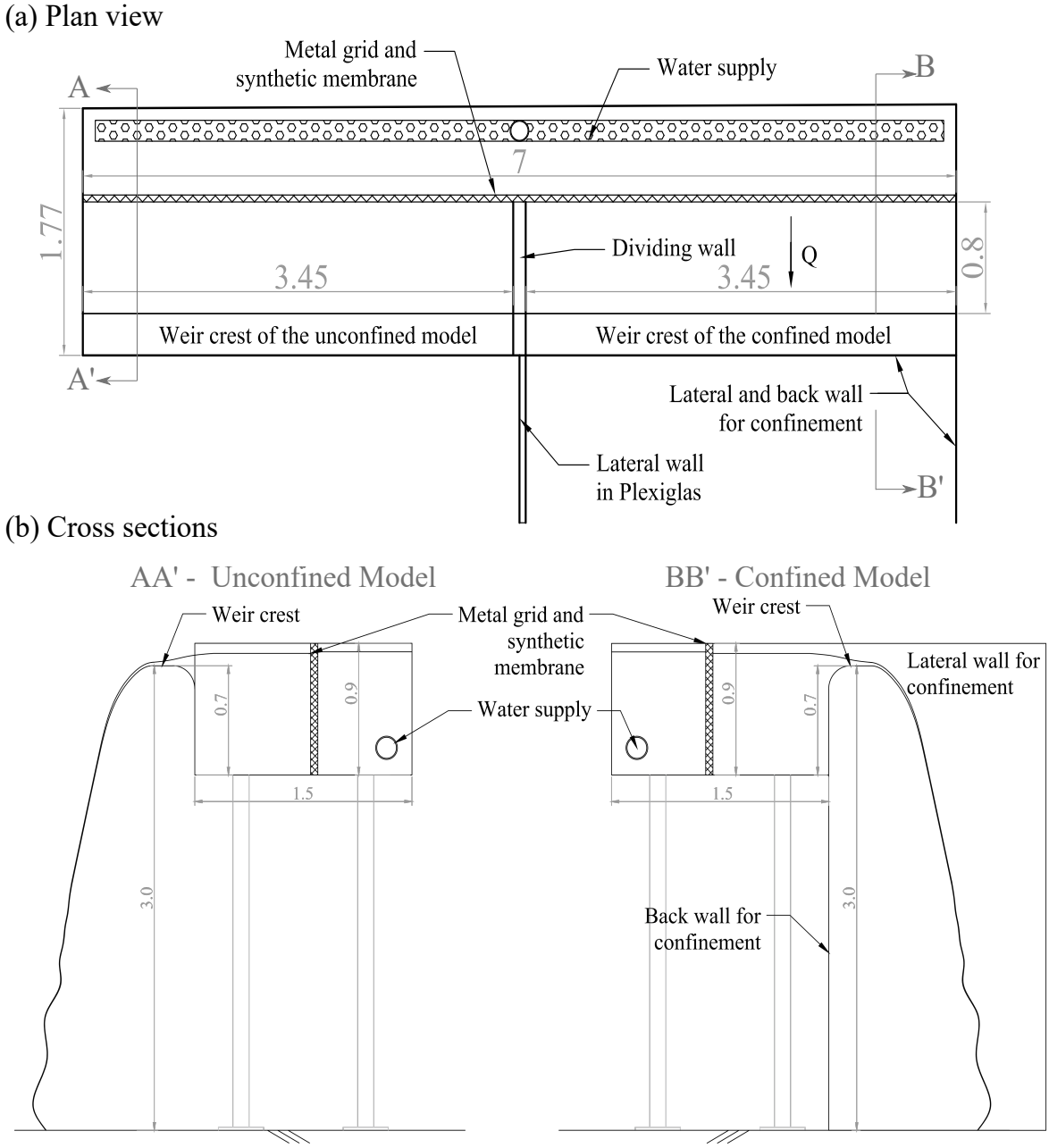

Figure II.3: Fig.3. (a) Plan view and (b) cross sections of the Model 1 (dimensions in m)

As shown in Fig.II.4, three specific crest profiles, located at the downstream extremity of the headbox, were tested during this study: a quarter round (QR), a half round (HR) and a truncated half round (THR) crest. For this large scale model, the characteristic dimension R was equal to 15 cm for all profiles. These crests were made with metal sheets, supported by machined PVC supports every 0.3 m.

In addition to the crest profile, the width and fall height were two geometric parameters that could be modified. For width modifications, pannels were placed along the crest weir in the reservoir to reduce the flow area while a wooden movable apron was use to reduce the fall height. All the configurations tested during this research are reported in the Table II.1.

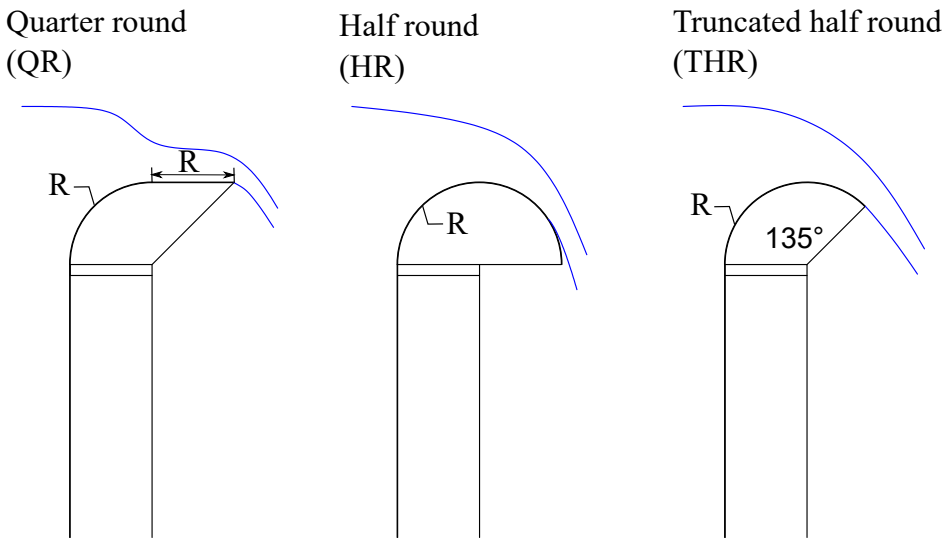

Figure II.4: Schematic of the three crest profiles

Table II.1: Summary of the configurations tested in the framework of this thesis

	Abbreviation	Confinement	Crest shape R- (cm)	Width W (cm)	Fall height L (cm)
Model 1	$C-QR1-W1-L1$	Confined C	QR- 15	345	300
	$C-THR1-W1-L1$		THR- 15	345	300
	$C-THR1-W1-L2$				250
	$C-THR1-W1-L3$				200
	$C-THR1-W1-L4$				150
	$C-THR1-W1-L5$				100
	$C-THR1-W2-L1$			250	300
	$C-THR1-W2-L2$				250
	$C-THR1-W2-L3$				200
	$C-THR1-W2-L4$				150
	$C-THR1-W3-L1$			200	300
	$C-THR1-W3-L2$				250
	$C-THR1-W3-L3$				200
	$C-THR1-W3-L4$				150
	$C-THR1-W4-L1$			150	300
	$C-THR1-W4-L2$				250
	$C-THR1-W4-L3$				200
	$C-THR1-W4-L4$				150
	$C-THR1-W6-L1$			100	300
	$C-THR1-W6-L2$				250
	$C-THR1-W6-L3$				200
	$C-THR1-W6-L4$				150
	$C-HR1-W1-L1$		HR- 15	345	300
	$C-HR1-W1-L5$				100
	$C-HR1-W1-L7$				50
	$UC-QR1-W1-L1$	Unconfined UC	QR- 15	345	300
	$UC-QR1-W1-L2$				250
	$UC-QR1-W1-L3$				200
	$UC-QR1-W1-L4$				150
	$UC-QR1-W1-L5$				100
	$UC-QR1-W1-L7$				50
	$UC-QR1-W2-L1$			250	300
	$UC-QR1-W2-L2$				250
	$UC-QR1-W2-L3$				200
	$UC-QR1-W2-L4$				150
	$UC-QR1-W2-L7$				50
	$UC-QR1-W3-L3$			200	200
	$UC-QR1-W3-L4$				150
	$UC-QR1-W3-L5$				100
	$UC-QR1-W3-L7$				50

	Abbreviation	Confinement	Crest shape R- (cm)	Width W (cm)	Fall height L (cm)
Model 1	$UC-QR1-W4-L1$	Unconfined UC	QR- 15	150	300
	$UC-QR1-W4-L2$				250
	$UC-QR1-W4-L3$				200
	$UC-QR1-W6-L1$			100	300
Model 2	$C-QR2-W5-L5$	Confined C	QR- 5	120	100
	$C-QR2-W5-L6$				75
	$C-QR2-W5-L7$				50
	$C-THR2-W5-L5$		THR- 5		100
	$C-THR2-W5-L6$				75
	$C-THR2-W5-L7$				50
	$C-R-W5-L5$		R		100
	$C-RR-W5-L5$		RR		100

II.2.2 Small scale model – Model 2

To investigate the potential size scale effect (Chapter IV), a second model was built. This small scale model, called Model 2 in the following manuscript, was a rectangular flume 4.7-m long, 1.2-m wide and 1.2-m deep (Fig.II.5 and Fig.II.6). The flume was supplied with water up to 0.075 m^3/s via a 0.3-m diameter pipe which contained a calibrated orifice plate flow meter. A flow straightener was placed near the upstream end of the flume to minimize the turbulence and improve flow conditions. A linear weir supported by a wooden frame was set up 3.5 m downstream from the flume inlet. The fall height was 1.0 m and confined by two sidewalls (acrylic) and a back wall (wood).

Two crest profiles with identical shape to the ones tested for Model 1 but with smaller dimensions were tested for this model: the quarter round (QR) and the truncated half round (THR). The characteristic dimension R was equal to 5 cm, i.e., 3 times smaller than for Model 1 (Fig.II.4). It should be noted that the crest at the downstream extremity ended vertically which slightly differed from the cantilevered metal sheet and support used for Model 1 (Fig.II.7). For both crest profiles, intermediate fall heights were also tested. All the tests with Model 2 were done with the confined configuration.

In addition to the QR and THR crest profiles, two additional crest profiles, illustrated in Fig.II.8, were tested for Model 2 : a rectangular (R) crest and a rectangular crest with a 1-cm rounded upstream edge (RR). The configurations tested for this small scale model are also reported in Table II.1.

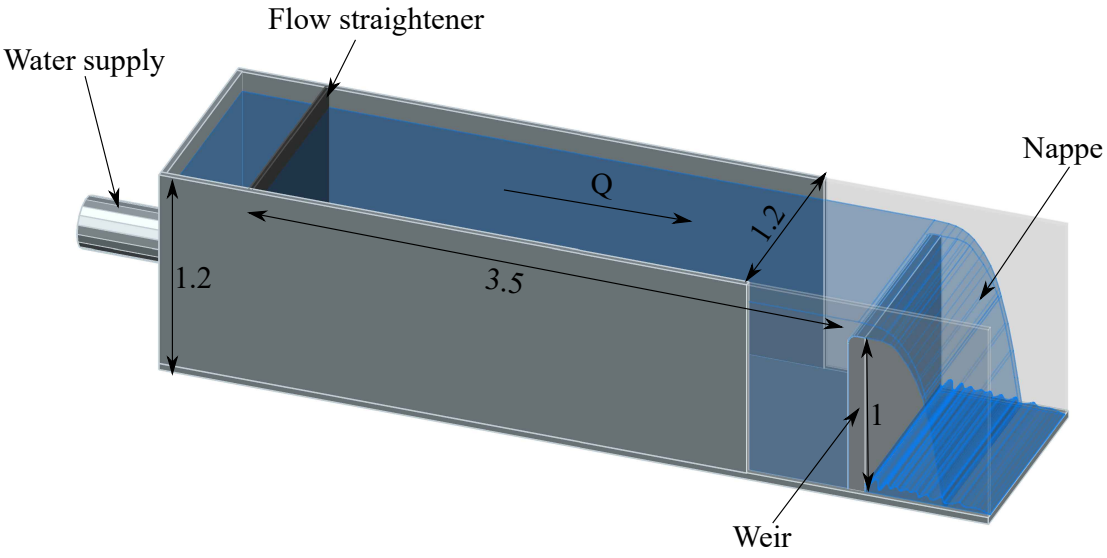

Figure II.5: Schematic of the small scale model – Model 2 (dimension in m)

Figure II.6: View of the small scale model – Model 2

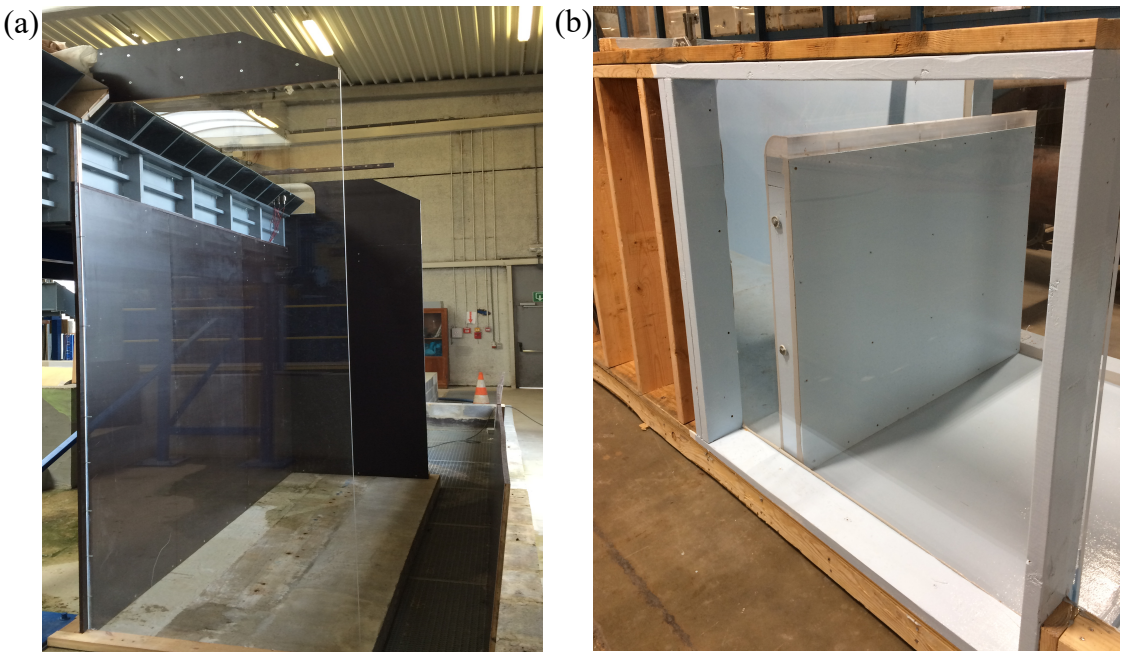

Figure II.7: Photographs of (a) the confined model of Model 1 and (b) Model 2

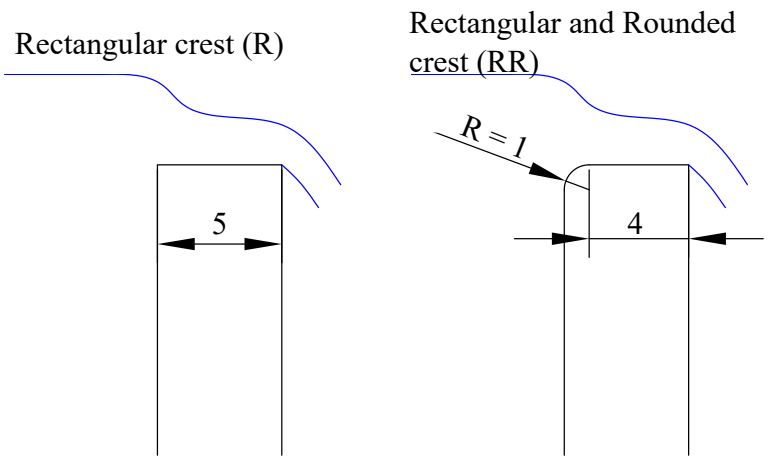

Figure II.8: Schematic of additional crest profiles tested on Model 2 (dimension in cm)

II.3 Measurement tools

The oscillations of the thin flow nappe cascading downstream from the crest and the noise production are respectively the visible and audible characteristics of the nappe oscillations. These characteristics were recorded respectively by the use of a high speed camera and a microphone, and analyzed by a specific method developed in the context of this research. Additionally, hydraulic characteristics of the flow, i.e., discharge and water levels, were measured using a flow meter, ultrasonic sensors or point gauges. These measurement tools are detailed in the following sections.

II.3.1 Microphones

To get data on the noise produced by the oscillations, a free-field microphone, MC212 (01dB-Metravib, Limonest, France) or Behringer ECM 8000 (Behringer GmbH, Willich, Germany) depending on the test, was placed along the centerline of the weir crest, 2.5 m downstream in front of the falling nappe. After testing several positions around the model, it was found that placing the microphone in front of the nappe as specified above makes it possible to obtain, on the one hand, the sound that is least affected by ambient noise, in particular the noise generated by the pumps and, on the other hand, the most direct sound produced by the oscillations. The MC212 and Behringer ECM 8000 microphones have respectively a frequency range of 6 Hz to 20 kHz and 15 Hz to 20 kHz. The recording of audio data was carried out for the MC212 microphone with dBFA from the dB1-Metravib software suite and with SIGVIEW software for the Behringer microphone. Both microphones were calibrated by the Cedia, the research department of acoustic and vibrations of the ULiège. For each test, the sound measurements were performed during 4 minutes and repeated at least twice.

II.3.2 High Speed Cameras

The second method used to characterize the nappe oscillations is based on image analysis. For this purpose, two high speed cameras, Go-Pro Hero 4 (GoPro, San Mateo, California) and ImagerMX4M Lavision (Lavision, Goettingen, Germany), were available in the Laboratory. As both cameras have an acquisition frequency higher than 200 Hz, they allow the capture of visible oscillations up to a maximum frequency of 100 Hz according to the Nyquist-Shannon sampling theorem (Shannon, 1949). Assuming the frequencies of interest in this study were lower than this limit of 100 Hz, both cameras were used indifferently depending on their availability. This assumption is verified in Chapters III and V. Horizontal bands being the visible characteristics of the nappe oscillations phenomenon, the camera was placed along the centerline of the weir crest, 2.5 m

downstream in front of the falling nappe. This location allowed to capture, using appropriate lighting, the visible horizontal bands on the images of the falling water as illustrated in Fig.II.9.

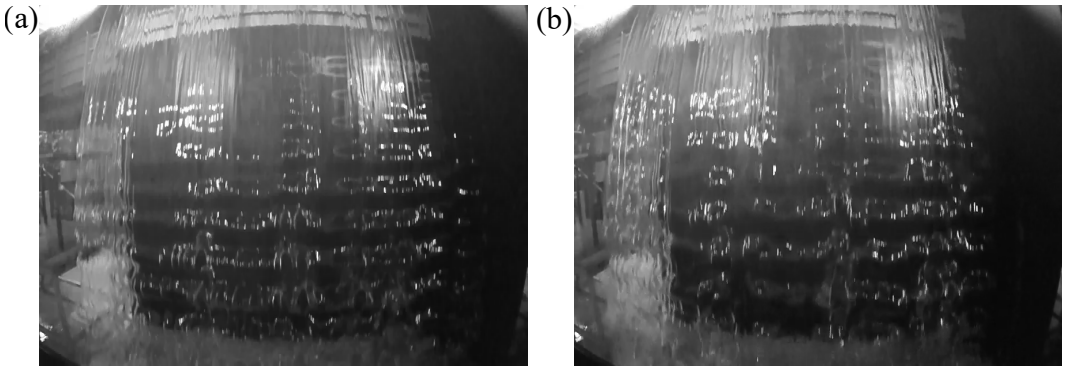

Figure II.9: Nappe visualization for Configuration $C - QR1 - W1 - L1$ (a) $q = 0.02$ m^2/s and (b) $q = 0.03$ m^2/s (images recorded at 240 frame per second with camera Go-Pro Hero 4)

II.3.3 Flow meters

The discharge provided to the model was the only parameter controlled by the experimenter through the opening or closing of valves and adjustment of pump rotation speed. For Model 1, the measurement of this parameter was performed with a flow meter Endress+Hauser PROMAG 50W connected to the main 0.3 m diameter supply pipe. The accuracy of the flow meter Endress+Hauser is $\pm 0.5\%$ of the full scale (0.4 m^3/s) according to the calibration sheet of the device, which is $\pm 2 \times 10^{-3}$ m^3/s.

For Model 2, an orifice plate, connected to the 0.203 m diameter supply pipe, was used. This measurement tool was calibrated and had a total uncertainty of $\pm 0.25\%$ of the discharge which gave for the maximum discharge tested an accuracy of $\pm 2 \times 10^{-4}$ m^3/s.

In the following discussions of this research, the use of a unit discharge $q = \frac{Q}{W}$ in m^2/s, ratio of the total discharge Q (m^3/s) to the crest width W (m), has been preferred to the total discharge Q. The maximum unit discharge tested was 0.07 m^2/s for Model 1 and Model 2 which corresponds respectively to 241.5×10^{-3} m^3/s and 84×10^{-3} m^3/s.

II.3.4 Ultrasonic sensors and point gauges

Water levels, in the reservoir and on the crest, were acquired for each discharge and crest profile (except for HR). The position of the measuring instruments is illustrated for Model 1 in Fig.II.10 and for Model 2 in Fig.II.11.

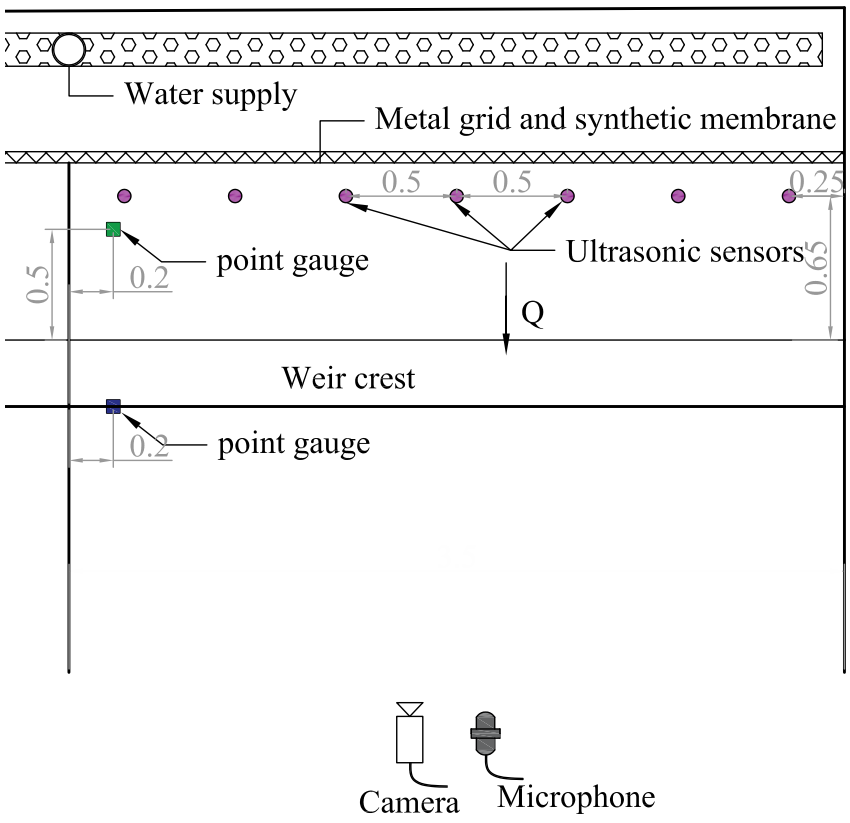

Figure II.10: Position of ultrasonic sensors and point gauge in Model 1 (dimensions in m)

For Model 1, measurements of the upstream water level were performed in the headbox either 0.65 m upstream of the weir using 7 calibrated ultrasonic sensors (Microsonic pico+35/WK/I) placed parallel to the weir crest or 0.5 m upstream of the weir using a unique point gauge located about 0.2 m from the dividing wall. The water level at the flow detachment (crest downstream extremity) was also measured with a point gauge. Whatever the measurement device, the measurement accuracy was ± 1 mm.

For Model 2, a point gauge was placed 1.5 m upstream of the crest extremity while a second one was movable from 0.5 m upstream to the extremity of the crest. Water level measurements for this model were performed with an accuracy of ± 0.6 mm.

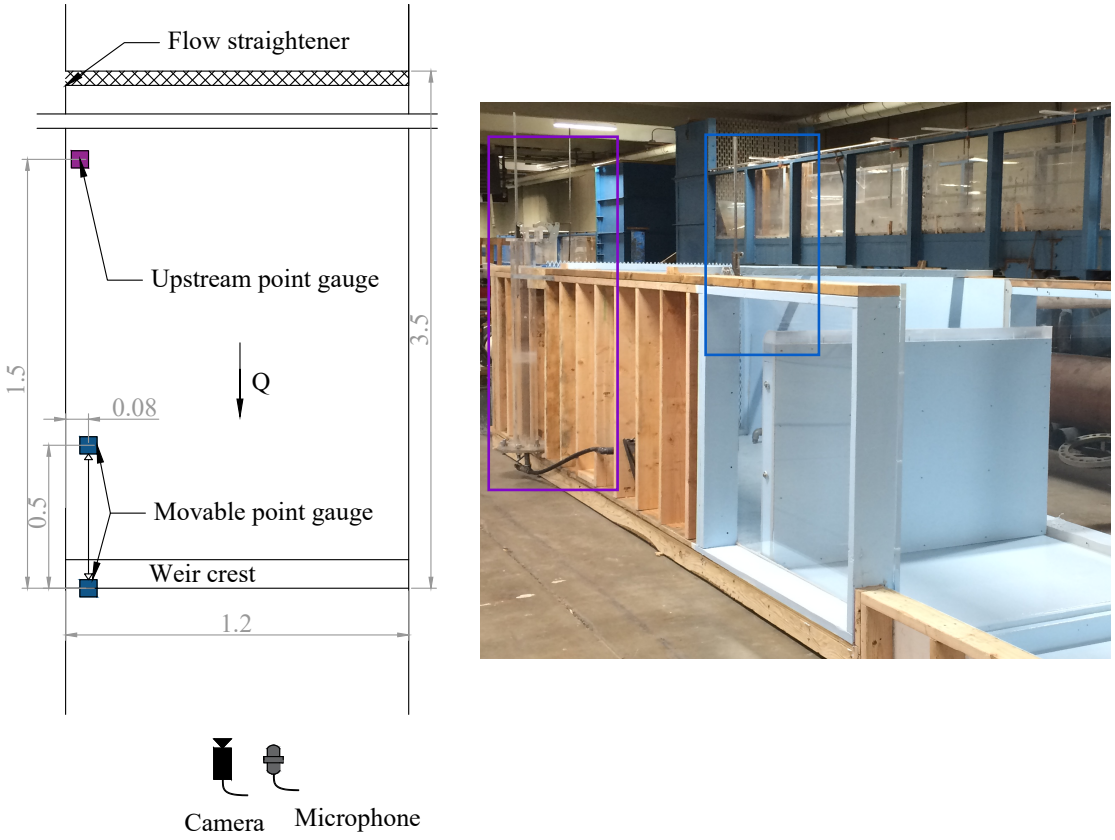

Figure II.11: Position of point gauges in Model 2 (dimensions in m)

II.4 Data processing

To collect relevant and quantitative data from sound measurements and videos, specific analysis methods were developed. These two methods allowed the identification of the oscillations occurrence and a quantification of their main characteristics.

II.4.1 Sound analysis

II.4.1.1 Processing of sound signal

Sound recording provided a time evolution of a pressure which is correlated to the sound pressure level, measured in dB, by $20 \log_{10} \frac{p}{p_0}$ with the root mean square of p the sound pressure around the microphone and p_0 the reference sound pressure (commonly set at 20 µPa in air). Fig.II.12 shows two sound recordings (time evolution of p) that illustrate the occurrence and the non-occurrence of the characteristic noise production related to the nappe oscillations. A clear periodic sound can be detected in the case of nappe oscillations occurrence as illustrated in Fig.II.12(a) while it is not observed in Fig.II.12(b). This periodic sound is often clearly audible to the human ear and can be unpleasant.

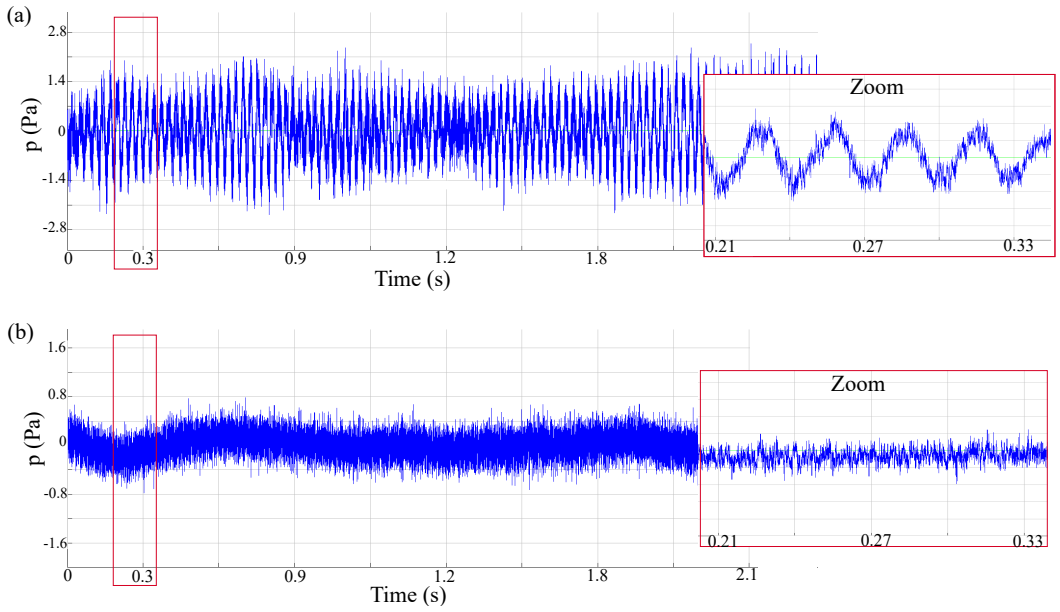

Figure II.12: Sound recording illustrating (a) the occurrence and (b) the non-occurrence of the characteristic periodic noise production of the nappe oscillations

Based on these sound data, the sound analysis was carried out by the software used for the recording, i.e., dBFA v4.9 (01dB Metravib, ACOEM, 2008)

or SIGVIEW v3.0.2 (SignalLab, 2017). The dBFA software supplied the auto-spectrum of the audio signal by applying a narrow-band analysis of the audio signal. The audio auto-spectrum provides an image of the sound level for each frequency of the noise. This spectral analysis is based on a classical periodogram or Gabor analysis, with the selection of an overlap and a weighting window (01dB Metravib, 2008). The result, named sound level or intensity in the following discussions, is expressed in dB and is equal to $20\log_{10}\frac{|G_{xx}|}{2\times10^{-5}}$ with $|G_{xx}|$ being the modulus of the complex auto-spectrum. Based on audio recording, this spectral analysis was applied considering an overlap of 50%, a Hanning window and a frequency resolution of 0.25 Hz. The analysis resulted in a narrow-band multi-spectrum with a time step of 125×10^{-3} s. This result was exported as a text file and analyzed with the MatLab software. The representation of the narrow-band multi-spectrum in time showed that this acoustic property was stationary for all the configurations or the unit discharges (q) as illustrated in Fig.II.13. For a fixed frequency, the standard deviation of the sound level has been computed. The maximum standard deviation of the sound level, among all the available frequencies, remained, for all tests, below 7 dB while the standard deviation never exceeded 1.5 dB at the characteristic local peak. Therefore, the temporal mean of the multi-spectrum was calculated for each test (Fig.II.14).

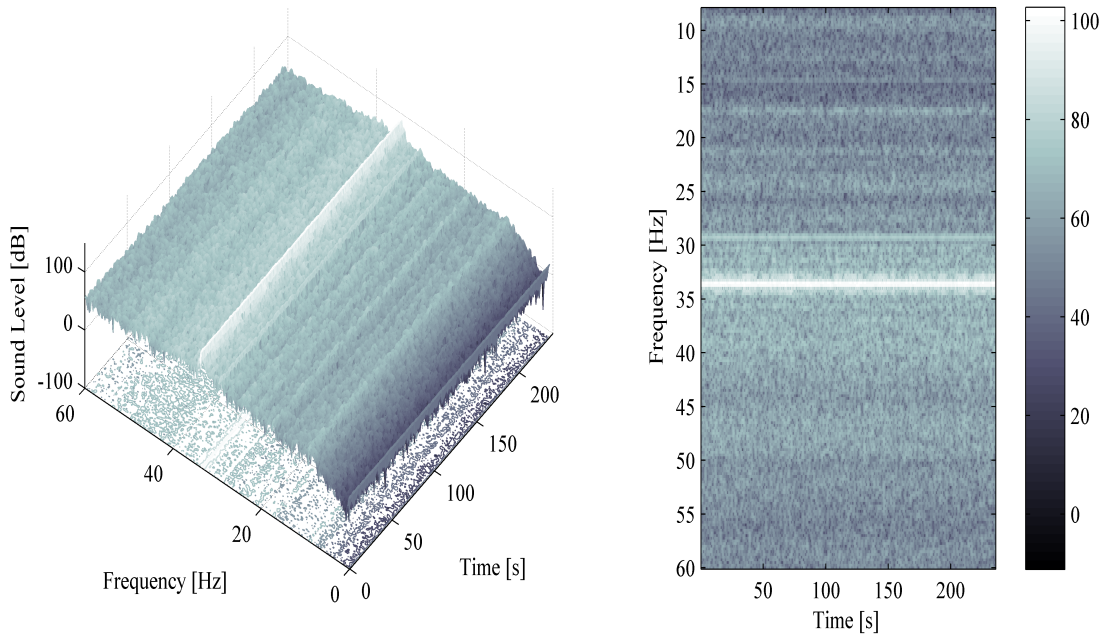

Figure II.13: Auto-spectrum of audio signal for Configuration $C-QR1-W1-L1$ and $q = 0.03$ m²/s

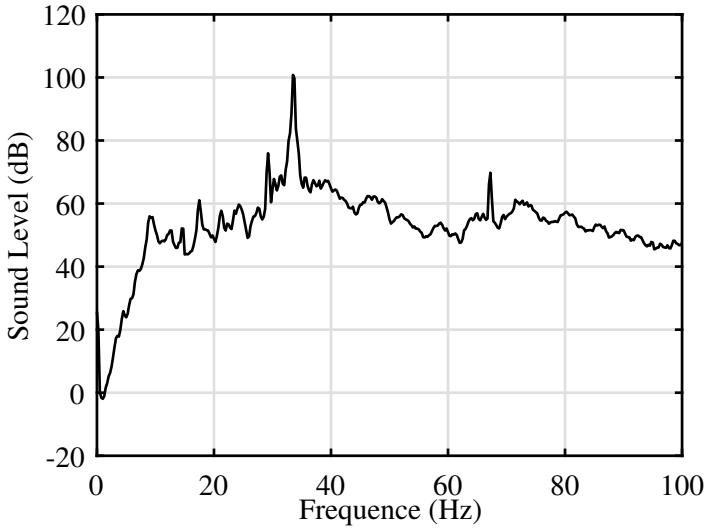

Figure II.14: Mean auto-spectrum of audio signal for Configuration $C - QR1 - W1 - L1$ and $q = 0.03$ $\mathrm{m^2/s}$

The SIGVIEW software (SignalLab, 2017) provided directly the mean auto-spectrum with a frequency resolution of 0.01 Hz with the application of the same filtering (Hanning window). For example, the spectral analysis performed with this software (recording with the Behringer microphone in April 2018) is reported and compared with the one obtained from dBFA software (using the MC212 microphone in October 2016) for an identical configuration ($UC - QR1 - W1 - L1$, 0.03 $\mathrm{m^2/s}$) in Fig.II.15. It shows that similar results are collected with these two different tools. Indeed, for the same configuration and some q, both spectra present a clear peak related to the oscillations. The frequency of the peak is similar, considering the different resolution of the software. However, the intensity of the spectrum varies due to the use of a different microphone. More generally, sound intensities extracted from spectra are not comparable if the sound signals were recorded with different microphones and/or in different laboratory acoustics. Therefore, to compare sound intensities recorded with different microphones and processed with different softwares, these intensities measured for a defined configuration (i.e., for fixed confinement and geometric parameters) were normalized by the maximum intensity measured for the tested configuration.

Finally, the sound signal processing generated a mean auto-spectrum, simply called spectrum in the following analyses. From this result two quantitative parameters were extracted to characterize the oscillations: the maximum sound level and its associated frequency.

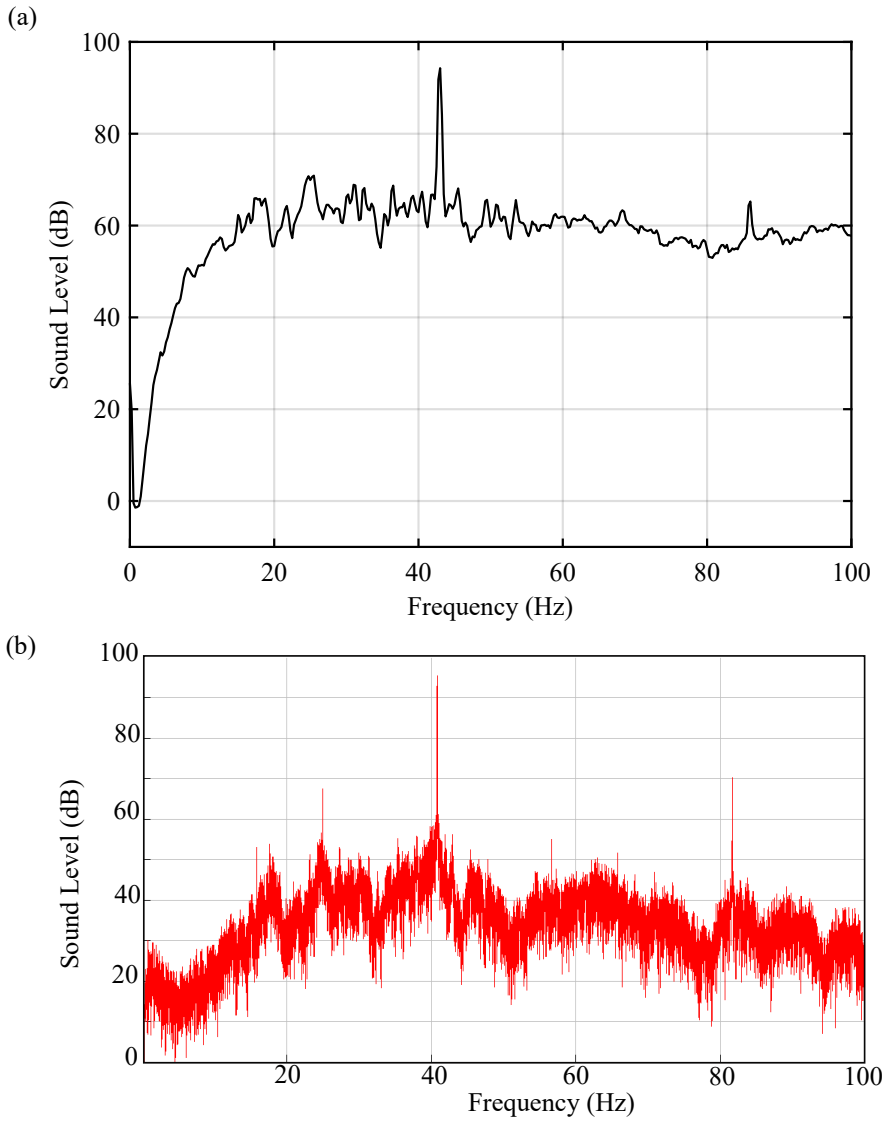

Figure II.15: Mean auto-spectrum for Configuration $UC - QR1 - W1 - L1$ and $q = 0.03$ m^2/s. (a) Signal recorded with the MC212 microphone and processed with dBFA (b) Signal recorded with the Behringer microphone and processed with SIGVIEW

A third parameter extracted from these results was the numerical integral of the spectrum S. This parameter increased with q as the sound production increased with the discharge, independently of the nappe oscillations occurrence. However, the magnitude of this increase depended on the occurrence or absence of oscillations. To help the comparison between the configurations, this third parameter may also be divided by the maximum integral (S_{max}) of the configuration to provide a dimensionless comparison.

II.4.1.2 Interpretation of audio spectrum

As mentioned above, the sound analysis focused on the mean auto-spectrum, or spectrum, obtained from the processing of the sound recording with the specific software (dBFA or SIGVIEW). This spectrum provided an image of the sound level for each frequency of the noise generated by the nappe cascading downstream from the weir. It allowed to determine the occurrence or non-occurrence of the nappe oscillations phenomenon which is characterized by the presence of a local peak in the spectrum with its corresponding frequency. Indeed, the spectra extracted from sound measurements were typically of two types, as illustrated in Fig.II.16a for Configuration $C-QR1-W1-L1$ and two q. Fig.II.16a shows, for $q = 0.03$ m^2/s, a spectrum in which a clearly visible peak in sound level appears for a specific frequency while for $q = 0.06$ m^2/s, there is no obvious dominant peak. For $q = 0.03$ m^2/s, nappe oscillations were characterized by a sound level up to 100 dB. This maximum quantified the magnitude of the phenomenon while the frequency of oscillations, 33.25 Hz, was directly given by the associated frequency of the peak in the audio spectrum. For $q = 0.06$ m^2/s, nappe oscillations were weak or non-existent as there was no local maximum in the spectrum. The distinction between these two examples is also illustrated in Fig.II.16b by the cumulative frequencies of the spectra, which exemplifies the concept of "dominant" peak. For $q = 0.03$ m^2/s, 2% of the frequencies increased the sound level by 26% while for the non-oscillating configuration (0.06 m^2/s) the frequencies distribution over the sound level was more uniform.

The nappe oscillations are characterized by a local peak in the spectrum. However, it should be mentioned that the oscillations were not the only process able to create a local peak in the audio spectrum. Acoustic recordings also included background noise, such as the pum, associated with its characteristic frequencies such as the pump rotation speed. As an example, the second maximum of the spectrum in Fig.II.17 was due to the pump rotating at a 25 Hz frequency. To overcome this problem, special care has been paid in every test to adapt the pump frequency so as not to match the frequency of other local peaks in the spectrum. In addition, when repeating the tests, different pump frequencies were used to isolate unequivocally the sound signal from the oscillations. Therefore, all the intensities and associated frequencies of spectra presented in this study are unequivocally related to the nappe oscillations. This procedure is illustrated in Fig.II.18 for Configuration $UC - QR1 - W1 - L1$ and $q = 0.025$ m^2/s. For an identical q, four different pump frequencies were tested, i.e., 27, 29, 31.5 and 40 Hz, respectively illustrated by the blue asterisk in Fig.II.18a-d while the maximum sound level is encircled in red. Figs.II.18a,b,d show a peak for a frequency of 50.75 Hz, which is clearly different from the pump frequency and therefore linked to the oscillations while in Fig.II.18c the pump frequency is the maximum of the spectrum and the second maximum is the frequency of the oscillations.

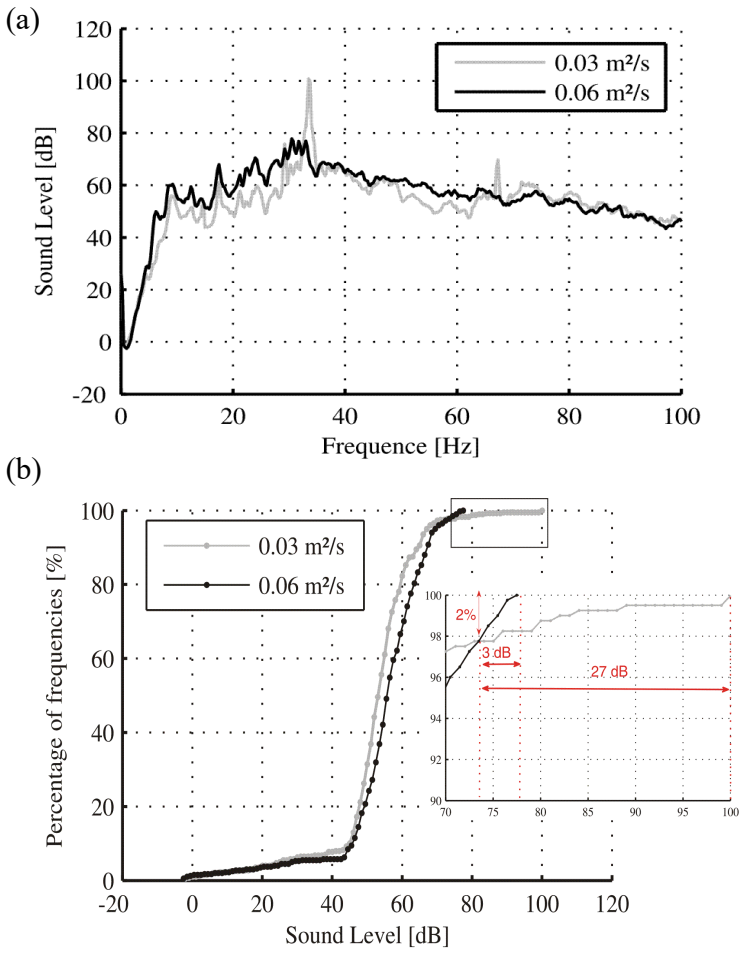

Figure II.16: (a) Spectrum of sound measurement for Configuration $C - QR1 - W1 - L1$ and (b) the corresponding cumulative frequencies of the spectrum

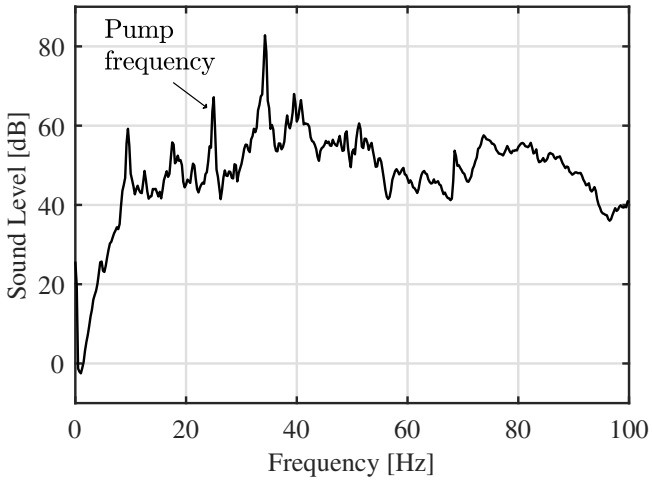

Figure II.17: Spectrum of sound measurements for Configuration $C - QR1 - W1 - L1$ and $q = 0.015$ m²/s

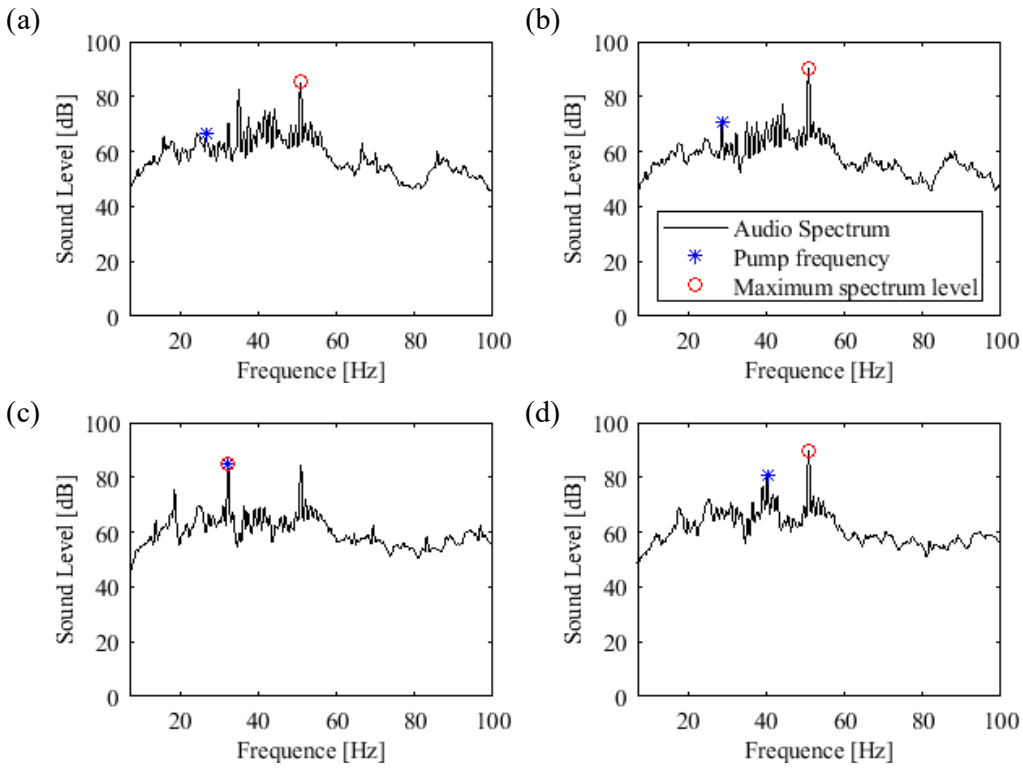

Figure II.18: Audio spectrum collected for variable pump frequencies, Configuration $UC - QR1 - W1 - L1$ and $q = 0.025$ m^2/s

The analysis presented above to characterize the nappe oscillations is based on the assumption that the oscillations noise results from the action of the nappe on the surrounding air and not from the impact on the apron. To verify this assumption, measurements were carried out for Configuration $UC-QR1-W2-L1$ by adding on the concrete apron two 4-cm thick synthetic horsehair panels. The resulting 8-cm thick mattress modified the impact conditions and in particular smoothened the noise. Fig.II.19 illustrates the audio spectra acquired with and without this modified configuration of the zone of impact for $q = 0.02$ m^2/s. It can be observed that the main peak in sound level appeared in both cases for similar frequency and amplitude, i.e., 47.5 Hz and 84.4 dB for the initial configuration and, 47.0 Hz and 81.7 dB with the impact condition modification. With the modification of the impact area, the harmonics of this main peak frequency were still visible. The integral of the spectrum, illustrated in Fig.II.20 for various discharges, is similar to the one for the configuration without impact modification for $q \leq 0.025$ m^2/s with a relative difference varying between -2.3% and 2.5%. For higher q, this integral averaged less than 3.2% the one without impact mitigation. A maximum relative difference of 4.4% was measured for $q = 0.04$ m^2/s. These results confirm the hypothesis that the sound

generated by the nappe oscillations originates from an action of the falling sheet of water on the surrounding air and is not merely related to the impact of the nappe. Identical findings were pointed out by Anderson (2014) who tested the influence of a more cushioned apron material (foam pad) and showed that the presence of this foam pad did not cause the oscillations to cease.

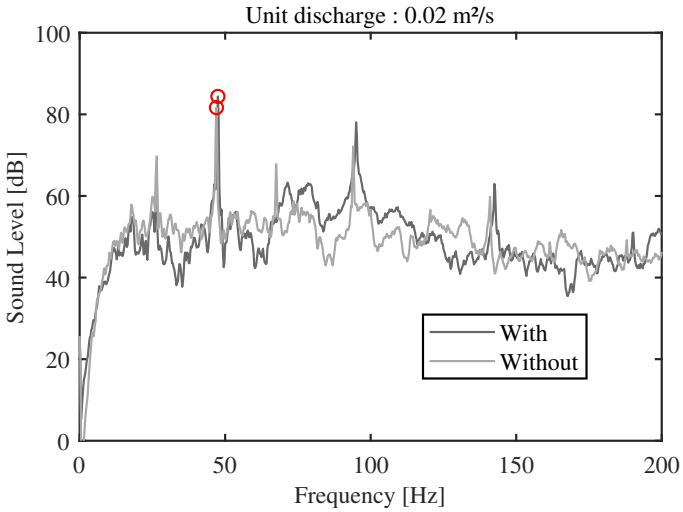

Figure II.19: Spectrum of sound measurement for Configuration $UC - QR1 - W2 - L1$ with a modification of the ground surface with synthetic membranes and without modification, i.e., concrete slab

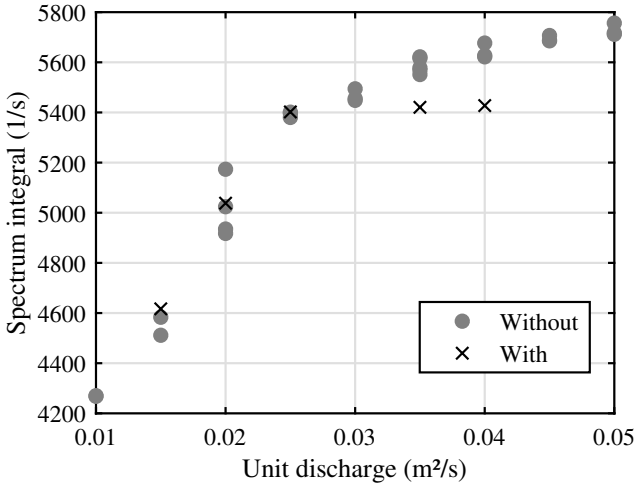

Figure II.20: Integral of sound spectra for Configuration $UC - QR1 - W2 - L1$ with a modification of the ground surface with synthetic membranes and without modification, i.e., concrete slab

II.4.2 Image analysis

II.4.2.1 Processing of video recordings

As shown in Fig.II.21, the viewing of an oscillating nappe with a high speed camera allows the detection of horizontal bands. These are the visible characteristics of the nappe oscillations phenomenon as referred in the literature (Anderson and Tullis, 2018; Casperson, 1993a; Crookston et al., 2014; Khodier and Tullis, 2018). In addition, the analysis of successive images shows the propagation of the oscillations along the nappe according to the flow direction (Fig.II.21). This figure is in accordance with the theory exposed in Pariset (1955) suggesting that oscillations are created by a periodic direction change of the nappe at the crest detachment. After the crest detachment, the particules follow a trajectory almost parabolic but different from other particules located downstream or upstream. The general picture of the nappe is an oscillating trajectory. Also, the direction change is amplified along the nappe fall as the oscillations grow in amplitude throughout the nappe trajectory(Khodier and Tullis, 2018).

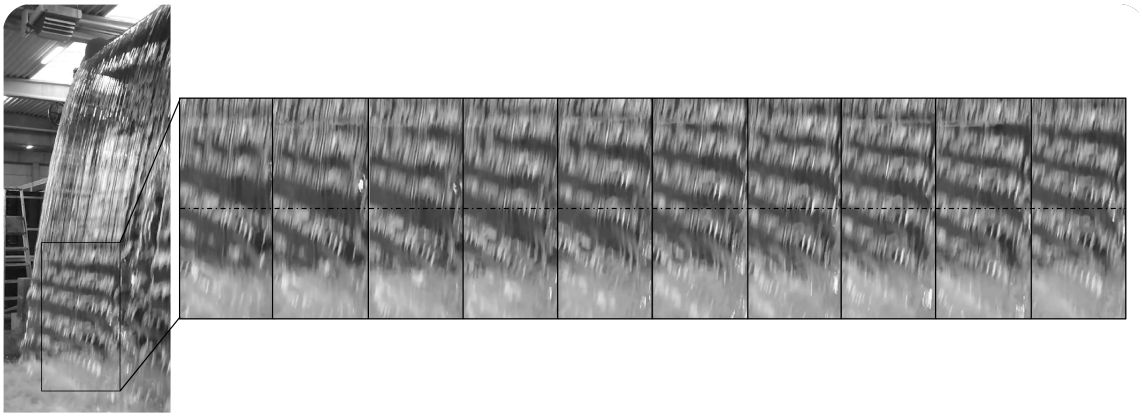

Figure II.21: Downstream side view of the oscillations; tracking of the oscillations along the nappe in a set of 10 successive images (8.3×10^{-3} s between the images)

An image analysis procedure has been developed to quantify the frequency related to horizontal bands displacement along the nappe. Assuming that the horizontal bands are due to the lighting on the undulating surface, the frequency of the bands was determined by the time evolution of data carried by a set of pixels on a succession of raw images. The method is conceptually sketched in Fig.II.22. In this figure, the undulating nappe surface, represented at three successive time steps, shows horizontal bands (lit or unlit bands) moving according to the flow direction. For a fixed image frame, a chosen line of pixels (represented by a thick black line in the image frame) carries information which varies in time. The numerical value associated to each pixel depends on whether the pixels are

on the illuminated zone of the oscillations or not, which represents the curvature of the nappe undulation (concave or convex). This numerical value, for images in grayscale and encoded in 8 bits, is between 0 (white) and 255 (black). Considering the average value on a line of pixels, the oscillations frequency is calculated by the Fast Fourier Transform (FFT) of its time evolution. In order to illustrate this methodology, an analysis on 600 images (recorded at 240 Hz, i.e., 2.5 s long movie) is shown in Fig.II.23 for the configuration $UC - QR1 - W1 - L1$ and $q = 0.045$ m^2/s. This figure illustrates (1) the time evolution of a chosen line of 300 pixels, (2) the fluctuation of the average value of this line and (3) the FFT of this fluctuating signal.

The resolution of this frequency calculation is given by the ratio between the acquisition frequency and the number of snapshots. The acquisition frequency of the camera was either 240 Hz for the Go-Pro Hero4 or 300 Hz for the ImagerMX4M. Image analysis was conducted with the number of snapshots needed to get a resolution at least identical to that of sound analysis (0.25 Hz), i.e., 960 images for the Go-Pro Hero4 and 1200 images for the ImagerMX4M.

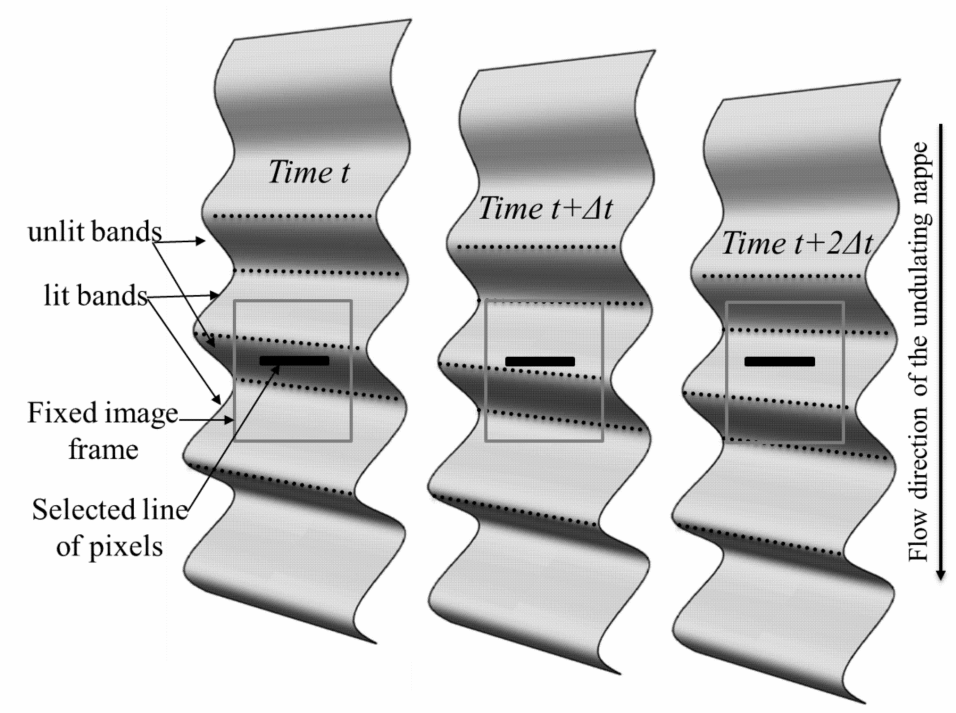

Figure II.22: Conceptual representation for image analysis

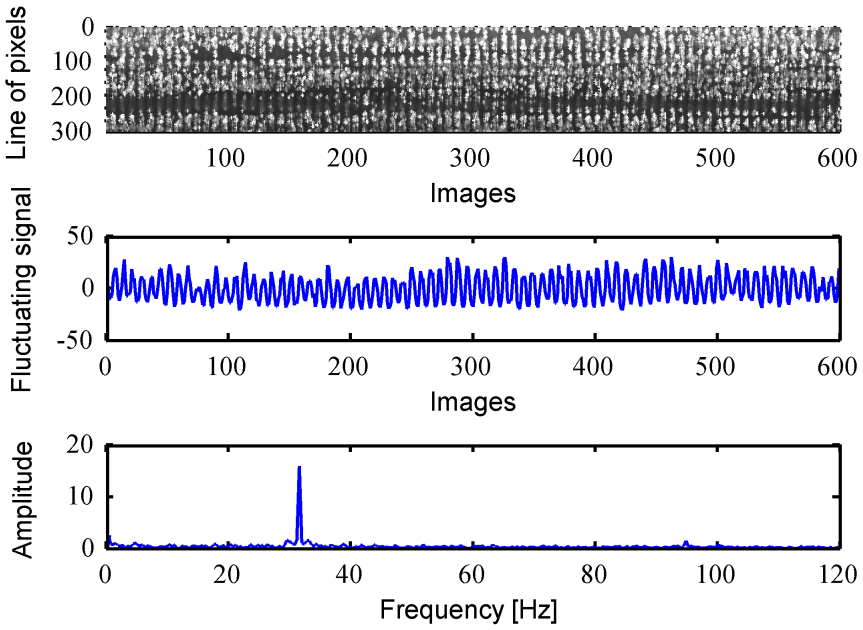

Figure II.23: Steps of image analysis on 600 images for Configuration $UC - QR1 - W1 - L1$ and $q = 0.045$ m^2/s

For each test, a minimum of 6 lines of 300 pixels were considered per snapshot and at least 5 sets of images were analyzed. Therefore the image analysis led to a minimum of 30 calculated points per tested unit discharge. The horizontal lines of pixels taken into consideration for the image analysis were distributed evenly along the frame. The application of this methodology for various configurations showed that a better detection of the bands was obtained for the lines positioned near the crest (within a distance of 1 m), due to the fact that the nappe is more uniform close to the detachment. However, data collected for lines positioned far downstream from the crest provided identical results in terms of frequency, only the amplitude of the peak in the FFT was affected by the position of the line. The number of lines was set at 6 to get robust data and may be increased depending on the fall height of the nappe. Nevertheless, the application of the method showed that for a set of images, the frequency extracted from the different lines did not vary by more than the accuracy of the method, i.e., 0.25 Hz. Finally, the choice of a minimum of 300 pixels per line has been fixed to correspond to the entire length of the narrowest nappe. The position of the camera being fixed, the number of pixels was increased according to the width of the nappe so that the line corresponds to the nappe width.

The variability of the frequency gained from the image analysis is lower than 1.5 Hz, considering a fixed configuration and a discharge. However, higher vari-

ability was detected in some configurations for which several distinct frequencies may coexist for the same discharge. This specificity was also detected for identical configurations by the sound analysis.

II.4.2.2 Application and interpretation of image analysis

Some results of the image analysis performed for Configurations $C-QR1-W1-L1$ and $C-THR1-W1-L1$ and various q are illustrated in Fig.II.24 and Fig.II.25. Although the image analysis was always performed on 6 lines of 300 pixels and a minimum of 960 images (for an acquisition frequency of 240 Hz) to get a relevant accuracy, these figures exemplify the data extracted from only one line of 300 pixels for 240 images. In Fig.II.24, it is first possible to link the detection of oscillations on an instantaneous picture, for $q = 0.02$ m^2/s and $q = 0.04$ m^2/s, to an oscillating signal (in time) as illustrated by the time evolution of the chosen line. The x-axis named Images in these figures corresponds indeed to a time evolution as it corresponds to a set of successive images, shot at 240 Hz. This signal finally allows the calculation of the frequency of the visual characteristic by the application of the FFT.

In contrast, in Fig.II.25a, for $q = 0.06$ m^2/s, the absence of oscillations on the instantaneous picture was also confirmed by the non-fluctuating signal and relevant spectrum. However, if the image analysis could confirm the visual observations, the application of this analysis on a set of images that at first sight did not show oscillations allowed also to confirm the existence of oscillations observed by sound analysis. As an example, Fig.II.25b illustrates an instantaneous picture of Configuration $C-THR1-W1-L1$ and $q = 0.055$ m^2/s which did not display any clear oscillation. The image analysis also reported in Fig.II.25b shows the existence of a particular low frequency also observed with the sound analysis.

As part of the image analysis, the amplitude of the oscillations was not analyzed. The reason is that the amplitude was very variable and could depend on the ambient lighting (depending on the season and the time of the day) which was not fully controlled in the laboratory.

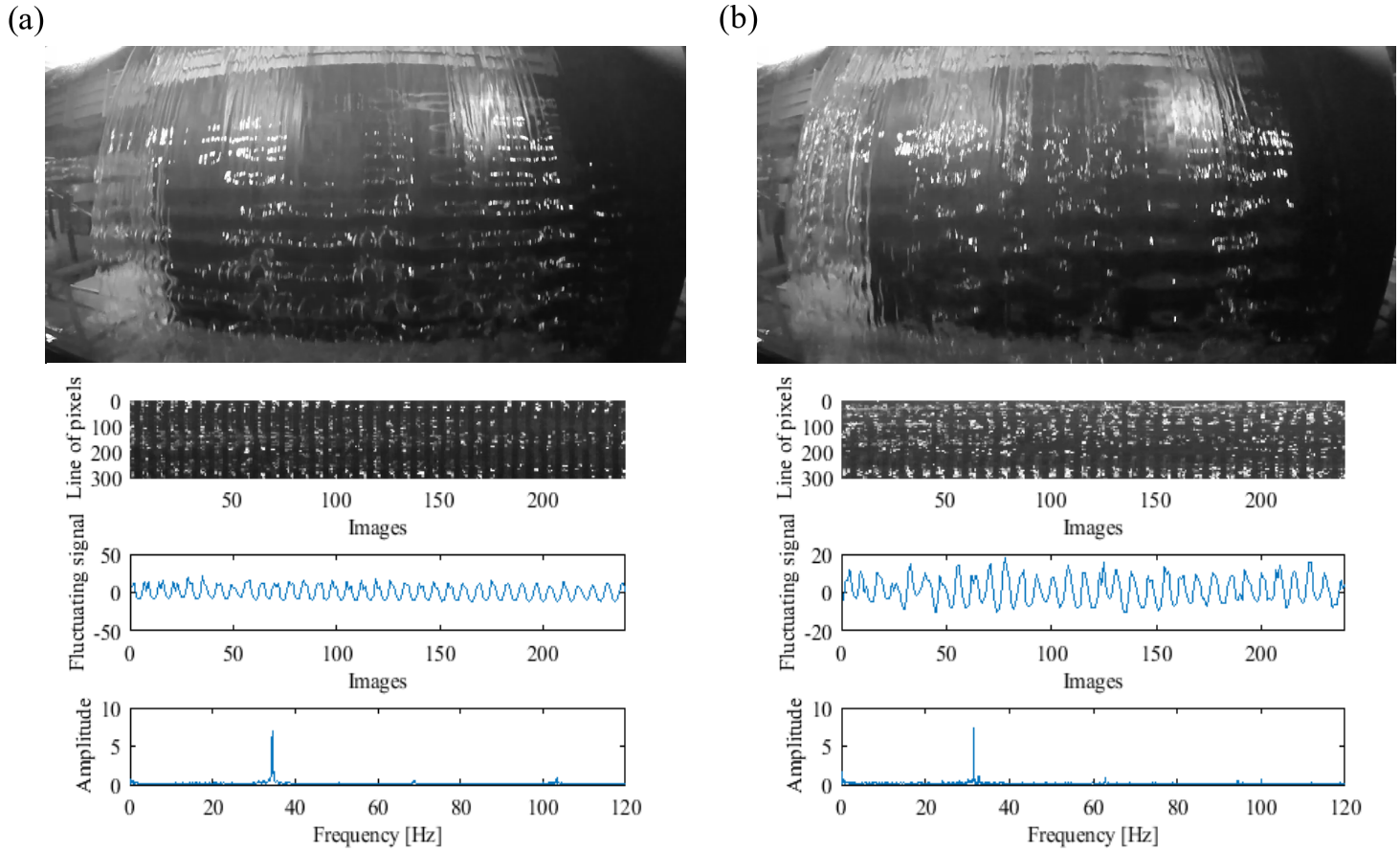

Figure II.24: Illustration of the image analysis for Configuration $C - QR1 - W1 - L1$ and (a) $q = 0.02$ m²/s and (b) $q = 0.04$ m²/s

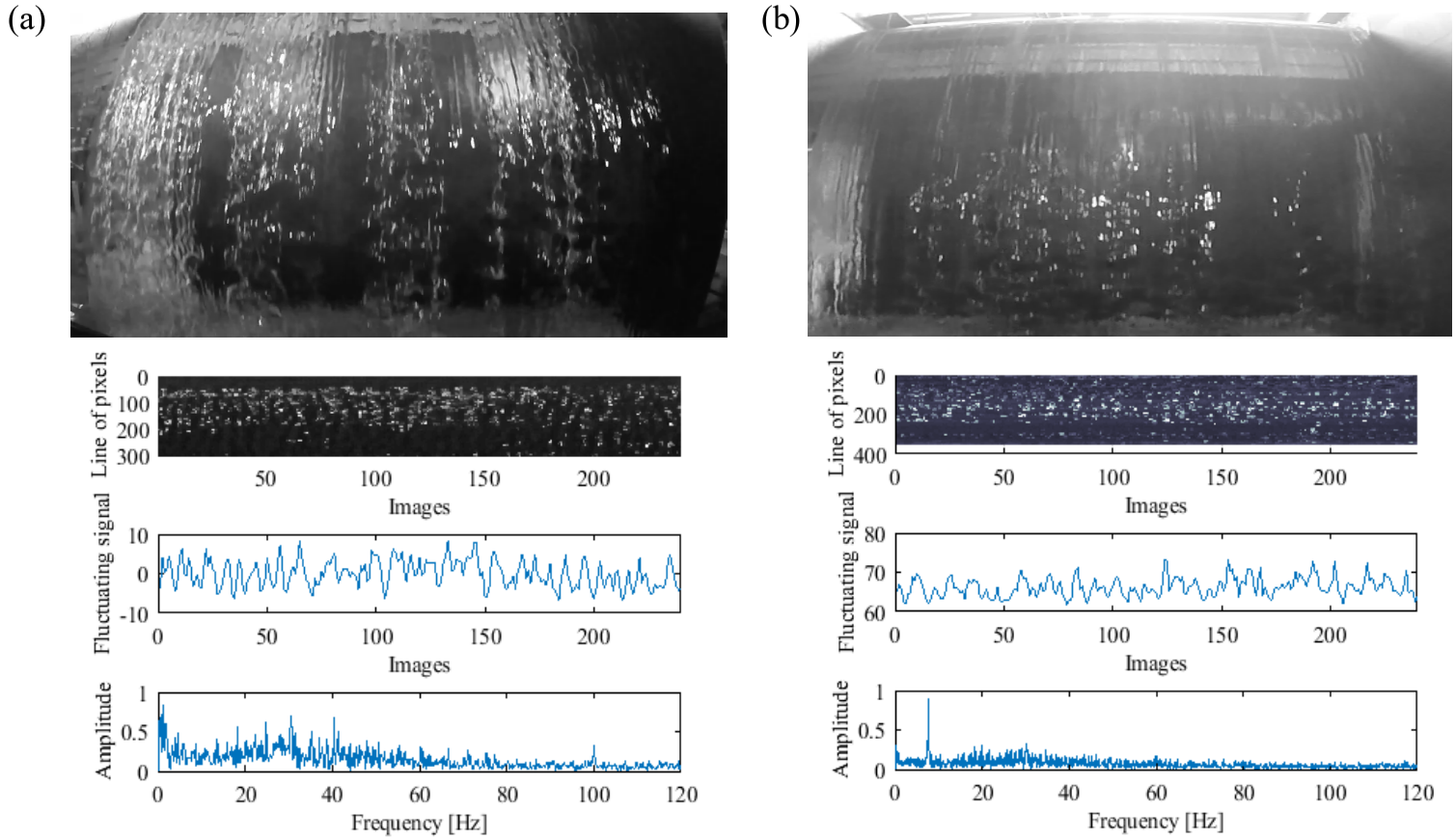

Figure II.25: Illustration of the image analysis for (a) Configuration $C - QR1 - W1 - L1$ and $q = 0.06$ $\mathrm{m^2/s}$ and (b) Configuration $C - THR1 - W1 - L1$ and $q = 0.055$ $\mathrm{m^2/s}$

II.5 Conclusions

The first effort of this research was the design of a prototype-scale linear weir with a geometry known to produce nappe oscillations. Great attention was paid to get a flexible physical model to investigate the influence of geometric parameters such as the fall height and width of the weir, the crest profile of the weir and the confinement. Then, a small scale model was derived from the design of the large scale model as a geometric similitude of the first facility with a 1/3 scale regarding the fall height and the crest profile. The second task was the selection of adapted measurement tools, in particular microphone and high speed camera, to collect audible and visual characteristics of nappe oscillations. Finally, for these measurement tools, systematic methodologies of data acquisition and processing were developed to extract quantitative results, i.e., frequency of sound signal, sound intensity and frequency of visible oscillations. These data analysis procedures were applied to the 52 configurations tested in the framework of this research (Chapter V) as well as to two prototypes (Chapter VII) and provided a set of relevant data for the nappe oscillations knowledge enhancement. Before that, in the next chapter (Chapter III), the sound and images analyses exposed above have been applied to three particular configurations in order to exemplify the characterization of the nappe oscillations and point out specificities of this phenomenon.

Chapter III

Characterization of nappe oscillations

This Chapter is based on the following articles:

Lodomez, M., Pirotton, M., Dewals, B., Archambeau, P., Erpicum, S., 2018c. Nappe oscillations on free-overfall structures: Experimental analysis. Journal of Hydraulic Engineering 144 (3), 04018001.

Lodomez, M., Tullis, B., Dewals, B., Archambeau, P., Pirotton, M., Erpicum, S., 2019. Nappe oscillation on free-overfall structures : Size scale effects. Journal of Hydraulic Engineering 145(6), 040119022.

III.1 Introduction

This chapter focuses on the characterization of the nappe oscillations phenomenon using the results collected from the sound and image analyses techniques presented in Chapter II. This characterization has been performed considering three specific Configurations; $C-QR1-W1-L1$, $UC-QR1-W1-L1$ and $C-THR1-W1-L1$. The two first configurations only differed by the confinement and were the highest (3-m high) and widest (3.45-m wide) weirs tested with a QR crest profile while the third one only differed from the first one by the crest profile. In this chapter, the occurrence of the oscillations was first evaluated by means of qualitative observations (Section III.2). Then, the development of these oscillations in terms of sound intensity and frequencies were examined based on sound and image analyses (Section III.3 and Section III.4). Section III.5 compares the characteristic frequencies collected by these two analyses and Section III.6 presents the hydraulic characteristics of the tested configurations. General findings and key points are summarized in Section III.7.

III.2 Nappe oscillations occurrence

As already mentioned, nappe oscillations are characterized visually by horizontal bands in the nappe flowing downstream of the weir crest (Anderson and Tullis, 2018; Casperson, 1993a; Crookston et al., 2014). Fig.III.1 and Fig.III.2 illustrate respectively the flowing nappe of Configurations $C-QR1-W1-L1$ and $C-THR1-W1-L1$ for various q. For Configuration $C-QR1-W1-L1$ (Fig.III.1), oscillations were clearly visible for q between 0.01 and 0.04 $\mathrm{m^2/s}$. The oscillations decreased for $q = 0.05$ $\mathrm{m^2/s}$ and finally disappeared for $q = 0.06$ $\mathrm{m^2/s}$. Likewise the visual characteristics of nappe oscillations for Configuration $C-THR1-W1-L1$, reported in Fig.III.2, illustrate clear horizontal bands for q lower than 0.04 $\mathrm{m^2/s}$. For higher q, horizontal waves still existed but were disordered and finally vanished.

In addition to the horizontal bands, intense acoustic pressure waves and the associated noise that have been aptly described as sounding similar to a helicopter or an amplified bass note (Casperson, 1993a), may support the detection of the oscillations. Both flow visualizations and sound measurement techniques were therefore analyzed in order to define the flow range affected by nappe oscillations. Horizontal bands and acoustic waves are the elements associated to nappe oscillations. However, it is possible that only one of these characteristics is detectable. Indeed, for lower q, horizontals bands were usually predominant while they disappeared faster than the typical noise for higher q.

Based on qualitative observation, i.e., *"Are horizontal bands visible and/or specific noise audible?"* the range of flow discharge affected by nappe oscillations was first estimated. For the three configurations investigated in this chapter, the

range of q affected by the nappe oscillations is reported in Table III.1. This table shows that a similar range of q produced nappe oscillations for all configurations. This finding led to a systematic investigation of videos and sound data for q between 0.01 and 0.06 m^2/s whatever the geometric configuration.

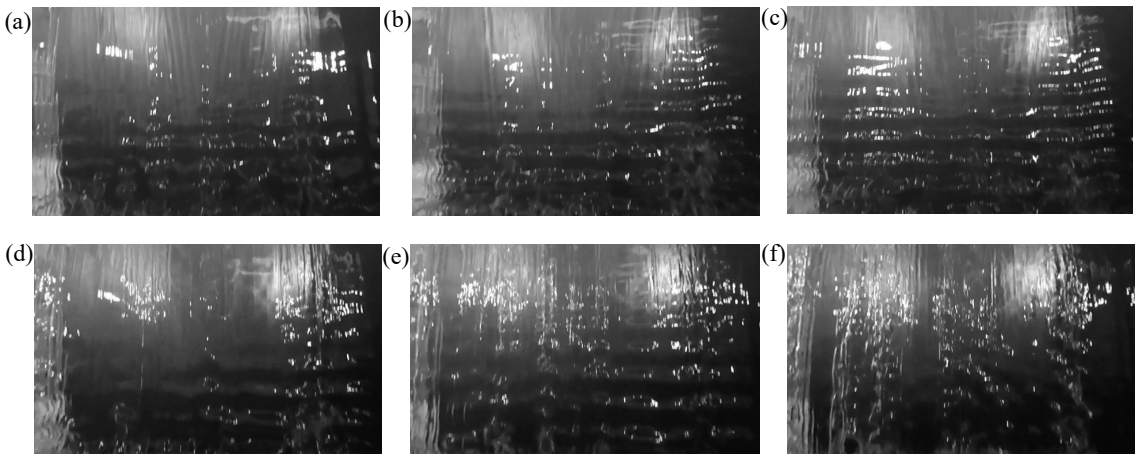

Figure III.1: Nappe snapshots for Configuration $C - QR1 - W1 - L1$: (a) $q = 0.01$ m^2/s, (b) $q = 0.02$ m^2/s, (c) $q = 0.03$ m^2/s, (d) $q = 0.04$ m^2/s, (e) $q = 0.05$ m^2/s and (f) $q = 0.06$ m^2/s

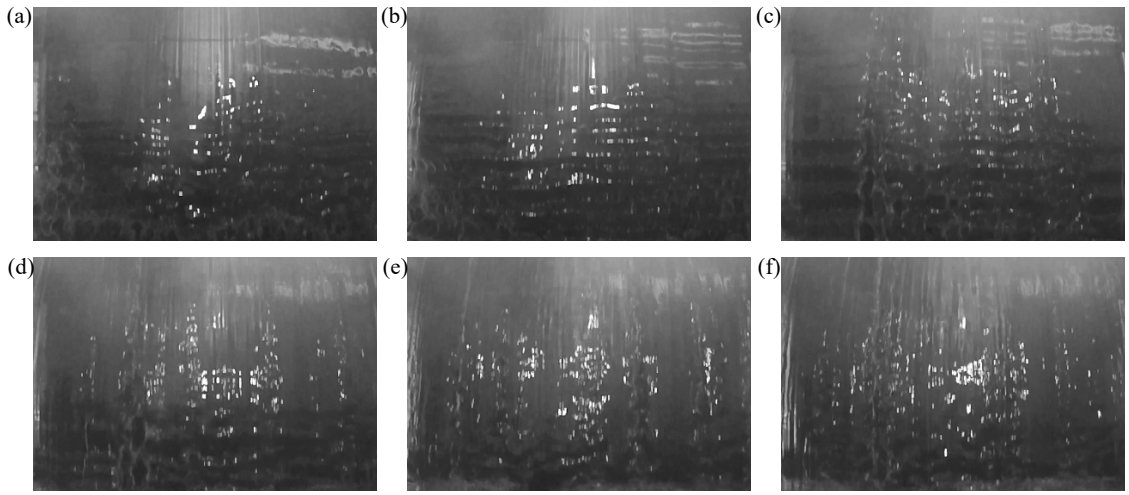

Figure III.2: Nappe snapshots for Configuration $C - THR1 - W1 - L1$: (a) $q = 0.01$ m^2/s, (b) $q = 0.02$ m^2/s, (c) $q = 0.03$ m^2/s, (d) $q = 0.04$ m^2/s, (e) $q = 0.05$ m^2/s and (f) $q = 0.06$ m^2/s

Table III.1: Range of unit discharge affected by nappe oscillations

Configuration	Range of q affected by the oscillations (m^2/s)
$C-QR1-W1-L1$	0.01 - 0.055
$UC-QR1-W1-L1$	0.01 - 0.045
$C-THR1-W1-L1$	0.015 - 0.06

In order to get a reference situation without oscillation, an effective and simple mitigation technique was added to Configuration $C-QR1-W1-L1$. This mitigation technique was a continuous step along the entire width of the weir added at the downstream edge of the crest (details regarding mitigation techniques are developed in Chapter VI). Results gained with this countermeasure are presented in Fig.III.3 and Fig.III.4 by comparison with the same configuration without countermeasure. These figures illustrate the absence of the two nappe oscillations characteristics, namely the horizontal banding and the local peak in the spectrum that refers to an oscillating noise.

Another way to get a configuration without nappe oscillation would have been to remove the baffle wall in the reservoir. Indeed, at the beginning of this research, nappe oscillations were not detected until the addition of synthetic membranes in the reservoir, i.e., two 4-cm thick synthetic horsehair panels, to establish smooth approach flow conditions. This finding whereby nappe oscillations were not observed without uniform smooth flow conditions could support the theory on nappe oscillations origin introduced by Schwartz (1966a) and related to the development of the boundary layer along the crest.

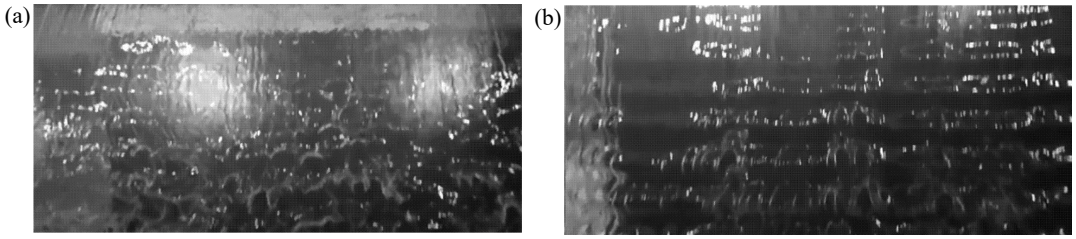

Figure III.3: Nappe snapshot for Configuration $C-QR1-W1-L1$ and q=0.02 m^2/s: (a) with a mitigation technique and (b) without mitigation

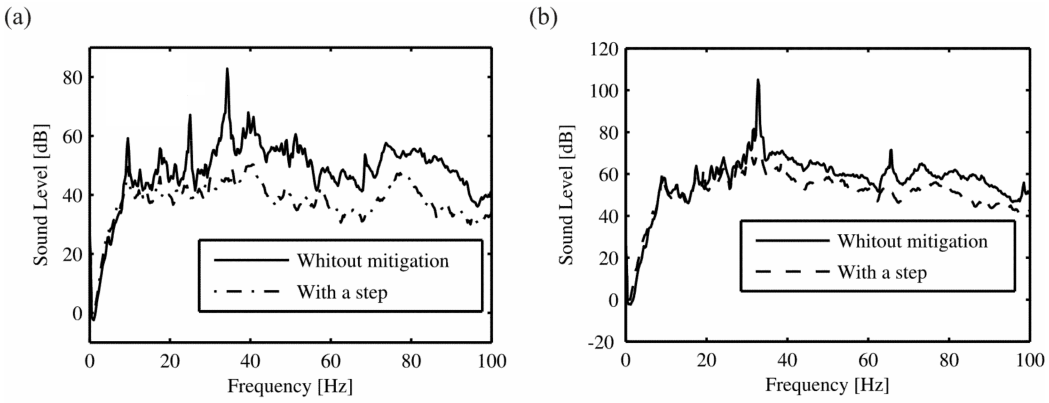

Figure III.4: Spectrum of sound measurements for Configuration $C - QR1 - W1 - L1$ with and without mitigation technique for (a) $q = 0.015$ m^2/s and (b) $q = 0.045$ m^2/s

III.3 Sound analysis

As a first step, the dominant peaks in audio spectra were detected for Configurations $C - QR1 - W1 - L1$, $UC - QR1 - W1 - L1$ and $C - THR1 - W1 - L1$ respectively between 0.01 and 0.055 m^2/s, 0.01 and 0.045 m^2/s and, 0.015 and 0.06 m^2/s which is in agreement with the detection of nappe oscillations using the coupling of a qualitative audible and visual detection.

Second, the intensity of the highest peak in the spectrum was plotted as a function of the unit discharge for Configuration $C - QR1 - W1 - L1$ with and without a mitigation technique in Fig.III.5a. The resulting graph shows, for the configuration experiencing nappe oscillations, a sound level evolution in four successive phases (represented schematically in Fig.III.5b): growing, maximum intensity stabilization, damping and finally a new stabilization phase. The occurrence of nappe oscillations was related to the three first stages which were bounded by the discharges leading to a local dominant peak in the audio spectrum and horizontal bands in flow visualization. In contrast, the sound level for the configuration with a mitigation technique evolved monotonously with the discharge.

The dimensionless intensity, obtained by dividing the intensity by the maximum intensity of the data set (i.e., all data collected from a fixed configuration but with various discharge), is reported in Fig.III.6a for Configurations $C - QR1 - W1 - L1$, $UC - QR1 - W1 - L1$ and $C - QR1 - W1 - L1$. This figure illustrates the same behavior composed of 4 phases for all configurations. However, for Configuration $C - THR1 - W1 - L1$, the damping phase was not marked for all tests and the new stabilization phase was rather a continuous decrease of the sound intensity. Despite these minor differences, the analysis of the intensity evolution, i.e., graph of the intensity or dimensionless intensity as a

function of q, was a good way to determine the flow range affected by the nappe oscillations.

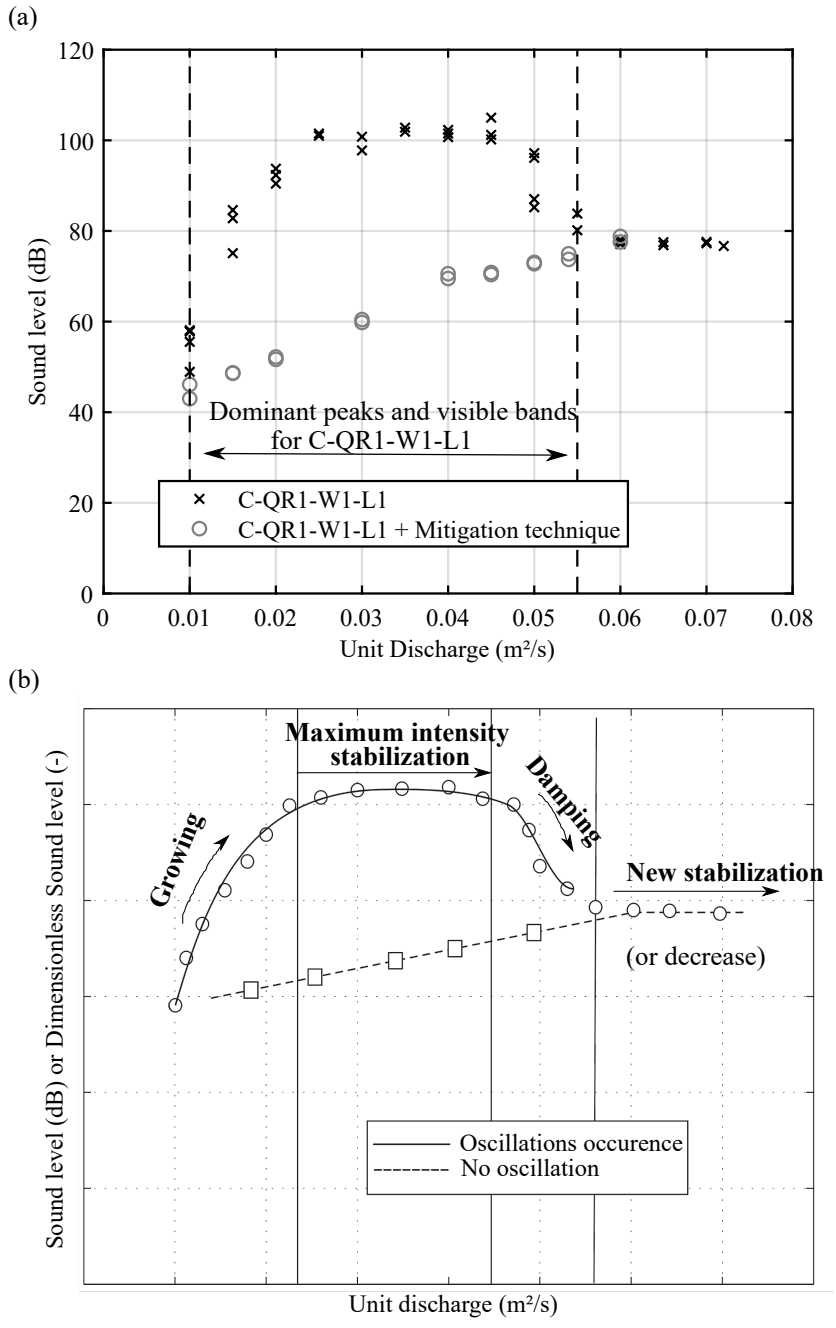

Figure III.5: (a) Results of sound analysis for configurations $C-QR1-W1-L1$ and $C-QR1-W1-L1$ with a mitigation technique (b) Typical evolution of the highest peak intensity in the spectrum as a function of the unit discharge for oscillating and non-oscillating nappes

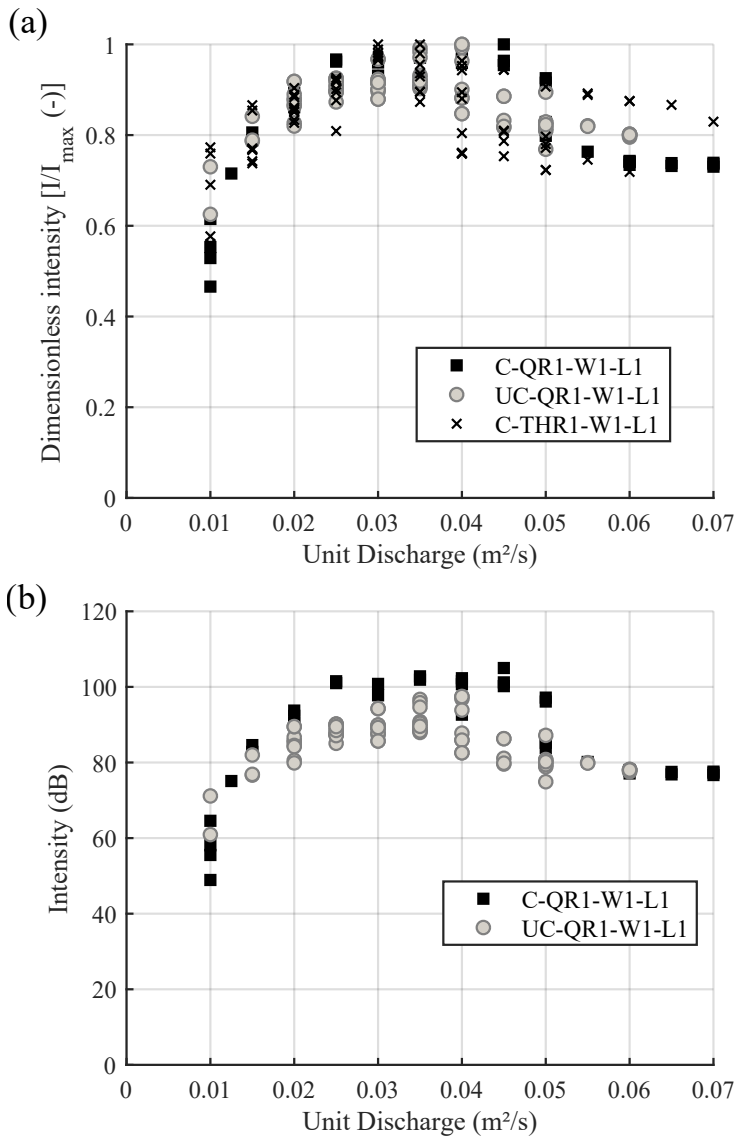

Figure III.6: (a)Dimensionless intensity as a function of the unit discharge for configurations $C-QR1-W1-L1$, $UC-QR1-W1-L1$ and $C-THR1-W1-L1$ (b) Evolution of the dimensional intensity as a function of the unit discharge for configurations $C-QR1-W1-L1$ and $UC-QR1-W1-L1$

The intensity expressed in dB is reported as a function of the unit discharge for Configurations $C-QR1-W1-L1$ and $UC-QR1-W1-L1$ in Fig.III.6b. These intensities may be compared as they result from sound recordings and data processing made from identical conditions. The comparison of the intensity between the confined ($C-QR1-W1-L1$) and the unconfined ($UC-QR1-W1-L1$) configurations shows sound intensities higher in case of confinement.

In addition, for the unconfined model, the data were more scattered than for the confined configuration. Fig.III.6b thus illustrates that the confinement helps in stabilizing the oscillations, but is not a requirement to produce them.

The frequency associated to the maximum of the spectrum was collected and is reported in Fig.III.7 for the three configurations and for the flow range affected. Beyond the flow range affected by nappe oscillations, the sound peak frequency is meaningless as there was no oscillation. Considering the three configurations of this chapter, three different evolutions of the oscillations frequency may be identified.

- For Configuration $C - QR1 - W1 - L1$ (Fig.III.7a), a unique frequency (33 Hz) was recorded for $0.015 \leq q \leq 0.06$ m^2/s. Indeed, the frequency variability (represented by the dashed lines) in the q range affected by the oscillations did not exceed 3.5 Hz, as represented by the dashed lines in Fig.III.7a. This variability was close to the maximum variability of the frequency for a fixed q, i.e., 2.25 Hz for this configuration. In contrast, for $q = 0.01$ m^2/s, the oscillations frequency was more variable and even reached 39 Hz.

- For Configuration $UC - QR1 - W1 - L1$, three distinct frequencies (49.4, 42.9 and 36.4 Hz) were detected as illustrated in Fig.III.7b. The range of q affected by the oscillations was from 0.01 to 0.025 m^2/s, 0.03 to 0.045 m^2/s and 0.025 to 0.04 m^2/s respectively from highest to lowest frequency. Distinct frequencies were therefore detected for a fixed q when repeating measurements. The three frequencies had a constant difference of 6.5 Hz. The variability of these frequencies (represented by the dashed lines) in the q range was of 2.75 Hz for the highest frequency and 2.5 Hz for the others which is similar to the highest variability of frequency measurement for a fixed configuration and q.

- For Configuration $C - THR1 - W1 - L1$, four distinct frequencies were detected (Fig.III.7c): 7.5 Hz between 0.035 and 0.06 m^2/s, 22.5 Hz between 0.015 and 0.035 m^2/s, 31 Hz between 0.015 and 0.05 m^2/s and 41.8 Hz between 0.035 and 0.04 m^2/s. The variability of the frequencies in these ranges was equal or lower than 1 Hz except for the frequency of 31 Hz for which a variability of 4 Hz was observed. As already mentioned for Configuration $UC - QR1 - W1 - L1$, different distinct frequencies were observed for the same q. However, in that case, these frequencies were multiples of the lowest frequency ($\approx$7-8 Hz) and therefore corresponded to harmonics.

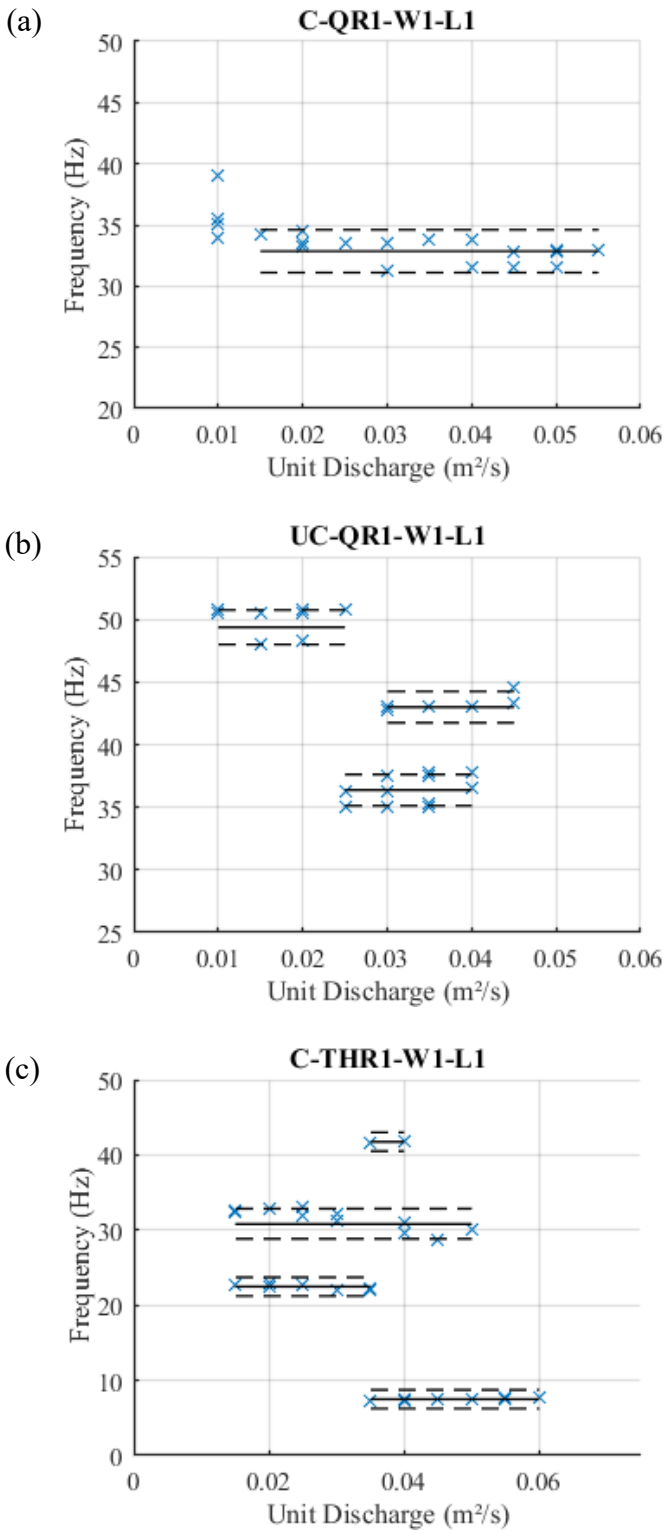

Figure III.7: Sound frequency associated to the maximum intensity of the spectrum for Configurations (a) $C - QR1 - W1 - L1$, (b) $UC - QR1 - W1 - L1$ and (c) $C - THR1 - W1 - L1$. Solid lines are the mean frequency and dashed lines illustrate the variability (from 2.5 to 4 Hz)

Finally, the integral of the audio spectrum was calculated and presented in Fig.III.8 for the three oscillating configurations and the configuration with the mitigation technique. As expected, the integral increased with q as the overall sound level increased with q. In addition, the figure illustrates a clear increase of the spectrum integral in case of nappe oscillations occurrence. To help the comparison between configurations, the calculated integral may be divided by the maximum integral of the configuration for each configuration separately to provide a dimensionless integral. In particular, results collected for Configuration $C-QR1-W1-L1$ with and without the mitigation technique are reported as a function of q in Fig.III.9. This figure is comparable to Fig.III.5a. However, the use of the sound energy did not provide as much information as the intensity. The use of the dimensionless intensity was therefore preferred in the following analyses of this research.

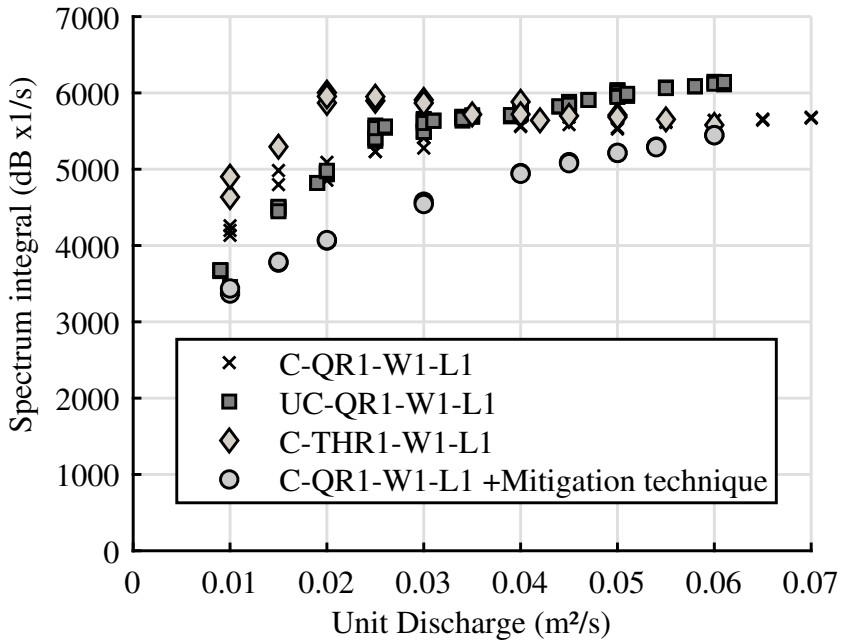

Figure III.8: Integral of sound spectrum for Configurations $C-QR1-W1-L1$, $UC-QR1-W1-L1$, $C-THR1-W1-L1$ and $C-QR1-W1-L1$ with mitigation technique

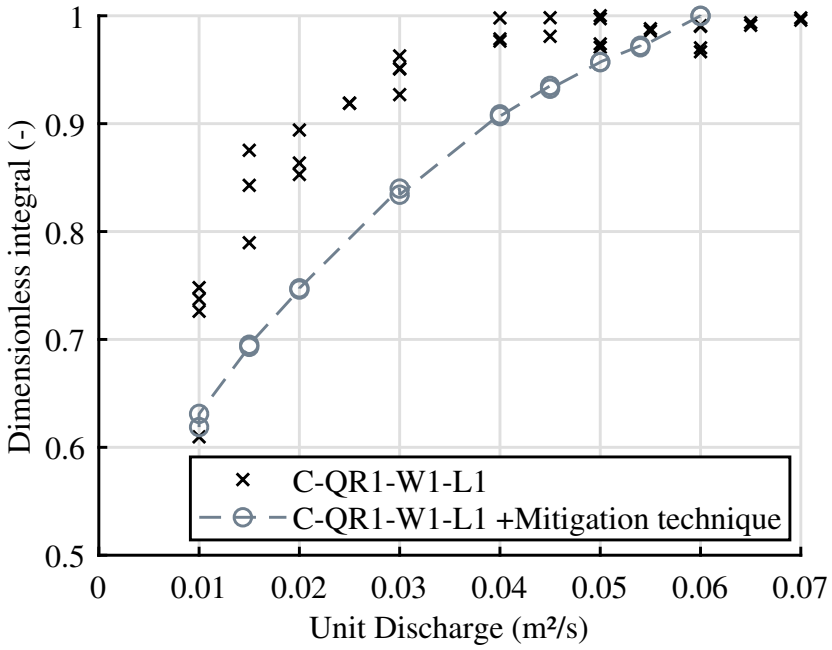

Figure III.9: Evolution of the dimensionless energy of sound with q

III.4 Image analysis

The flow range for which oscillations were visible did not always correspond perfectly to the one defined by acoustic measurements. Indeed, we found that the visual characteristics were more pronounced for low unit discharges while the noise increased for larger unit discharges in the affected flow range. However, the image analysis was applied in the same range as the sound analysis for all configurations.

For Configurations $C-QR1-W1-L1$ and $UC-QR1-W1-L1$, results are presented in Table III.2 as the mean, minimum and maximum frequencies resulting from a minimum of 30 data points (6 lines of pixels for 5 different sets of images) per discharge (except for one discharge). The frequency of the nappe oscillations did not change by more than 2.5 Hz for Configuration $UC-QR1-W1-L1$ and q between 0.025 and 0.04 m^2/s. The mean oscillations frequency was 36.3 Hz in this range while for lower q, between 0.01 and 0.02 m^2/s, it was equal to 50.61 Hz. For Configuration $C-QR1-W1-L1$, the frequency of the oscillations was between 31.25 and 34 Hz for q varying between 0.015 and 0.045 m^2/s. In contrast a frequency of 39 Hz was observed for a unit discharge of 0.01 m^2/s.

Table III.2: Frequencies from the image analysis for Configurations $UC-QR1-W1-L1$ and $C-QR1-W1-L1$ Line of 300 pixels, 6 lines per frame, a minimum of 0.25 Hz Fast Fourier Transform resolution and a minimum of 5 image sets were used, excepted for the confined model and a unit discharge of 0.025 m/s (in grey) only 2 different sets of images were used

$UC-QR1-W1-L1$					$C-QR1-W1-L1$				
q (m^2/s)	Frequency (Hz)			Number of data	q (m^2/s)	Frequency (Hz)			Number of data
	Mean	Max.	Min.			Mean	Max.	Min.	
0.01	50.76	50.8	50.75	36	0.01	39.12	39.25	39	30
0.015	50.52	50.6	50.49	42	0.015	34.25	34.27	34.25	30
0.02	50.56	50.65	50.5	48	0.02	34.46	34.5	34.38	36
0.025	36.24	36.25	36.2	54	0.025	33.56	33.63	33.5	12
0.03	36.27	36.3	36.25	30	0.03	31.25	31.27	31.24	30
0.035	35.10	35.25	35	30	0.035	33.68	33.75	33.6	30
0.04	35.42	36	35	36	0.04	31.5	31.5	31.5	30
0.045	37.46	41.75	37.7	42	0.045	31.52	31.6	31.5	30

For Configuration $C-THR1-W1-L1$, the frequencies of the horizontal bands are reported in Fig.III.10 for each tested q between 0.015 and 0.06 m^2/s. Contrary to the two others configurations, various frequencies are provided by the image analysis, for the same discharge. In addition, despite disordered horizontal waves for q higher than 0.04 m^2/s, a frequency pattern of 7.25-8 Hz was noted. For q lower than 0.03 m^2/s, two particular frequencies, i.e., 22.3±0.5 Hz and 32.55±0.65 Hz, were detected. These particular frequencies seemed to be harmonics of the small frequency (≈7.25-8 Hz) observed for the higher q. For q between 0.035 and 0.045 m^2/s various harmonics were also detected by the image analysis.

In the same way as exposed by the sound analysis, the three configurations exemplify different behaviors regarding the frequency variation as a function of q. For Configuration $C-QR1-W1-L1$, a unique frequency (mean value of 32.9 Hz) is observed on the entire q range (excluding the smallest q) while two distinct frequencies (mean value of 36 Hz and 50.6 Hz) were detected for Configuration $UC-QR1-W1-L1$ and 6 frequencies, i.e, ≈7.25-8 Hz and harmonics were recorded for Configuration $C-THR1-W1-L1$.

Finally, the hyposthesis according to which a camera acquisition frequency of 240 or 300 Hz is enough to capture nappe oscillations, is thus satisfied as the frequencies do not exceed 51 Hz for the three configurations tested in this chapter.

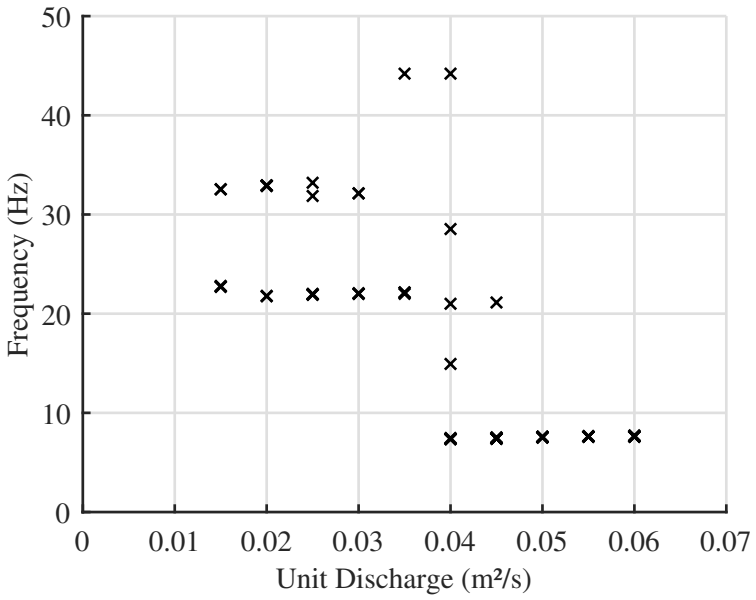

Figure III.10: Frequencies from the image analysis for Configuration $C-THR1-W1-L1$

III.5 Comparison of the characterization parameters

The sound analysis and the image analysis being two independent procedures, the results extracted from these methods were compared. First of all, for the three configurations considered in this chapter, both analyses detected the dominant frequency of oscillations in a similar flow range. Second, the frequencies extracted by the different methods are compared in Fig.III.11 for the three configurations. For each configuration, this figure shows that both methodologies provided globally the same oscillations frequency. However, this figure also shows that image analysis did not provide all the distinct frequencies found by sound analysis for Configuration $UC-QR1-W1-L1$. In contrast, for Configuration $C-THR1-W1-L1$, image analysis provided a frequency of 14 Hz which was not supplied by the sound.

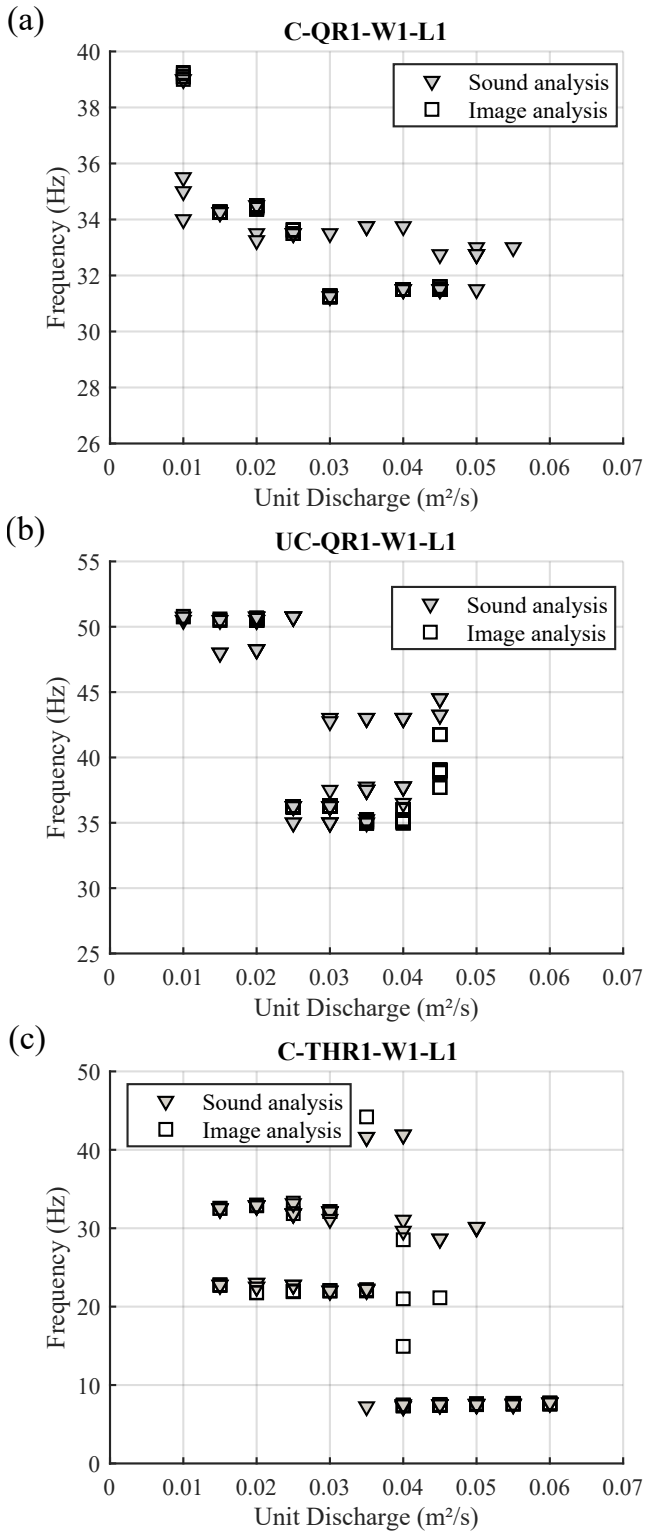

Figure III.11: Comparison of frequencies extracted from sound and image analyses, Configurations (a) $C-QR1-W1-L1$, (b) $UC-QR1-W1-L1$ and (c) $C-THR1-W1-L1$

Another comparison of the oscillations frequency collected by sound and image analyses is also presented in Fig.III.12. This figure only compares, for a fixed q, the same level of frequency in particular for Configurations $UC-QR1-W1-L1$ and $C-THR1-W1-L1$. Fig.III.12 shows that sound and image analyses provide for a fixed q, oscillations frequencies that are similar to a 2.5 Hz variability (dashed lines). Finally, based on this frequency similarity for identical tested configurations and q, a link between the visible nappe oscillations and the associated noise is obvious and suggests that the sound is generated by the oscillations action on the surrounding air and not by the impact of the nappe on the ground. This was also verified by modifying the rigidity of the impact apron as exposed in Chapter II.

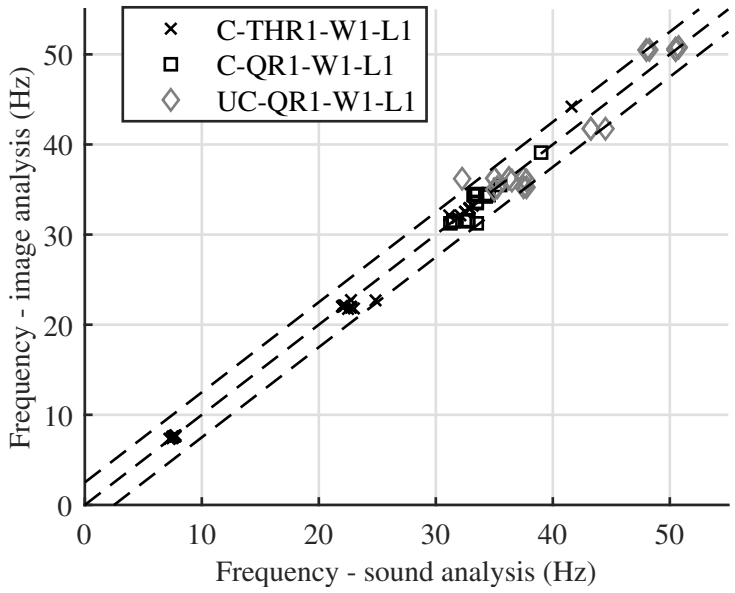

Figure III.12: Comparison of sound and image analyses for the three configurations

As part of the comparison of the characteristic parameters between the three tested configurations, the effect of the confinement, pointed out in the sound analysis regarding its effect on the sound level intensity, may be mentioned. Indeed, the comparison between the confined ($C-QR1-W1-L1$) and the unconfined ($UC-QR1-W1-L1$) weir showed that the confinement helped in stabilizing the noise production as the intensities are higher for the confined configuration. In addition, the frequencies measured, both by sound and image analyses, showed more variability for the unconfined model. Three distinct frequencies were detected in the q range affected by the oscillations in case of unconfined weir while only one frequency was observed for the confined model. This finding is in agreement with the theory suggesting that the air entrapped

behind the nappe may amplify the oscillations but is not required to initiate the instability.

Then, the comparison between Configurations $C-QR1-W1-L1$ and $C-THR1-W1-L1$, shows that the profile of the crest affects the occurrence of the oscillations and their characteristics. Indeed, the flow range and the oscillations frequencies were different. In addition, the existence of harmonics was observed for the THR crest profile while it was not observed for the other profile. Finally, despite some geometric differences between the configurations, nappe oscillations appeared in the same range of q, i.e., 0.01-0.06 m^2/s.

III.6 Hydraulic parameters

As exposed in Chapter II, the discharge Q (in m^3/s) was the only parameter controlled by the experimenter through the opening or closing of valves. Knowing the width of the weir, the unit discharge q was thus known.

In parallel to the oscillation characteristic measurements developed above, the upstream water depth as well as the water depth at the detachment point were also measured for both crest profiles considered in this chapter. These measurements were performed for Configurations $C-QR1-W1-L1$ and $C-THR1-W1-L1$ but may be extended for a similar crest profile to all configurations varying in terms of width, fall height and confinement.

The evolution of the water depths as a function of the unit discharge is reported in Fig.III.13 for the QR and THR crest profiles (prototype scale model). For the upstream water levels, the reference ($h=0$) was imposed as the top of the crest. The upstream water depths reported in Fig.III.13 correspond thus to water depths measured positively over this reference point. For the water level at the nappe detachment point, the point gauge allowed to measure vertically the nappe thickness. In that case, the reference was the crest level (at the detachment). In the case of THR crest profile, this measurement was thus projected according to the angle of the weir crest at the downstream end, i.e., 45° with horizontal, to define the water depth. The water level at the crest detachment point is thus the water thickness perpendicular to the bottom at the crest detachment point.

Based on the water level measurements (Fig.III.13), the Head-Discharge curve that links the discharge and the upstream head was defined for both crests in the following format :

$$q = C_d\sqrt{2gH^3}$$

with H the upstream head calculated as follows:

$$H = h + \frac{u^2}{2g}$$

with $u = \frac{q}{(h+z)}$the velocity, h the upstream water depth in the reservoir measured relative to the weir crest elevation and z the weir height.

At the crest detachment point, a similar relation $\left(q = K\sqrt{2gH^3}\right)$ between the discharge q and the head at the detachment point may be calculated considering in that case the water level at the crest detachment point and $z = 0$. The values of the C_d and K coefficients are reported for both crest profiles in Table III.3.

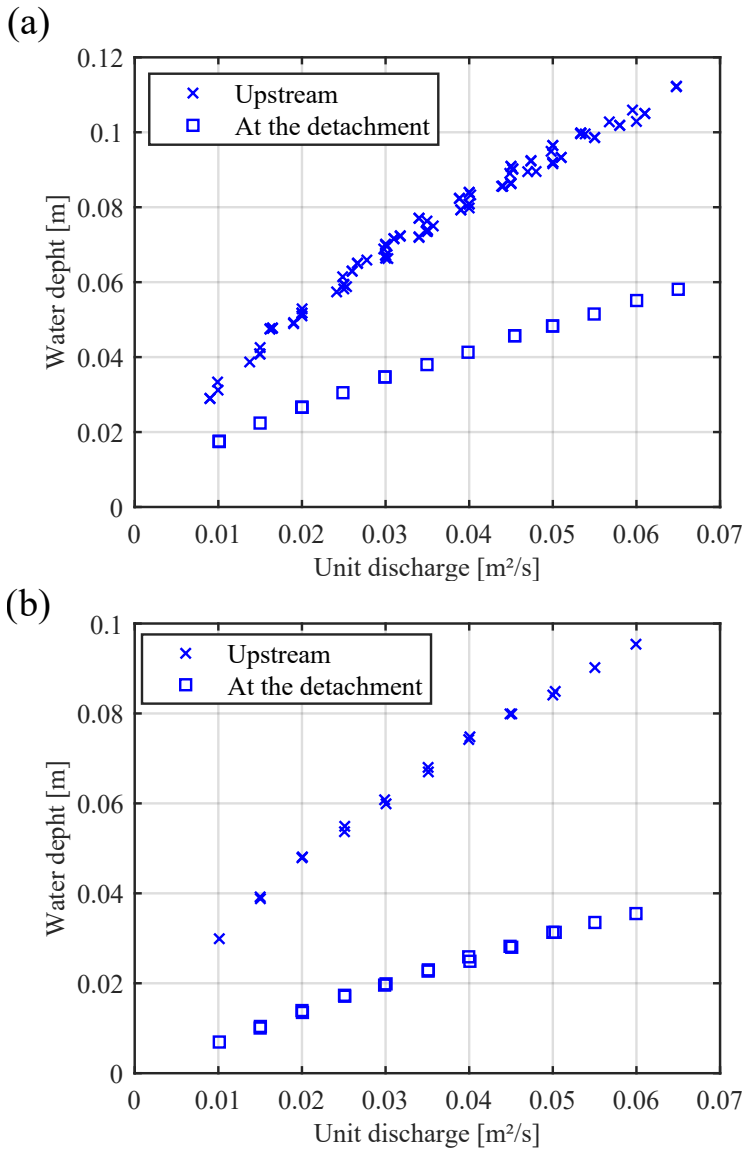

Figure III.13: Evolution of the water depths with the unit discharge (a) for the QR crest profile and (b) the THR crest profile

Table III.3: Coefficients of the Head – Discharge curves

	QR	THR
Upstream	0.3998	0.4515
At the detachment	0.3439	0.2848

During the measurements, no water level fluctuation (higher than the measurement accuracy, i.e., 1 mm) was observed in the case of occurrence (and also non-occurrence) of nappe oscillations.

Finally, for Configuration $C-QR1-W1-L1$, water pressure was measured along the crest (details of these measurements are also presented in Appendix A). These measurements showed that a positive pressure existed along the crest and no pressure fluctuation higher than 0.1 Pa was observed along the QR crest profile in case of nappe oscillations. The positive pressure profile, close to hydrostatic pressure along the crest, supports the existence of a pressure discontinuity at the crest extremity which is perceived by Chanson (1996) as part of the initiating event of the nappe oscillations phenomenon.

For the other crest profiles tested in the framework of this thesis, the hydraulic characteristics are reported in Appendix A.

III.7 Conclusions

The aim of this chapter was the characterization of nappe oscillations. This has been done through the interpretation of quantitative data collected from sound and image recording analyses for three particular configurations on the large scale model (Model 1).

First, the discharge range for the occurrence of nappe oscillations was investigated based on qualitative observations. Then, based on sound and image analyses exposed in Chapter II, the flow range affected by nappe oscillations and the associated frequencies were carefully assessed.

A typical sound intensity behavior was identified as a function of q in case of nappe oscillations. It is composed of 4 successive phases (a growing, a stabilization, a damping and a new stabilization) while in absence of nappe oscillations, it has been verified that the evolution of the sound intensity with q was continuous. Then, the comparison of frequencies collected simultaneously by sound and image analyses shows an adequacy for identical configurations and q. In addition, the analyses applied for three slightly different configurations, either by the confinement of the crest shape, pointed out the influence of the crest geometry configuration on the main oscillations characteristic, i.e., its frequency, while the discharge range is poorly affected.

To conclude, both methods applied in this chapter proved their capability to characterize the nappe oscillations phenomenon in terms of affected q range,

sound intensity and frequency and can be extended to other facilities. In particular, their application to the small scale model and to the other configurations of the prototype scale model, respectively with the aim of deepening the knowledge of the nappe oscillations scaling and studying the influence of geometric parameters, are exposed and discussed respectively in Chapters IV and V. The application of these techniques to case studies is proposed in Chapter VII.

Chapter IV

Nappe oscillations on scale model and size scale effects

This Chapter is based on the following article:

Lodomez, M., Tullis, B., Dewals, B., Archambeau, P., Pirotton, M., Erpicum, S., 2019. Nappe oscillation on free-overfall structures : Size scale effects. Journal of Hydraulic Engineering 145(6), 040119022.

IV.1 Introduction

This chapter focuses on the analysis of the size scale effects affecting the nappe oscillations phenomenon. To that end, the prototype scale model, Model 1 and its geometrically similar laboratory-scale facility with a geometric scale factor of 3 regarding the fall height and the crest profile, Model 2 (Section II.2) were used. In particular, Configurations $C-QR1-W1-L1$ and $C-THR1-W1-L1$ and their equivalent on scale model (Model 2), i.e., Configurations $C-QR2-W5-L5$ and $C-THR2-W5-L5$ were assessed and compared. The geometric parameters of these configurations are reported in Table II.1. Out of the four configurations evaluated in this chapter, two (for Model 1) have been analyzed in detail in Chapter III. For the other two, the methodologies of sound and image analyses explained in Chapter II and exemplified in Chapter III were used to first assess the presence of nappe oscillations and if so, to define the flow range affected by the oscillations and their associated frequencies. The frequencies collected from image and sound analyses being identical as shown in Chapter III, nappe oscillations frequencies are quantified without distinction between both detection methods. Section IV.2 presents the results collected from scale model (Model 2) operation while Section IV.3 discusses the impact of the model size by comparing the results gained for Models 1 and 2.

IV.2 Nappe oscillations on small scale model

IV.2.1 Quarter round crest profile

According to Froude similarity, the flow range leading to nappe oscillations for the prototype scale model, i.e., Configuration $C-QR1-W1-L1$ [0.01-0.055 m^2/s (Fig.IV.1a)] would correspond to 0.002-0.011 m^2/s on the small scale model, i.e., Configuration $C-QR2-W5-L5$. However, for these discharges, nappe oscillations were not detected. In contrast, nappes tend to break up at such lower discharges and exhibit thus a completely different behavior. This behavior is in agreement with the literature as the break-up length is lower than the fall height (1 m) for $q < 0.004$ m^2/s according to Horeni's formula (Castillo et al., 2014; Ervine et al., 1997). However, nappe oscillations were observed between 0.015 and 0.06 m^2/s, while the flow range that generated high noise disturbance was limited between 0.015 and 0.03 m^2/s as illustrated in Fig.IV.1a by the dimensionless sound intensity plotted as a function of q. For higher discharges, a continuous decrease of the sound intensity was observed.

In parallel, Fig.IV.2 illustrates the horizontal bands that characterize the nappe oscillations, in particular between 0.015 and 0.04 m^2/s. For higher discharges, these horizontal bands were visible at the crest but seemed to vanish during the fall. Based on sound and image analyses, frequencies varying from

48.85 to 36.5 Hz for q lower than 0.03 m^2/s were detected. For a higher q, several frequencies coexisted at the same time as shown by the audio spectrum in Fig.IV.3. These frequencies were equal to 34.25, 36.5, 38.85, 41.3 and 42.85 Hz for $q = 0.04$ m^2/s (Fig.IV.1b).

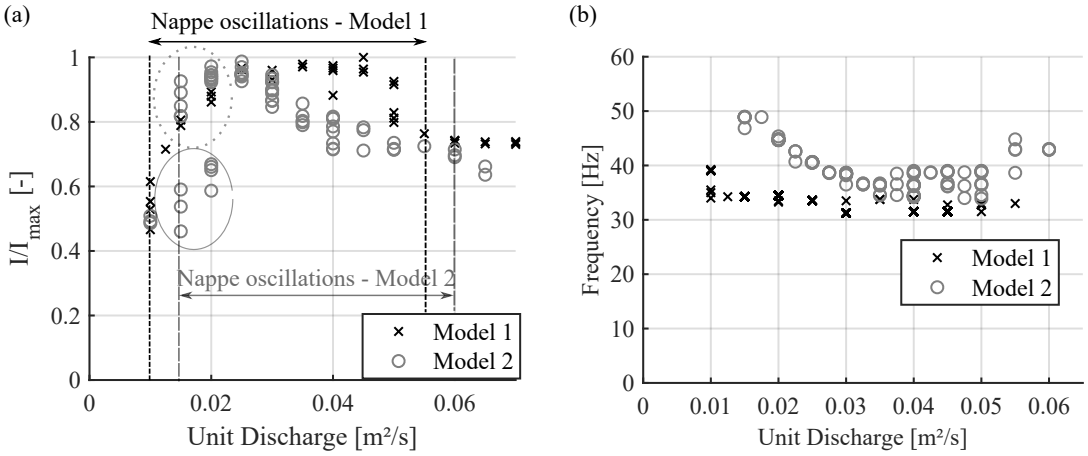

Figure IV.1: (a) Results of sound analysis for the QR crest profiles. Hysteretic behavior for the scale model illustrated by oscillating data (doted circle) and no oscillating data (plain circle) and (b) Frequencies of nappe oscillations

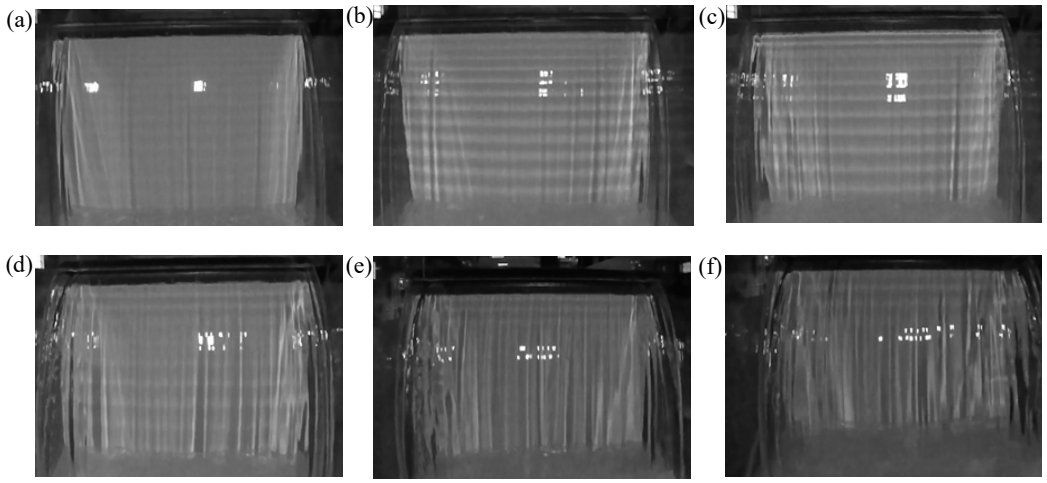

Figure IV.2: Nappe characteristics for Configuration $C - QR2 - W5 - L5$: (a) $q = 0.015$ m^2/s, (b) $q = 0.02$ m^2/s, (c) $q = 0.03$ m^2/s, (d) $q = 0.04$ m^2/s, (e) $q = 0.05$ m^2/s and (f) $q = 0.06$ m^2/s

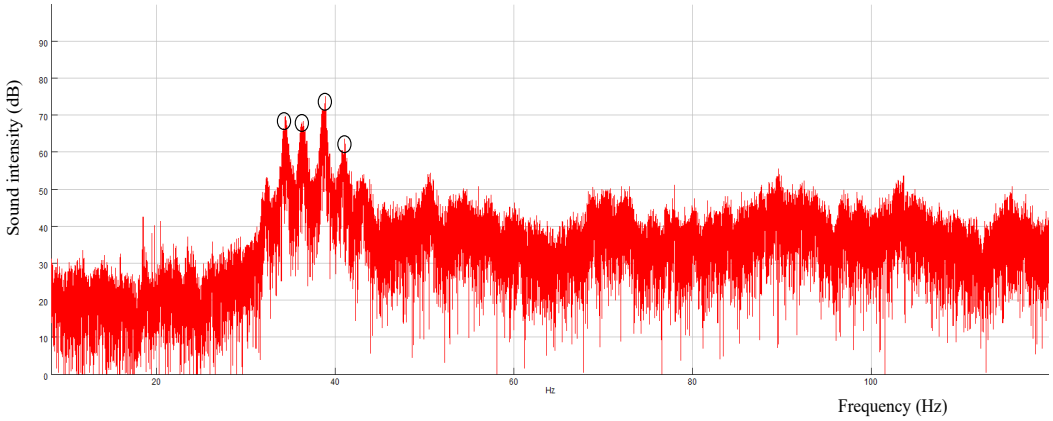

Figure IV.3: Audio spectrum for Configuration $C - QR2 - W5 - L5$ and $q = 0.04$ m^2/s

In addition, a hysteretic behavior was observed for q smaller than 0.02 m^2/s (Fig.IV.1a). For an increasing discharges variation, the oscillating nappes experienced intermittent periods of nappe stability. Oscillating periods lasting approximately 20 to 50 seconds were observed approximately every 5 minutes. In contrast, for a decreasing discharge from an oscillating unit discharge, i.e., for q decreasing from $q = 0.06$ m^2/s to $q = 0.01$ m^2/s, oscillations remained and were temporally constant.

IV.2.2 Truncated half round crest profile

In the same way as for the QR profile, no oscillation was observed in Configuration $C - THR2 - W5 - L5$ for the scaled q range of the prototype scale configuration (Fig.IV.4a), i.e., between 0.003 and 0.012 m^2/s. Nonetheless, nappe oscillations were detected, in Configuration $C - THR2 - W5 - L5$, between 0.015 and 0.05 m^2/s. High levels of sound intensity were recorded between 0.015 and 0.03 m^2/s with a maximum intensity for $q = 0.03$ m^2/s (Fig.IV.4a). Then, for $q > 0.03$ m^2/s, a continuous decrease of the intensity was observed. In parallel, Fig.IV.5 illustrates the horizontal bands that characterized the nappe oscillations in particular between 0.02 and 0.04 m^2/s and their disappearance for $q > 0.05$ m^2/s. The frequencies of the nappe oscillations varied from 58.75 to 37.65 Hz based on sound and image analyses. The highest frequencies were observed between 0.015 and 0.03 m^2/s with a decrease in that range from 58.75 to 44.15 Hz (Fig.IV.4b). Then for higher q, a stabilization of the frequency was observed with frequencies varying from 44.15 to 37.65 Hz.

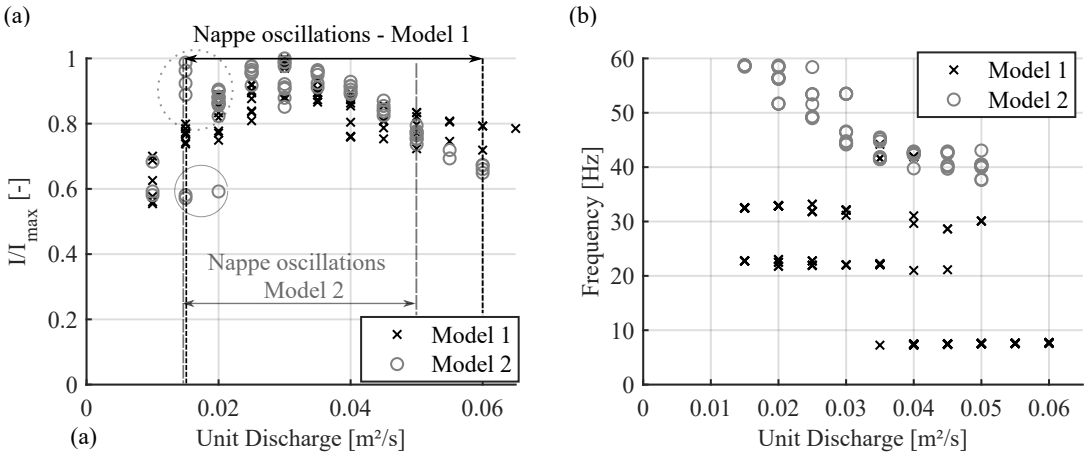

Figure IV.4: (a) Results of sound analysis for the THR crest profiles. Hysteretic behavior for the scale model illustrated by oscillating data (doted circle) and no oscillating data (plain circle) and (b) Frequencies of nappe oscillations

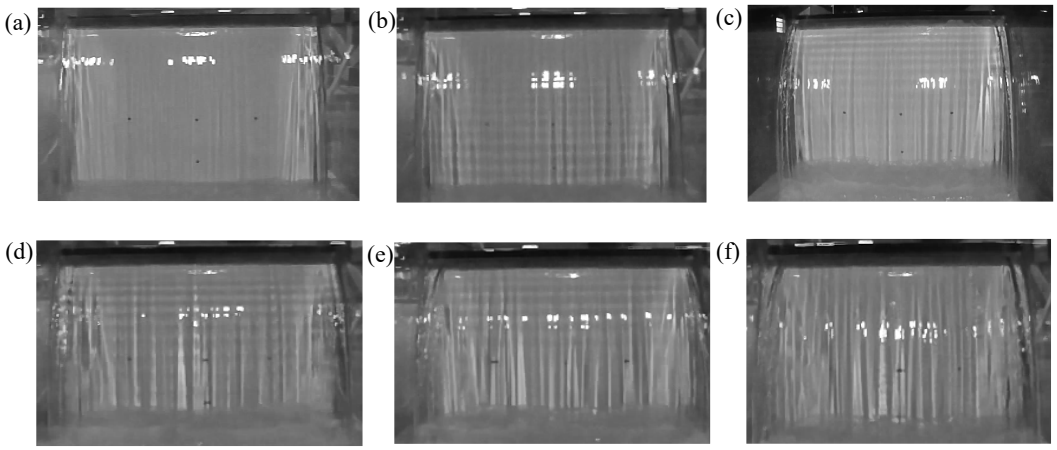

Figure IV.5: Nappe characteristics for Configuration $C - THR2 - W5 - L5$: (a) $q = 0.01$ m^2/s, (b) $q = 0.02$ m^2/s, (c) $q = 0.03$ m^2/s, (d) $q = 0.04$ m^2/s, (e) $q = 0.05$ m^2/s and (f) $q = 0.06$ m^2/s

For $q = 0.015$ m^2/s and $q = 0.02$ m^2/s, nappe oscillations showed a hysteretic behavior. With these conditions, nappe oscillations occurrence was dependent upon the unit discharge prior to changing the flow. In addition, some temporal variability was observed for this configuration as illustrated in Fig.IV.6 based on the air pressure (sound) measurement.

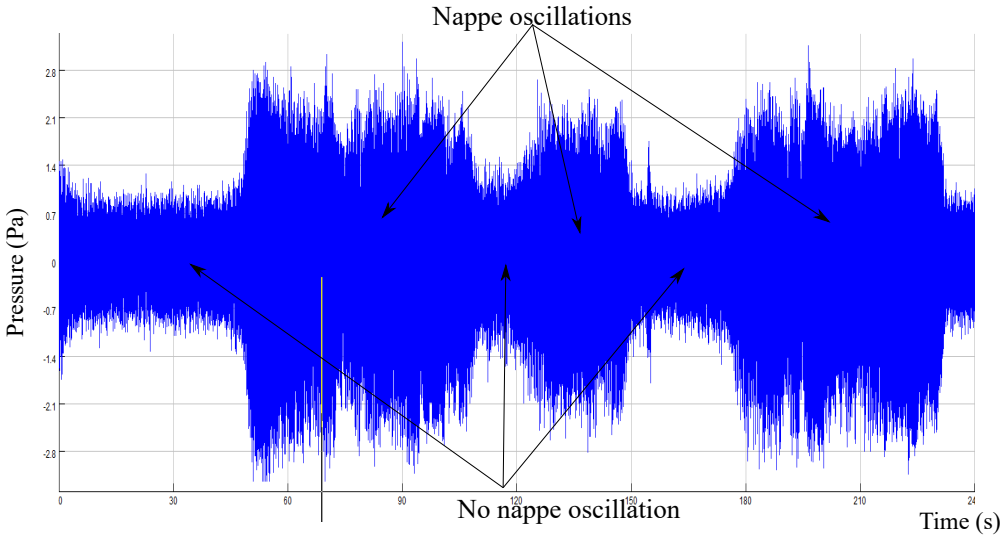

Figure IV.6: Time evolution of the air pressure signal (sound) for Configuration $C - THR2 - W5 - L5$ and $q = 0.03$ m^2/s. Alternation of oscillating and non-oscillating behavior along time

IV.3 Discussion

The first key finding of this chapter is that nappe oscillations always appeared in the same range of unit discharge independent of size scale. The occurrence of nappe oscillations was indeed observed, for both facilities and crest shapes, between 0.015 and 0.05 m^2/s approximately as reported for both models in Fig.IV.1 and Fig.IV.4. This suggests that the nappe oscillations phenomenon cannot be scaled according to Froude similitude and is thus not driven solely by gravity and inertia.

Within this flow range, oscillations characteristics were slightly affected by the model scale. In particular, the sound intensity evolution as a function of q varied. For the tests with a QR crest profile, a clear decrease in sound intensity was observed for $q > 0.045$ m^2/s in the larger model (Model 1), while a more gradual decrease was observed for the smaller model (Model 2). For the THR crest profile, Model 1 produced a slight damping of the sound intensity between 0.03 and 0.04 m^2/s and then reached a stabilized sound level for $q > 0.04$ m^2/s; Model 2 produced continuously decreasing sound levels for $q > 0.03$ m^2/s. The frequencies of the nappe oscillations also varied with the model size. For a QR crest profile, Models 1 and 2 frequencies varied for $q < 0.03$ m^2/s and became similar for $q > 0.03$ m^2/s. For the THR, Models 1 and 2 frequencies were completely different except for three tests at $q = 0.035$ m^2/s and $q = 0.04$ m^2/s.

The second observation concerns the variability of the nappe oscillations and

their frequencies. The smaller model (Model 2) results showed substantially more variation in the nappe oscillations characteristics than the larger model (Model 1). Specifically, nappe oscillations with the smaller model were more inclined to exhibit temporal fluctuations: periodically, the nappe oscillations stopped for a short period of time and then started again. With the larger model, nappe oscillations were temporally stable. Another variability was related to the frequencies of these oscillations and the coexistence of various frequencies at the same time.

Finally, hysteresis was observed with respect to nappe oscillations in the smaller model, while no hysteresis was observed in the larger model. These findings are in agreement with the first investigations on nappe oscillations scaling in Anderson and Tullis (2018).

IV.4 Conclusions

The experimental tests depicted in this chapter investigated the possible size scale effects on nappe oscillations. The nappe oscillations occurrence assessment and frequency evaluation were performed using sound and image analyses for both experimental facilities depicted in Chapter II, i.e., a prototype-scale linear weir (fall height of 3 m) and a scale model (1/3) of the same weir (fall height of 1 m). Experiments showed that nappe oscillations cannot be scaled according to the traditional similitude for free overfall structures, i.e., Froude similitude. Indeed, the nappe oscillations always appeared in the same unit discharge, i.e., 0.015 - 0.05 m^2/s, independently of the weir size scale and test facility.

This research also indicated that the nappe oscillations development and their characteristics (intensity and frequencies) are affected by the dimension of the model, i.e., the fall height and the crest profile. In addition, the variability of the frequencies and the coexistence of various frequencies at the same time were highlighted in case of scale model. A hysteretic behavior and a variability of the oscillations in time were also observed for the scale model.

Chapter V

Occurrence and frequencies of oscillations

V.1 Introduction

Based on the literature review and the characterization of nappe oscillations presented in Chapter III and IV, it appears that the phenomenon depends on both hydraulic and geometric parameters. In particular, the occurrence of the oscillations, their development and their characteristic frequency are related to the discharge or the upstream head, the geometric parameters of the weir, i.e. the crest shape, the width and the fall height, and finally the confinement of the nappe (as shown in Chapter III).

In the framework of this research, thanks to the experimental model's flexibility, varied geometric parameters have been tested in a large range as reported in the Table II.1. The results of the 52 configurations are analyzed in this chapter in order to assess and if possible identify the parameters influence on nappe oscillations occurrence (Section V.2) and characteristic frequencies (Section V.3).

V.2 Occurrence of nappe oscillations

V.2.1 Main findings

For all tested configurations presented in Table II.1, the occurrence of nappe oscillations has been assessed according to the methodologies detailed in Chapter II. The results are presented in Table V.1 in terms of discharge range affected by oscillations and associated frequency range. Evidences of the oscillations occurrence in terms of sound intensity evolution as well as flow visualization are reported in Appendix B.

As already mentioned in Chapter III, the range of q affected by the oscillations phenomenon is always between ~ 0.01 and 0.06 $\mathrm{m^2/s}$. Consistently with what is usually reported in literature, this corresponds to a low upstream head within a range of 3 to 12 cm for the tested crest profiles. Despite the fact that this range may be reduced depending on some geometric parameters, it is independent of the weir scale and the test facility. In addition, it should be noted that nappe oscillations are not "on/off" phenomenon but is more gradual as observed from the disappearance of the oscillations with increasing discharges (damping phase in the evolution of the sound intensity and progressive disappearance of the horizontal bands).

The results presented in Table V.1 show that nappe oscillations occurrence and the associated frequencies depend on the crest profile. For instance, for a fall height of 3 m ($L1$) and a width of 3.45 m ($W1$), nappe oscillations were detected for QR and THR crest profiles ($C-QR1-W1-L1$ and $C-THR1-W1-L1$) but not for a HR crest profile ($C-HR1-W1-L1$). The crest profile is thus a key parameter in the nappe oscillations occurrence. In the same way, for Model 2 and an identical fall height and width ($L5-W5$), the modification of the crest

profile influenced the occurrence of the nappe oscillations. Nappe oscillations were never observed in the case of a rectangular (R) crest while they appeared for the rounded rectangular (RR) crest as well as the QR and THR crest profiles. These findings may be linked to two distinct theories regarding the nappe oscillations mechanism. First, depending of the crest profile, the detachment of the nappe from the crest can be imposed by the geometry (QR, THR, RR, R crest profiles), this generates a pressure discontinuity and favors the oscillations according to Chanson (1996). In contrast, in case of a HR crest, the detachment point of the nappe occurs without sudden pressure transition and also varies along the weir width and with the discharge. The location of the detachment in that case refers to the position where the atmospheric/zero pressure is reached which generates the detachment from the crest. There is thus no sharp pressure discontinuity for this configuration and hence no nappe oscillation. These considerations can explain oscillations observed for the crests QR, THR and RR but not the ones observed for the HR crest.

Secondly , the upstream part of the crest profile also influences the appearance of the oscillations. Indeed, it controls the way the flow reaches the crest and thus the flow conditions along the crest (Schwartz, 1966b). For the rectangular crest (R), where the upstream face looks like a sharp direction change, no nappe oscillation was observed and the flow was disordered. In contrast, when a rounded upstream edge has been added to the rectangular profile (RR), nappe oscillations were observed.

For a given crest profile, the weir width and the fall height affect the occurrence or absence of oscillations. This will be discussed in Section V.2.2.2.

Finally, in the 52 configurations tested during this research study, 19 were with an unconfined nappe. Nappe oscillations were detected for 9 out of these 19 configurations. This confirms that the confinement is not a prerequisite for the oscillations, as already reported by Anderson and Tullis (2018); Binnie (1972); Crookston et al. (2014); Sato et al. (2007). However, the detailed analysis of Configurations $UC - QR1 - W1 - L1$ and $C - QR1 - W1$–L1 in Chapter III proved that the non-confinement of the nappe slightly reduces the range of discharge affected by oscillations and modifies the associated frequencies. In addition, an aeration of the small scale model (Model 2), modified the nappe oscillations development. In particular, the aeration of the nappe stopped nappe oscillations for all unit discharges. The confinement plays thus a significant role in this specific case of small width and fall height. Based on these two contradictory findings, it can be concluded that the confinement is not the unique cause that generates nappe oscillations but is an integral part of the complex mechanism.

Table V.1: Occurrence of nappe oscillations, related discharge range and associated frequencies extreme depending on geometric configuration

	Abbreviation	Range of q affected by the oscillations (m^2/s)	Extreme frequencies (Hz)
Model 1	$C-QR1-W1-L1$	0.01-0.055	31.3;39.1
	$C-THR1-W1-L1$	0.015-0.06	7.4;44.2
	$C-THR1-W1-L2$	0.01-0.045	6;44.4
	$C-THR1-W1-L3$	0.01-0.035	7.3;36.6
	$C-THR1-W1-L4$	0.01-0.025	11;28.9
	$C-THR1-W1-L5$	0.015-0.06	17.4;20.9
	$C-THR1-W2-L1$	0.015-0.035	8.9;23.2
	$C-THR1-W2-L2$	0.01-0.035	18;33.3
	$C-THR1-W2-L3$	0.01-0.02	7.4;33.2
	$C-THR1-W2-L4$	No nappe oscillation	/
	$C-THR1-W3-L1$	0.015-0.035	10;24.6
	$C-THR1-W3-L2$	0.01-0.035	9.4;31
	$C-THR1-W3-L3$	0.01-0.02	14.8;16.9
	$C-THR1-W3-L4$	No nappe oscillation	/
	$C-THR1-W4-L1$	0.015-0.03	16;24.8
	$C-THR1-W4-L2$	0.01-0.035	13.2;15.5
	$C-THR1-W4-L3$	0.01-0.0175	18.1;60.5
	$C-THR1-W4-L4$	No nappe oscillation	/
	$C-THR1-W6-L1$	0.015-0.02	22.8;23
	$C-THR1-W6-L2$	0.01-0.035	20.9;23.3
	$C-THR1-W6-L3$	0.01-0.015	14.6;44.5
	$C-THR1-W6-L4$	No nappe oscillation	/
	$C-HR1-W1-L1$	No nappe oscillation	/
	$C-HR1-W1-L5$	0.01-0.045	20.5;51.2
	$C-HR1-W1-L7$	0.01-0.04	34.5;41.3
	$UC-QR1-W1-L1$	0.01-0.045	32.3;50.8
	$UC-QR1-W1-L2$	0.01-0.045	38.8;50.2
	$UC-QR1-W1-L3$	0.01-0.04	24.5;46.3
	$UC-QR1-W1-L4$	No nappe oscillation	/
	$UC-QR1-W1-L5$	No nappe oscillation	/
	$UC-QR1-W1-L7$	No nappe oscillation	/
	$UC-QR1-W2-L1$	0.01-0.04	43;53
	$UC-QR1-W2-L2$	0.01-0.04	24.9;47.3
	$UC-QR1-W2-L3$	0.01-0.04	25.3;37.4
	$UC-QR1-W2-L4$	No nappe oscillation	/
	$UC-QR1-W2-L7$	No nappe oscillation	/
	$UC-QR1-W3-L3$	0.02-0.025	34.8;35.3

	Abbreviation	Range of q affected by the oscillations (m^2/s)	Extreme frequencies (Hz)
Model 1	$UC-QR1-W3-L4$	No nappe oscillation	/
	$UC-QR1-W3-L5$	No nappe oscillation	/
	$UC-QR1-W3-L7$	No nappe oscillation	/
	$UC-QR1-W4-L1$	0.01-0.025	48.3;54.6
	$UC-QR1-W4-L2$	0.01-0.015	29.7;29.9
	$UC-QR1-W4-L3$	No nappe oscillation	/
	$UC-QR1-W6-L1$	No nappe oscillation	/
Model 2	$C-QR2-W5-L5$	0.01-0.06	33.9;49
	$C-QR2-W5-L6$	0.02-0.06	32.1;48.3
	$C-QR2-W5-L7$	No nappe oscillation	/
	$C-THR2-W5-L5$	0.015-0.05	37.6;58.75
	$C-THR2-W5-L6$	0.03-0.05	46.2;50.1
	$C-THR2-W5-L7$	No nappe oscillation	/
	$C-R-W5-L5$	No nappe oscillation	/
	$C-RR-W5-L5$	0.02-0.025	38.17;42.47

V.2.2 Conditions for nappe oscillations occurrence

V.2.2.1 Minimum requirements

As already mentioned, it is clear that nappe oscillations development occurs only for discharges included between ~0.01 and 0.06 m^2/s. Then, based on the expertise gained from hours of nappe oscillations observations and in order to identify other necessary conditions for nappe oscillations occurrence, the results have been analyzed considering the following five questions:

1. Is the upstream face of the crest profiled?
2. Is a fixed detachment point imposed by the crest geometry?
3. Is the approach flow velocity low and uniformly distributed along the weir width?
4. Is the nappe confined?
5. Is the nappe coherent along the fall height and at the impact?

Answers Yes or No for these questions have been reported in Table V.4 for all tested configurations. Nevertheless, to avoid unnecessary duplication, these configurations have been classified in sets of configuration(s) (which correspond to the different columns of the table), mainly according to the crest profile

(QR, HR, THR, R or RR) and the confinement (Confined or UnConfined). The first column in particular corresponds to all configurations of the unconfined large scale model (Model 1) with a QR crest profile (19 configurations) for which L and W vary. The second column collects all the configurations performed with Model 1, confined and equipped with the THR crest profile (21 Configurations). The 3rd and 4th columns correspond to the configurations related to the small scale model (Model 2), confined and equipped respectively with a QR and THR crest profile (3 configurations for each crest profile). The 5th and 6th columns refer to Configuration $C-QR1-W1-L1$ and only differ by the set up (or not) of the metal grid and synthetic membrane in the reservoir, as baffle wall. The 7th and 8th columns respectively refer to Configurations $C-R-W5-L5$ and $C-RR-W5-L5$ while the 9th column relates to Configuration $C-HR1-W1-L1$ and the 10th column to $C-HR1-W1-L5$ and $C-HR1-W1-L7$.

For a given crest profile, the answers to questions 1 and 2 are identical for all sets of configuration(s) while answers to questions 3 to 5 vary, such as the reservoir condition and confinement for QR (5th and 6th columns) and nappe coherence for HR (9th and 10th columns).

For each set of configurations, the occurrence of nappe oscillations is reported as yes if at least one of the configurations of the set produced oscillations. Indeed, the aim of this analysis is the identification of necessary conditions for nappe oscillations occurrence.

The set of answers, and therefore configurations, that produced nappe oscillations are of three kinds as reported in Table V.5.

Table V.5 shows that the nappe confinement and the existence of a fixed detachment point imposed by the crest geometry are not required together to produce nappe oscillations. It has to be pointed out that the case of an unconfined nappe without detachment point imposed by the crest geometry was not tested in this research. It can however be concluded that at least one of these two conditions has to be satisfied to have nappe oscillations.

Based on this analysis, the necessary conditions for nappe oscillations might be summarized as follows:

- A unit discharge between 0.01 and 0.06 m^2/s;
- A profiled upstream face of the crest;
- Low and uniformly distributed approach flow velocities;
- A coherent nappe along the whole fall height;
- A fixed detachment point imposed by the crest geometry or a confined nappe.

Table V.4: Sets of answers to the five questions and assessment of nappe oscillations occurrence depending on sets of tested configurations – columns with **green** writing correspond to configurations showing oscillations

Column ♯	1	2	3	4	5
Questions	$UC-QR1$	$C-THR1$	$C-QR2$	$C-THR2$	$C-QR1$
1	**Yes**	**Yes**	**Yes**	**Yes**	**Yes**
2	**Yes**	**Yes**	**Yes**	**Yes**	**Yes**
3	**Yes**	**Yes**	**Yes**	**Yes**	**Yes**
4	**No**	**Yes**	**Yes**	**Yes**	**Yes**
5	**Yes**	**Yes**	**Yes**	**Yes**	**Yes**
Were nappe oscillations observed (at least once)?	**Yes**	**Yes**	**Yes**	**Yes**	**Yes**

Column ♯	6	7	8	9	10
Questions	$C-QR1$	$C-R$	$C-RR$	$C-HR1$	$C-HR1$
1	Yes	No	**Yes**	Yes	**Yes**
2	Yes	Yes	**Yes**	No	**No**
3	No	Yes	**Yes**	Yes	**Yes**
4	Yes	Yes	**Yes**	Yes	**Yes**
5	Yes	Yes	**Yes**	No	**Yes**
Were nappe oscillations observed (at least once)?	No	No	**Yes**	No	**Yes**

Table V.5: Conditions that lead to nappe oscillations

Questions	Sets of answers leading to oscillations		
1. Is the upstream face of the crest profiled?	Yes	Yes	Yes
2. Is a fixed detachment point imposed by the crest geometry?	Yes	Yes	No
3. Is the approach flow velocity low and uniformly distributed along the weir width?	Yes	Yes	Yes
4. Is the nappe confined?	Yes	No	Yes
5. Is the nappe coherent along the fall height and at the impact?	Yes	Yes	Yes

The conditions developed above are necessary but not sufficient. They justify the occurrence of the oscillations in the 34 concerned configurations reported in Table V.1. To analyze the non-occurrence of the oscillations for the 18 remaining configurations, the influence of other geometric parameters of the weir, i.e. W and L, has to be considered.

V.2.2.2 Width and fall height

The influence of the fall height and width on nappe oscillations is now analyzed in regard to the occurrence of the phenomenon. In particular, the occurrence of nappe oscillations for configurations with a fixed crest shape and confinement i.e., a QR crest profile and unconfined model and, a THR crest profile and confined model, is reported in Fig.V.1 by circles of which the diameters are proportional to the minimum and maximum unit discharges affected by the oscillations.

This figure shows, for the large scale (Model 1) and unconfined nappe equipped with a QR crest (Fig.V.1a), a non-occurrence of nappe oscillations for $L \leq 1.5$ m or $W \leq 1$ m. In addition, for a decreasing W and L, the unit discharge range affected by oscillations decreased.

Similarly, for the large scale and confined model equipped with a THR crest (Fig.V.1b), nappe oscillations were not detected for $L \leq 1.5$ m, except for $W = 3.45$ m. In contrast, for $L > 1.5$ m, nappe oscillations were detected for all tested widths. For $L > 1.5$ m and varying widths, it was also observed that nappe oscillations appeared within a similar unit discharge range.

For the smaller scale and confined model, Model 2, nappe oscillations were detected for both crest profiles, for a width of 1.2 m and until a fall height of 0.75 m as illustrated in blue in Fig.V.1.

In addition to the configurations with a QR and THR crest profile, the configurations with a HR crest profile showed nappe oscillations for a fall height of 1 m and 0.5 m, the width being kept constant to 3.45 m ($W1$).

Based on the set of experiments performed in the framework of this thesis, no general criterion in terms of$L$ or W or even L/W ratio that would predict the occurrence or non-occurrence of nappe oscillations were highlighted. Indeed, as reported in the paragraphs above, different conclusions in terms of value of W or L below which nappe oscillations were not observed, may be derived depending on the crest shape or the scale. The effect of these geometric parameters on the occurrence of the oscillations remains therefore unclear. However, it was observed that the possibility of nappe oscillations occurrence is all the more important when $W > 1.0$ m and $L > 1.5$ m. In addition, experiments showed that nappe oscillations occurred essentially for the largest L and W.

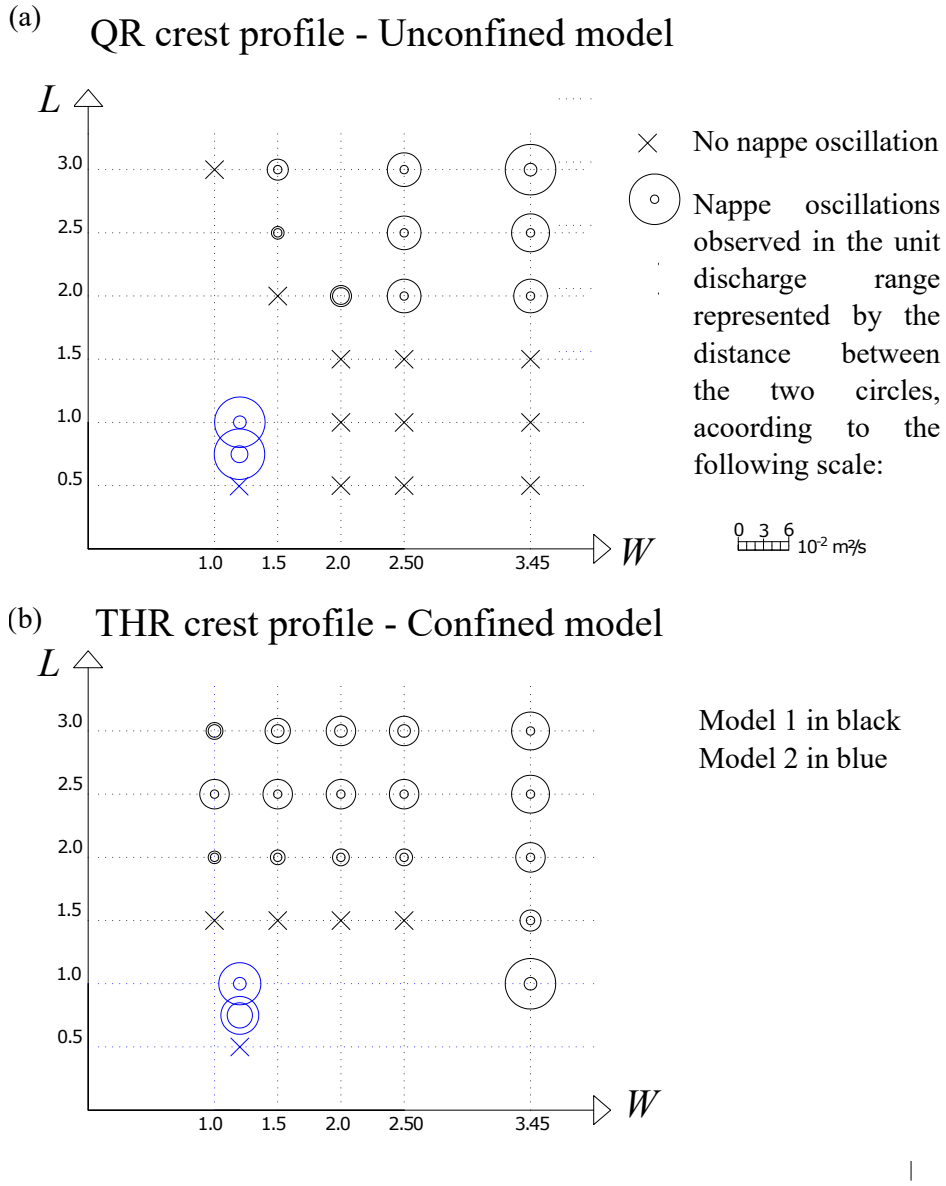

Figure V.1: Occurrence of nappe oscillations for (a) a QR crest profile and unconfined model and (b) a THR crest profile and confined model

V.3 Frequencies of nappe oscillations

V.3.1 Main findings

For all the configurations experiencing nappe oscillations, sound and image analyses were applied and provided the characteristic frequencies of the phenomenon. The frequencies extracted from sound and image analyses are presented in detail in Appendix B. The extreme frequencies are also reported in Table V.1.

As already mentioned in Chapter III, the frequencies extracted from image and sound analyses depended on the unit discharge, the confinement and the crest profile. In addition, the analysis of the frequencies extracted from the 34 configurations experiencing oscillations and tested in the framework of this research shows that the frequencies of the oscillations may depend on the fall height and, in some cases of the weir width.

The variability of the frequencies to L and W is illustrated for an unconfined model equipped with a QR crest profile for fixed W and L in Fig.V.2. Fig.V.2a-c shows that the frequency variation for a fixed W and variable L is even more important when the width is small. Indeed, for $W = 2$ m [$W4$ (Fig.V.2c)], a large difference in terms of measured frequencies is observed between Configurations $W4 - L1$ and $W4 - L2$. In contrast, for $W = 3.45$ m [$W1$(Fig.V.2a)], similar frequencies were observed for the fall height $L1$ and $L2$. For the intermediate width, $W2$ (Fig.V.2b), the frequencies measured for the intermediate fall height $L2$ coincide with the frequencies measured for the fall height $L1$ and $L3$ for different q. For fixed L, Fig.V.2d-e illustrates that the variation of W impacts the frequencies. However, for some specific q ranges, the frequencies observed for a fixed L and different W are identical as for $0.01 \leq q \leq 0.02$ m^2/s for $W1, W2$ and $W4$ in Fig.V.2d, $0.015 \leq q \leq 0.04$ m^2/s for $W1$ and $W2$ in Fig.V.2e. Therefore, for QR crest profile configurations, the fall height emerges as more influential than the width regarding the frequencies.

For a confined model and a THR crest profile, Fig.V.3 and Fig.V.4 illustrate the impact of L and W modification on the frequency variation. Mainly due to the detection of multiple frequencies for this type of crest, the difference with respect to the QR crest profile pointed out by these figures is the large variability of the frequencies from 6 to 44.4 Hz. For a fixed W, despite the detection of identical frequencies for some q (Fig.V.3b, c and e), a large variability of the frequencies is observed for the different tested L. An identical finding was drawn for a fixed L and variable W in Fig.V.4. Contrary to the case of a QR profile, none of the geometric parameters appear as the most influential on the frequencies and the effect of L and W is unclear.

Therefore, the systematic characterization of nappe oscillations showed that the frequency of oscillations varies with both W and L while no clear correlation has been found. In addition, Fig.V.3 and Fig.V.4 illustrate the existence of a different oscillation frequency for a fixed configuration and q. This observation

implies that it is not possible to establish a relationship that would predict the oscillations frequency since this one is not unique.

Finally, the analysis of the frequency showed that the frequencies were all within one order of magnitude, i.e. between 6 and 60 Hz.

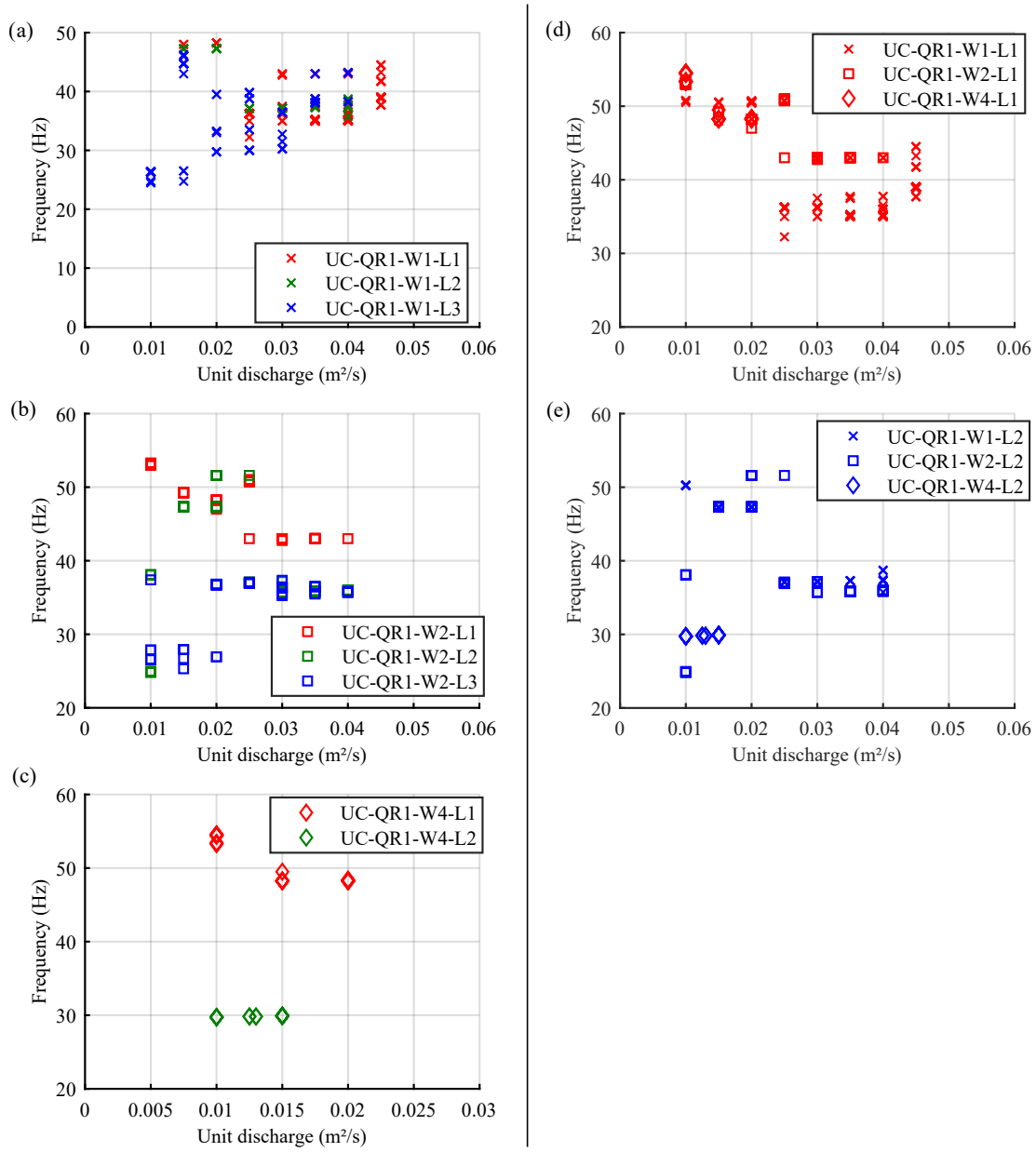

Figure V.2: Frequencies of nappe oscillations for Model 1, unconfined and equipped with a QR crest profile, and variable lengths and fixed width, i.e., (a) $W1$, (b) $W2$ and (c) $W4$ or, variable widths and fixed length i.e., (d) $L1$ and (e) $L2$

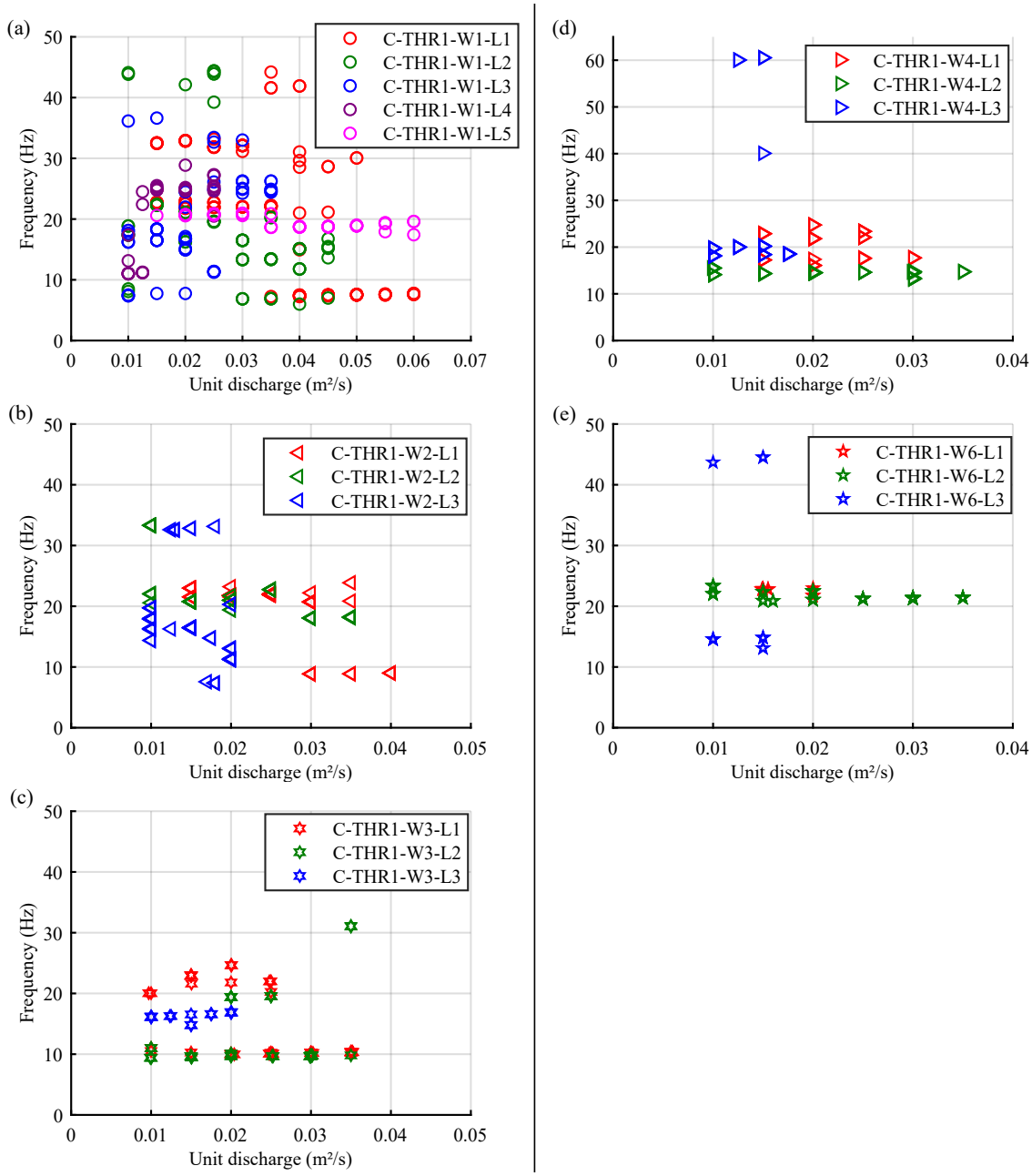

Figure V.3: Frequencies of nappe oscillations for Model 1, unconfined, equipped with a THR crest profile, variable lengths and fixed width, i.e., (a) $W1$, (b) $W2$, (c) $W3$, (d) $W4$ and (e) $W6$

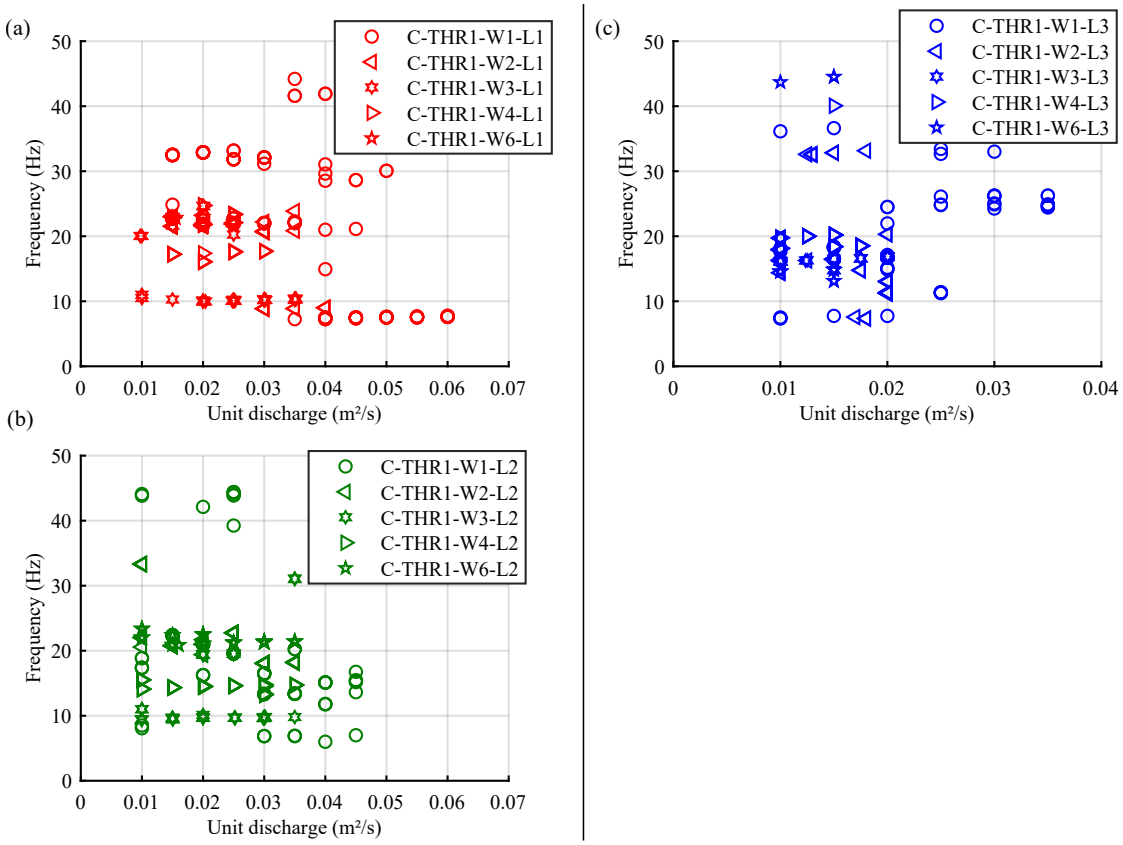

Figure V.4: Frequencies of nappe oscillations for Model 1, unconfined, equipped with a THR crest profile, variable widths and fixed length i.e., (a) $L1$ (b) $L2$ and (c) $L3$

V.3.2 Predition formulation from literature

A few authors propose empirical or theoretical formulations to predict the oscillations frequencies or their occurrence in the case of free overfall structures. In this section, these formulations have been applied to the 34 configurations tested in the framework of this research and experiencing oscillations.

Partenscky and Khloeung (1967) reported oscillations of thin nappe over flap gates. They focused on very small specific discharges ($q < 0.01$ m^2/s), for which nappe oscillations have not been reported in our study. However, it is interesting to look at their work because they have been able to proposed a criterion to predict flow configurations prone to produce oscillations:

$$\frac{1}{L/e} \leq \frac{5}{49}(1.308 - Fr) \tag{V.3.1}$$

where e is the water depth at the detachment point, $Fr = \frac{V}{\sqrt{ge}}$ the Froude

number calculated at the crest detachment where $V = \frac{q}{e}$ is the velocity at the detachement point.

In Fig.V.5a, this criterion is represented with the configurations experiencing nappe oscillations in terms of L/e and Fr. According to Partenscky and Khloeung (1967), nappe oscillations do not occur for configurations on the right of the blue curve in Fig.V.5a. However, it is observed that in our study all the data are located on the right and correspond to oscillating data. While our study considered the similar L/e ratio, we experienced oscillations for much more important Froude number than the aforementioned Authors. This difference may be explained by the fact that nappe oscillations were always observed for higher q in our study while Partenscky and Khloeung (1967) focused on $q < 0.01$ m²/s and thus smaller Froude number.

In addition to an occurrence criterion, Partenscky and Khloeung (1967) also linked the frequency of the oscillations to the ratio L/e as:

$$\begin{cases} S = \frac{fL}{V} = 181 \left(\frac{L}{e}\right)^{-0.276} & \text{for } \frac{L}{e} < 170 \\ S = \frac{fL}{V} = 44 & for\ \frac{L}{e} \geq 170 \end{cases} \tag{V.3.2}$$

As illustrated in Fig.V.5b, this formulation is not adapted to predict the frequency of the oscillations observed in our research. In particular, we observed much more variability in the dominant frequency. Contrary to our research, Partenscky and Khloeung (1967) focused on a single crest and nappe geometry. Unfortunately considering the dimensionless form of the results presented in their study and the lack of information to deduce their value in Hertz, it was impossible to deepen the discussion.

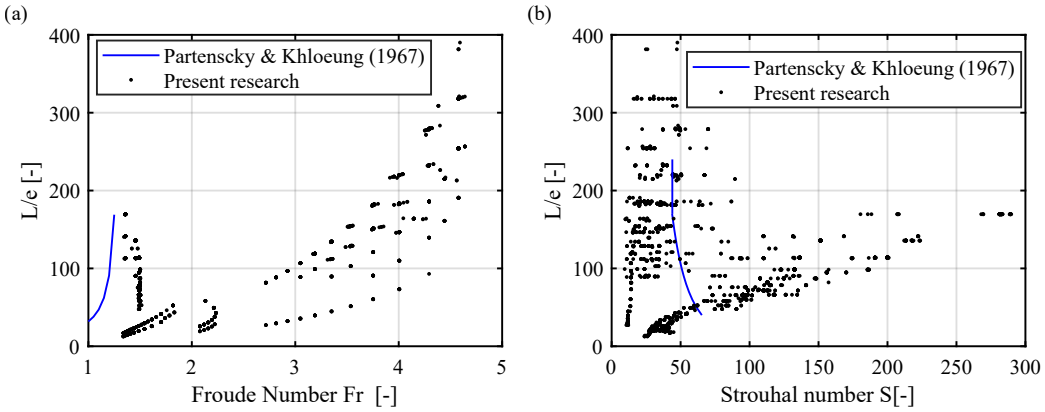

Figure V.5: Application of the Partenscky and Khloeung (1967) formulation regarding (a) the occurrence and (b) the frequency evaluation

Schwartz (1964a) expressed the possible oscillations frequencies based on the $K + 1/4$ criterion which relies on the fact that the number of wave-lengths con-

tained in an oscillating nappe could only be an integer plus 1/4 value. This formulation is presented in Eq.V.3.3. More recently, Casperson (1993b) expressed in his simplified model the possible oscillations frequencies using an identical formulation.

$$f = \frac{K + \frac{1}{4}}{-\frac{v_0}{g}\left[\sqrt{1 + \frac{2gL}{v_0^2}} - 1\right]} = \frac{g\left(K + \frac{1}{4}\right)}{\sqrt{v_0^2 + 2gL} - v_0} \tag{V.3.3}$$

Where v_0 is the initial vertical velocity and K is an integer. The 1/4 value, also named m_0 in Casperson formulation, measures the fundamental excess top-to-bottom phase shift necessary to ensure the positive feedback for sustaining the oscillations. To apply these formulae, in this research, the initial vertical velocity (v_0) was assumed equal to 0 for a QR crest profile, while for a THR crest, v_0 was deduced from nappe thickness (e), experimentally measured and then projected according to the angle (α) of the weir crest at the downstream end (i.e., 45° with horizontal).

The application of this formulation to define the integer, K in Eq.V.3.3 associated to the measured frequencies is exemplified for Configurations $C - QR1 - W1 - L1$ and $C - THR1 - W1 - L1$ in Fig.V.6 and Fig.V.7. For Configuration $C - QR1 - W1 - L1$, the measured frequencies and associated K reported in Fig.V.6b show that the variability of the frequency induces a variability of the calculated parameter K. Considering the frequency varying between 31.25 and 34.5 Hz, for q between 0.02 and 0.055 m^2/s, the associated parameter K varies from 24 to 27 and K varies thus with the discharge.

The uncertainty on K based on frequency measurements can be evaluated by Eq.V.3.4

$$|\Delta K| = \left|\frac{\partial K}{\partial f}\right| |\Delta f| + \left|\frac{\partial K}{\partial L}\right| |\Delta L| + \left|\frac{\partial K}{\partial e}\right| |\Delta e| + \left|\frac{\partial K}{\partial Q}\right| |\Delta Q| \tag{V.3.4}$$

where $\frac{\partial K}{\partial f}, \frac{\partial K}{\partial L}, \frac{\partial K}{\partial e}, \frac{\partial K}{\partial Q}$ the first derivative of K (Eq.V.3.5) with respect to measured variables f, e, L and Q while $\Delta f, \Delta L, \Delta e, \Delta Q$ correspond to the uncertainty of measurement of these variables. The total discharge Q appears from the initial vertical velocity in Eq.V.3.6 for the THR crest profile. By contrast $v_0 = 0$ for a QR crest profile.

$$K = \frac{f}{g}\left(\sqrt{v_0^2 + 2gL} - v_0\right) - \frac{1}{4} \tag{V.3.5}$$

$$v_0 = \frac{qsin\alpha}{e} = \frac{Qsin\alpha}{Le} \tag{V.3.6}$$

For Configuration $C - QR1 - W1 - L1$, considering an uncertainty on the variables f, L, e and Q respectively of 1.5 Hz, 5×10^{-3} m, 10^{-3} m and $2 \times$

10^{-4} m^3/s, the maximal uncertainty on K is 1.2 for the whole q range. This uncertainty explains part of the variability of the computed integer K value, but also shows that several values of K can be computed for a single geometry.

For Configuration $C - THR1 - W1 - L1$, similar conclusions are drawn (Fig.V.7), with much larger range for K. In addition, for a single geometry and discharge, we observe several values of K, which are multiple (a mean frequency of 22.5 Hz corresponds to 3 times the mean frequency of 7). The application of the Eq.V.3.5 to all the configurations with QR and THR crest profiles showed that K varies from 4 to 43. This formulation does not allow to predict the frequency if the oscillating mode is unknown. This analysis shows however that the $K + 1/4$ criterion applies to all of our measurements, at the uncertainty of the measurements.

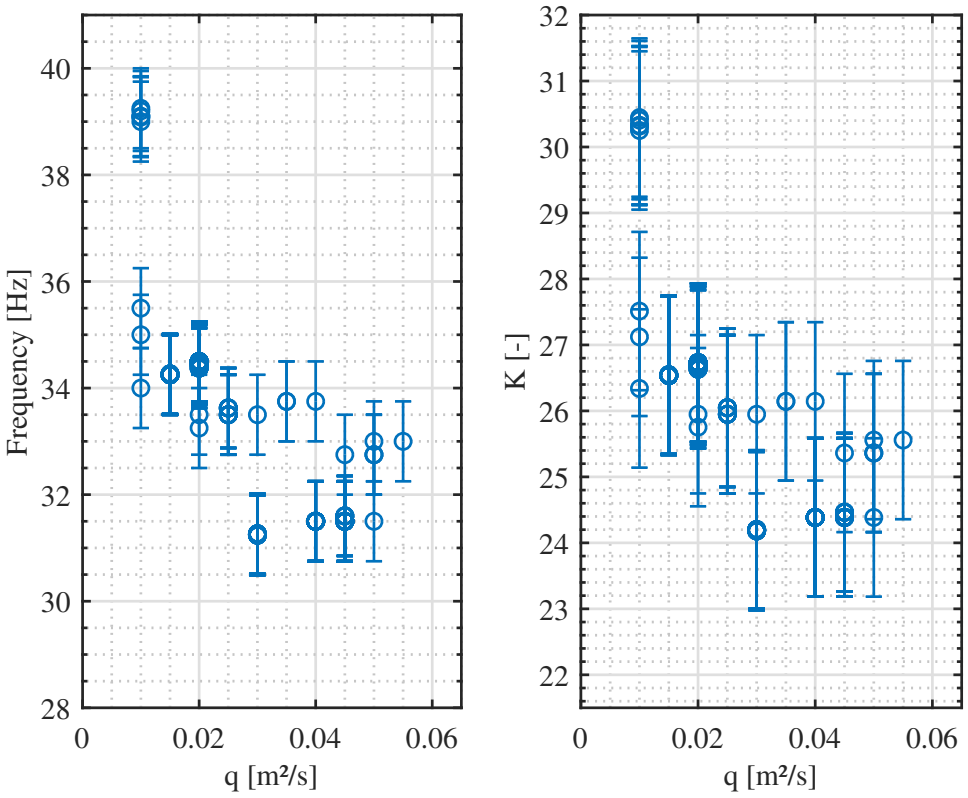

Figure V.6: Configuration $C - QR1 - W1 - L1$: (a) frequencies and (b) associated integer K, calculated according to Eq.V.3.3 (Schwartz, 1964a; Casperson, 1993b)) for each measured frequency

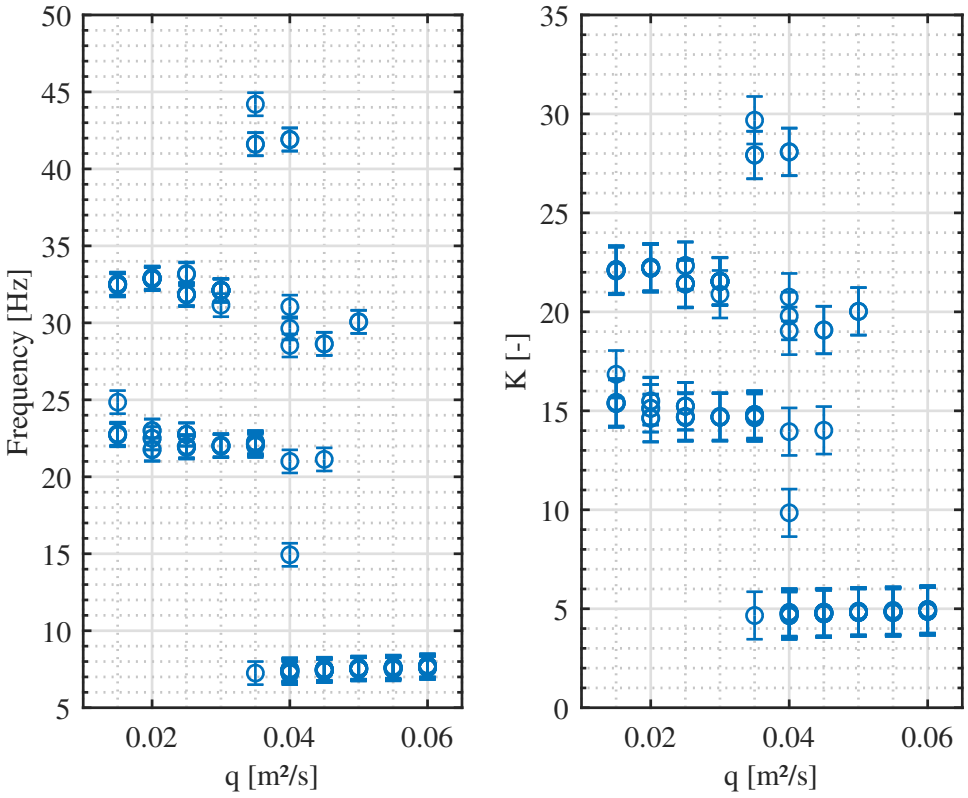

Figure V.7: Configuration $C - THR1 - W1 - L1$: (a) frequencies and (b) associated integer K, calculated according to Eq.V.3.3 (Schwartz, 1964a; Casperson, 1993b)) for each measured frequency

V.3.3 Dimensional analysis

Based on the previous section, it appears that no formulation in the literature allows the prediction of the frequency of the oscillations for the 34 oscillating configurations of this research. In an effort to link the geometric characteristics of a configuration to the oscillations frequencies, a dimensional analysis was thus undertaken. As a first step, 10 independent characteristic parameters of the phenomenon, called variables in the following, have been listed in Table V.6. The number of Π-parameters, dimensionless and independent numbers, is equal to 10-3 = 7. [1]

[1]The list of variables is not exhaustive : addition data relative to the fluids and flow characteristics of air may indeed be taken into consideration as well as other geometrical parameters such as the crest height (elevation of the weir crest with respect to the upstream bottom level of the headbox). However, the listed variables are, to the knowledge of the author, those that have a major influence on nappe oscillations.

Table V.6: Dimensional analysis: variables and Π-parameters. Variables used for expressing the dimension of the problem are in bolt

Types	Variables	Notations	SI unit	Π-parameters
Geometry	Fall height	L	m	$\Pi_1 = L/e$
	Weir width	W	m	$\Pi_2 = W/e$
Hydraulics	**Water depth at the crest detachment**	e	**m**	**-**
	Characteristic fall velocity	v	**m/s**	**-**
	Characteristic frequency of the oscillations	f	1/s	$\Pi_3 = fe/v$
	Unit discharge	q	$\mathrm{m^2/s}$	$\Pi_4 = q/(ve)$
	Gravitational acceleration	g	$\mathrm{m/s^2}$	$\Pi_5 = v/\sqrt{ge} = Fr$
Fluid	**Density**	ρ	$\mathbf{kg/m^3}$	**-**
	Surface tension	σ	$\mathrm{kg/s^2}$	$\Pi_6 = \rho v^2 e/\sigma = We$
	Dynamic viscosity	μ	kg/ms	$\Pi_7 = \rho ve/\mu = Re$

The Π-parameters in Table V.6 were classified into three groups: geometry, hydraulics and fluid. The choice of the water depth at the detachment point, e, the fall velocity, v, and the water density, ρ, as independent variables has been driven by the literature review, various trials performed during this thesis but also the wish to have a variable linked to the crest shape (e) and another one linked to the nappe (v). Another analysis has been published in Lodomez et al. (2018c). It provided less interesting and complete findings than the one presented below. This analysis is thus not presented in this manuscript. The water depth at the crest was chosen by Partenscky and Khloeung (1967) for their dimensional analysis of the nappe oscillations problem. Aside from the fact that the proposed formulations using e in Partenscky and Khloeung (1967) did not provide conclusive results in our case, this parameter was easily measured during the experiments. This parameter reflects the characteristics of the crest profile.

The characteristic velocity was defined as the velocity differential between the vertical velocity at the crest detachment and the vertical velocity at the impact. Based on the equations of the free fall (without air resistance, with positive axis in the fall direction):

$$\begin{cases} y(t) = y_0 + v_0 t + \frac{1}{2} g t^2 \\ v(t) = v_0 + gt \end{cases} \tag{V.3.7}$$

With v_0 the initial vertical velocity, y_0 the initial altitude (assumed equal to 0), $v(t)$ the vertical velocity with respect to time, $y(t)$ the altitude with respect to time and t the time elapsed. The vertical velocity at the impact, v_L which is

the velocity when $y(t) = L$, is obtained by replacing the expression of the fall time, $t_f = \frac{v_{L-v_0}}{g}$, in the equation of the vertical position (Eq.V.3.7) and is:

$$v_L = \sqrt{v_0^2 + 2g(L - y_0)} = \sqrt{v_0^2 + 2gL} \tag{V.3.8}$$

The characteristic velocity used in the dimensional analysis is thus defined as follows:

$$v = \sqrt{v_0^2 + 2gL} - v_0 \tag{V.3.9}$$

As reported in Section V.3.2, the initial vertical velocity (v_0) was assumed equal to 0 for a QR crest profile. For a THR crest profile, it was deduced from e, experimentally measured and then projected according to the angle of the weir crest at the downstream end. The choice of this characteristic velocity is identical to what has been proposed by Casperson (1993b) in his simplified model to express the possible oscillations frequencies Eq.V.3.3. This formulation is compatible with the observation of multiple frequencies for some configurations with a THR crest profile despite the fact that it does not provide an accurate prediction of the frequency.

Focusing on the characteristics of nappe oscillations, the parameters Π_3 and Π_4 were multiplied to define a new parameter :

$$F = \Pi_3\Pi_4 = \frac{fq}{v^2} \tag{V.3.10}$$

This parameter is reported as a function of the parameter Π_1 since, in addition to literature content, experiments showed a large influence of the fall height on frequencies. In a first step, these parameters, F and Π_1, are reported for QR crest profile configurations in Fig.V.8.

A remarkable tendency is presented in this figure although the variability of the frequencies is measured as reported in Fig.V.2. For these data sets, the following fitting curve, based on a least mean square estimation of linear relation between the logarithms of F and Π_1, was defined by:

$$\Pi_1 = 3.2642F^{-0.8} \tag{V.3.11}$$

Then, despite the effect of the width is not taken into account in this dimensionless representation, the parameters F and Π_1 are reported for the configurations equipped with a THR crest profile, without taking into account the configurations presenting harmonics in Fig.V.9. The fitting curve derived by maintaining the coefficient affected to the dimensionless frequency identical to the one of Eq.V.3.11 for the QR configuration, i.e., -0.8, is the following:

$$\Pi_1 = 4.5449F^{-0.8} \tag{V.3.12}$$

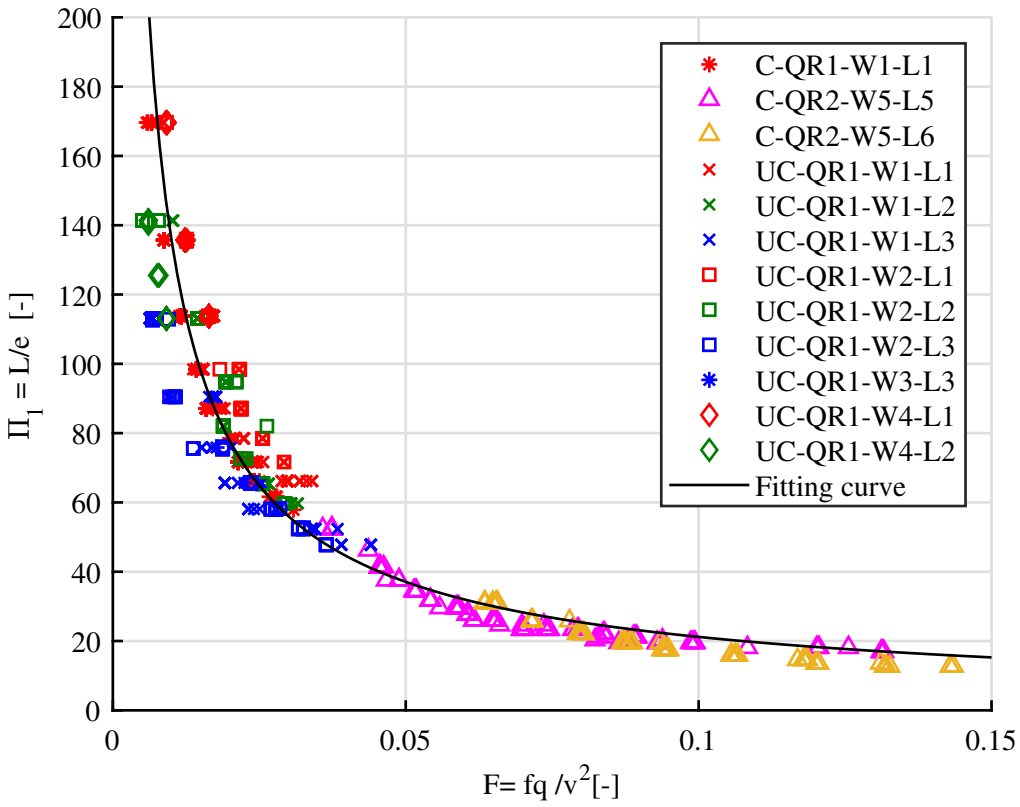

Figure V.8: Dimensionless frequency of nappe oscillations, F, for the configurations with a QR crest profile as a function of Π_1

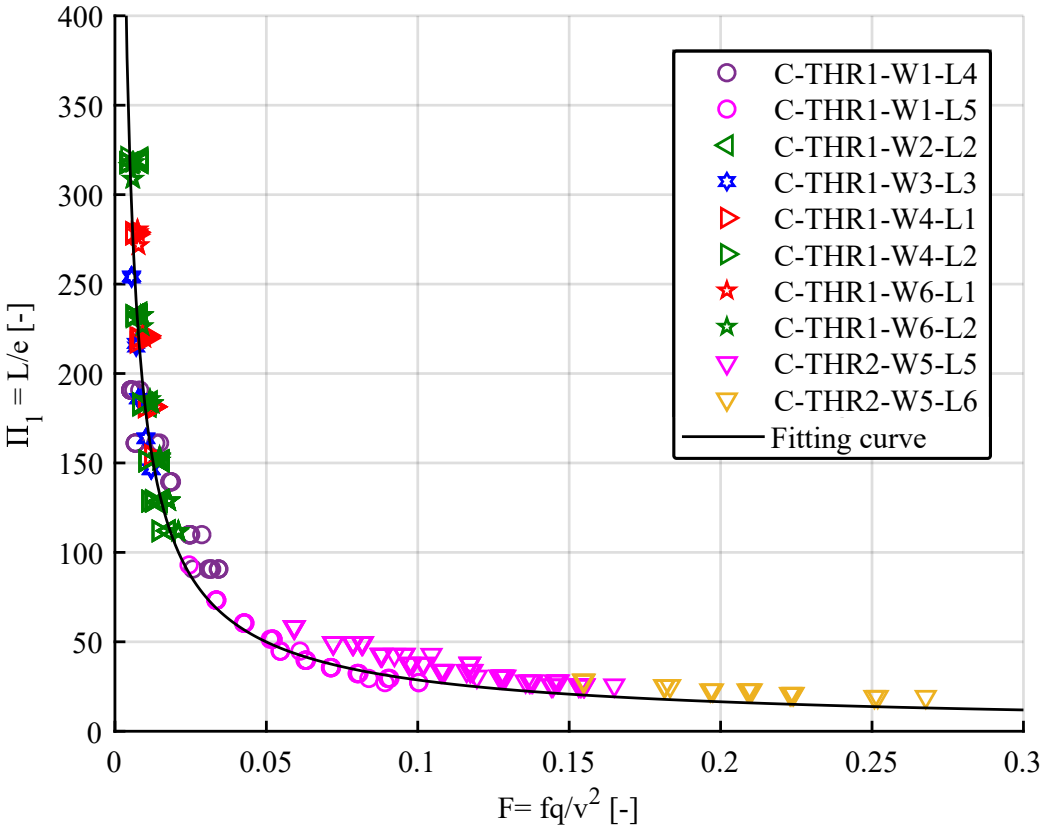

Figure V.9: Dimensionless frequency of nappe oscillations F for the configurations with a THR crest profile as a function of Π_1. Data sets for which harmonics were measured are not taken into consideration

Then, for all the configurations with the THR crest profile, the evolution of F and Π_1 is reported in Fig.V.10.

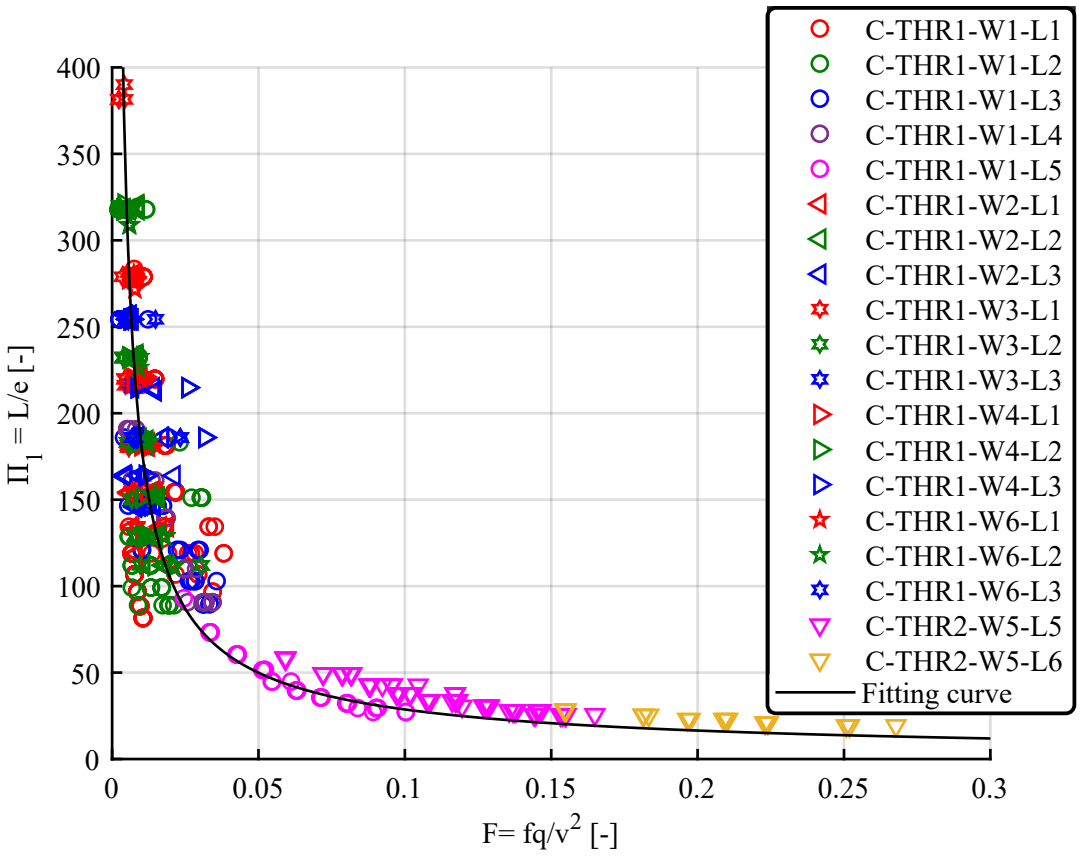

Figure V.10: Dimensionless frequency of nappe oscillations F for all configurations with a THR crest profile as a function of Π_1

In spite of a significant adequacy of the results to the curve in Fig.V.9, a dispersion is observable when all the configurations were taken into account (Fig.V.10, Eq.V.3.12). This dispersion is investigated for a set of configurations in Fig.V.11. These configurations show nappe oscillations at one, two, three or even four distinct frequencies (also called levels in the following discussion). The mean value of these distinct levels, reported in Fig.V.11a by the black lines, are 7.4, 15.2, 22, 32.3 and 43.4 Hz. In parallel, Fig.V.11b shows that configurations oscillating at a same frequency level follow the same fitting curve. These fitting curves reported in Eq.V.3.13 show an increase of the constant factor of the power law with increasing frequencies.

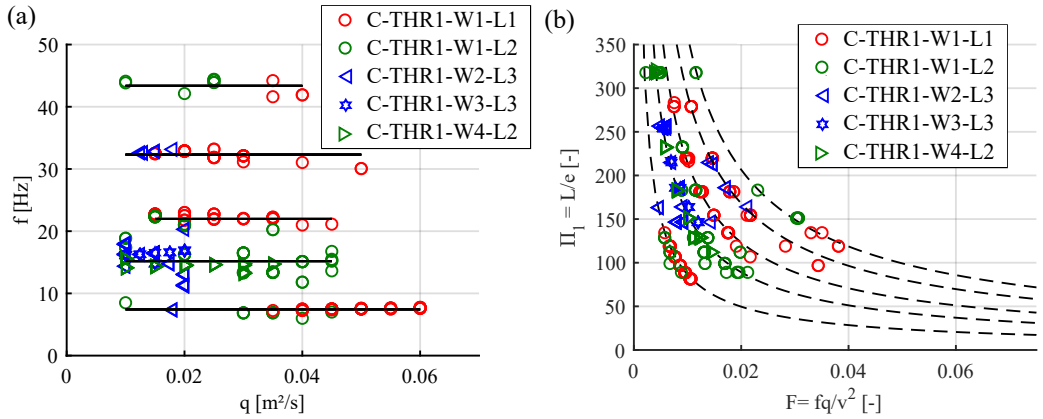

Figure V.11: Analysis of frequency dispersion

$$\Pi_1 = \begin{pmatrix} 2.17 \\ 3.90 \\ 5.39 \\ 7.35 \\ 9.03 \end{pmatrix} F^{-0.8} = 0.45 f^{0.8} \left(\frac{fq}{v^2}\right)^{-0.8} \tag{V.3.13}$$

This analysis of the dispersion, in particular Eq.V.3.13, shows thus that the tendency observed both for QR and THR crest profiles is due to a characteristic relationship between L/e and q/v^2 which mainly links hydraulic and geometric parameters like a discharge rating curve. The frequencies thus only positioned the curve along the x-axis and maintained the tendency provided by the relation between L/e and q/v^2 for all configurations due to the fact that all frequencies are in the same order of magnitude, i.e., between 6 and 60 Hz.

This statement is confirmed by the fact that the application of Eq.V.3.11 or Eq.V.3.12 do not predict the oscillating frequency with accuracy. In case of a QR crest profile, the approximation of the oscillations frequencies based on Eq.V.3.11 is compared to the measured frequencies in Fig.V.12a. The relative error calculated for each data point is reported in Fig.V.12b and shows that 65% of the approximated frequencies have a relative error included between 0 and ±20%. Even if these results can be described as satisfactory for a QR crest, this figure shows nevertheless that 5% of the approximated data have a relative error higher than 60%. In addition, the distribution of the relative error on the approximated frequencies in case of THR crest profile (Fig.V.13) indicates that only 45% of these frequencies have a relative error included between 0 and ±20%. It can therefore be concluded that an accurate approximation of the nappe oscillations frequency cannot be provided.

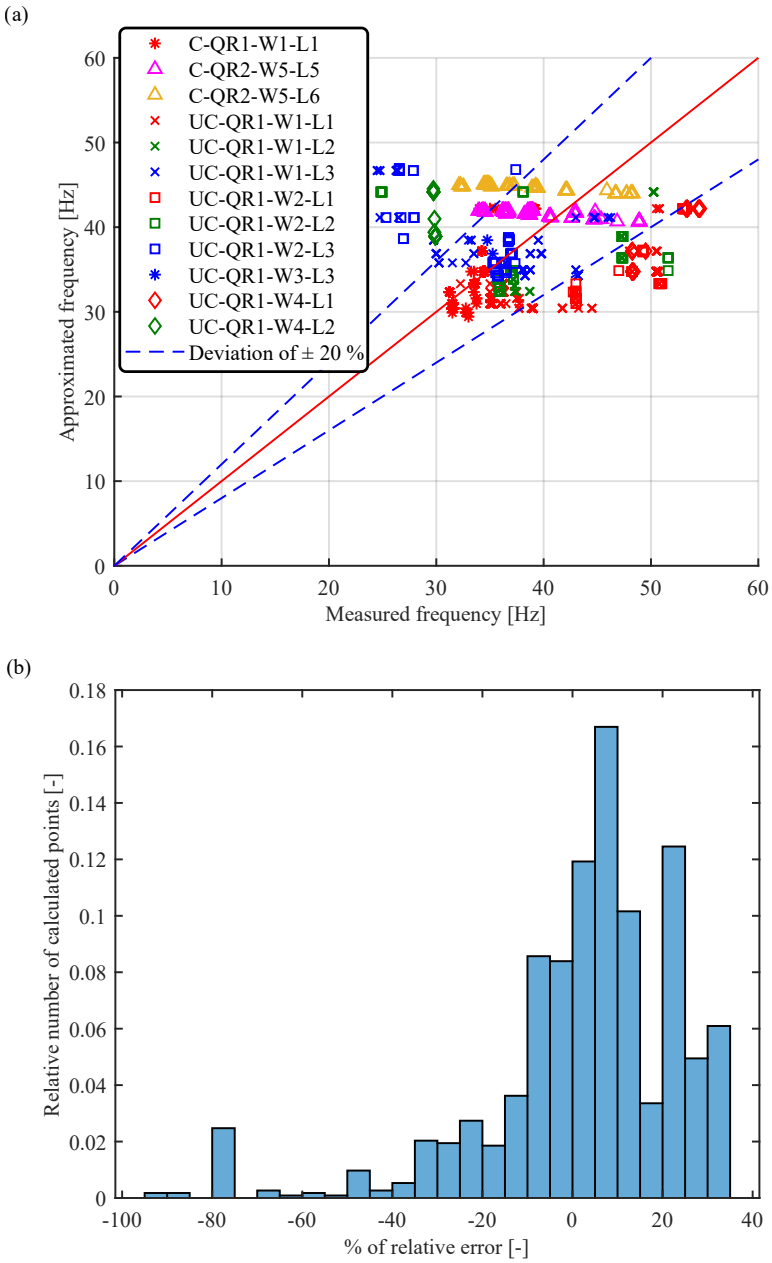

Figure V.12: (a) Approximation of the oscillations frequencies based on Eq.V.3.11 for configurations equipped a QR crest profile and (b) distribution of the relative error

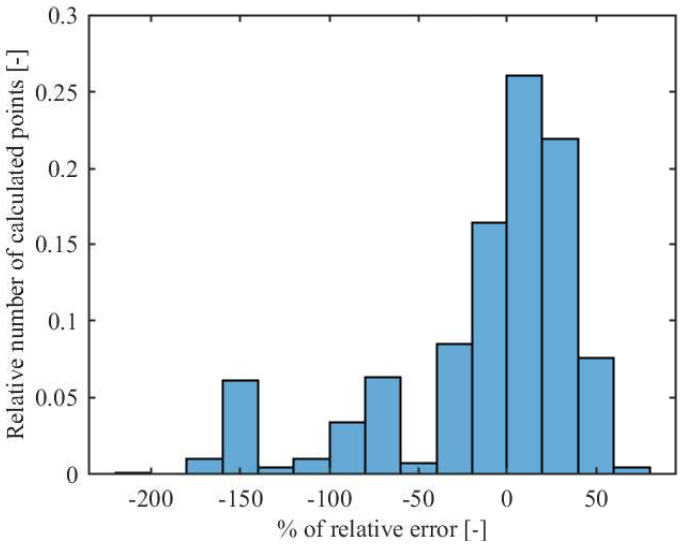

Figure V.13: Distribution of the relative error in case of frequency approximation via Eq.V.3.12 for configurations equipped with a THR crest profile

As a conclusion, only the order of magnitude of the nappe oscillations can be predicted on the basis of the experiments performed in the framework of this thesis. Anderson and Tullis (2018); Sumi and Nakajima (1990) studied the nappe oscillations for an experimental model with similar geometric parameters as reported in Table V.7. None of these researches derived a formulation of the oscillations frequency. Nonetheless, the measured frequencies were in the same range (6-60 Hz) as the frequencies measured in this thesis.

Table V.7: Geometric parameters of the experimental facilities and range of measured oscillations frequency

	Fall height (m)	Width (m)	Crest profile	Frequency (Hz)
Anderson and Tullis (2018)	1-3.6	1.8-4.9	QR	16-40
Sumi and Nakajima (1990)	1.5-3.1	0.9-5.5	Sharp edge 40°	20-27
Lodomez (present research)	0.5-3	1-3.45	QR, THR, HR, R, RR	6-60.5

Another conclusion of this dimensionless analysis is also that another/other variable(s) than the ones measured and reported in this section should exist in order to justify the measured frequencies.

Finally, the other Π-parameters of this dimensional analysis, Π_2, Π_5, Π_6 and Π_7 defined in Table V.6 were not detailed in this section because they did not provide relevant information linked to the oscillations frequency. However, their evolution according to Π_1 were reported in Appendix C.

V.4 Conclusions

First, from hours of nappe oscillations observations and analysis, necessary conditions for nappe oscillations occurrence have been defined. Along with geometric criteria regarding the fall height and width of the structure, these conditions, although not sufficient, allow to predict the possible occurrence of the oscillations in many cases. The condition for nappe oscillations were presented in the form of a questionnaire (Table V.8) which is a practical and valuable tool for designers.

The definition of these necessary conditions to nappe oscillations underlined the influence of the crest geometry on the oscillations development. Some crest characteristics in particular are linked to the imposition of a pressure discontinuity at the crest detachment or the flow condition along the crest which impact the initiation of the oscillations.

Secondly, the analysis of the results varying L and W showed first that the effect of these geometric parameters on the occurrence remains unclear. However, it was observed that the possibility of nappe oscillations occurrence is all the more important that $W > 1$ m and $L > 1.5$ m for QR and THR crest profiles. Regarding the oscillations frequency, the systematic characterization of nappe oscillations showed that the frequency of the oscillations varies with both W and L while no clear correlation has been found. Finally, the analysis of the frequencies measured for the 34 configurations experiencing nappe oscillations comes to the conclusion that the frequencies of the oscillations cannot be approximated on the basis of the geometric and hydraulic parameters measured during the experiments. However, the order of magnitude is always between 6 and 60 Hz and fits with comparable studies in literature.

Table V.8: Questionnaire - Conditions that lead to nappe oscillations

Questions (Possible answers are Yes or No)	Sets of answers leading to oscillations		
Is the unit discharge between 0.01 and 0.06 m^2/s?	Yes		
Is the upstream face of the crest profiled?	Yes		
Is the approach flow velocity low and uniformly distributed?	Yes		
Is the nappe coherent along the fall height and at the impact?	Yes		
Is a fixed detachment point imposed by the crest geometry?	Yes		No
Is the nappe confined?	Yes	No	Yes
	Nappe oscillations		

Chapter VI

Mitigation techniques for weirs

This Chapter is based on the following articles:

Lodomez, M., Pirotton, M., Dewals, B., Archambeau, P., Erpicum, S., 2017. Could piano key weirs be subject to nappe oscillations? In: Labyrinth and Piano Key Weirs III. CRC Press, London, pp. 135144.

Lodomez, M., Crookston, B., Tullis, B., Erpicum, S., 2018b. Mitigation techniques for nappe oscillations on free-overfall structures. Journal of Hydraulic Engineering 145 (2), 04018086.

VI.1 Introduction

Nappe oscillations are an oscillating phenomenon that affects various free overfall structures as exposed in the literature review (Chapter I). Usually two types of structure were distinguished: the gates and the weirs. In the case of flow over a gate, the nappe oscillations have been mitigated for decades through the use of splitters (Naudascher and Rockwell, 1994; Reclamation, 1964; Sumi and Nakajima, 1990). In contrast, a few researches have focused on mitigation techniques for weirs. As reported in Chapter I, only nappe splitters and increased roughness were investigated (Anderson and Tullis, 2018; MWSB, 1980; Reclamation, 1964). Nowadays, no standard regulation exists and mitigations are still developed on a case by case basis. This position led us to investigate other original solutions. To that end, this study has been performed in collaboration with Schnabel Engineering who provided insight regarding ease of installation and durability.

The objective of the study, presented in Section VI.2, was to investigate the effectiveness of three alternative nappe oscillations mitigation techniques and any corresponding impacts to hydraulic efficiency, using Model 1 (large-scale physical linear weir model). Three evaluated mitigation techniques are included herein: a crest roughening via projecting elements (bolts), the fragmentation of the nappe through deflectors, and a boundary layer and nappe trajectory modification created through the use of a small downstream step. These mitigation techniques were defined based on the literature review and best practice related to gates. Indeed, the impact of the crest roughness on the oscillations disappearance was discussed in Anderson and Tullis (2018) and Schwartz (1966a) while the fragmentation of the nappe by the use of splitters proved its effectiveness for a long time (MWSB, 1980; Naudascher and Rockwell, 1994; Reclamation, 1964; Sumi and Nakajima, 1990).

In addition to the study investigating countermeasures which modify the flow conditions at the crest, another mitigation technique has been revealed throughout the investigation of the risk of nappe oscillations development for Piano Key Weir (PKW). It consists of an inclined apron at the nappe impact which refers, in case of PKW, to the inclined ramp downstream of the linear sidewalls. This solution is presented in Section VI.3.

VI.2 Innovative mitigation techniques setup at the crest

In the following sections, the experimental setup and tools are described (Section VI.2.1). Then, experimental results and discussions are developed respectively in Sections VI.2.2 and VI.2.3. It should be noted that this study regarding the mitigation techniques imposed at the crest has been undertaken at the beginning of

this thesis, before the definition of the characterization method based on the image analysis developed in Chapter II. However, image analysis was performed in a second phase. The additional information collected through the image analysis is consistent with the initial study and completes it.

VI.2.1 Experimental setup

In the framework of this study, the confined prototype-scale linear weir with a quarter round crest profile, i.e., Configuration $C - QR1 - W1 - L1$ was used (Fig.II.1). As previously noted, practicing engineers and contractors were consulted in an effort to identify practical mitigation techniques with respect to constructability, durability, performance, maintenance. Three approaches were identified and tested: projecting elements (i.e., bolts), deflectors, and a small downstream step as illustrated in Fig.VI.1. In order to optimize the configuration and geometry of these mitigation techniques (height, spacing, position), 12 projecting elements configurations, 5 deflectors configurations, and one step configuration were tested (Table VI.1).

To assess the occurrence of the nappe oscillations and therefore the effectiveness of the mitigations, sound recordings and processing (MC 212 microphone and dBFA software) were performed and analyzed according to the methodology developed in Section II.4.1. The use of identical tools for all tested configurations justified the use of dimensional intensity in dB.

In addition to sound measurements, flow over the weir was shot with the GoPro Hero 4. The image analysis of videos was performed and examined according to the methodology presented in Section II.4.2 to provide the frequency of the horizontal bands visible on the flowing nappe.

VI.2.2 Experimental results

VI.2.2.1 Reference configuration

To evaluate the effectiveness of a mitigation alternative, a reference configuration, i.e., with intense nappe oscillations, was required. This reference configuration is called Configuration A in the following discussions and has already been discussed in detail in Chapter III. As a reminder, this chapter identified for this configuration the flow range [0.01 to 0.05 m^2/s (Fig.VI.2)] corresponding to nappe oscillations and the associated frequencies (31.25 to 35.5 Hz). In addition, the sound analysis of this reference configuration allowed the definition of an intensity threshold of 80 dB on the mean auto-spectrum above which nappe oscillations are considered uncomfortable and thus undesirable. This threshold value also corresponds to an intensity slightly higher than the intensity of the 4th characteristic phase in the sound intensity evolution graph (presented in Section III.3) as illustrated in Fig.VI.2.

Table VI.1: List of mitigation techniques

Projecting elements				
N°	Characteristics			
	Diameter ϕ (cm)	Height H (cm)	Spacing s (cm)	Position (see Fig.VI.1)
PE1	2	1.5	10	1
PE2		2.5		
PE3		3.5		
PE4		4		
PE5		2.5	20	
PE6		4		
PE7		4	40	
PE8		4	80	
PE9		4	10	2
PE10		8	20	
PE11		4	20	3
PE12		8		

Deflectors			
N°	Characteristics		
	Length L (cm)	Width W (cm)	Spacing s (cm)
D1	5	50	100-200
D2	10		
D3	15		
D4	5	20	20
D5	5	30	30

Step			
N°	Characteristics		
	Length L (cm)	Height H (cm)	Width W (cm)
S1	10	5	345

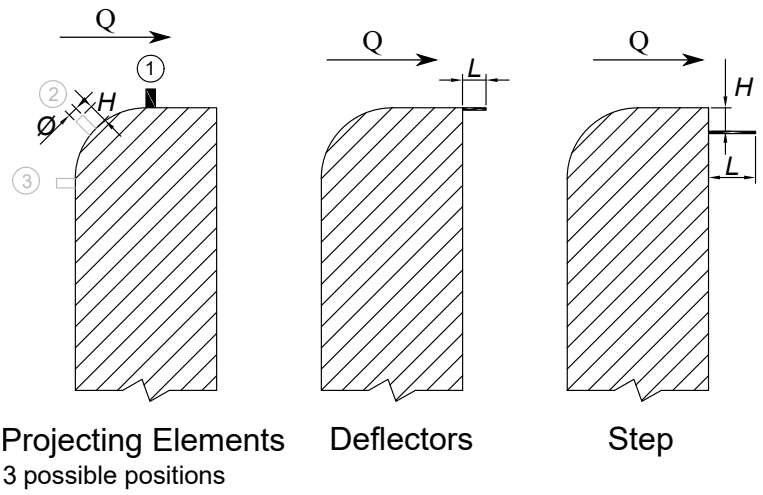

Figure VI.1: Cross section of the weir with the three mitigation techniques

Based on the study made for this reference configuration, the 18 configurations (listed in Table VI.1) were first systematically tested for discharges generating the most intense noise disturbances, i.e., 0.03 m^2/s, 0.04 m^2/s and 0.05 m^2/s. Then, the optimized countermeasure of each type (projecting element, deflectors and step) was tested over the whole range of discharges from 0.01 to 0.06 m^2/s.

VI.2.2.2 Projecting elements (PE)

Projecting element parameters that were optimized included: element location, spacing, and height. The first optimization stage of the projecting elements countermeasure identified the minimum required element height for a specific spacing, i.e., 10 cm, and position 1, i.e., downstream of the curved portion of the crest profile (Configurations PE1 to PE4). The sound analysis for these 4 element heights showed that elements at least 2.5-cm high (PE2) are necessary to mitigate the nappe oscillations. Fig.VI.2a illustrates the maximum sound intensity extracted from the mean auto-spectrum and shows a large decrease of this value, below the intensity threshold of 80 dB, for configurations PE2, PE3 and PE4. In addition, image analysis did not detect any regular horizontal bands as illustrated in Fig.VI.3. Results for PE1 are close to those for Configuration A.

Subsequently, the spacing was optimized for a fixed height (Configurations PE5 to PE8). Experimental results clearly show that element spacing affects the minimum required element height. Fig.VI.2b shows that a 2.5-cm projection height is not sufficient when the spacing is greater than 10 cm. In addition, it appears that for a spacing of 20 cm, a 4-cm tall projecting element is required

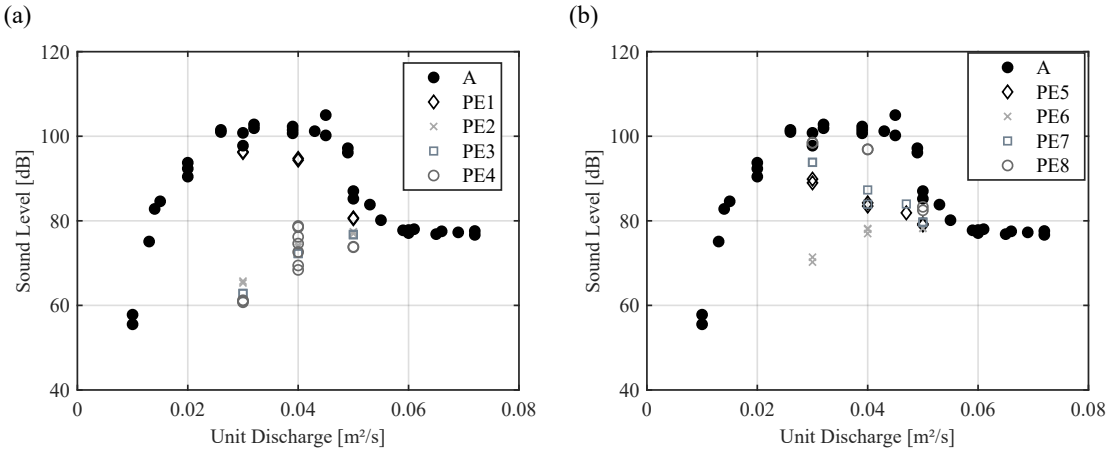

Figure VI.2: Results of sound analysis for Configurations (a) PE1 to PE4 and (b) PE5 to PE8

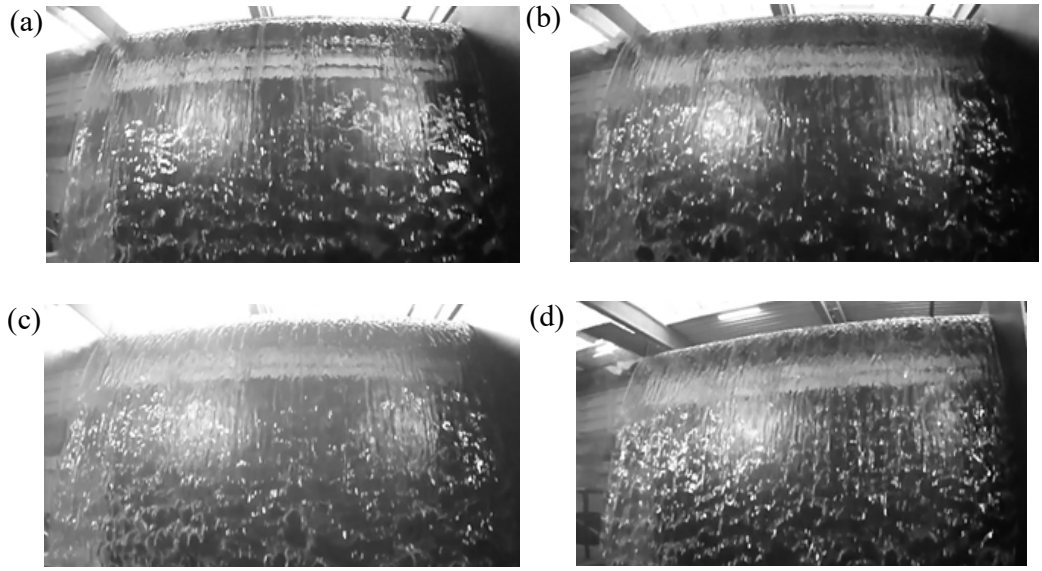

Figure VI.3: Nappe wave characteristics at $q = 0.03$ m²/s for Configurations (a) PE1, (b) PE2, (c) PE3 and (d) PE4

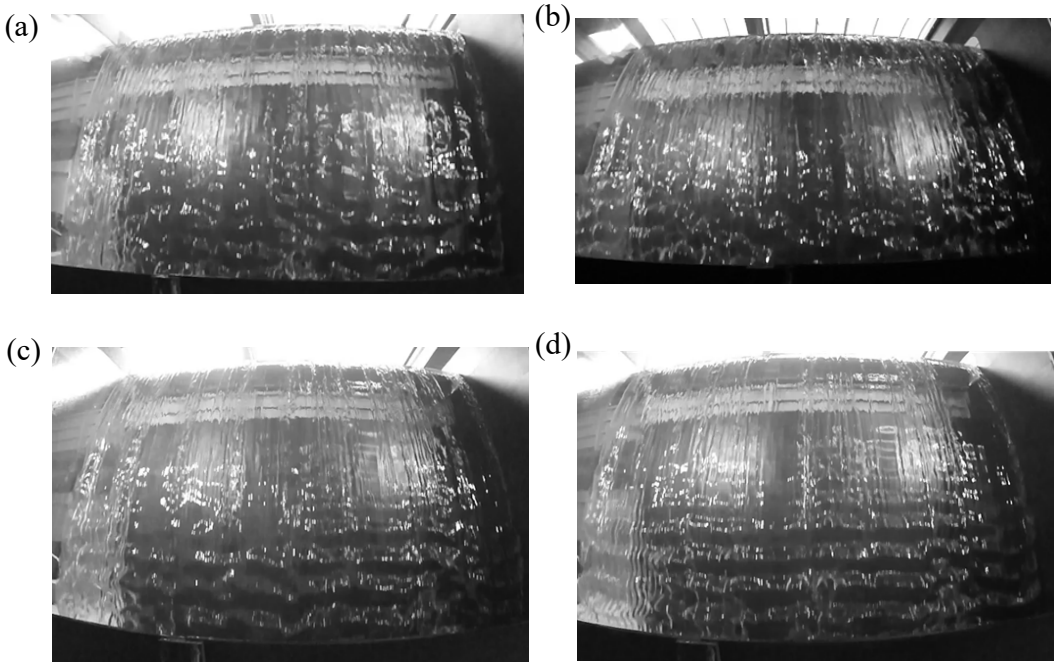

Figure VI.4: Nappe wave characteristics at $q = 0.03$ m^2/s for Configurations (a) PE5, (b) PE6, (c) PE7 and (d) PE8

which is the largest tested height (maximum height was limited based on potential for debris collection). The scope of this study did not investigate the required element heights for spacing greater than 20 cm. Flow visualization for these configurations is consistent with the sound analysis results as horizontal bands are detected for the configurations PE7 and PE8 (Fig.VI.4).

Finally, in order to reduce the potential for debris collection, two additional positions, i.e., positions 2 and 3 respectively in the middle and upstream of the curved portion of the quarter-round crest, were tested (Configurations PE9 to PE12). The results from these experiments are illustrated in Fig.VI.5a. This graph shows that unfortunately these configurations were relatively ineffective in reducing or eliminating nappe oscillations. In spite of significant reduction of the maximum intensities of the mean auto-spectrum for the Configuration PE10, these measurements are over the intensity threshold. The inefficiency of the projecting elements in positions 2 and 3 gives credence to the hypothesis that the nappe oscillations are initiated at the nappe detachment point from the crest and may be affected by the boundary layer development. The effect of the projecting elements in position 2 and 3 on the developing boundary layer and flow structure may be minimal or vanish before the flow passes over the crest and to the point of nappe detachment, and thus this configuration is ineffective. On the contrary, for the projecting elements in position 1, the effect on the developing

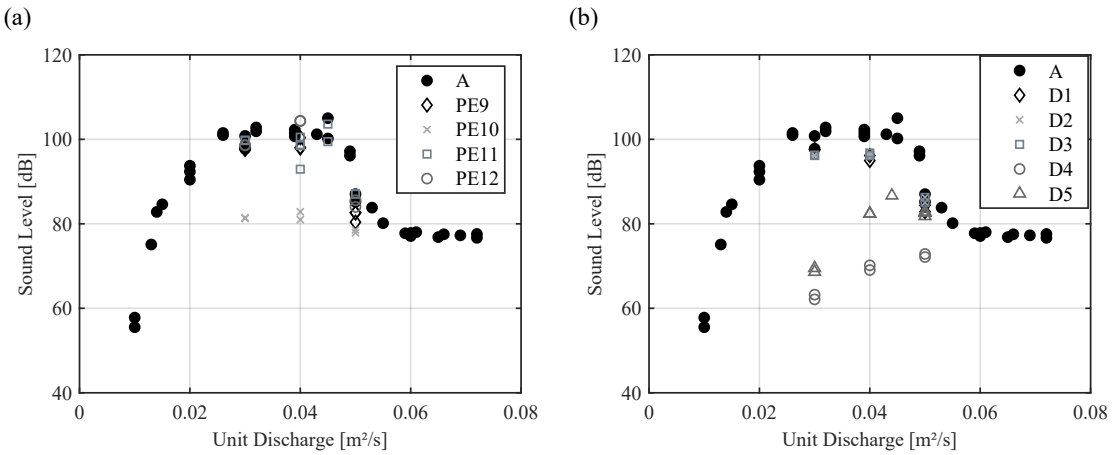

Figure VI.5: Results of sound analysis for Configurations (a) PE9 to PE 12 and (b) D1 to D5

boundary layer and flow structure occurs close enough to the detachment point to mitigate the oscillations development.

Therefore, from this test matrix Configuration PE6, i.e., 4-cm high projecting elements, 20-cm spaced and placed downstream of the curved portion of the crest, was chosen as the optimized projecting elements countermeasure.

VI.2.2.3 Deflectors (D) and downstream step (S)

Initial deflector experiments focused on a single deflector 50-cm wide with streamwise lengths of 5, 10 and 15 cm, located 1.0 m from the right side of the weir and 1.96 m from the left (Configurations D1 to D3). Then, considering the results gained with this single deflector as well as the projecting elements results, 5-cm long deflectors with widths of 20 cm and 30 cm, were tested with a spacing equal to the deflector width (Configurations D4 to D5). The results of these experiments are illustrated in Fig.VI.5b. For Configurations D1 to D3, the maximum intensity of the mean auto-spectrum exceeds 90 dB and is therefore higher than the intensity threshold. In addition, horizontal bands are clearly visible (Fig.VI.6 a,b) for these configurations and the associated frequencies (31.5 to 33.8 Hz) are comparable to those obtained for the reference configuration (Configuration A). In contrast, noise production decreased for Configurations D4 and D5. However, for Configuration D5, two of the three tested q produced sound intensity higher than 80 dB (Fig.VI.6d). Although horizontal bands were visible on the 20-cm wide nappe (Fig.VI.6c), Configuration D4 did not generate acoustic pressure waves. This deflector configuration (5-cm long, 20-cm wide, 20-cm spaced) is therefore the preferred tested combination herein.

Finally, a continuous small downstream step located along the entire length

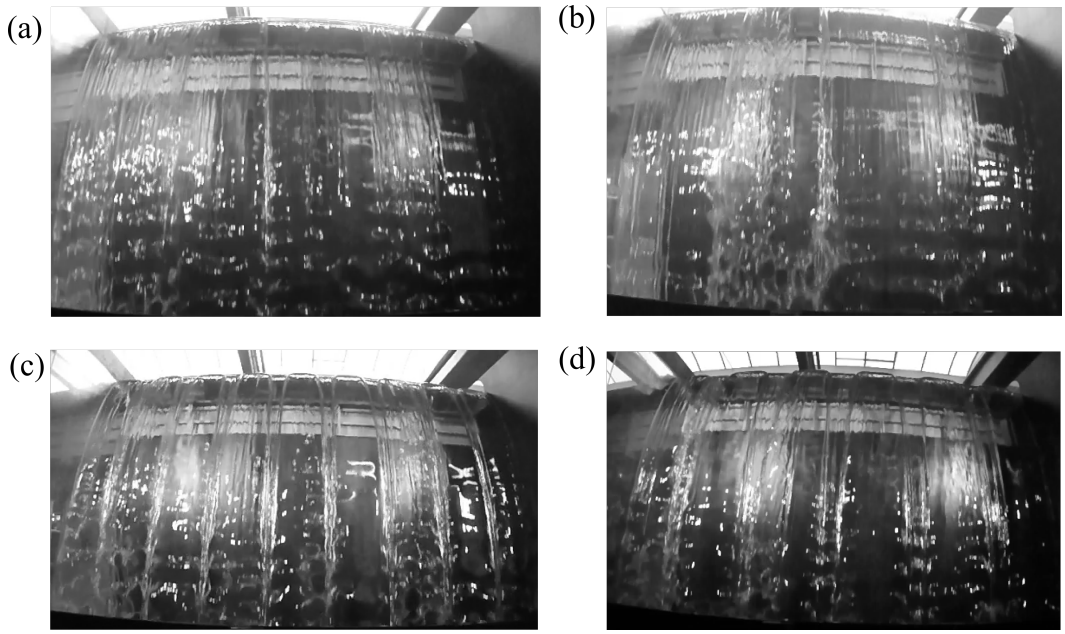

Figure VI.6: Nappe wave characteristics at $q = 0.03$ m^2/s for Configurations (a) D1 (b) D3, (c) D4 and (d) D5

of the weir was attached to modify the boundary layer and nappe trajectory. This step was designed to be impacted by the nappe for q between 0.01 and 0.05 m^2/s. Fig.VI.7 shows the measured lower and upper nappe trajectories for $q = 0.01$ m^2/s and $q = 0.05$ m^2/s as well as the designed 5-cm high and 10-cm long step. This step modified the nappe trajectory and increased the turbulence of the flow in the range of q affected by the oscillations. For q higher than 0.06 m^2/s, nappe trajectory was not impaired by the step.

The experimental results with a downstream step are illustrated in Fig.VI.8 for $0.01 \leq q \leq 0.06$ m^2/s. This mitigation technique is simple and was found to be highly effective. For the same flow range, the sound intensities of the optimal projecting element and deflectors configurations i.e., Configurations PE6 and D4, were also plotted for comparison in Fig.VI.8. It shows that the sound intensity decreases for the downstream step and the deflectors are of the same order and slightly lower for the projecting elements between 0.03 and 0.05 m^2/s.

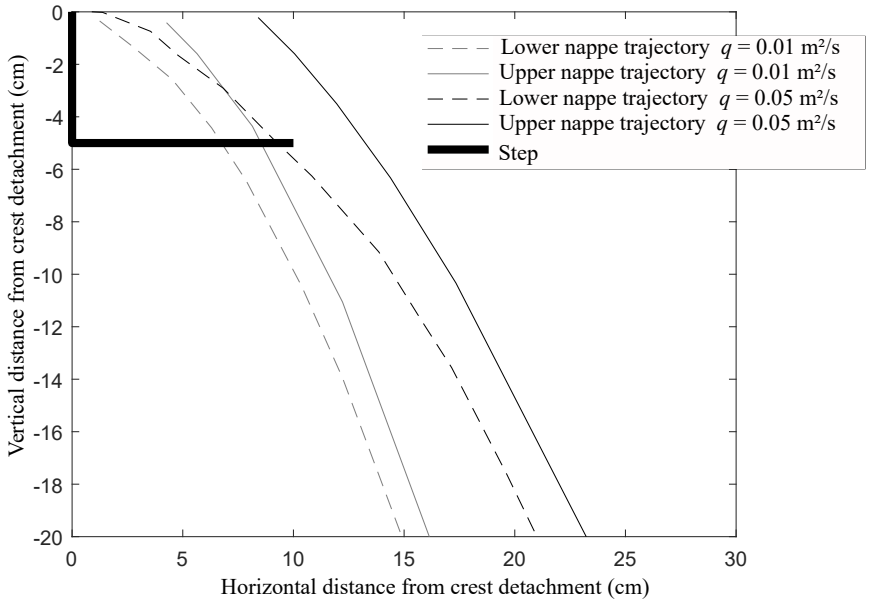

Figure VI.7: Lower and upper nappe trajectories for $q = 0.01$ m^2/s and $q = 0.05$ m^2/s and designed step (S1)

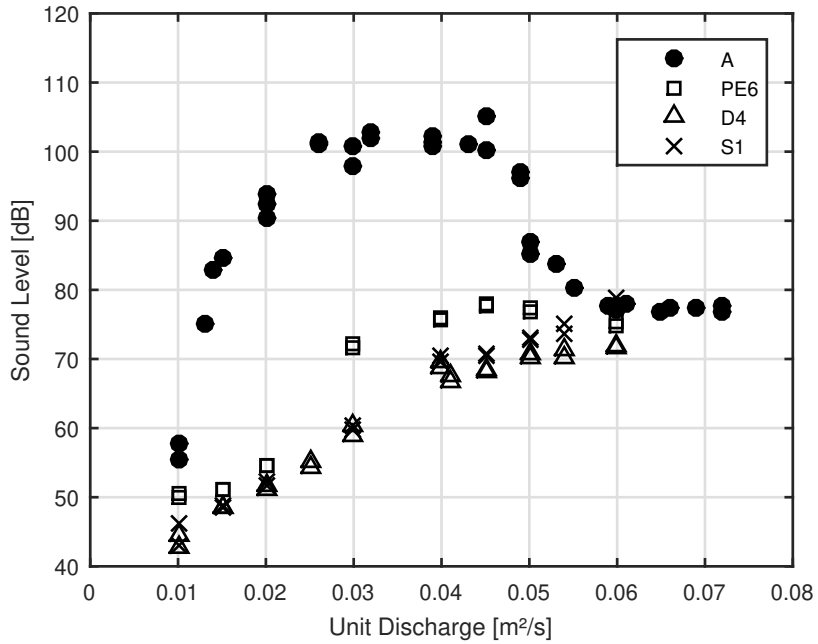

Figure VI.8: Results of sound analysis for the reference configuration (Configuration A) and the 3 optimized mitigation techniques (Projecting elements - PE6, Deflectors - D4 and Step - S1)

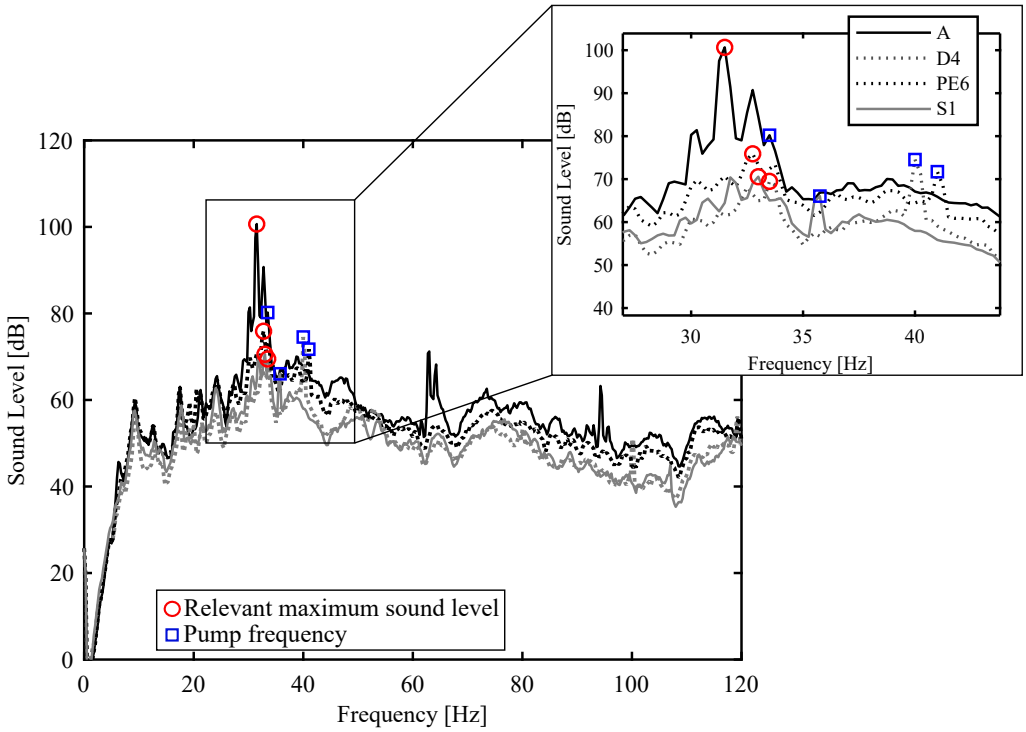

Figure VI.9: Mean auto-spectrum for Configurations A, PB 6 - projecting elements, D4 - deflectors and S1 - step, at q =0.04 m^2/s. Circle is the relevant maximum in sound level and rectangle is the pump frequency imposed during the test.

VI.2.3 Discussion

Feasible crest modification mitigation solutions that reduce the sound production related to nappe oscillations have been investigated herein. This decrease is illustrated in Fig.VI.9 for $q = 0.04$ m^2/s. It shows that the countermeasures decreased the intensity of the peak from 100 dB to 75 dB, 70 dB and 69 dB, respectively for the projecting elements (PE), deflectors (D) and step (S) configurations. In addition to this decrease of the peak intensity, a decrease of the integral of the spectrum was measured and thus supported the effectiveness of the crest modification mitigation solutions.

Fig.VI.10 illustrates nappe wave characteristics for the reference configuration (Configuration A) and the three effective mitigation techniques at $q = 0.03$ m^2/s. Although clear continuous horizontal bands were detectable for Configuration A, it was observed that these bands were disrupted and not synchronized for the projecting elements and downstream step. For these effective configurations, the noise production was also decreased. This decrease is linked to the disorganization of the oscillations along the weir crest. In contrast, the use of deflectors

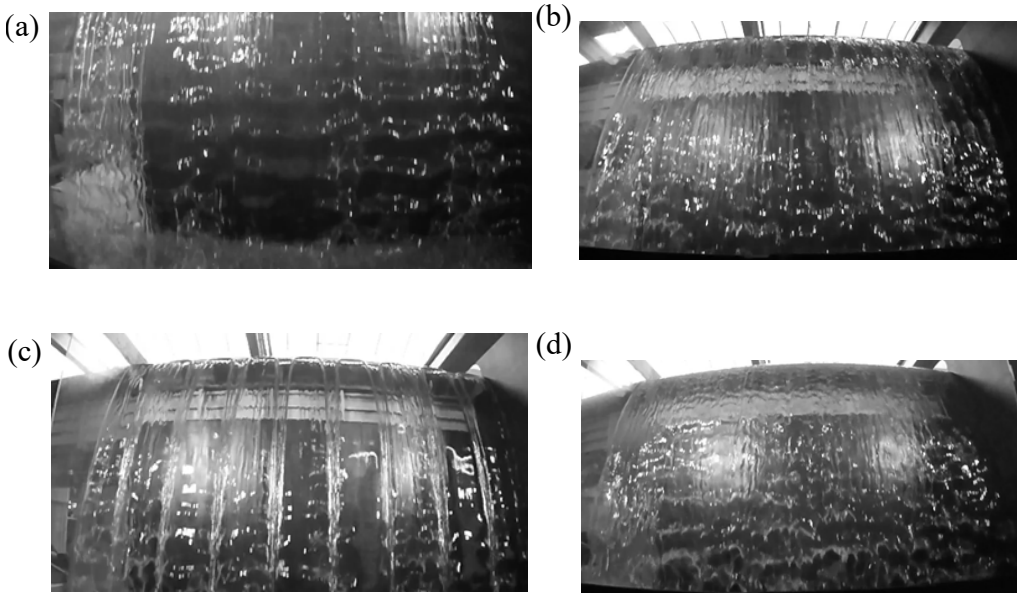

Figure VI.10: Nappe wave characteristics at $q = 0.03$ m^2/s for (a) Configuration A, (b) PE6 – Optimal projecting element configuration, (c) D4 – Optimal deflector configuration and (d) S1 – Step configuration

divides the nappe into several parts along which horizontal bands can be identified. In this case, the application of the image analysis detected frequencies between 31.25 and 32.5 Hz, identical to frequencies detected for Configuration A. There are thus nappe oscillations despite the presence of the deflectors, but they are not synchronized on each segmented nappe section and do not generate sufficient sound energy to create noise disturbance. Consequently, the noise disturbance created by nappe oscillations requires organized oscillations of a sufficient longitudinal length (parallel to weir crest).

The application of the image analysis on the configurations considered as non-effective provided frequencies between 31.4 and 33.8 Hz, for 0.03 m^2/s and 0.04 m^2/s (Table VI.2). The frequencies, associated with image analysis, are identical to sound frequencies and to the ones without mitigation techniques. This outcome shows that the presence of projecting elements or deflectors does not modify the oscillations frequency when oscillations occur.

The discharge capacity of a weir being a key parameter for the dam's safety, the hydraulic efficiency of the three optimized mitigation techniques was analyzed. The water level was measured at 7 locations along the crest width, spaced 0.5 m apart, and positioned 0.65 m upstream from the downstream end of the crest (Section II.3.4).

Table VI.2: Nappe oscillations frequencies extracted from image and sound analyses

Configurations	q (m^2/s)	Frequency (Hz)	Configurations	q (m^2/s)	Frequency (Hz)
A	0.03	31.25-33.5	PE10	0.03	33.5
	0.04	31.5		0.04	32.75
	0.05	31.5-32.75		0.05	32.75
PE1	0.03	33.5	PE11	0.03	33.5
	0.04	33.25-33.5		0.04	31.5-32.75
	0.05	32.75		0.05	32.75
PE5	0.03	33.5	PE12	0.03	33.5
	0.04	32.75-33.5		0.04	32.75
	0.05	32.75		0.05	32.75
PE7	0.03	33.75	D1	0.03	33.5
	0.04	32.75		0.04	31.5
	0.05	32.75-33		0.05	31.5
PE8	0.03	33.75	D2	0.03	33.5
	0.04	33.25		0.04	32.75
	0.05	32.75		0.05	32.75
PE9	0.03	33.5	D3	0.03	33.75
	0.04	32.75		0.04	32.75-33.75
	0.05	32.75		0.05	32.75

The discharge coefficient of the weir was calculated as follows:

$$C_d = \frac{Q}{\sum_{i=1}^{7} l_i \sqrt{2gH_i^3}}$$

where Q is the total discharge, l_i the distance attributed to the sensor i (i.e., 0.5 m) and H_i the upstream head at the sensor i, calculated as $H_i = h_i + \frac{u_i^2}{2g}$ with $u_i = \frac{Q}{L(h_i+z)}$ the flow velocity, h_i the water depth in the reservoir relative to the weir crest measured at sensor i and z the weir height.

The resulting discharge coefficient evolution with the mean upstream head is shown in Fig.VI.11 for the reference configuration (Configuration A) and the three effective mitigation techniques. This figure shows that the discharge coefficient increases monotonously with the upstream head for all configurations. For the range of tested heads (30 to 120 mm), it shows that the use of projecting elements decreased the discharge coefficient from 6.7% to 3.9% with increasing upstream head. For the low heads investigated in this study, the projecting elements impeded the flow and led to a reduction of the weir discharge efficiency. However, this effect decreased with the increasing head as suggested by the trend of the discharge capacity in Fig.VI.11. In contrast to projecting elements, the step did not affect the discharge coefficient for low upstream heads but decreased by 2.5% the discharge efficiency for the highest upstream head. Finally, the discharge coefficient decreased by 2.5% for all tested upstream heads when using deflectors. For the step and deflectors, the trend illustrated in Fig.VI.11 should not continue for higher heads and should be equivalent to the initial or unmodified configuration. In particular, for q higher than 0.06 m^2/s, the configuration with the step should be identical to the initial configuration as no step impact is expected. However, due to discharge limitations of the experimental facility, higher discharges were not tested.

The three mitigation techniques of this research, based upon the constructability in the field, were studied in a controlled environment, i.e., clear water, controlled air temperature, and for a limited flow range. The selection and installation of a crest modification scheme requires multi-disciplinary considerations particularly if the structure is made of reinforced concrete. Special attention is needed regarding the location of the hydraulic structure (populated area, remote location, etc.), frequency of flows with low heads, presence of floating debris and/or ice, accessibility during installation, new construction vs. retrofit, hydraulics, etc. Potential head-discharge relationship modification may also result depending on the selected mitigation strategy (e.g., roughness elements, potential for debris collection). A recent retrofit using a downstream step, that considered hydraulics, constructability, economy and durability is the labyrinth weir of the Linville Dam (USA) shown in Fig.VI.12. The advantage of this approach is that it is simple to design (based upon nappe trajectory), inexpensive compared to other approaches, easy to install, and can be installed as a retrofit if nappe

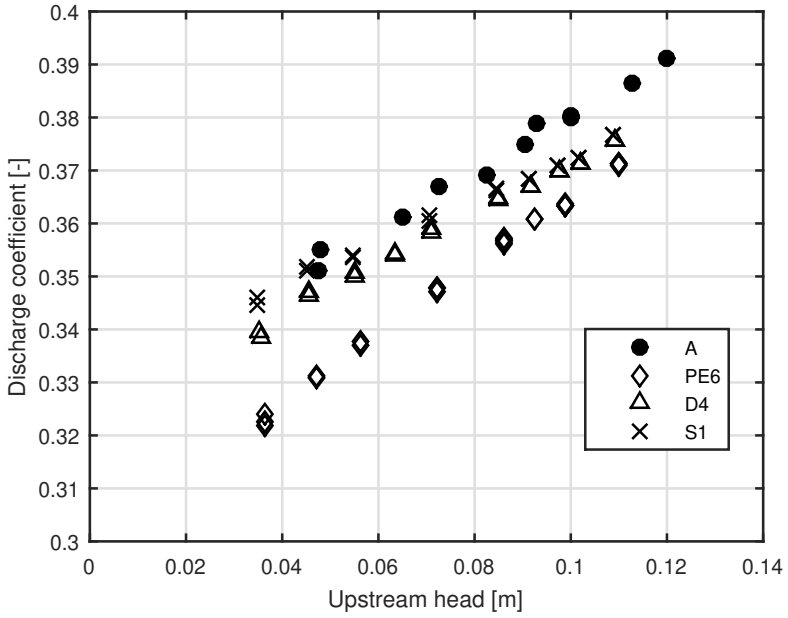

Figure VI.11: Evolution of the discharge coefficient with the upstream head (A - initial configuration, PE6 – Optimal projecting element configuration, D4 – Optimal deflector configuration and S1 – Step configuration)

oscillations problems arise.

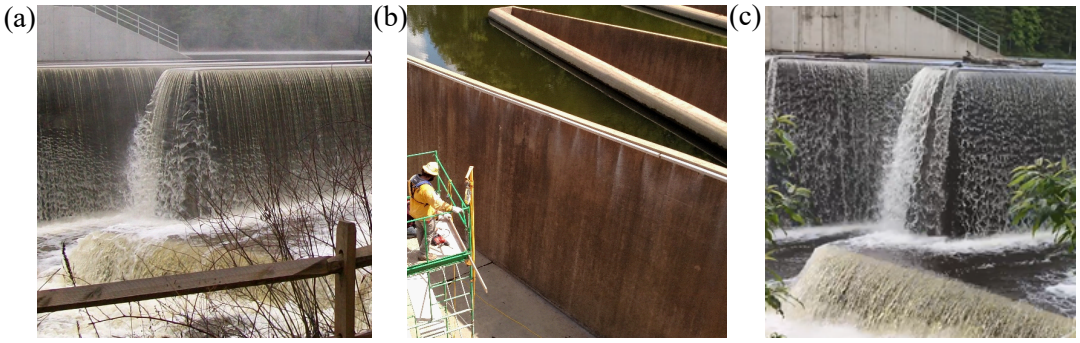

Figure VI.12: Example of successful nappe oscillations mitigation via a small downstream step, pre-fix with oscillations (a), modification installation (b), and post-fix without oscillations (c). Photos courtesy of Schnabel Engineering

VI.3 Risk of nappe oscillations for piano key weirs and inclined apron

In the framework of the thesis, the prototype scale model has been used to assess the risk of nappe oscillations occurrence on PKW (Lodomez et al., 2017). Indeed, most of the documented cases of nappe oscillations in the literature are related to linear and labyrinth weirs. The PKW is a relatively new hydraulic structure (Blanc and Lempérière, 2001) with geometric aspects similar to a labyrinth weir. The risk of nappe oscillations development for PKW could not be neglected and therefore had to be evaluated.

By comparison with linear or labyrinth weirs, two specific geometric parameters of PKW were identified as significant when considering the risk of nappe oscillations occurrence: the width of the downstream crest, i.e., the inlet apex, and the inclined ramp downstream of the linear sidewalls. The influence of the width regarding the nappe oscillations occurrence has been developed in Chapter V and showed that nappe oscillations may appear only if the width is higher than 1 m. Thus, the following sections focus only on the influence of an inclined apron on nappe oscillations development.

VI.3.1 Experimental setup

The experimental facility used was the unconfined prototype scale model (Model 1) equipped with a QR crest profile ($UC - QR1$). The weir width was equal to 2.45 m ($W2$) and an inclined apron, parallel to the crest, with a slope of 1/1.8 positioned at two different elevations, i.e., a fall height varying from 1.65 to 3.00 m (Configuration B1) and another varying from 0.70 to 2.05 m (Configuration B2). This slope of 1/1.8 corresponds to the slope proposed by Hydrocoop (2015) for the inclined ramp of the PKW. The varying fall height was created by the setting up of an inclined wooden plate and is sketched in Fig.VI.13 for Configuration B1.

The effect of the inclined apron on nappe oscillations development was assessed by comparing these two configurations (B1 and B2) with Configuration $UC - QR1 - W2 - L1$, i.e., for a fall height of 3 m, constant over the width.

Once again, the occurrence and characterization of nappe oscillations were determined by means of sound and image analyses following audio and video recordings (Chapters II and III). Sound measurements being performed and analyzed with identical tools (i.e., MC212 and dBFA software) for all tested configurations, maximum sound intensities extracted from the auto-spectra are always reported in dB.

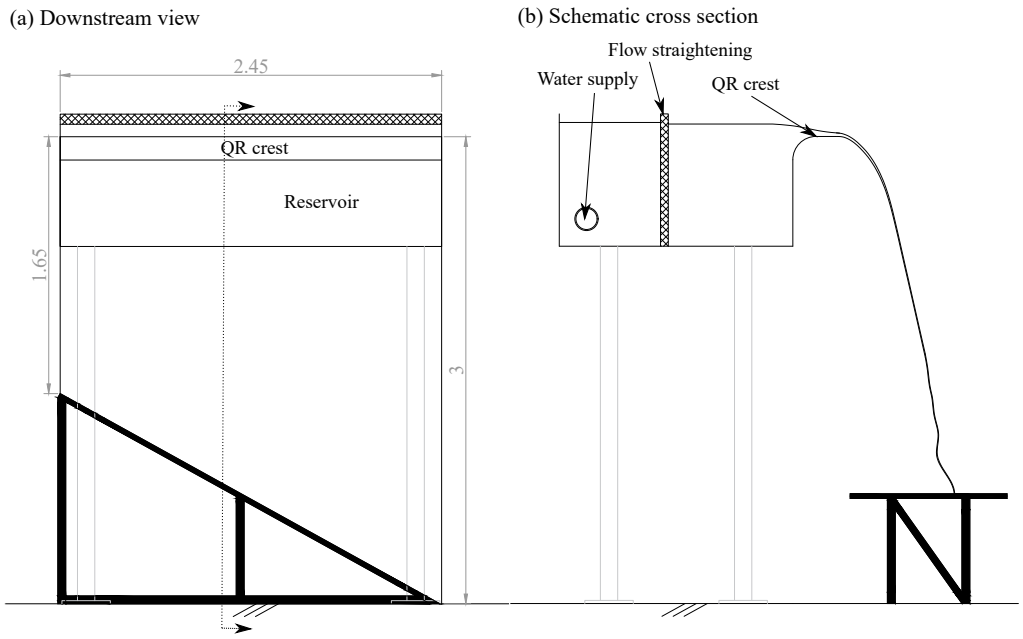

Figure VI.13: Schematic view of the weir equipped with a inclined apron: (a) downstream view and (b) cross section (dimension in m)

VI.3.2 Results and discussions

As mentioned in Chapter V, nappe oscillations were detected for the reference configuration, i.e., $UC - QR1 - W2 - L1$, for q between 0.01 and 0.04 m^2/s. These oscillations are illustrated for various q in Fig.VI.14 while the maximum sound intensities extracted from the mean auto-spectra are reported as a function of q in Fig.VI.15.

For Configurations B1 and B2, no horizontal bands were detected for any of the unit discharges evaluated. Additionally, no high intensity noise production was noted for these cases. These findings are confirmed by the maximum sound intensity extracted from the mean auto-spectrum illustrated in Fig.VI.15. This figure illustrates identical results to those from the optimized mitigation techniques presented previously, i.e., low maximum intensity of spectra that evolves monotonously with the unit discharge. In addition, photographs of the nappe flow are reported in Fig.VI.16 for q affected by nappe oscillations for the case of a horizontal apron. No horizontal band was visually detected and no frequency emerged from the image analysis.

To corroborate this finding, an additional configuration with an inclined apron was tested for the confined model with a THR crest profile and the maximum width of 3.45 m. This configuration, named B3 in the following discussion, corresponds to Configuration $C - THR1 - W1 - L1$ equipped with the inclined apron with a slope identical to Configurations B1 and B2 ($1.1 \leq L \leq 3$ m).

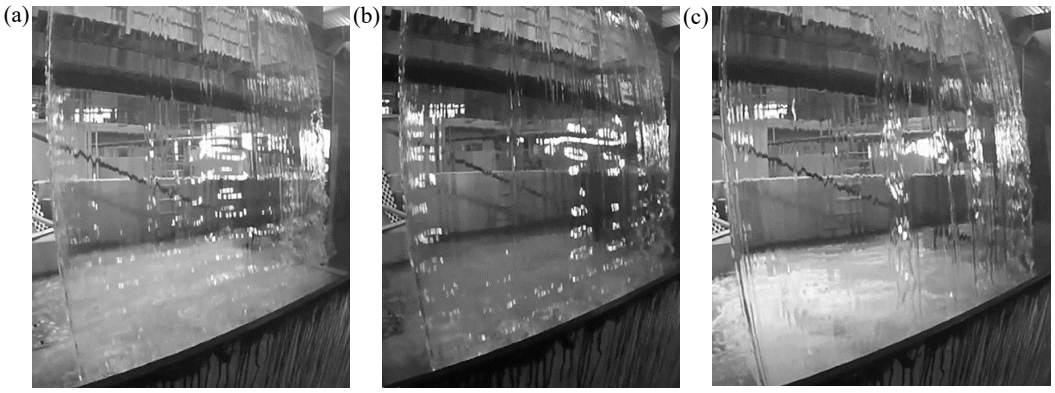

Figure VI.14: Nappe wave characteristics for $UC - QR1 - W2 - L1$ at (a) $q = 0.01$ m²/s, (b) $q = 0.02$ m²/s and (c) $q = 0.03$ m²/s

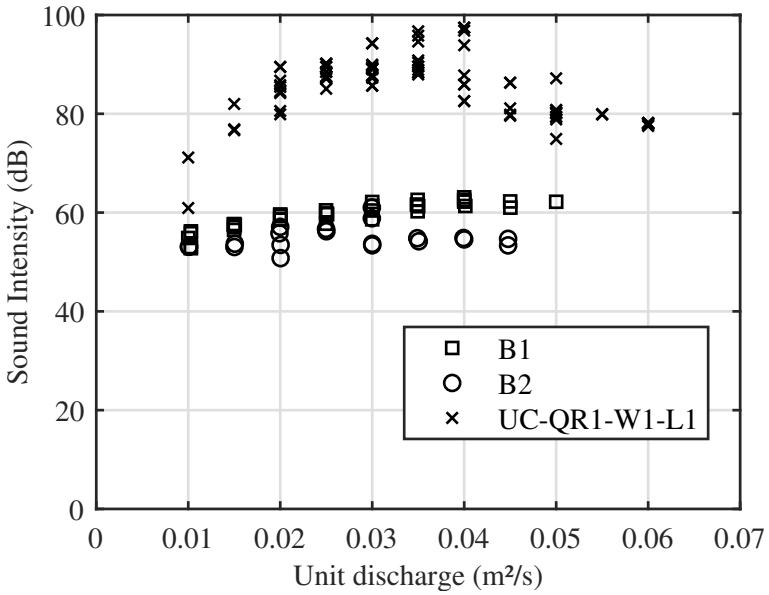

Figure VI.15: Results of sound analysis for the reference configuration ($UC - QR1 - W2 - L1$) and both configurations with inclined apron (Configurations B1 and B2)

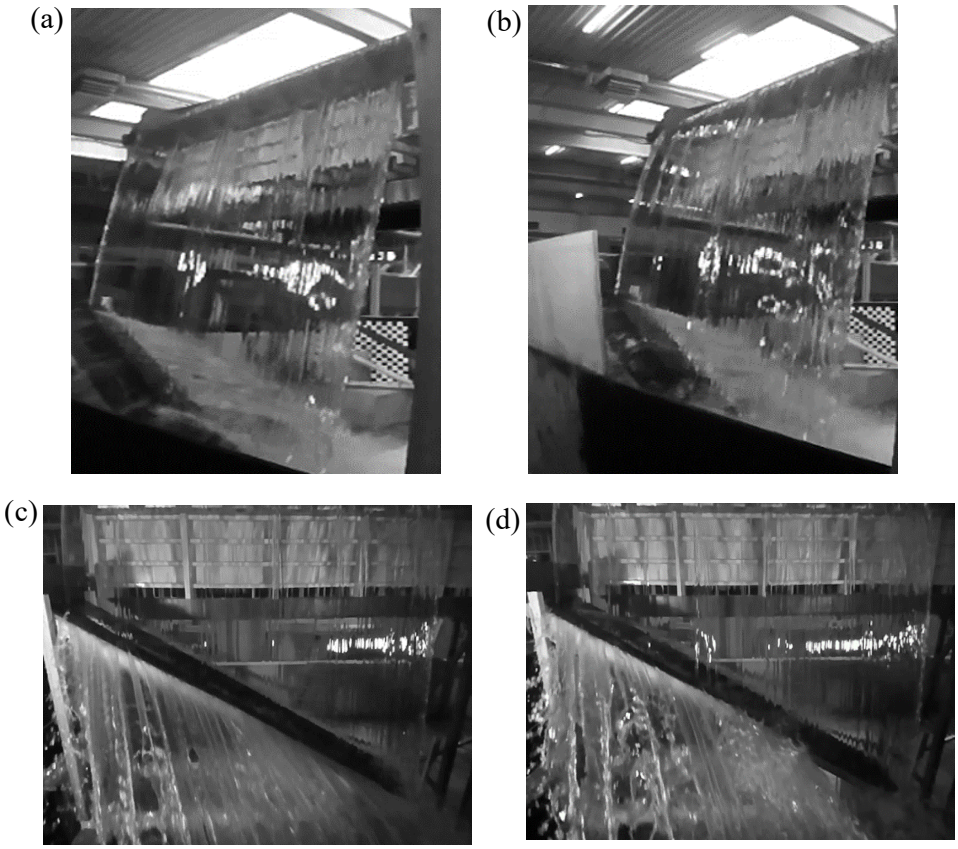

Figure VI.16: Nappe wave characteristics for Configuration B1 at (a) $q = 0.015$ m^2/s and (b) $q = 0.02$ m^2/s and, for Configuration B2 at (c) $q = 0.015$ m^2/s and (d) $q = 0.02$ m^2/s

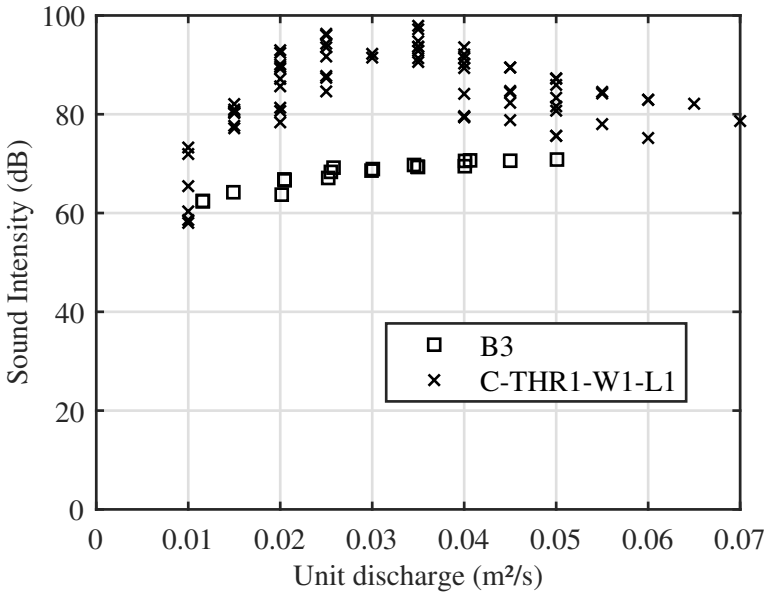

Figure VI.17: Results of sound analysis for Configuration $C-THR1-W1-L1$ and Configuration B3

The maximum sound intensities extracted from the mean auto-spectra for the reference configuration ($C-THR1-W1-L1$) and Configuration B3 are reported in Fig.VI.17 as a function of q. This figure confirms the findings already made for Configurations B1 and B2, namely the disappearance of the nappe oscillations for a nappe impacting an inclined apron with a slope of 1/1.8 (parallel to the crest).

This finding is in accordance with the results present in Nagamine et al. (2011) that showed the suppression of nappe oscillations by setting an inclined board (slope of 1/2.95) at the lower end of the falling sheet to modify the impact conditions. The use of an inclined plate (steel covered with rubber) was even implemented on site for a gate and proved its effectiveness. To the knowledge of the author, this mitigation technique was never installed for weirs. This may be explained by the fact that, this mitigation technique was relatively unknown to date. In addition, more studies are required to improve the characterization and evaluation of the effectiveness of this solution. Indeed, there should be a minimum slope required to avoid the oscillations, of which the evaluation would be valuable for designers and contractors. As with the other mitigation techniques tested herein, a complete technique analysis would require multi-disciplinary considerations regarding cost, ease of installation and durability.

Finally, the disappearance of nappe oscillations due to an inclined apron should be kept in mind when looking at a theory to explain the nappe oscillations phenomenon.

VI.4 Conclusions

The nappe oscillations phenomenon is generally not taken into consideration at the design step of a weir. Therefore, practical mitigation techniques have to be developed to avoid the nuisances generated by this instability phenomenon, considering suitability for retrofits and new construction, ease to construct, durability, hydraulic efficiency and a minimal potential for debris collection.

In the framework of this research, three innovative mitigation techniques were found to be effective regarding noise reduction for the prototype scale linear weir with a QR crest profile (Configuration $C - QR1 - W1 - L1$). The optimized solutions are projecting elements (4-cm high and 20-cm spaced along the crest), deflectors (5-cm long and 20-cm wide with a 20-cm spacing) and a small downstream step (5-cm deep and 10-cm long), continuous along the crest. These solutions proved their effectiveness regarding noise reduction. In particular, deflectors and step provided the maximum noise reduction with a less than 3% reduction in weir discharge efficiency and lower debris blocking risk. A step is perhaps the most economical mitigation technique for existing or new hydraulic structures. Nevertheless, the choice among one of these effective countermeasures will require the analyses of hydraulics, constructability, economy and durability aspects which are specific to the considered site.

Besides these practical considerations, experiments showed that the spacing of projecting elements and deflectors is a fundamental parameter. The efficiency of the downstream step as well as the optimal position of projecting elements also indicated the sensitivity of the nappe vibrations phenomenon to flow conditions at the crest or close to the crest. Finally, the nappe visualization of the optimal mitigation configurations showed waves in the nappe, however the out-of-phase waves that occurred instead of the horizontal banding waves did not produce the disturbing characteristic acoustic wave energy. All these experimental findings could be reflective components regarding the cause and mechanism of the nappe oscillations.

Finally, through the assessment of the risk of nappe oscillations for PKW, the effectiveness of a mitigation technique which does not affect the crest of the weir was found. This mitigation is the setting up of an inclined apron. Even if it would require additional studies for on-site application, this mitigation proved its effectiveness (considering a slope of 1/1.8) for QR and THR crest profiles and weir width of 2.45 and 3.45 m. It is also another key reflective component regarding the cause and mechanism of the nappe oscillations.

Chapter VII

In situ measurements

This Chapter is based on the following article:

Lodomez, M., Bousmar, D., Dewals, B., Archambeau, P., Pirotton, M., Erpicum, S., 2018a. In-situ measurement and mitigation of nappe oscillations : The Papignies and Nisramont dams in Belgium. In: 7th IAHR International Symposium on Hydraulic Structures.

VII.1 Introduction

In the case of flow over a gate, the nappe oscillations have been mitigated for decades by the use of splitters (Naudascher and Rockwell, 1994; Pariset, 1955; Reclamation, 1964; Schwartz, 1966b; Sumi and Nakajima, 1990). Although many of these references assigned the effectiveness of splitters to a sufficient aeration of the air pocket behind the nappe, the literature (Anderson and Tullis, 2018; Falvey, 1980; Sato et al., 2007) as well as the various unconfined and oscillating configurations tested during this research (Chapter V) showed that the aeration does not necessarily prevent the nappe oscillations occurrence. In contrast, the effectiveness of splitters could be assigned to the division of the nappe into narrower nappes as shown in Section V.2.2 by analyzing the impact of the width on the oscillations occurrence.

However, while good practices in flap gate design recommend adding splitters on the crest, some dams with gate(s) are still not or inappropriately equipped with this mitigation technique. In Belgium, oscillations problems have been detected on the flap gates of the recently commissioned Papignies weir on the Dendre River. These oscillations were causing vibrations of the actuators, which could lead to malfunctioning. Similar problems were reported for the down lift gates of the Nisramont weir on the Ourthe River, also in Belgium. For these two prototypes, the Service Public de Wallonie (SPW - DGO2) gave the opportunity to perform in situ measurements using the characterization methods presented in Chapters II and III. The aim of these measurement campaigns was the definition of the range of upstream heads prone to cause nappe oscillations and the quantifiation of the effectiveness of additional splitters to mitigate the problem. This study also allowed the application of the characterization method to prototype cases varying from the experimental model by their geometry and upstream flow conditions. Finally, these campaigns were also undertaken to compare the characterization techniques based on sound and image analyses to other measurement techniques, i.e., acceleration and velocity measurements, that were performed by the Service Public de Wallonie (Bousmar and Libert, 2015, 2017).

In the following sections, Section VII.2 presents the two dams. Section VII.3 introduces the additional measurement tools and the methodology of the tests applied by the SPW during the campaigns. Finally, results are presented and discussed in Section VII.4.

VII.2 Papignies and Nisramont Dams

Papignies dam (Fig.VII.1) is a water level regulating structure on the River Dendre (Belgium) in operation since August 2016. The dam consists of two flap gates 3.885-m high and 8-m wide. Each gate is operated through an actuator asymmetrically placed on the central pile. As illustrated in Fig.VII.2 , the gate

is a thin sheet of metal (15-mm thick) reinforced by a beam structure on the downstream face. Torsional rigidity is provided by a cylinder with a diameter of 0.813 m, located at the gate basis. The gate crest is equipped with splitters every 1.65 m. The width of these splitters varies from 40 mm at the connection with the gate to 100 mm at the free extremity (Fig.VII.2). The mean upstream water level is 23.65 m DNG (Belgian altitude reference system) while the downstream is 21.20 m DNG, which gives a fall height of 2.45 m.

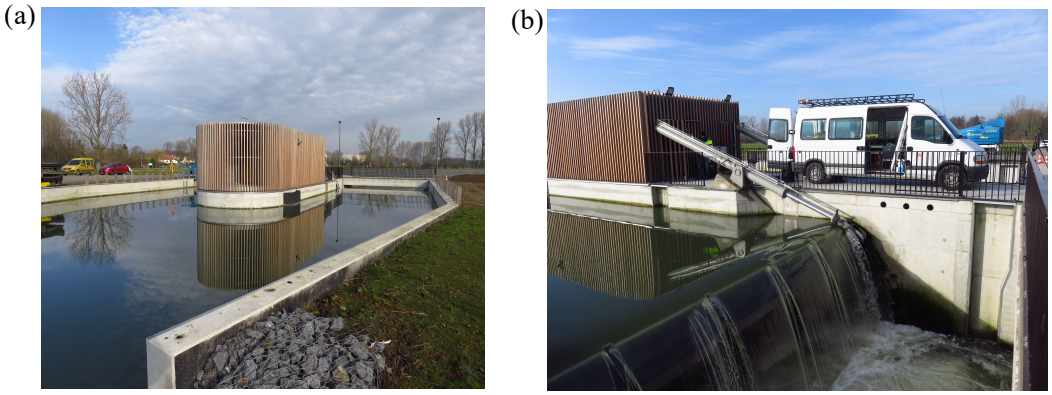

Figure VII.1: Papignies dam: (a) View from upstream, (b) View from downstream

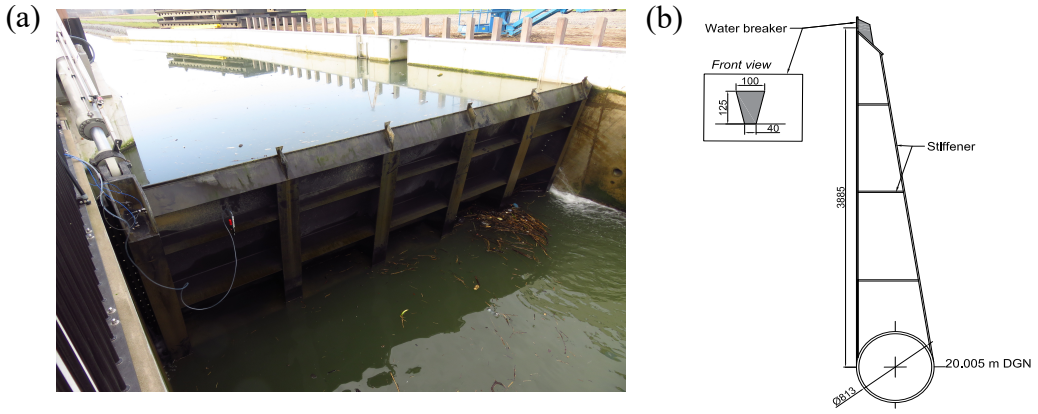

Figure VII.2: Papignies flap gate: (a) View from downstream, (b) Details of the gates, dimension in mm

Nisramont dam (Fig.VII.3) was built in 1958 on the River Ourthe to create a 3.10^6 m^3 reservoir intended for drinking water supply. The spillway is controlled by three down lift gates, also refered to as crest gates, that can be lowered behind a concrete weir. Each gate is 12.5-m wide and 3-m high. The gate crest is profiled

like an arc to complete an ogee profile when the gate is in the lowered position. There is no splitter on the gate crest as illustrated in Fig.VII.3c. The gates are actuated on both extremities with symmetrical cables and pulleys. Nappe oscillations risk was well known by local operators. They managed an uneven position of the gates in order to avoid the occurrence of these oscillations. When the regulation system of the dam was upgraded 5 years ago, the three gates were set to operate at the same level. As a result, low and medium discharges are now equally distributed among the gates and the nappe thickness is reduced. The nappe oscillations occurrence sharply increased with this new operational setup. This observation justified the in situ measurement campaign and the design of splitters.

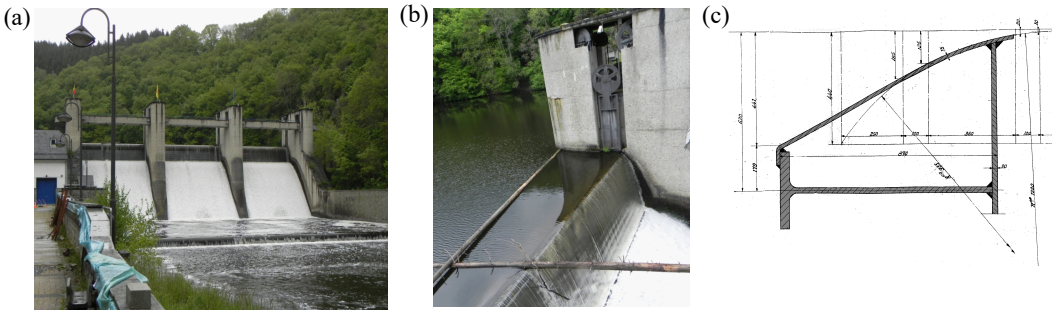

Figure VII.3: Nisramont dam: (a) View from downstream, (b) View of the lifting mechanism, (c) Details of the gate crest

VII.3 Instrumentation and methodology of in situ measurements

To assess the occurrence of nappe oscillations and to characterize them, three types of devices were used during both in situ measurement campaigns. To collect data on structure acceleration, noise production, and visible oscillations of the nappe, a set of accelerometers, a microphone, and a high speed camera were used. Simultaneously, the hydraulic characteristics of the flow were monitored. The gates being identical on each dam, only one gate per dam was instrumented. In Papignies, the in situ measurements were performed in two phases (Bousmar and Libert, 2017). The first one considered the existing configuration (Fig.VII.2). Then, additional splitters were added as illustrated in Fig.VII.4a-b. They were 50-m wide, 125-mm high, and decreased the existing splitters spacing from 1.65 to 0.825 m. The measurement methodologies were identical for both configurations. To investigate the range of upstream heads that generates oscillations, the gate was operated to generate heads between 8 and 74 mm for the existing

configuration while a range between 19 and 103 mm was tested for the configuration with additional splitters. In Nisramont, a first measurement campaign focused on the vibrations of the gate, using only accelerometers (Bousmar and Libert, 2015). Three configurations were tested: without splitters, with temporary splitters spaced 0.95 m apart (Fig.VII.4c) and with temporary splitters spaced 1.95 m apart. The temporary splitters were 50-mm wide and 150-mm high. Flow conditions covered upstream heads between 25 and 230 mm. Acoustic and video investigations were performed during a second campaign. During this second campaign, only the gate without splitter was tested, and upstream heads ranged between 60 and 180 mm.

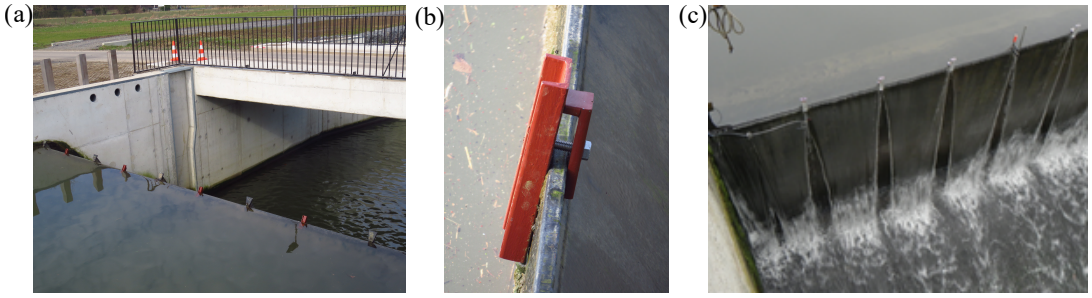

Figure VII.4: Additional splitters: (a,b) on Papignies weir and (c) on Nisramont weir (at 0.95 m spacing)

VII.3.1 Hydraulic characteristics

The upstream and downstream water levels and the actuator/gate crest position were monitored through the dam monitoring system and provided the head at the crest. In addition, an ultrasound distance sensor was added to verify the upstream head measurement during the tests. For each test, measurements were performed continuously for 2 minutes with a sample rate of 1 kHz in Papignies while, a sample rate of 500 Hz and a duration of 1 minute were considered in Nisramont.

VII.3.2 Oscillations characteristics

VII.3.2.1 Sound measurement and flow visualization

To get data on the noise produced by the oscillations, the free-field microphone MC212 was placed in front of the nappe on a bridge at Papignies dam and on the downstream right bank of the stilling basin at Nisramont dam. In addition, the flow visualization was performed with a Go-Pro Hero 4 camera (acquisition rate of 240 Hz) placed in front of the falling nappe.

Sound and image analyses were applied according to the methodology developed in Chapter II. As already mentioned, both analyses supported the detection of the oscillations and provided the magnitude of the noise and its associated frequency (sound analysis) and the frequency of horizontal waves (image analysis).

VII.3.2.2 Accelerometers

At Papignies, two types of monoaxial accelerometers were positioned at the connection between the actuator and the gate: piezoelectric sensors PCB 393B12 (range 0.5g) and capacitive sensors PCB 3701D1 (range 3g). Three sensors of each type were used to obtain data according to the three axes as displayed in the Fig.VII.5. Oscillations characteristics were assessed by the analysis of the standard deviation of the accelerometer measurements, representative of the oscillations intensity around the mean value and on the acceleration spectrum that enables to differentiate periodic vibrations at a clearly identified frequency from a high level noise with no dominant frequency.

In Nisramont, monoaxial accelerometers (PCB 393B12) and velocimeters (Syscom MS2003+) were positioned on both sides of the gate, at the connection between the pulleys and the gate. Accelerations and velocities were recorded along the vertical and the longitudinal (normal to the gate) axes. The analysis of these data was also based on the standard deviation of the measurements.

These measurements were performed, processed and analyzed by the SPW (Bousmar and Libert, 2015, 2017).

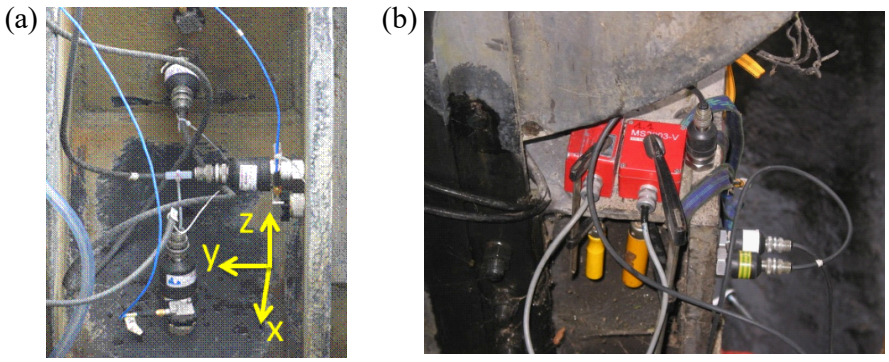

Figure VII.5: Set of accelerometers: (a) Papignies and (b) Nisramont

VII.4 Results of in situ measurements

VII.4.1 Occurrence of nappe oscillations for the existing configuration

VII.4.1.1 Papignies Dam

Based on acceleration measurements, noise analysis, and flow visualization results, nappe oscillations were detected for upstream heads between 20 and 40 mm for the existing configuration. In this range of head, the standard deviation of the acceleration increases significantly and leaves the linear trend as illustrated in Fig.VII.6. This figure illustrates these increases in acceleration for both types of accelerometers, especially in the y-direction (perpendicular to the flow direction). In the same conditions, the maximum sound level of the mean auto-spectrum increases significantly (Fig.VII.6) and is associated with a dominant peak. Horizontal bands were also visible for upstream heads between 20 and 40 mm as illustrated in Fig.VII.7. For lower heads, some oscillations are visible. However, the nappe breaks before impact and the intensity of the acceleration and noise generated are not strong.

The frequencies associated with the noise and horizontal bands are between 21 and 23 Hz. As already observed in Chapter III, sound and image analyses give, for a given head, the same frequency of oscillations (to the uncertainty of the measurements, i.e., 0.25 Hz). In the present measurements, it was additionally possible to confirm that these dominant frequencies are coherent with the spectrum obtained from the gate vibrations measurements. As an example, Fig.VII.8 shows an oscillations spectrum for a head of 30 mm. A significant peak is observed around 23 Hz. Secondary lower peaks are observed around 14 and 21 Hz, while additional large peaks are observed for higher frequency harmonics.

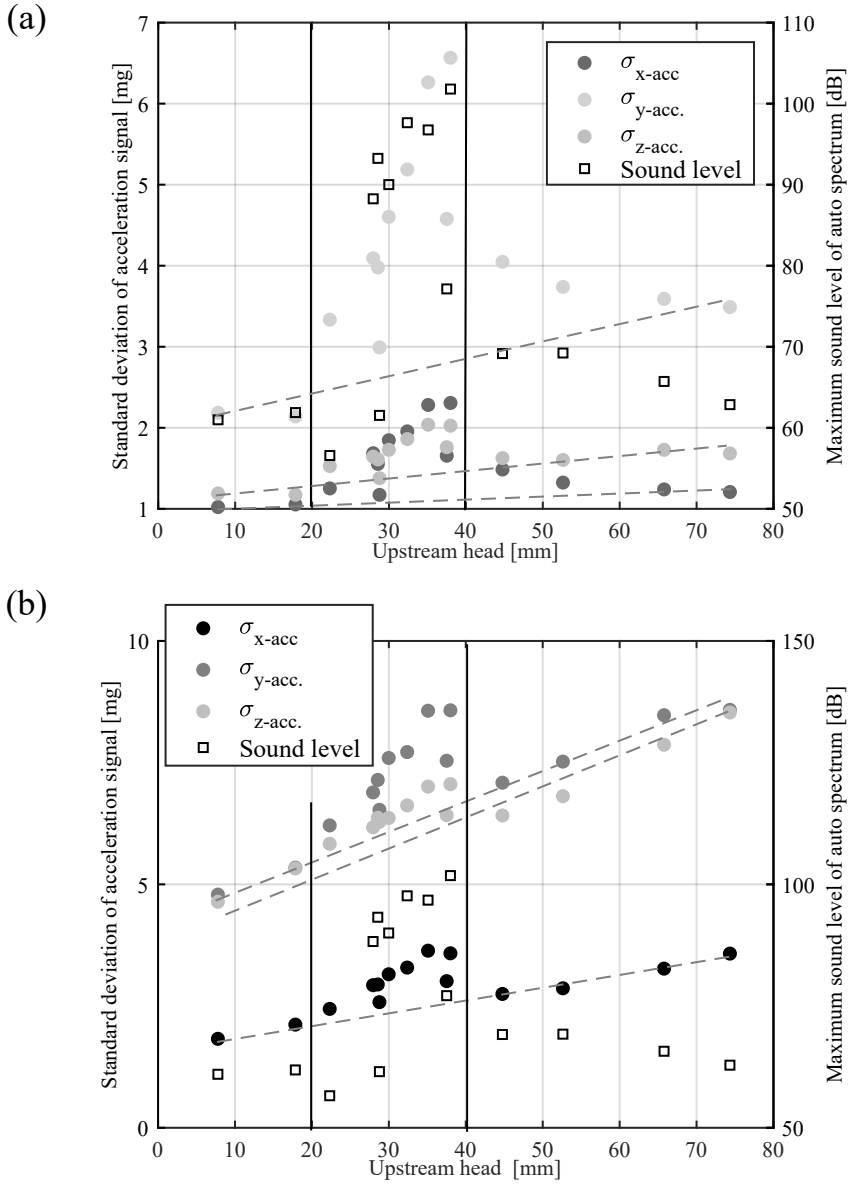

Figure VII.6: Papignies: Standard deviation of acceleration measurement according to x, y and z: (a) for a piezoelectric accelerometer and (b) for a capacitive accelerometer, and maximum sound level of the mean auto-spectrum

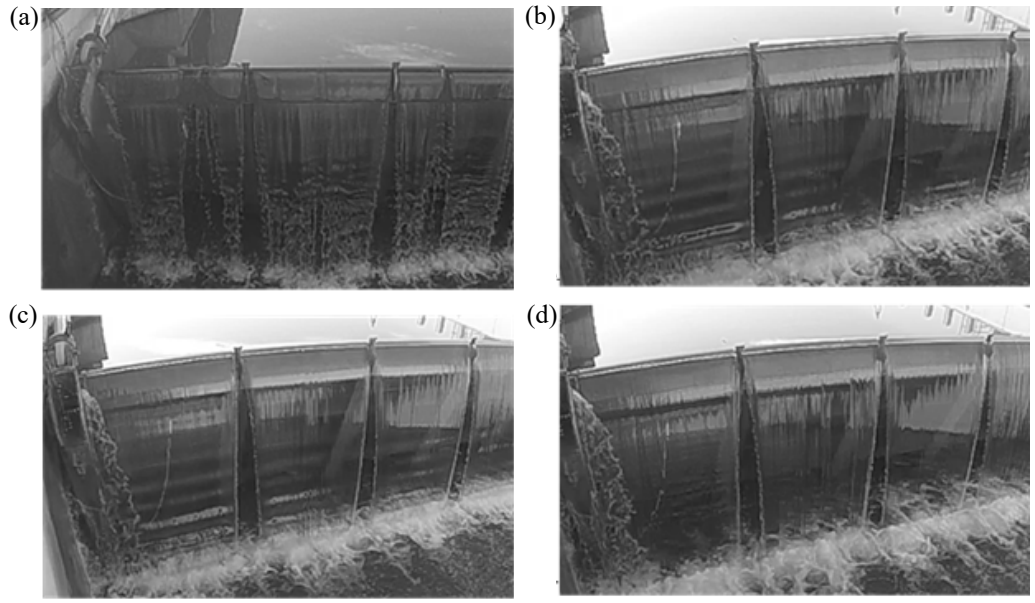

Figure VII.7: Papignies: Flow visualization of the flowing nappe for an upstream head of: (a) 18 mm, (b) 30 mm, (c) 35 mm and (d) 40 mm

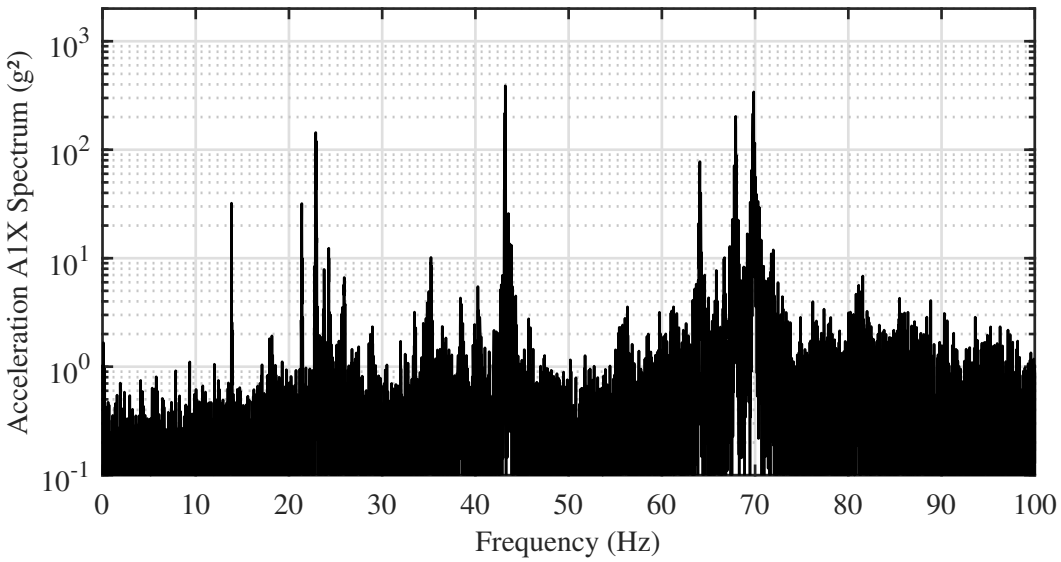

Figure VII.8: Papignies: acceleration spectrum for an upstream head of 30 mm, longitudinal piezoelectric accelerometer

VII.4.1.2 Nisramont Dam

Based on vibrations measurements and flow visualization results, nappe oscillations were detected for upstream heads between 50 and 230 mm, in the case of the existing configuration. Horizontal bands are clearly visible for upstream heads between 50 and 125 mm as illustrated in Fig.VII.9. For upstream heads lower than 30 mm, the thin sheets of water break up. Horizontal bands are visible, especially in the bottom of the nappe, for an upstream head of 50 mm. As the upstream head increases, the visual inception point of the horizontal bands moves higher up the nappe as illustrated for an upstream head of 100 mm in Fig.VII.9c. Finally, from visual observations, the bands tend to decrease for the upstream heads higher than 125 mm. However, severe vibrations were still recorded up to upstream heads as high as 230 mm. As an illustration of these vibrations, Fig.VII.10a shows the amplitude of the horizontal acceleration. A local minimum of the acceleration is observed for upstream heads around 125 mm, corresponding to the vanishing of the visible horizontal bands. Then, for higher heads, vibrations increase again. The analysis of the vibrations spectrum (Fig.VII.10b) shows that the energy of the vibrations for these higher heads is concentrated at frequencies between 14 and 20 Hz in particular for upstream heads higher than 100 mm. For lower heads, the spectrum illustrates higher frequencies. However, it is not clear at this stage if this is still nappe oscillations or another kind of flow/structure instability.

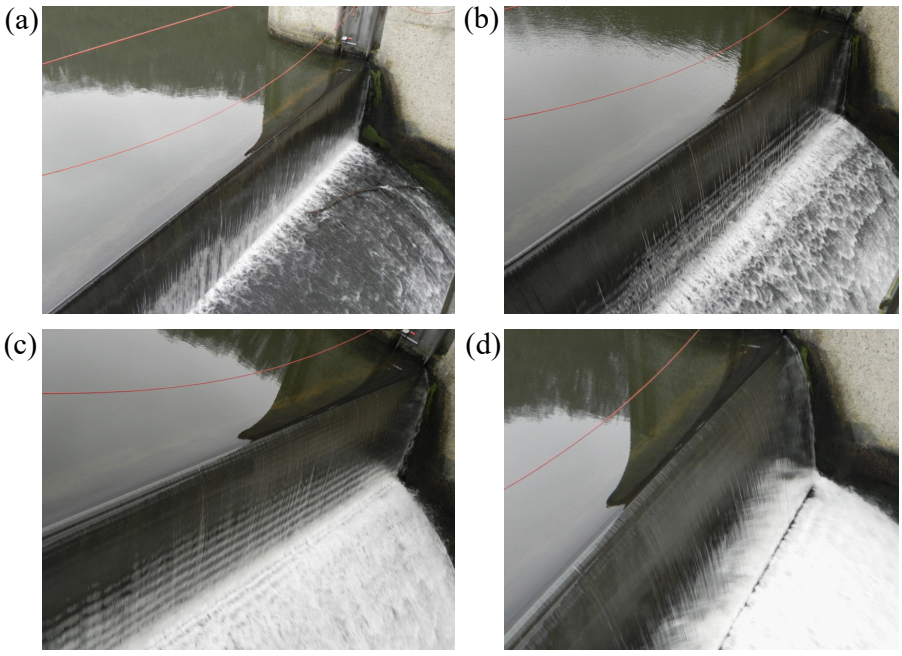

Figure VII.9: Nisramont: Flow visualization for an upstream head of (a) 26 mm; (b) 51 mm; (c) 105 mm; (d) 124 mm

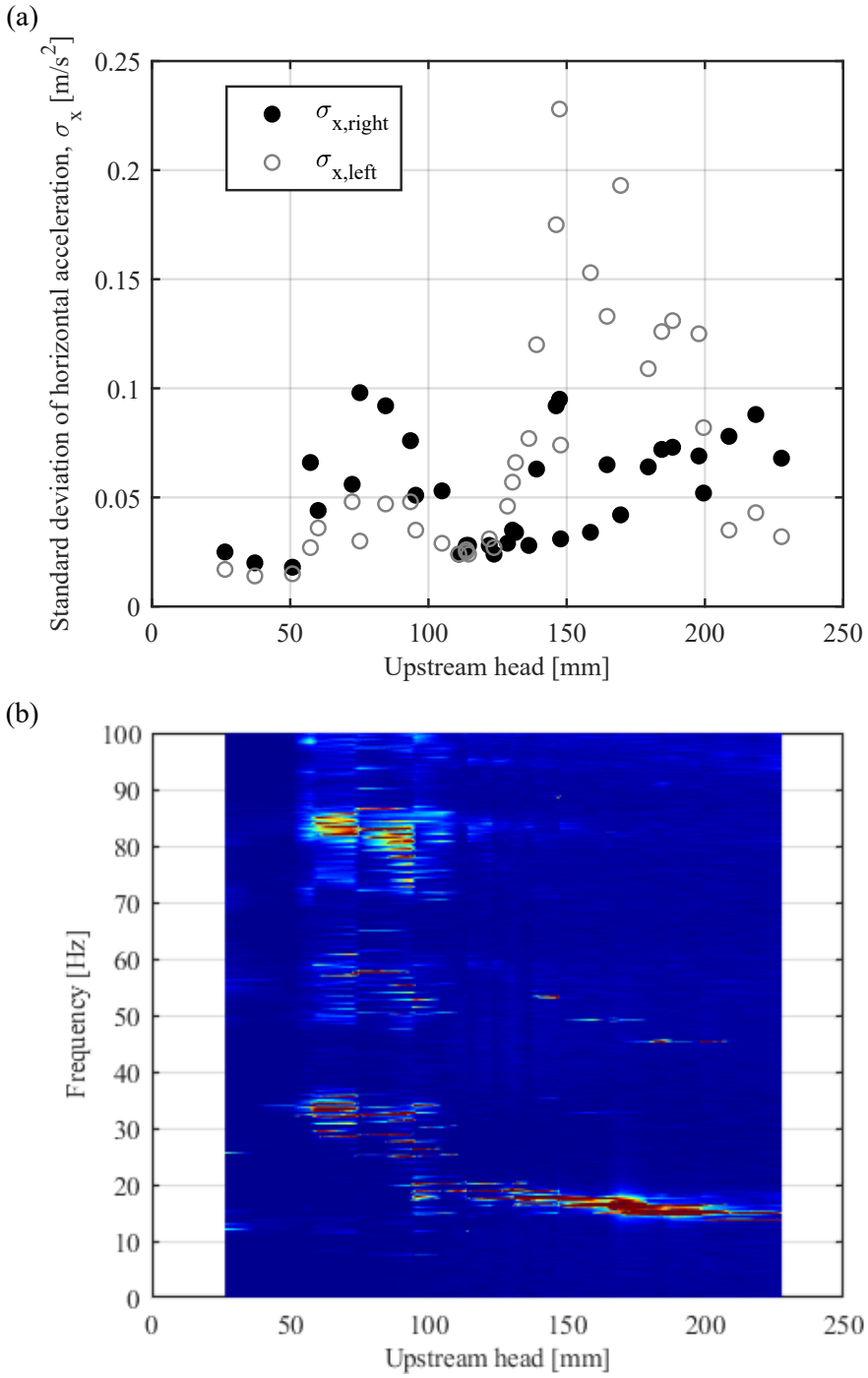

Figure VII.10: Nisramont, acceleration in the longitudinal axis: (a) standard deviation and (b) spectrum

Regarding the sound measurements, a dominant peak was detected in the mean auto-spectrum for upstream heads between 60 and 180 mm. Image analysis also highlights a dominant peak for upstream heads up to 180 mm. The frequencies associated to these vibrations are reported in Fig.VII.11 and compared to the frequencies of the acceleration signals and image analysis. This figure shows that the frequencies are identical whatever the measurement techniques and even if measurements were not recorded during the same test campaign. It also illustrates a decrease of the frequency from 35 to 14 Hz with increasing upstream head. Finally, it confirms that the vibrations recorded for heads larger than 125 mm with an accelerometer are also due to nappe oscillations as their frequencies are identical to those extracted from sound and image analyses.

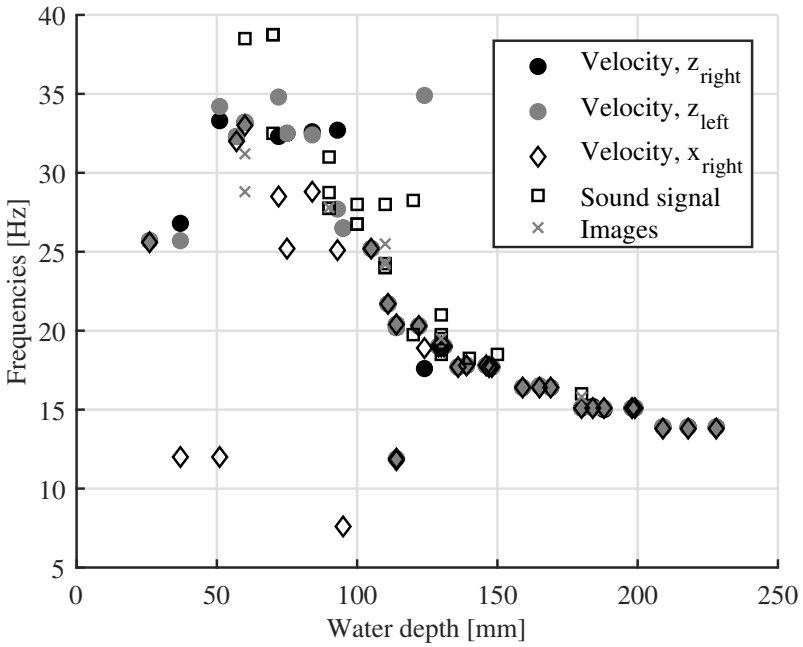

Figure VII.11: Nisramont: Frequencies from sound, image and velocities analyses

VII.4.2 Efficiency of additional splitters

VII.4.2.1 Papignies Dam

The addition of splitters between each existing water breaker prevents the occurrence of nappe oscillations as illustrated in Fig.VII.12. For the whole range of tested upstream heads, this figure shows no increase of the standard deviation of the acceleration and a regular smooth increase of the sound level with the usptream head. In addition, horizontal bands are not visible as illustrated in Fig.VII.13b for upstream heads that initially generated oscillations. However, in

the case of lower upstream heads, nappe oscillations are still visible but do not generate significant noise or acceleration on the actuator.

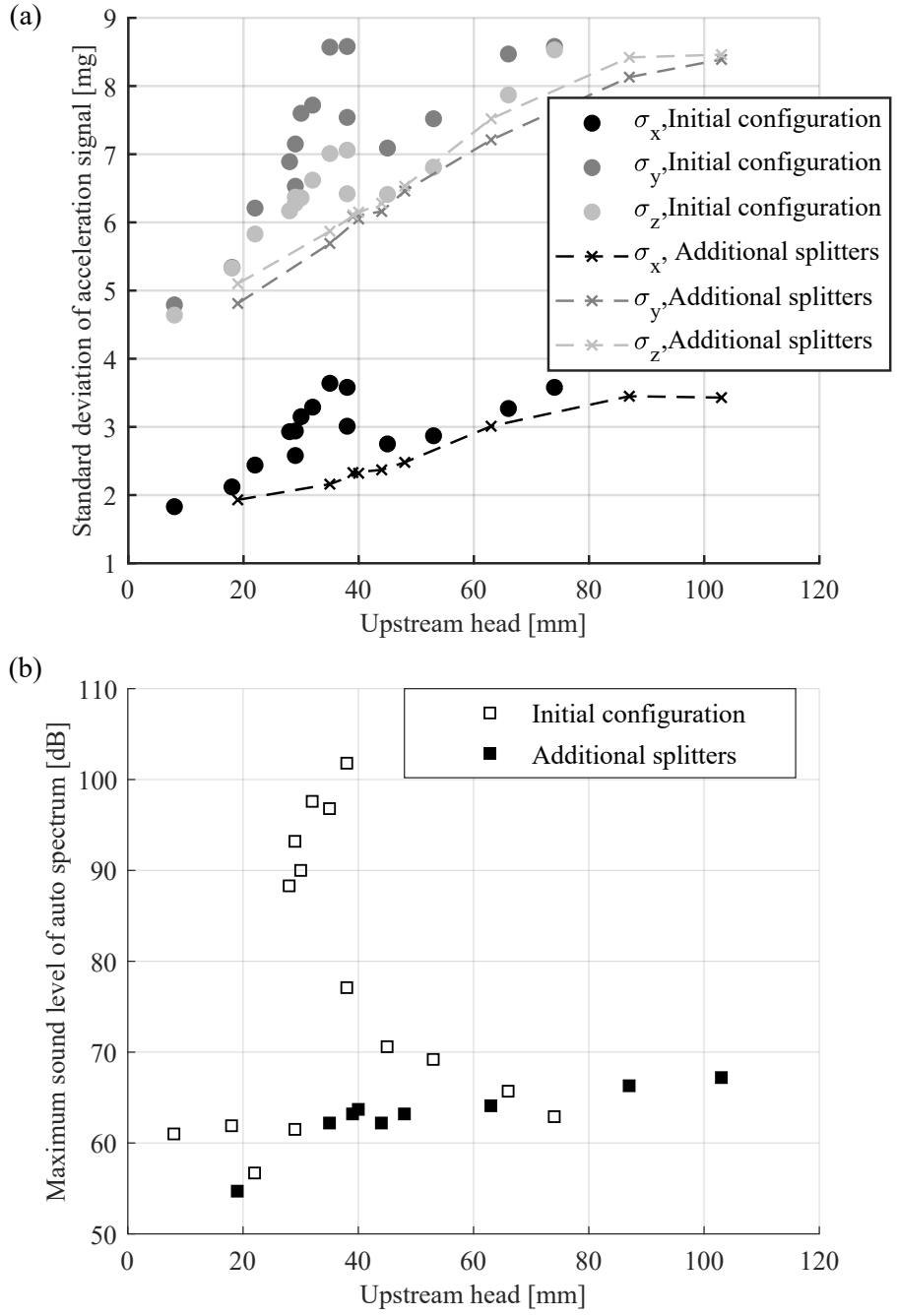

Figure VII.12: Papignies: Impact of additional splitters on (a) the standard deviation of acceleration measurement according to x, y and z (for piezoelectric accelerometer) and (b) the maximum sound level of the mean auto-spectrum

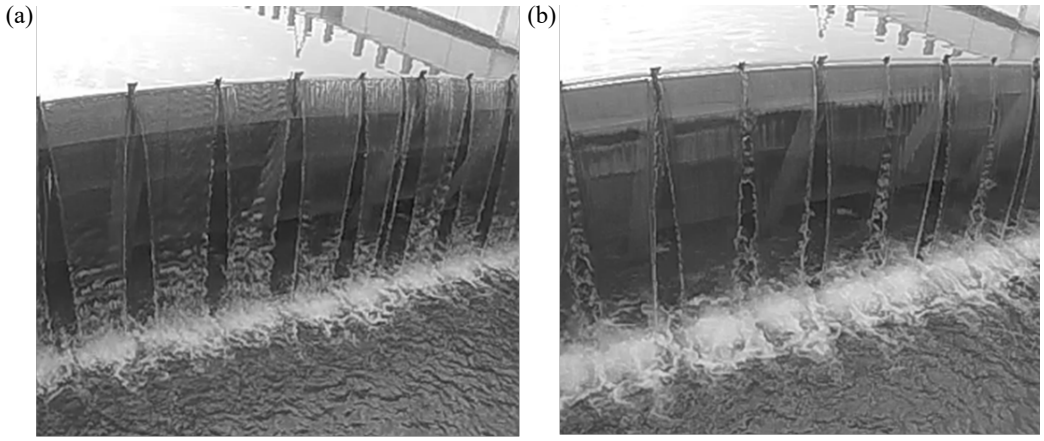

Figure VII.13: Papignies: Flow visualization of the flowing nappe for the configuration with additional splitters and an upstream head of: (a) 18 mm and (b) 35 mm

VII.4.2.2 Nisramont Dam

The addition to the crest of splitters with a spacing of 0.95 m eliminates the occurrence of the nuisance due to nappe oscillations as illustrated by the acceleration measurements in Fig.VII.14. Some horizontal bands are still observed for the lower upstream heads but do not generate significant noise or vibrations.

When increasing the spacing of splitters to 1.95 m, the nappe oscillations were more perceptible. For upstream heads between 40 and 70 mm, significant vibrations were observed as depicted in Fig.VII.14. Accordingly, it was recommended to fix the spacing of the splitters to be installed at 0.95 m.

VII.5 Comparison of nappe oscillations on site and in a controlled environment

In Chapter V, necessary conditions for nappe oscillations occurrence have been developed in the form of a questionnaire. This survey has been filled for Nisramont and Papignies in Table VII.1. The answers to these questions indicate that both case studies satisfied the conditions for nappe oscillations. To justify some of the answers, it has to be mentioned that in Nisramont the crest is clearly profiled as illustrated in Fig.VII.3c while in Papignies, the crest is similar to a sharp crest and its upstream face is supposed profiled considering that this face is the gate itself which does not generate sudden direction change of the flow upstream of the detachment point.

In addition to these conditions, the geometric parameters in terms of fall height and width have to be checked for the existing configurations and the

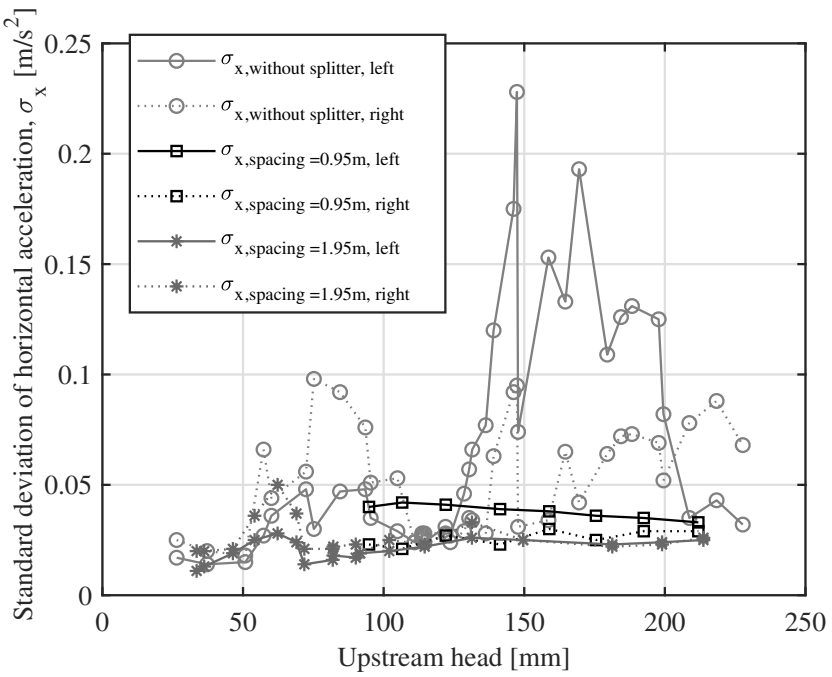

Figure VII.14: Nisramont: Impact of additional splitters on the standard deviation of longitudinal acceleration measurement

configurations with additional splitters (Table VII.2). While all conditions for nappe oscillations were satisfied in the existing configuration, this table shows that with additional splitters, reducing the nappe width, the conditions for nappe oscillations occurrence are no more satisfied. This explains the effectiveness of the countermeasures, as the experiments presented in Chapter V showed that nappe oscillations tend to vanish for widths lower than 1 m.

Considering a QR crest profile, the study also showed that the flow range (or upstream head) affected by the nappe oscillations decreases with the nappe width. For a crest 3.45-m wide with a QR profile, the upstream heads affected by oscillations are between 17 and 50 mm, while for a crest 1.45-m wide these upstream head range is reduced between 17 and 30 mm. The same tendency was observed on Nisramont dam. Nappe oscillations are observed for upstream heads between 40 and 70 mm using 1.95-m spaced splitters, while they are observed for upstream heads between 50 and 230 mm without splitter.

The applicability of the necessary conditions developed for fixed weirs in controlled environments seems therefore applicable for other structures such as crest gates. The in situ measurements also showed that the impact conditions, different from laboratory ones, did not influence the phenomenon. Indeed, the nappe impacted a concrete horizontal apron in the laboratory while in Papignies the nappe plunged into water. At Nisramont, the apron was inclined in the

Table VII.1: Answers to questions related to necessary conditions for nappe oscillations

	Nisramont	Papignies
Is the upstream face of the crest profiled?	Yes	Yes
Is a fixed detachment point imposed by the crest geometry?	Yes	Yes
Is the approach flow velocity low and uniformly distributed?	Yes	Yes
Is the nappe confined?	Yes	Yes
Is the nappe coherent along the fall height and at the impact?	Yes	Yes

Table VII.2: Fall heights (L) and widths (W)

	Nisramont	Papignies
Existing configurations		
Is $L > 1.5$ m ?	Yes	Yes
Is $W > 1.0$ m ?	Yes	Yes
With additional splitters		
Is $L > 1.5$ m ?	Yes	Yes
Is $W > 1.0$ m ?	Yes/No	Yes

direction of the flow. In that case the inclined apron is different from the inclined apron presented in Chapter VI as the inclinaison is in the flow direction. Indeed, the fall height is constant along the width in Nisramont while in Chapter VI, the apron was inclined in parallel to the crest and the fall height varied therefore along the width.

Finally, it should be noted that for the existing configurations, the frequencies of oscillations are reported in Papignies and Nisramont respectively between 14 and 23 Hz and, 14 and 35 Hz. The range of the frequencies observed on site is included in the range observed for the prototype scale model.

VII.6 Conclusions

In situ measurements were performed on two Belgium dams subject to nappe oscillations under low head conditions. These measurements illustrated the reproducibility of the phenomenon observation, independently of the measurement techniques used to characterize the oscillations, i.e., accelerometers, velocimeters, microphone and high speed camera. In particular, oscillations frequencies were identical whatever the measurement technique and the time of the measurements.

These measurements are rather unique and illustrate the reproducibility of the phenomenon and the robustness of the developed measurement techniques.

In addition, the tests showed the effectiveness of splitters spaced less than 1 m to prevent nappe oscillations. This spacing is in line with results exposed in Chapter V for a prototype scale linear weir. They also indicated that too large of a splitter spacing does not prevent nappe oscillations and that the range of upstream heads prone to induce oscillations reduces with the increase of crest width, i.e., with the splitters spacing.

Chapter VIII

General conclusions

The instability of falling thin water sheets, reported as nappe oscillations, has been explored theoretically for decades. A number of theories regarding the cause or the origin of the oscillations appearance and development have been put forward, such as a Kelvin-Helmoltz instability, a pressure discontinuity at the weir crest or an instability of the boundary layer. However, no definitive understanding of the phenomenon has been proposed to date. Experimentally, while most of the researches focused on vertically falling water sheets generated at a thin slot in a pressurized tube, few attempts explored the nappe oscillations problem on free surface weirs. Such systems, widely used as dam safety structures for flood evacuation, may however experience nappe oscillations, with significant societal and environmental impacts. In this context, considering the practical importance of free surface weirs in hydraulic structures engineering and the inchoate understanding of the dominant processes underpinning nappe oscillations occurrence, this PhD thesis aimed at providing a thorough characterization of the phenomenon occurring on free overfall structures such as weirs, crest gates and fountains on an experimental basis.

In what follows, Section VIII.1 summarizes the different contributions and findings of this research while Section VIII.2 presents its limitations and paves the way for future works.

VIII.1 Contributions and findings

The first effort of this PhD thesis was the design of a prototype-scale linear weir able to produce nappe oscillations while ensuring flexibility to investigate the influence of geometric parameters of the weir such as the fall height, the weir width, the crest profile and the nappe confinement. In parallel, a selection of measurement devices able to capture the physical characteristics of the nappe oscillations was performed.

Based on the distinct audio and visual features of the phenomenon, two original characterization methods have been developed to quantify the nappe oscillations properties. The application of these methods allows the determination of the occurrence of the phenomenon and the identification of its dominant frequency. Nappe oscillations were observed, whatever the crest profile, for unit discharges between 0.01 and 0.06 m^2/s, which corresponds to upstream heads between 3 and 12 cm (depending on the crest profile). The frequency associated to these oscillations was included between 6 and 60 Hz. The original and complementary methods, coupled to the experimental model's flexibility, provided for the first time a large dataset of quantitative nappe oscillations characteristics depending on systematic variation of geometric and hydraulic parameters. The results of these systematic experimental tests enabled to provide information never noticed before. In particular, a quantitative description of the nappe oscillations development on a free surface weir has been performed. A specific

evolution depending on the discharge and key geometric parameters has been identified. It is made of 4 successive phases in sound intensity evolution (growing, stabilization, damping and new stabilization), while it has been verified that in absence of nappe oscillations, sound intensity increases continuously with the discharge. It has been shown that the frequencies of the visible oscillations and the main frequency of the associated sound are identical, but may vary with the system geometry and the discharge. It has also been confirmed that the nappe confinement is not a prerequisite to nappe oscillations development but acts more as an amplificator of the phenomenon.

Besides the laboratory experiments, the characterization methods have been applied to two Belgian dams experiencing nappe oscillations. The in situ measurements proved the robustness of the measurement methodologies and their applicability to real outdoor structures.

Significant time has been devoted to the study of scale effects. Indeed, scale physical modeling is very common in hydraulic structures design such as weirs. A 1/3 geometric scale model of the prototype scale facility has been built and operated during a 3 months' research stay at the Utah Water Research Laboratory (USA). The same characterization techniques applied to both models showed that the nappe oscillations phenomenon cannot be scaled according to the traditional similitude for free surface flow, i.e., Froude similitude. Indeed, the nappe oscillations always appeared in the same unit discharge range, independently of the weir size scale and test facility. However, the characteristics of the oscillations on the small scale model showed more variability in terms of occurrence and dominant frequency, including the coexistence of various dominant frequencies in some configurations, as well as some hysteresis not observed on the prototype scale model.

Based on the dataset build from the systematic analysis of 52 geometric configurations and on the expertise gained from hours of nappe oscillations observations and analysis, the necessary conditions for nappe oscillations occurrence on free surface weirs have been defined in terms of unit discharge, crest profile and nappe confinement. Along with criteria on the fall height and the weir width, these conditions, although not sufficient, allow to predict the occurrence of the oscillations. They have been summarized in a questionnaire which is a practical and valuable tool for engineers and designers. This tool has been validated in the case of two Belgian dams recently modified to avoid nappe oscillations occurrence.

Given the environmental and societal impacts of nappe oscillations, a particular effort has been put into the development of mitigation techniques specifically suited for free surface weirs. Indeed, nappe oscillations are commonly avoided on overflow gates thanks to nappe splitters fixed to the gate crest. However, this solution is not suitable for fixed weirs because of their impact on discharge capacity and floating debris blockage. Three efficient innovative mitigation tech-

niques have been developed in collaboration with the Schnabel company (USA) and with the help of practicing engineers and contractors. Their techniques include crest roughening via projecting bolts, fragmentation of the nappe using deflectors as well as a boundary layer and nappe trajectory modification with a small step downstream of the weir crest. Designed with respect to constructability, durability and maintenance, all these solutions turn effective regarding noise disturbance reduction, on the prototype scale linear weir, without impacting the hydraulic efficiency and the floating debris disposal. The spacing of projecting bolts and deflectors emerged as a fundamental parameter to avoid noise disturbance. The efficiency of the downstream step as well as the optimal position of projecting bolts also indicated the sensitivity of the nappe oscillations phenomenon to flow conditions at the crest or close to the crest. The choice among one of these effective countermeasures will usually require the analysis of hydraulic, constructability, economy and durability aspects which are specific to each site. In practical terms, the step is perhaps the most economical mitigation technique for existing or new hydraulic structures. Further to this research, such a step has been setup as retrofit of the labyrinth weir of the Linville Dam (USA).

Another effective solution to avoid the negative effects of nappe oscillations development is to set up an inclined impact apron, parallel to the crest. Such an apron is naturally present downstream of Piano Key weirs side walls. Its effectiveness has been proven for confined and unconfined nappes downstream of various crest profiles and crest widths.

Finally, although it has not been possible during this research to clearly identify the cause of nappe oscillations apparition and development, some observations that support or infer existing theories were gained:

- Uniform low turbulence approach flow conditions are required to get nappe oscillations. A small step deflecting the nappe downstream of the crest, projecting bolts upstream or at the crest apex or a squared crest profile are effective to prevent nappe oscillations appearance. All these points support the theory linking the initiation of nappe oscillations to an instability in the turbulent boundary layer development when the flow accelerates over the crest.

- Nappe oscillations appear generally for crest profiles that impose the nappe detachment point geometrically, i.e. with a sudden transition from a positive pressure on the crest to the atmospheric pressure. No nappe oscillation is observed on a half rounded crest, where the detachment occurs when the pressure at the crest is atmospheric. In some confined nappe configurations with limited fall heights, the oscillations phenomenon was strongly affected by significant pressure variation behind the nappe compared to atmospheric pressure. These observations support the assumption linking the oscillations appear-

ance to the sudden pressure variation at the crest.

- Oscillations development and disturbing noise generation is related to the nappe geometry. This assumption is supported by observations such as the non-occurrence of nappe oscillations in case of an inclined downstream apron or in case of nappe division with deflectors downstream of the crest (or nappe splitters on gates).

The expertise gained during these four-year research lead us to believe that the nappe oscillations phenomenon is generated at the crest or close to the crest by a complex mechanism which implies more than one theory.

VIII.2 Limitations and perspectives

Four years were definitively not enough to address all the topics related to the nappe oscillations. This study suffers thus from some limitations and opens the door to future works.

The understanding of the dominant processes underpinning nappe oscillations is still incomplete. Indeed, irrefutable proof of an initiation mechanism and the associated theory have not been found during this experimental thesis. Additional measurements such as air pressure fluctuations close to the detachment point or the turbulence conditions on the crest would be valuable to confirm and support the possible theories.

If it is my belief that the nappe oscillations of thin nappes generated through a slot should be classified as another type of nappe oscillations than the one observed on free overfall structures, proofs to support this hypothesis are to be explored. The inadequacy of critical conditions and predictive formulations reported in literature to explain the oscillations frequencies measured during this thesis is indeed not sufficient to support my belief. A complete review of the diverse nappe oscillations reported in the literature would be helpful to objectively classify the nappe instabilities.

This research considered 52 configurations corresponding to 5 crest profiles, 7 fall heights and 5 crest widths. Additional crest profiles, fall heights and widths, and additional combinations of the tested parameters, should be considered in order to validate the findings of this thesis and extend the understanding of geometric parameters influence. For instance, it would be useful to consider an unconfined nappe downstream of a half rounded crest. Additional tests would validate and complete the existing analysis. These additional experiments along with additional measurement techniques could help to identify sufficient conditions for oscillations initiation and predictive formulation of the oscillations frequency which are, at this stage, impossible to establish.

The influence of the impact conditions is a topic that would require more attention in the future research. Despite they do not seem linked to the generation

of the oscillations, they play a role in the development and maintenance of the oscillations. For instance, the definition of the minimum downstream apron slope to avoid the development of the oscillations would be interesting to identify.

Finally, besides experimental considerations, it would be interesting to investigate the nappe oscillations phenomenon using numerical tools. They could help to validate or invalidate potential mechanisms of oscillations initiation and development.

I hope this work will serve as a solid basis for additional studies on the nappe oscillations affecting free overfall structures and in particular for the suggested investigations tracks. To conclude, I do trust that this PhD thesis will provide practical answers for designers and contractors for which the nappe oscillations phenomenon is an actual issue.

Bibliography

01dB Metravib, july 2008. dBFA: Frequency analysis software suite and much more... User manual. France.

01dB Metravib, ACOEM, 2008. dBFA.
URL https://www.01db.com/

Anderson, A., Tullis, B., 2018. Finite crest length weir nappe oscillation. Journal of Hydraulic Engineering 144 (6), 04018020.

Anderson, A. A., 2014. Causes and countermeasures for nappe oscillation. Master's thesis, Utah State University, Logan, UT, US.

Binnie, A., 1972. The stability of a falling sheet of water. In: Royal Society of London A: Mathematical, Physical and Engineering Sciences. Vol. 326. The Royal Society, pp. 149–163.

Binnie, A., 1974. Resonating waterfalls. In: Royal Society of London A: Mathematical, Physical and Engineering Sciences. Vol. 339. The Royal Society, pp. 435–449.

Blanc, P., Lempérière, F., 2001. Labyrinth spillways have a promising future. International Journal on Hydropower & Dams 8 (4), 129–131.

Bousmar, D., Libert, Y., 2015. Barrage de Nisramont, Ourthe. Vibration de la vanne. mesures in-situ du 26 novembre 2014. Tech. Rep. 1- Avis 2014/6, Direction de Recherches hydrauliques, Service Public de Wallonie.

Bousmar, D., Libert, Y., 2017. Barrage de Papignies, Dendre. Oscillations de la nappe déversante : Mesures in-situ. Tech. Rep. Mod.064, Direction de Recherches hydrauliques, Service Public de Wallonie.

Casperson, L. W., 1993a. Fluttering fountains. Journal of Sound and Vibration 162(2), 251–262.

Casperson, L. W., 1993b. Fluttering fountains: Simplified models. Journal of Applied Physics 74 (8), 4894–4898.

Casperson, L. W., 1994. Fluttering fountains: Stability criteria. Journal of Applied Physics 75 (10), 4892–4894.

Casperson, L. W., 1996. Fluttering fountains: Annular geometry. Journal of Applied Physics 79 (3), 1275–1278.

Castillo, L. G., Carrillo, J. M., Sordo-Ward, Á., 2014. Simulation of overflow nappe impingement jets. Journal of Hydroinformatics 16 (4), 922–940.

Chanson, H., 1996. Some hydraulic aspects during overflow above inflatable flexible membrane dam. Tech. Rep. CH47/86, The University of Queensland, Brisbane, QLD, Australia.

Crookston, B., Anderson, A., Shearin-Feimster, L., Tullis, B., 2014. Mitigation investigation of flow-induced vibrations at a rehabilitated spillway. In: 11th National Conference on Hydraulics in Civil Engineering & 5th International Symposium on Hydraulic Structures: Hydraulic Structures and Society-Engineering Challenges and Extremes. Engineers Australia, pp. 149–156.

Crookston, B. M., Tullis, B., 2012. Hydraulic design and analysis of labyrinth weirs I: Discharge relationships. Journal of Irrigation and Drainage Engineering 139 (5), 363–370.

Curle, N., 1953. The mechanics of edge-tones. In: Royal Society of London A: Mathematical, Physical and Engineering Sciences. Vol. 216. The Royal Society, pp. 412–424.

De Luca, L., Costa, M., 1997. Instability of a spatially developing liquid sheet. Journal of Fluid Mechanics 331, 127–144.

De Rosa, F., Girfoglio, M., De Luca, L., 2014. Global dynamics analysis of nappe oscillation. Physics of Fluids 26 (12), 122109.

Ervine, D. A., Falvey, H. T., Withers, W., 1997. Pressure fluctuations on plunge pool floors. Journal of Hydraulic Research 35 (2), 257–279.

Ettema, R., Arndt, R., Roberts, P., Wahl, T., 2000. Hydraulic modeling: Concepts and practice. ASCE.

Falvey, H., 1980. Bureau of reclamation experience with flow-induced vibrations. In: E. Naudascher, D. Rockwell (Eds.), Practical Experiences with Flow-induced Vibrations. Springer, New York.

Girfoglio, M., De Rosa, F., Coppola, G., De Luca, L., 2017. Unsteady critical liquid sheet flows. Journal of Fluid Mechanics 821, 219–247.

Guha, S., Luthra, S., 1963. Hydro-elastic vibration for dams. In: 10th General Meeting of the International Association of Hydraulic Research. Vol. 3. pp. 201–212.

Heller, V., 2011. Scale effects in physical hydraulic engineering models. Journal of Hydraulic Research 49 (3), 293–306.

Hydrocoop, June 2015. Piano key weirs (pk weirs) triple the spillway discharge.

ICOLD, 2018. World register of dams.
URL https://www.icold-cigb.org/GB/world_register/world_register_of_dams.asp

Khodier, M. A., Tullis, B. P., 2018. Piv measurements for oscillating liquid nappe. Journal of Hydro-environment Research 19, 237–242.

Knisely, C. W., 1989. On the acoustics of nappe oscillations. Tech. rep., HYDROCOMP 89.

Kyotoh, H., Nakamura, R., Baruah, P., 2002. Incipient oscillations of a sheet of falling water and the instability mechanisms. Journal of Hydroscience and Hydraulic Engineering 20 (1), 77–94.

Lempérière, F., Ouamane, A., 2003. The piano keys weir: a new cost-effective solution for spillways. International Journal on Hydropower & Dams 10 (5), 144–149.

Lodomez, M., Bousmar, D., Dewals, B., Archambeau, P., Pirotton, M., Erpicum, S., 2018a. In-situ measurement and mitigation of nappe oscillations : The Papignies and Nisramont dams in Belgium. In: 7th IAHR International Symposium on Hydraulic Structures.

Lodomez, M., Crookston, B., Tullis, B., Erpicum, S., 2018b. Mitigation techniques for nappe oscillations on free-overfall structures. Journal of Hydraulic Engineering 145 (2), 04018086.

Lodomez, M., Pirotton, M., Dewals, B., Archambeau, P., Erpicum, S., 2017. Could piano key weirs be subject to nappe oscillations? In: Labyrinth and Piano Key Weirs III. CRC Press, London, pp. 135–144.

Lodomez, M., Pirotton, M., Dewals, B., Archambeau, P., Erpicum, S., 2018c. Nappe oscillations on free-overfall structures: Experimental analysis. Journal of Hydraulic Engineering 144 (3), 04018001.

Lodomez, M., Tullis, B., Dewals, B., Archambeau, P., Pirotton, M., Erpicum, S., 2019. Nappe oscillations on free overfall structures : Size scale effects. Journal of Hydraulic Engineering 145 (6), 040119022.

Millet, J. C., Chambon, J., Soyer, G., Lefevre, C., 1988. Augmentation de la Capacité des Ouvrages d Evacuation de Divers Barrages. In: 16e Congrès Des Grands Barrages.

Mori, H., Nagamine, T., Ito, R., Sato, Y., 2012. Mechanism of self-excited vibration of a falling water sheet. Nihon Kikai Gakkai Ronbunshu, C Hen/Transactions of the Japan Society of Mechanical Engineers, Part C 78 (792), 2720–2732.

MWSB, 1980. Investigation into spillway discharge noise at Avon Dam. Metropolitan Water, Sewerage and Board, ANCOLD Bulletin 57, 31–36.

Nagamine, T., Minegishi, Y., Sekiya, A., Goto, M., Takaki, K., Mori, H., Sato, Y., 2011. Development of the equipment to suppress low frequency nappe oscillation. Nihon Kikai Gakkai Ronbunshu, C Hen/Transactions of the Japan Society of Mechanical Engineers, Part C 77 (778), 2211–2220.

Naudascher, E., 1965. Discussion on nappe oscillation. journal of the Hydraulics Division 91 (5), 223–229.

Naudascher, E., Rockwell, D., 1994. Flow-induced vibrations: An engineering guide. A.A. Balkema, Rotterdam, Netherlands.

Nishikawa, H., 1977. A study on nappe oscillation and associated noise. Theoretical and Applied Mechanics 26, 537–548.

Pariset, E., 1955. Etude sur la Vibration des lames déversantes. In: 6th IAHR Congress. Vol. 3. The Hague, The Netherlands, pp. 1–15.

Partenscky, H.-W., Khloeung, I. S., 1967. Oscillation de lames déversantes non aérées. In: XIIe Congrès de l'Association Internationale de Recherches Hydrauliques.

Peltier, Y., Dewals, B., Archambeau, P., Pirotton, M., Erpicum, S., 2018. Pressure and velocity on an ogee spillway crest operating at high head ratio: Experimental measurements and validation. Journal of Hydro-environment Research 19, 128–136.

Petrikat, K., 1958. Vibration tests on weirs and bottom gates. Water Power 190, 52–57.

Reclamation, 1964. Experience of the bureau of reclamation with flow-induced vibrations. Laboratory report 538, Hydraulics branch,U.S. Bureau of Reclamation.

Reclamation, 2014. Reclamation consequence estimating methodology : Dam failure and flood event case history compilation. Tech. rep., U.S. Bureau of Reclamation.

Sato, Y., Miura, S., Nagamine, T., Morii, S., Ohkubo, S., 2007. Behavior of a falling water sheet. Journal of Environment and Engineering 2 (2), 394–406.

Schmid, P. J., Henningson, D. S., 2002. On the stability of a falling liquid curtain. Journal of Fluid Mechanics 463, 163–171.

Schwartz, H. I., 1964a. Nappe oscillation. Journal of the Hydraulics Division 90 (6), 129–143.

Schwartz, H. I., 1964b. Projected nappes subject to harmonic pressures. In: The Institution of Civil Engineers - Engineering Sustainability. Vol. 28. pp. 313–326.

Schwartz, H. I., 1966a. Edgetones and nappe oscillation. Journal of the Acoustical Society of America 39 (3), 579–582.

Schwartz, H. I., Sep. 1966b. Some aspects of nappe oscillation. Ph.D. thesis, University of the Witwatersrand, Johannesburg ,Republic of South Africa.

Shannon, C. E., 1949. Communication in the presence of noise. In: IRE. Vol. 37. IEEE, pp. 10–21.

SignalLab, 2017. SIGVIEW.
URL https://www.sigview.com/

Squire, H., 1953. Investigaton of the instability of a moving liquid film. British Journal of Applied Physics 4 (6), 167–169.

Sumi, T., Nakajima, Y., October 1990. Three-dimensional characteristic of nappe oscillation and the estimation of sound pressure levels. Journal of Hydroscience and Hydraulic Engineering 8 (1), 89 –99.

USGS, 2016. How much water is there on, in, and above the earth?
URL https://water.usgs.gov/edu/earthhowmuch.html

Von Helmholtz, H., 1868. *Ü*ber discontinuierliche fl*ü*ssigkeits-bewegungen [on the discontinuous movements of fluids]. Tech. Rep. 23, Royal Prussian Academy of Philosophy, Berlin.

Xlyang, J., Cederström, M., 2007. Modification of spillways for higher discharge capacity. Journal of Hydraulic Research 45 (5), 701–709.

Appendix A

Hydraulic characteristics of the tested crest profiles

Water depth measurements

The discharge Q (in m^3/s) was the only parameter controlled by the experimenter through the opening or closing of valves. Knowing the width of the weir (W), the unit discharge q was thus known. In addition, for each crest profile tested in the framework of this thesis, the upstream water depth (h) as well as the water depth at the crest detachment (h_c) were measured using the ultrasonic sensors and point gauges described in Chapter II.

Therefore, for the $QR1$, $THR1$, $QR2$, $THR2$, R and RR crest profiles, the analytical relations between the (unit) discharge and the upstream head or the water depth at the detachment are reported below. The measurements were performed for configurations $C-QR1-W1-L1$, $C-THR1-W1-L1$, $C-QR2-W5-L5$, $C-THR2-W5-L5$, $C-R-W5-L5$ and $C-RR-W5-L5$ but the deduced relations may be extended for a similar crest profile to all configurations varying in terms of width, fall height and confinement.

The deduced relations link the discharges and the upstream heads in the following format :

$$q = C_d\sqrt{2gH^3} \tag{A.0.1}$$

with H the upstream head calculated as follows:

$$H = h + \frac{u^2}{2g}$$

with $u = \frac{q}{(h+z)}$the velocity, h the upstream water depth in the reservoir and z the weir height.

It should be noted that the reference point for the upstream water depth, h, was imposed to the crest top as illustrated for Model 1 in Fig.A.1. The reservoir height, z, is equal to 0.65 m for Model 1 and 0.95 m for Model 2, for all crest

profiles. The reference of the water depth at the crest detachment, h_c, is the crest itself. The reference is identical in case of QR, R and RR crest profiles but different for THR crest profile. In addition, for THR crest profile, measurement tools allowed to measure vertically the nappe thickness. This measure was thus projected according to the angle of the weir crest at the downstream end, i.e., 45° with horizontal to obtain the water depth at the crest detachment (Fig.A.1).

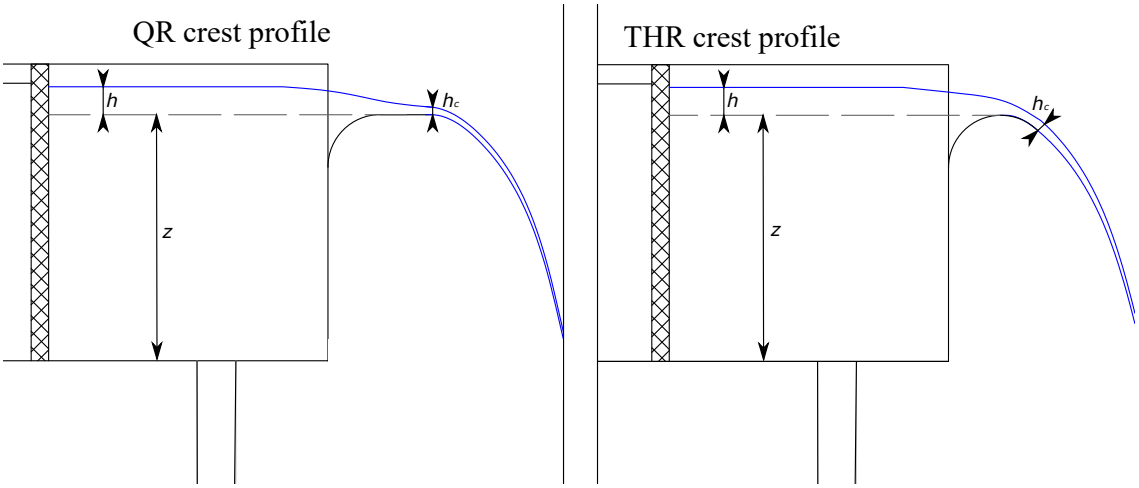

Figure A.1: Schematics of the water depths for QR and THR crest profiles on Model 1

At the crest detachment, a similar relation $\left(q = K\sqrt{2gH^3}\right)$ between the discharge q and the head calculated at the detachment may be derived (considering in that case the water level at the crest detachment and $z = 0$).

The values of the C_d and K coefficients are reported for all crest profiles in Table A.1.

Table A.1: Coefficients of the analytical relation between q and H

		Upstream	At the crest
Model 1	QR	0.3998	0.3439
	THR	0.4515	0.2848
Model 2	QR	0.4274	0.3389
	THR	0.4853	0.3708
	R	0.3500	-
	RR	0.3641	0.3328

On Model 1 and for the QR crest profile, measurements of the upstream water depth were performed in the headbox either 0.65 m upstream of the weir, using 7 calibrated ultrasonic sensors (Microsonic pico+35/WK/I) placed parallel

to the weir crest and spaced from 0.5 m, or 0.5 m upstream of the weir using a unique point gauge located about 0.2 m from the dividing wall. The water depth at the flow detachment (crest downstream extremity) was also measured with a point gauge. Using the 7 ultrasonic sensors, a variation of the upstream water depth of 1.7 mm around the average measurement was observed (for all tested discharges) due to the asymmetric water supply of the reservoir. This variability was almost twice the measurement accuracy ($\pm$ 1 mm) and taken into account be considering the mean value of these 7 measurement points. The upstream head varied from 0.029 to 0.120 m. Along with the measurements performed with the point gauge, these mean upstream water depths, expressed in m, are reported in Fig.A.2, depending on the unit discharge q in m^2/s. The fitting head-discharge curve for the coefficient reported in Table A.1 is also represented in this figure. The water depth at the crest detachment h_c, measured with a point gauge is reported as a function of q in Fig.A.3.

For the THR crest profile and Model 1, water depth measurements in the reservoir and at the crest detachment were only performed with the point gauges. The measurements are also reported in Fig.A.2 and Fig.A.3.

For Model 2, a point gauge was placed 1.5 m upstream of the crest extremity while a second one was movable from 0.50 m upstream to the extremity of the crest. The upstream head, H, is reported as a function of q in Fig.A.4 for the QR, THR, R and RR crest profiles. The analytical relation (Eq.A.0.1) are also reported in this figure. At the crest detachment, the water depth was measured thanks to the movable gauge. Fig.A.5 reports the evolution of this water depth for the QR, THR and RR crest profiles.

General comment

The range of discharges or unit discharges tested in this study is small and corresponds to very low discharges and heads. This finding is explained by the fact that nappe oscillations were only observed in that range which is in agreement with the literature review. For these discharges and heads (3 – 12 cm), the deduced discharge coefficients are low (0.29 – 0.49) as the weir acts as a broad weir.

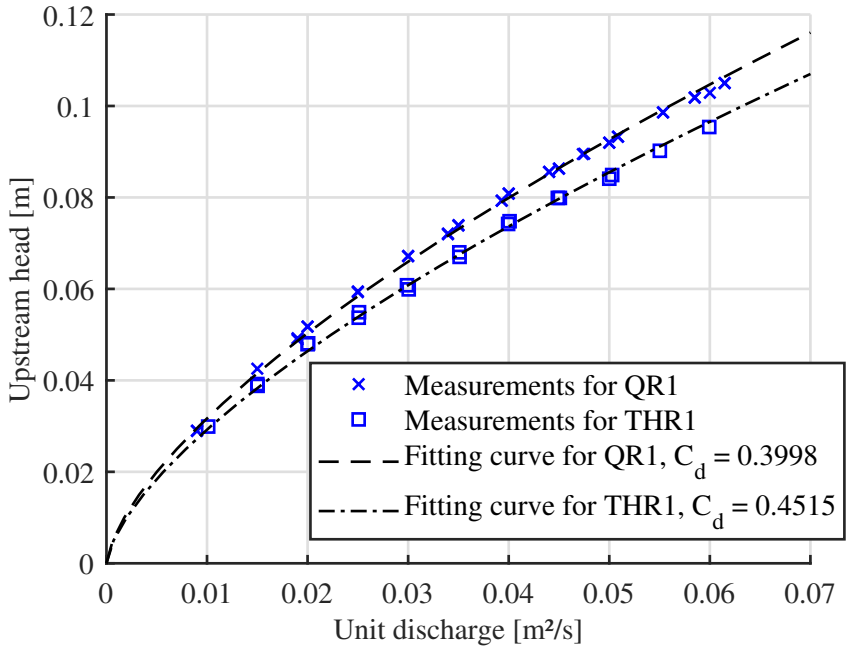

Figure A.2: $H - q$ curve for the QR and THR crest profiles on Model 1

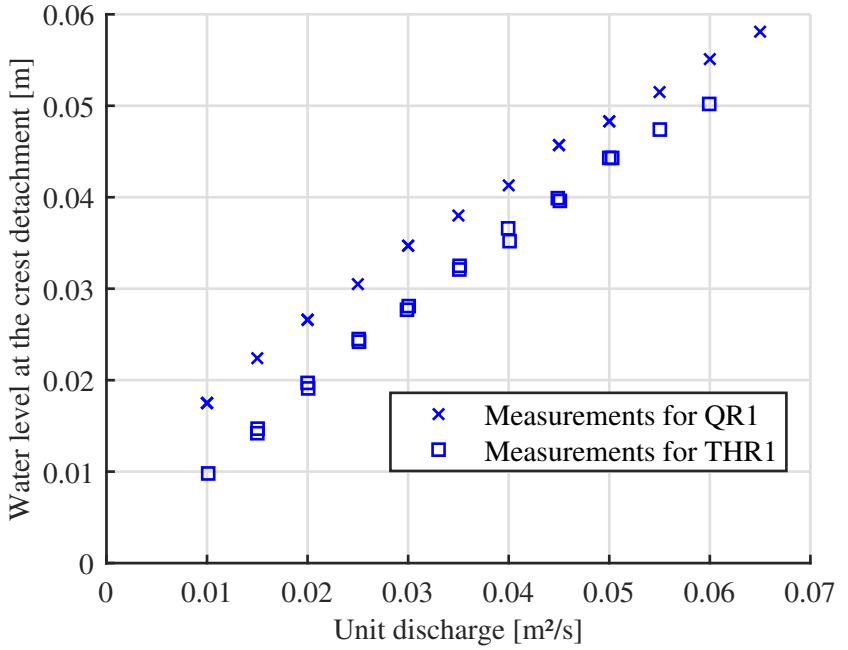

Figure A.3: $h_c - q$ measurements for the QR and THR crest profiles on Model 1

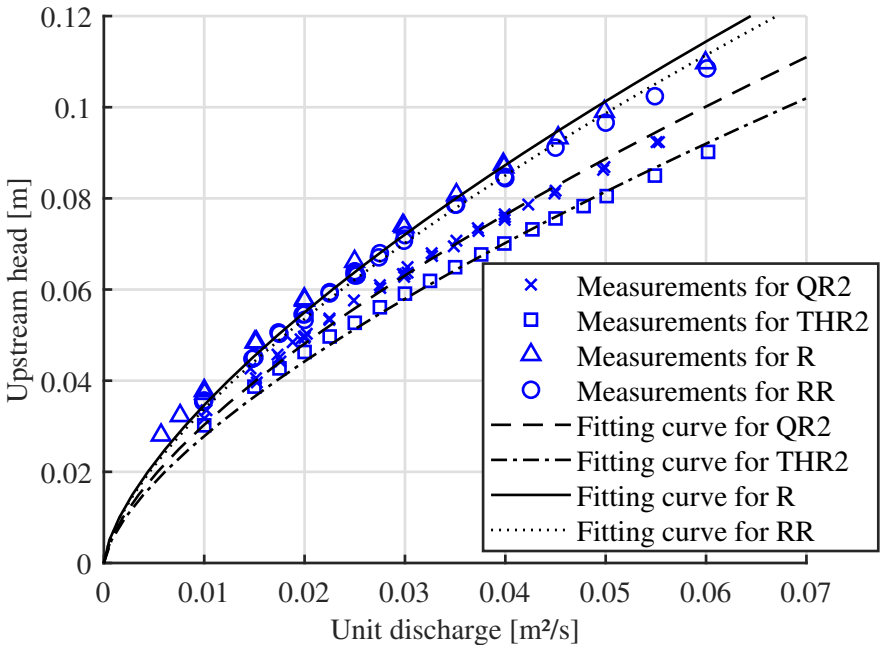

Figure A.4: $H - q$ curve for the QR, THR, R and RR crest profiles on Model 2

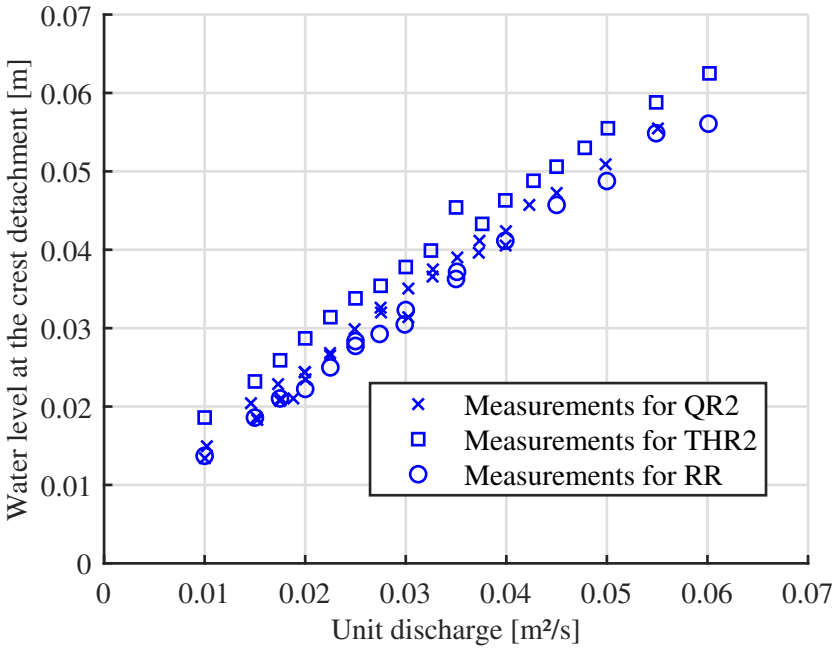

Figure A.5: $h_c - q$ measurements for the QR, THR, R and RR crest profiles on Model 2

Water pressure measurements

In addition to water depth measurements in the reservoir and at the crest detachment, the water pressure on the QR crest profile was measured for Model 1. To that end, 7 pressure sensors, placed along the flow axis and reported as C1 to C7 in Fig.A.6, were used. These sensors were capacitive pressure transmitters [Keller, series 41 X (PR-41X)] able to measure +300 to -30 mbar which correspond to +3 m to -0.3 m.

Pressure measurements were performed with a frequency acquisition of 1 kHz during 2 minutes. The mean pressure, expressed in m, is reported for various pressure in Fig.A.7 after the removal of the outliers, i.e., values outside the range of the mean value (μ) $\pm$ 5 times the standard deviation (σ) which only correspond to 1.1% of data. The analysis of the time evolution of the pressure showed only positive pressure along the crest profile. Therefore, the measurements confirm the existence of a pressure discontinuity at the crest extremity (Chanson, 1996). No periodic fluctuation of pressure was measured. In addition, the standard deviation of the signal was always lower than the measurement accuracy, i.e., 1 mm.

In addition to these pressure measurements, the water level in the flow direction was also measured for different discharges as reported in Fig.A.8. This measurement was performed thanks to 7 ultrasonic sensors, identical to those used to measure the upstream water level parallel to the crest weir. Measurements were also performed with a frequency acquisition of 1 kHz during 2 minutes and processed by a removal of the outliers (out of $\mu \pm 5\sigma$). The time evolution of the water depth also showed no periodic fluctuation. In addition, the comparison of the pressure and water depth along the crest shows that the pressure is a bit lower than the water depth and thus close to hydrostatic pressure.

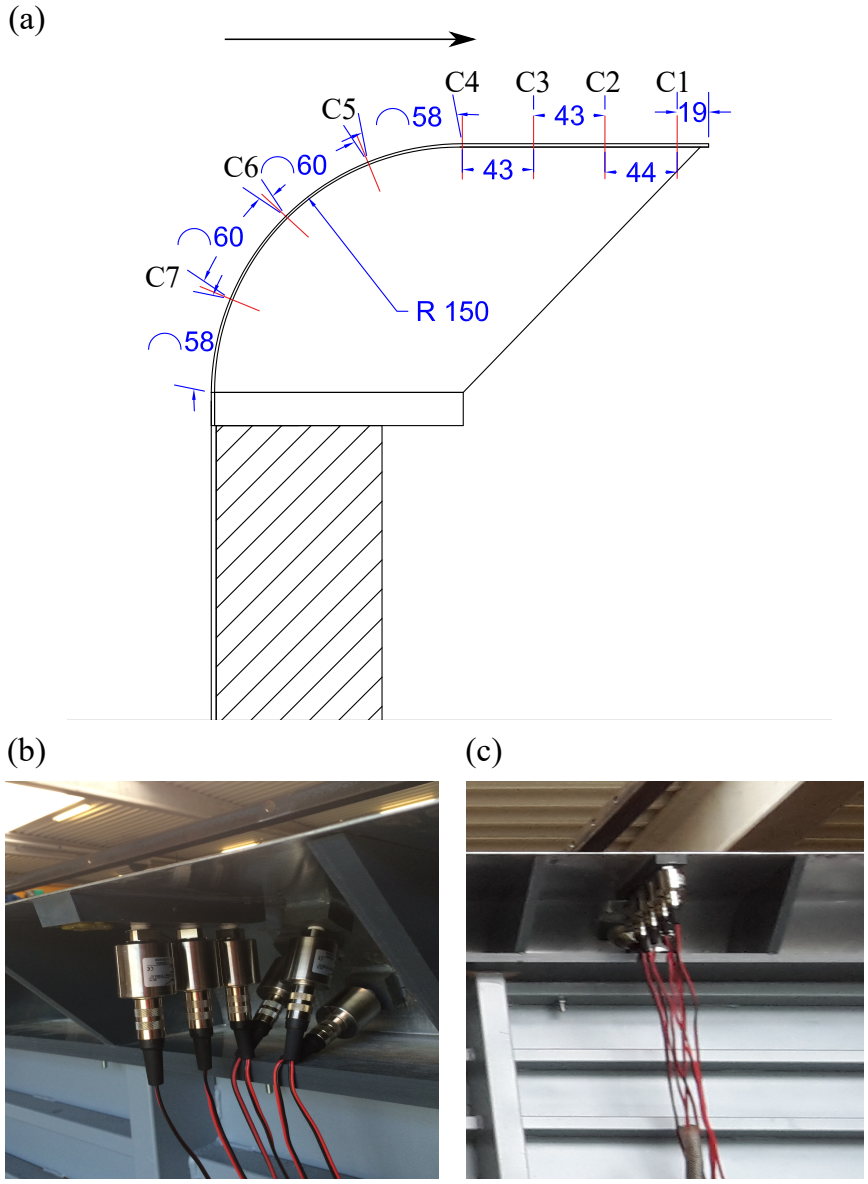

Figure A.6: (a) Schematic of the pressure positions and (b-c) Photographs of pressure sensor [in (b) the sensor at the downstream extremity is missing]

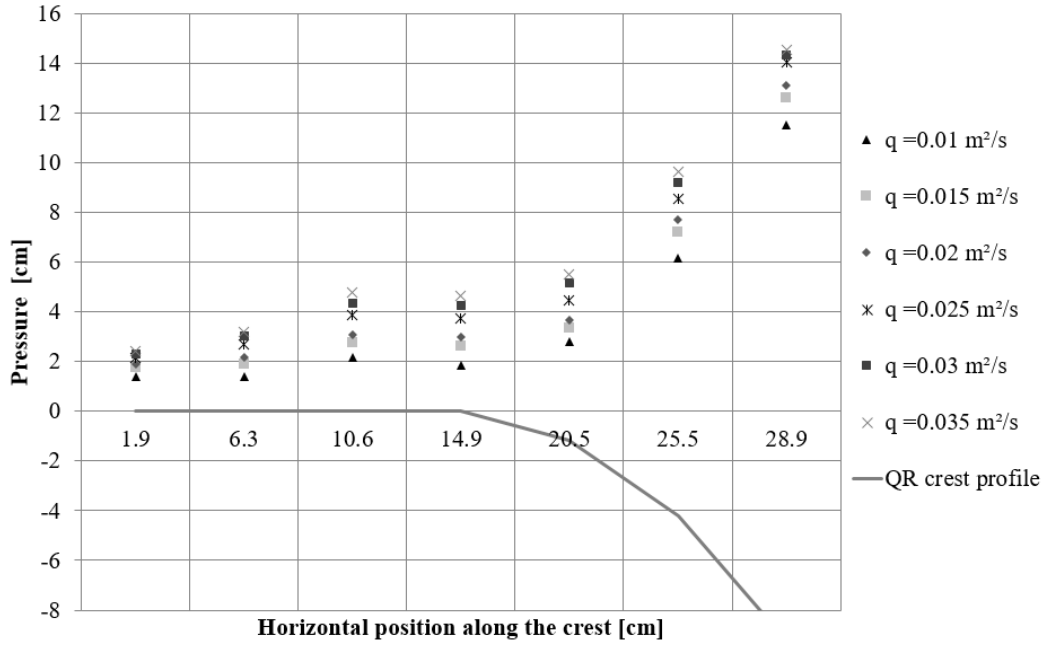

Figure A.7: Mean water pressure along the crest profile for different unit discharges

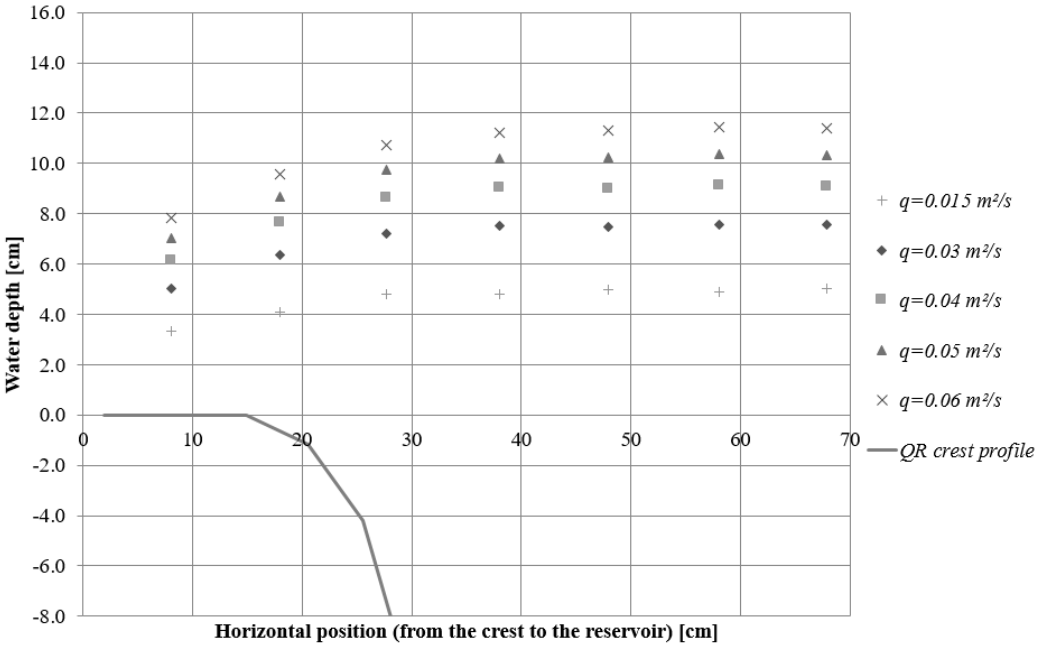

Figure A.8: Mean water depth along the crest profile for different unit discharges

Appendix B

Supplemental data to Chapter V

Characterization of the 52 configurations via sound and image analyses

For all the configurations tested in the framework of this PhD thesis, the occurrence of nappe oscillations has been assessed based on sound and image analyses. This appendix presents for all tested configurations the sound intensity evolution with q. In case of nappe oscillations occurrence, the associated sound frequency and the frequencies extracted from image analysis are also presented. In addition, when they are relevant, images of the visible oscillations are presented. In case of non-occurrence of nappe oscillations, the sound intensity evolution is compared with an oscillating configuration.

Configuration: $C - QR1 - W1 - L1$

Abbreviation	Model	Confinement	Crest shape - R	Width W	Height L	Range of q affected by the oscillations	Extreme frequencies
$C - QR1 - W1 - L1$	1	Confined	QR - 15 cm	345 cm	300 cm	0.01 - 0.055 m^2/s	31.5;39.1 Hz

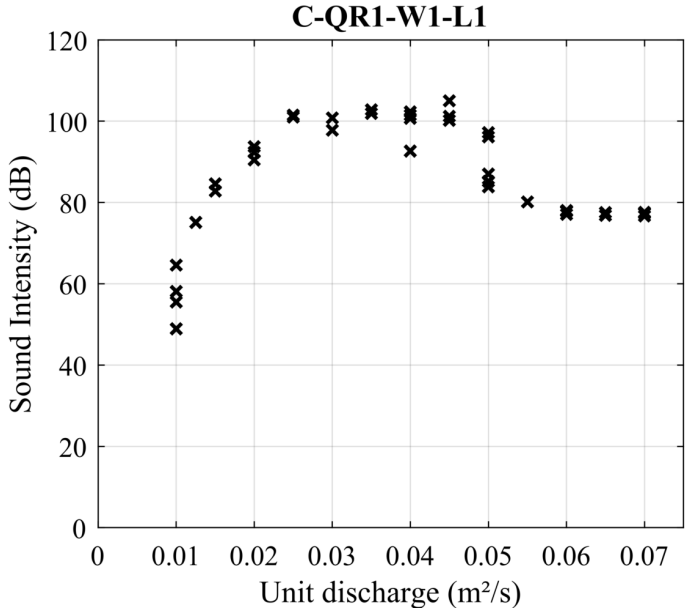

Results of sound analysis

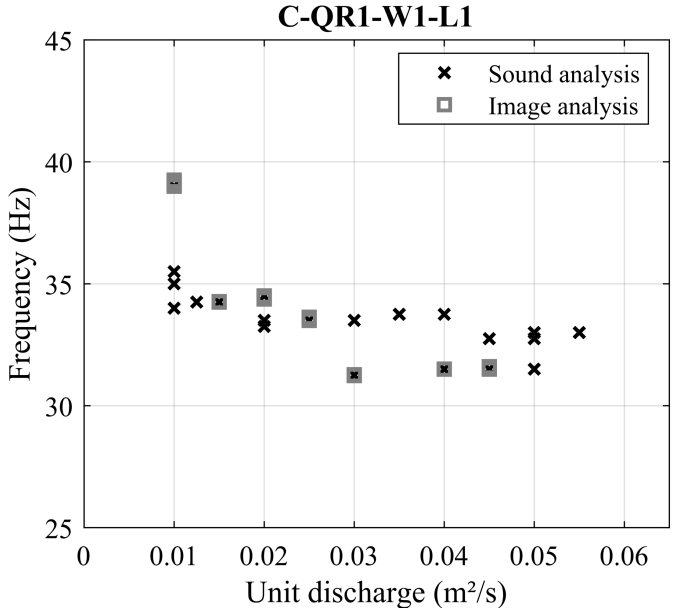

Frequencies obtained by sound and image analyses

Configuration: $C - QR1 - W1 - L1$

(a) (b)

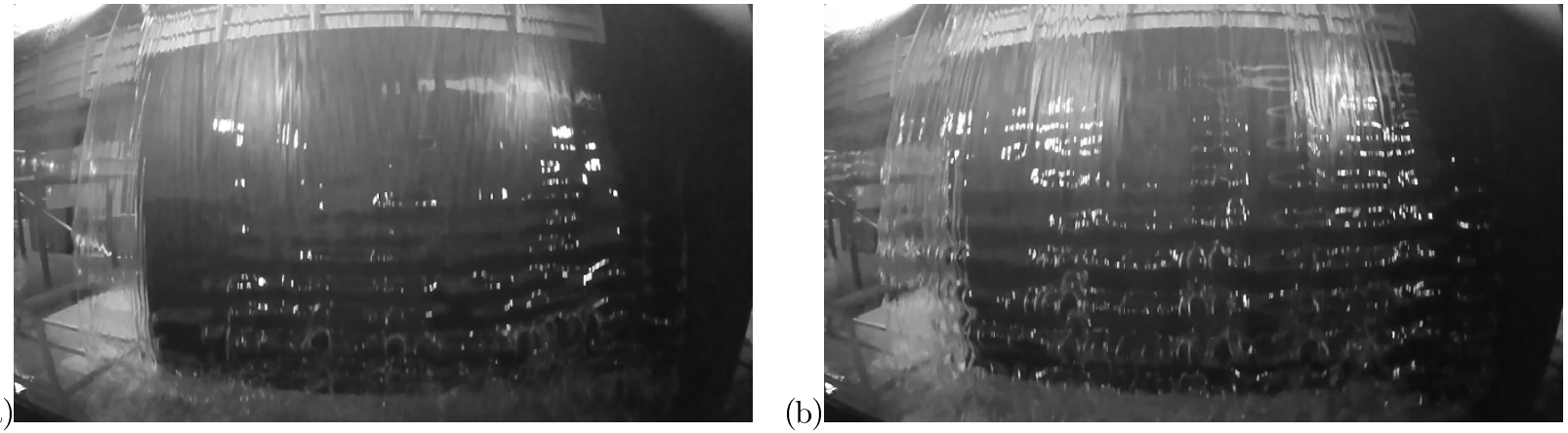

(c) (d)

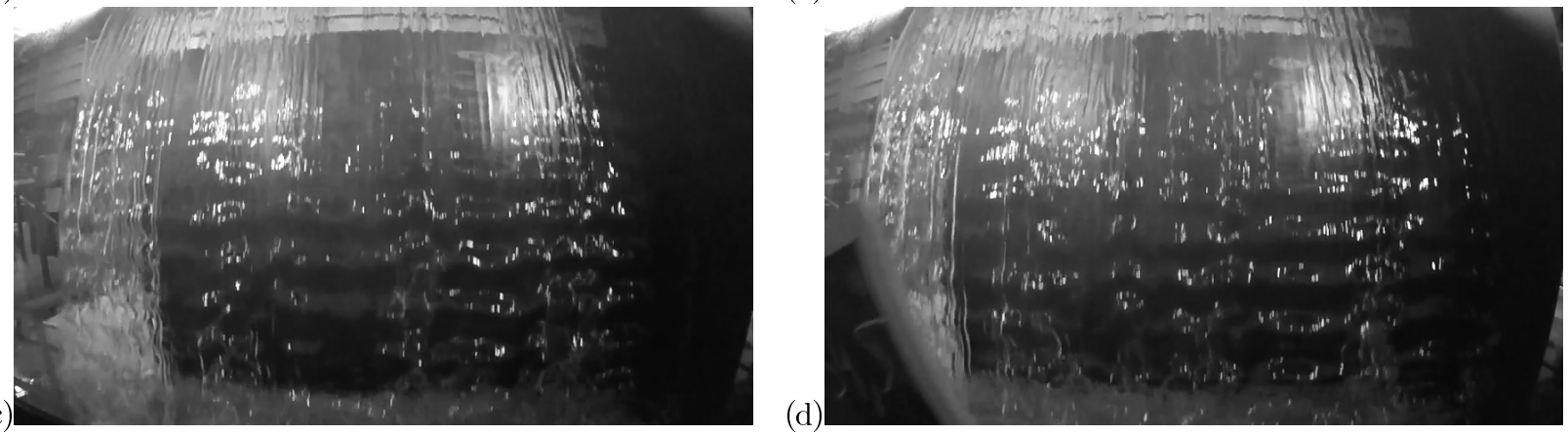

Flow characteristics : (a) $q = 0.01$ m^2/s, (b) $q = 0.02$ m^2/s, $q = 0.03$ m^2/s and $q = 0.04$ m^2/s

Configuration: $C - THR1 - W1 - L1$

Abbreviation	Model	Confinement	Crest shape - R	Width W	Height L	Range of q affected by the oscillations	Extreme frequencies
$C - THR1 - W1 - L1$	1	Confined	THR - 15 cm	345 cm	300 cm	0.015 - 0.06 m^2/s	7.6:44.2 Hz

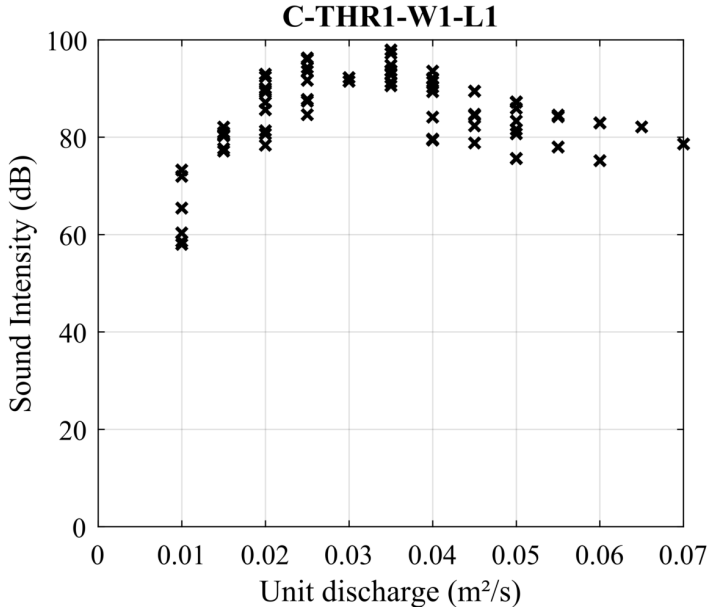

Results of sound analysis

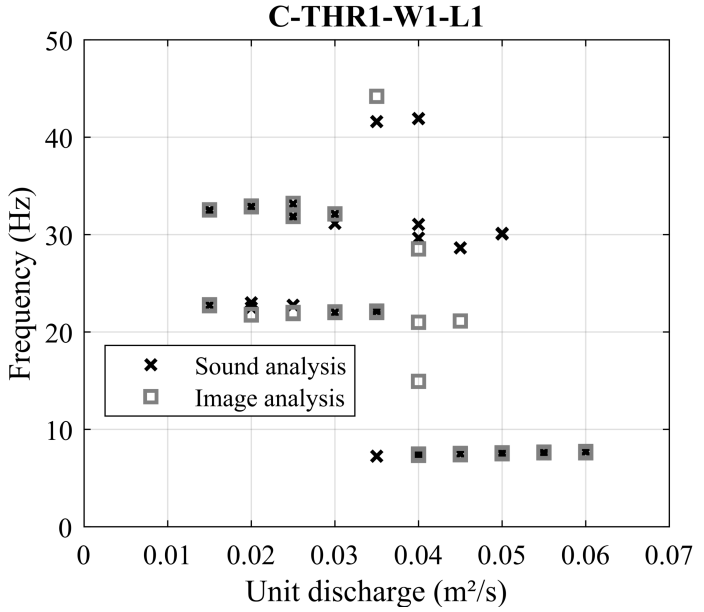

Frequencies obtained by sound and image analyses

Configuration: $C - THR1 - W1 - L1$

(a)

(b)

(c)

(d)

Flow characteristics : (a) $q = 0.01$ m^2/s, (b) $q = 0.02$ m^2/s, $q = 0.03$ m^2/s and $q = 0.04$ m^2/s

Configuration: $C - THR1 - W1 - L2$

Abbreviation	Model	Confinement	Crest shape - R	Width W	Height L	Range of q affected by the oscillations	Extreme frequencies
$C - THR1 - W1 - L2$	1	Confined	THR - 15 cm	345 cm	250 cm	0.01 - 0.045 m^2/s	6;44.1 Hz

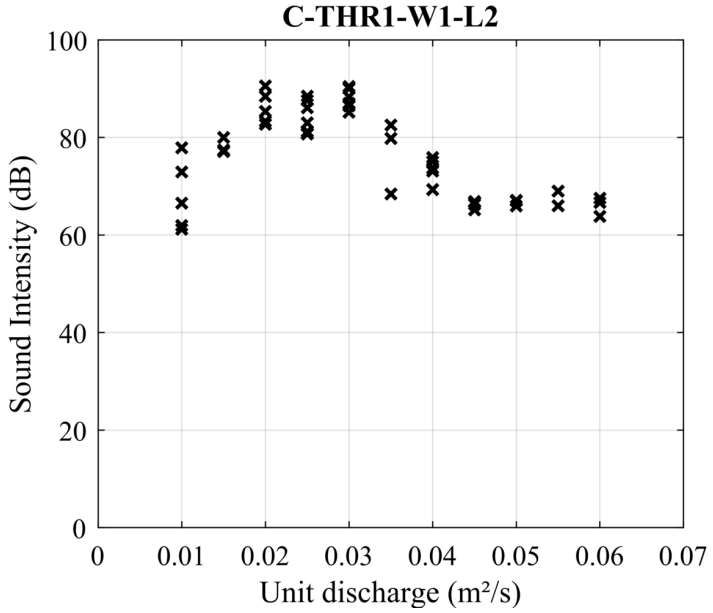

Results of sound analysis

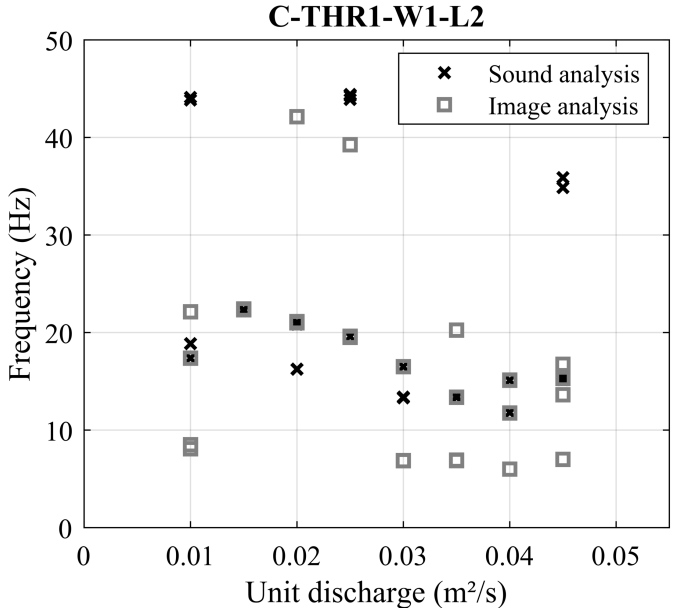

Frequencies obtained by sound and image analyses

Configuration: $C - THR1 - W1 - L3$

Abbreviation	Model	Confinement	Crest shape - R	Width W	Height L	Range of q affected by the oscillations	Extreme frequencies
$C - THR1 - W1 - L3$	1	Confined	THR - 15 cm	345 cm	200 cm	0.01 - 0.035 m^2/s	7.3;36.6 Hz

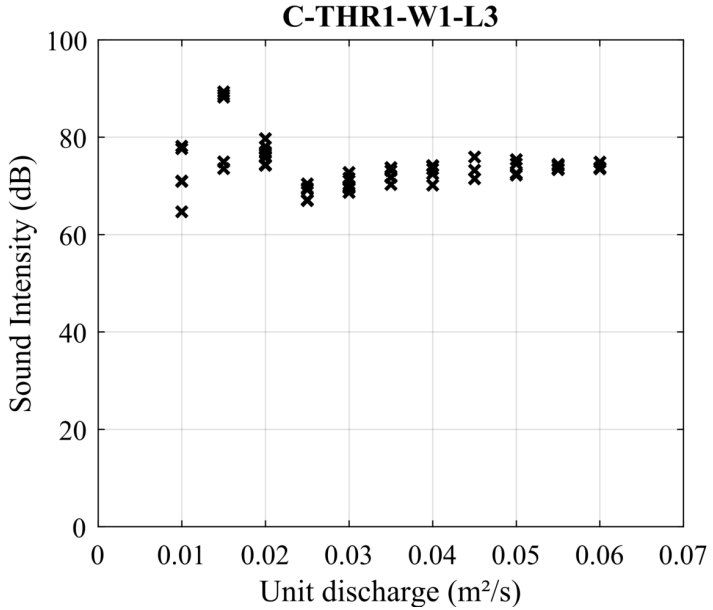

Results of sound analysis

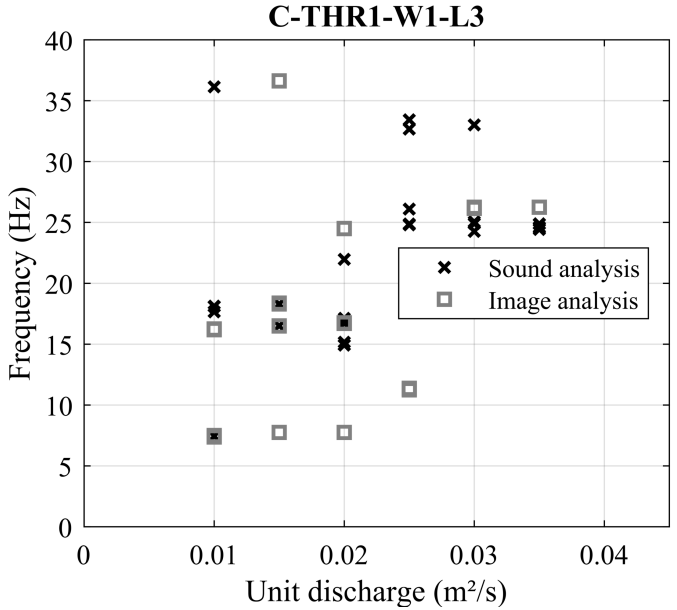

Frequencies obtained by sound and image analyses

Configuration: $C - THR1 - W1 - L4$

Abbreviation	Model	Confinement	Crest shape - R	Width W	Height L	Range of q affected by the oscillations	Extreme frequencies
$C - THR1 - W1 - L4$	1	Confined	THR - 15 cm	345 cm	150 cm	0.01 - 0.025 m^2/s	11;28.9 Hz

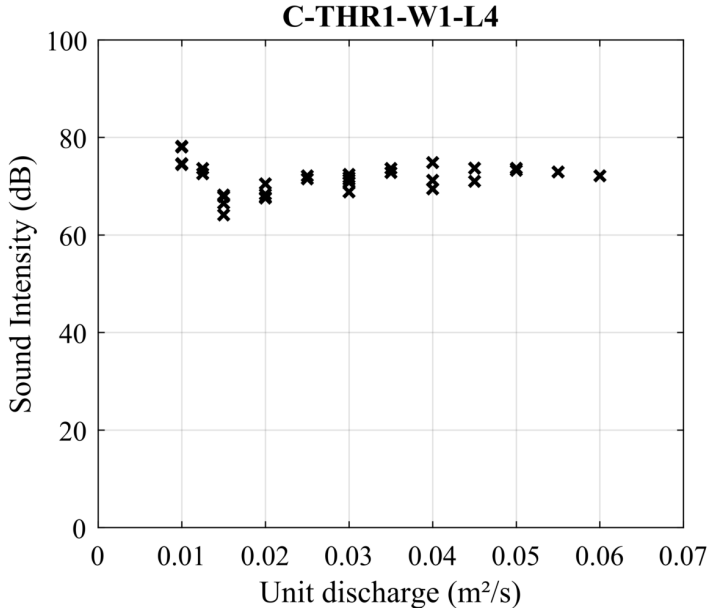

Results of sound analysis

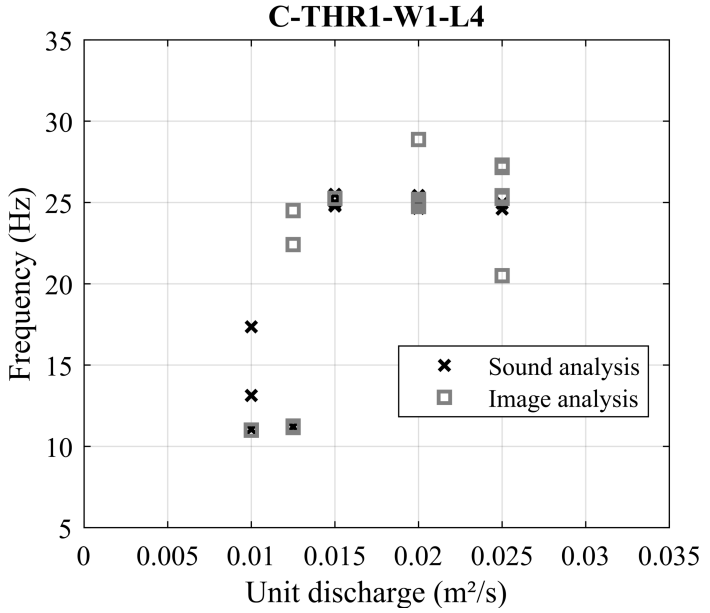

Frequencies obtained by sound and image analyses

Configuration: $C - THR1 - W1 - L5$

Abbreviation	Model	Confinement	Crest shape - R	Width W	Height L	Range of q affected by the oscillations	Extreme frequencies
$C - THR1 - W1 - L5$	1	Confined	THR - 15 cm	345 cm	100 cm	0.015 - 0.06 m^2/s	17.4;20.6 Hz

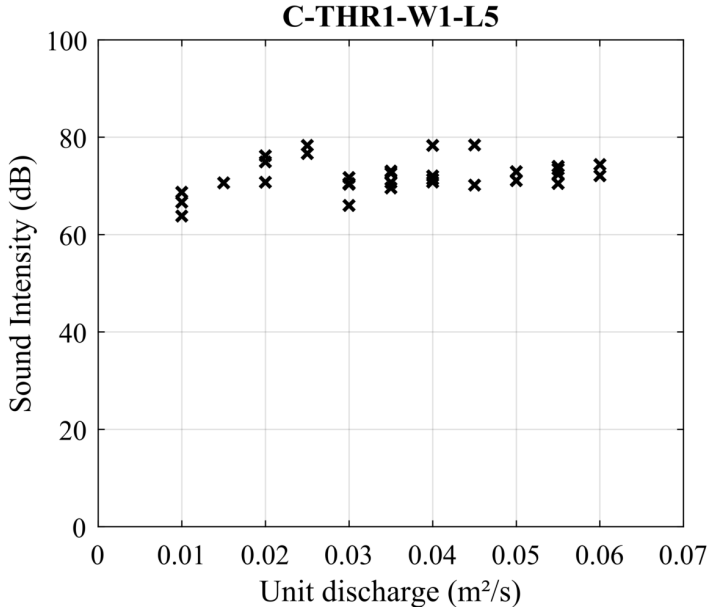

Results of sound analysis

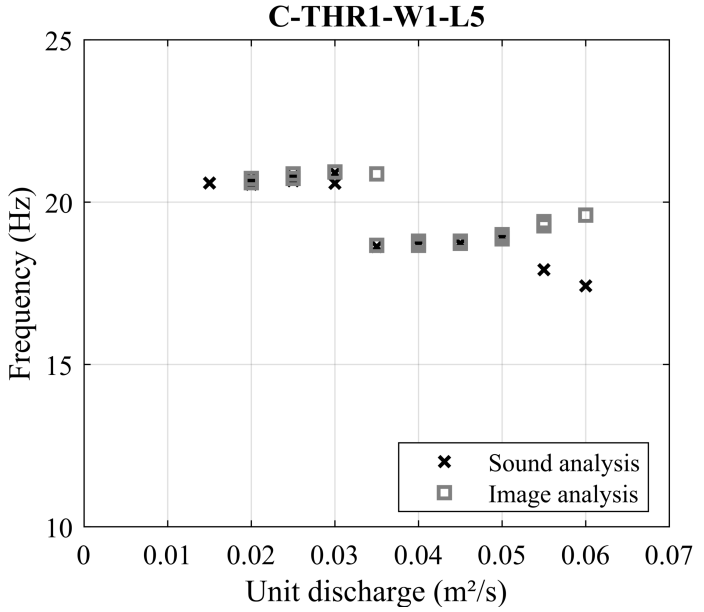

Frequencies obtained by sound and image analyses

Configuration: $C - THR1 - W2 - L1$

Abbreviation	Model	Confinement	Crest shape - R	Width W	Height L	Range of q affected by the oscillations	Extreme frequencies
$C - THR1 - W2 - L1$	1	Confined	THR - 15 cm	250 cm	300 cm	0.015 - 0.035 m^2/s	8.85;23.22 Hz

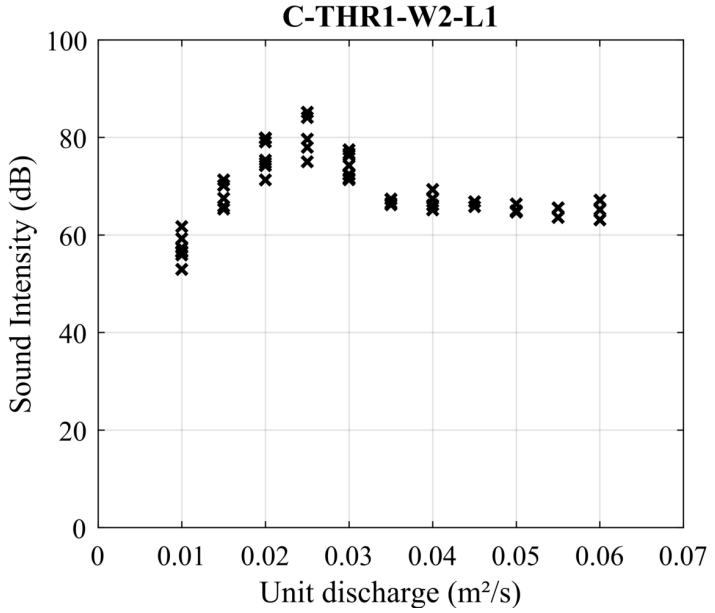

Results of sound analysis

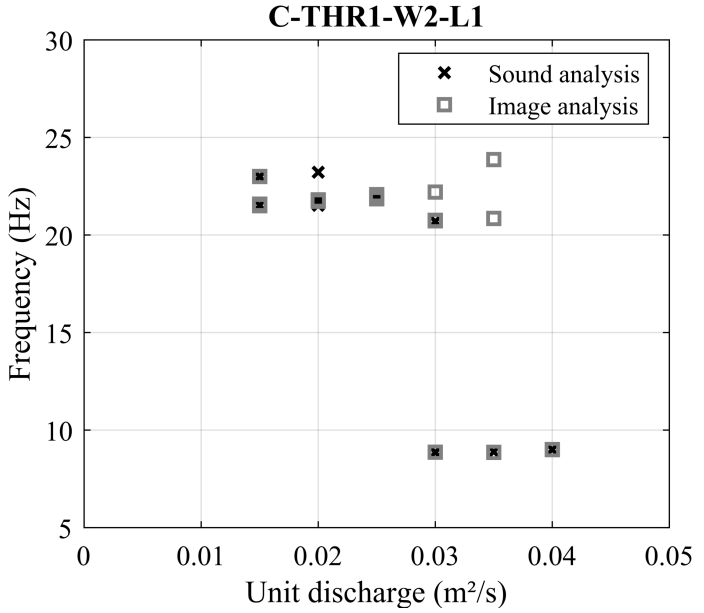

Frequencies obtained by sound and image analyses

Configuration: $C - THR1 - W2 - L2$

Abbreviation	Model	Confinement	Crest shape - R	Width W	Height L	Range of q affected by the oscillations	Extreme frequencies
$C - THR1 - W2 - L2$	1	Confined	THR - 15 cm	250 cm	250 cm	0.01 - 0.035 m^2/s	18.04;33.28 Hz

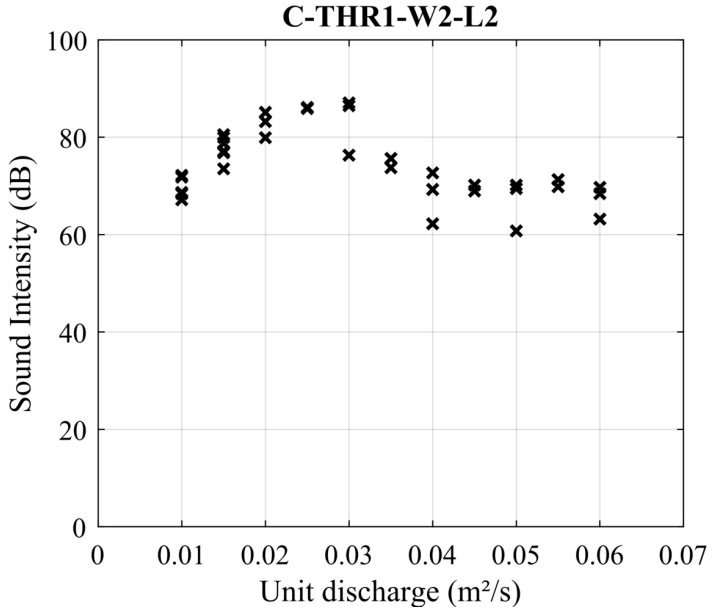

Results of sound analysis

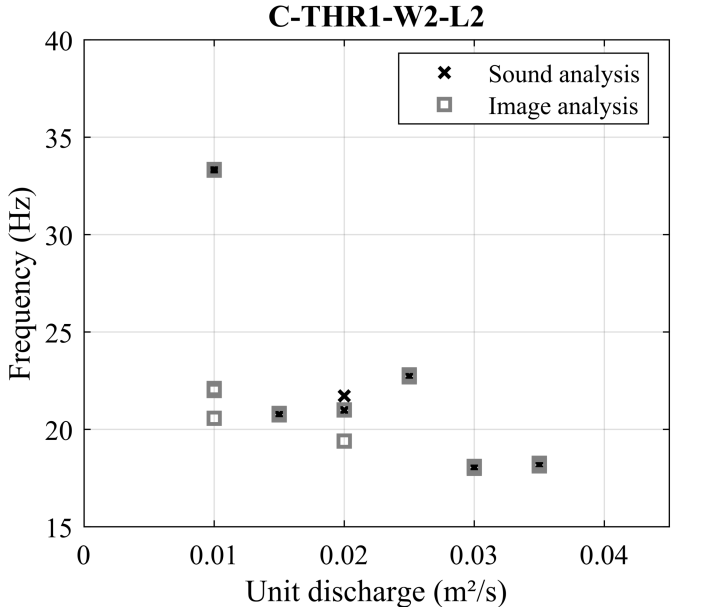

Frequencies obtained by sound and image analyses

Configuration: $C - THR1 - W2 - L3$

Abbreviation	Model	Confinement	Crest shape - R	Width W	Height L	Range of q affected by the oscillations	Extreme frequencies
$C - THR1 - W2 - L3$	1	Confined	THR - 15 cm	250 cm	200 cm	0.01 - 0.02 m^2/s	7.35;33.15 Hz

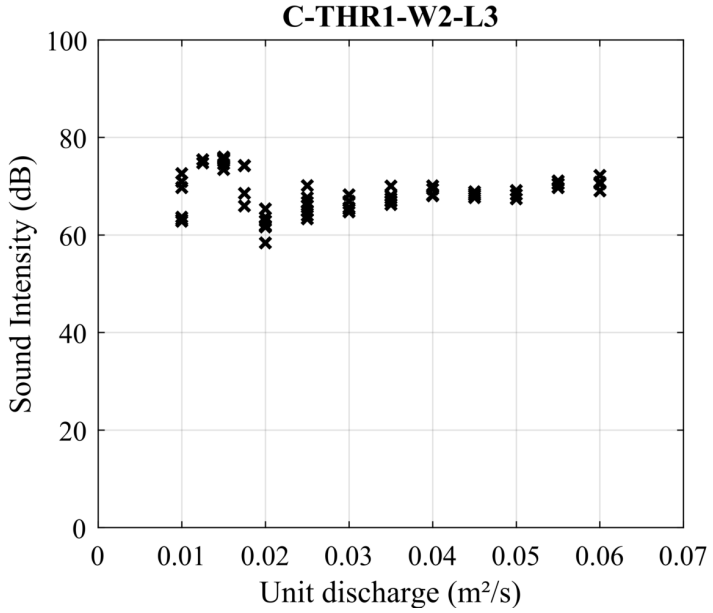

Results of sound analysis

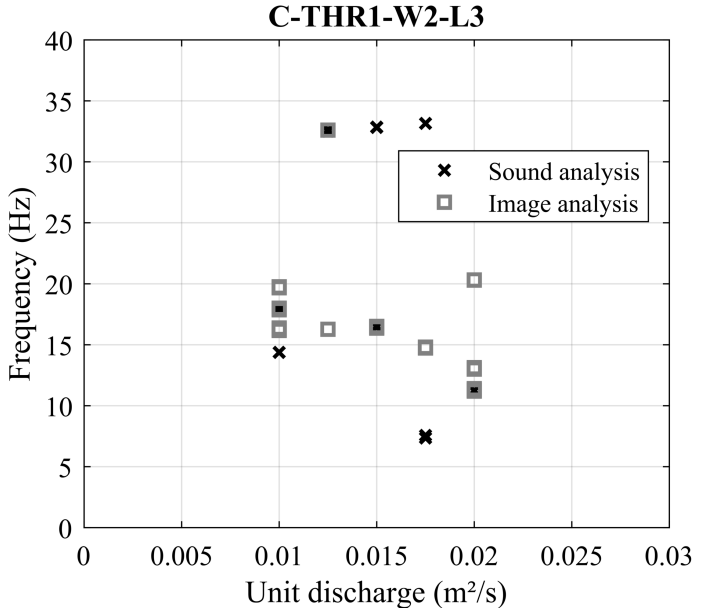

Frequencies obtained by sound and image analyses

Configuration: $C - THR1 - W2 - L4$

Abbreviation	Model	Confinement	Crest shape - R	Width W	Height L	Range of q affected by the oscillations	Extreme frequencies
$C - THR1 - W2 - L4$	1	Confined	THR - 15 cm	250 cm	150 cm	No nappe oscillation	

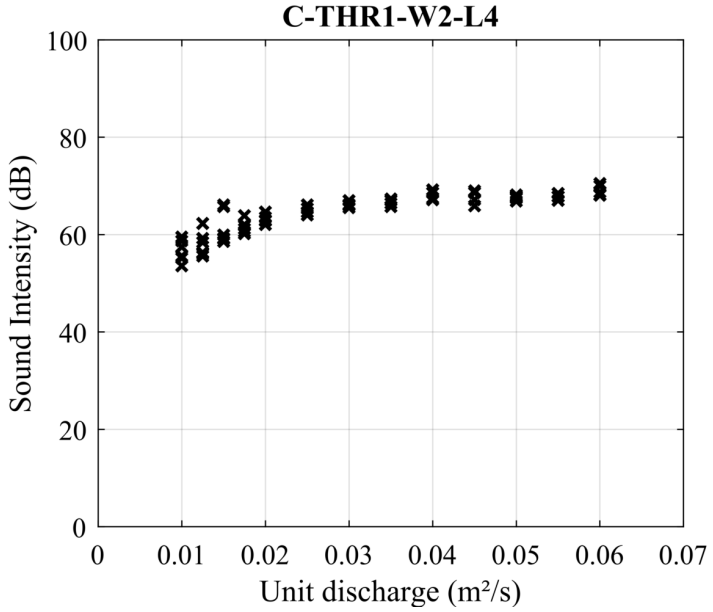

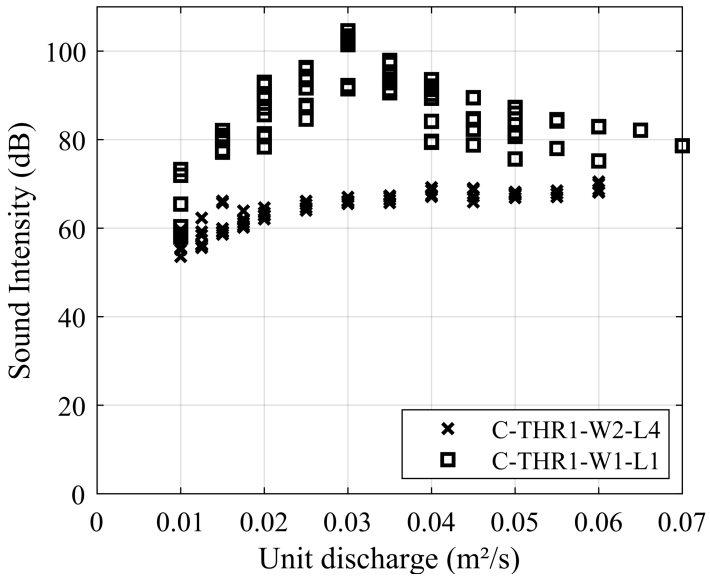

Results of sound analysis

Configuration: $C - THR1 - W3 - L1$

Abbreviation	Model	Confinement	Crest shape - R	Width W	Height L	Range of q affected by the oscillations	Extreme frequencies
$C - THR1 - W3 - L1$	1	Confined	THR - 15 cm	200 cm	300 cm	0.015 - 0.035 m^2/s	9.97;24.63 Hz

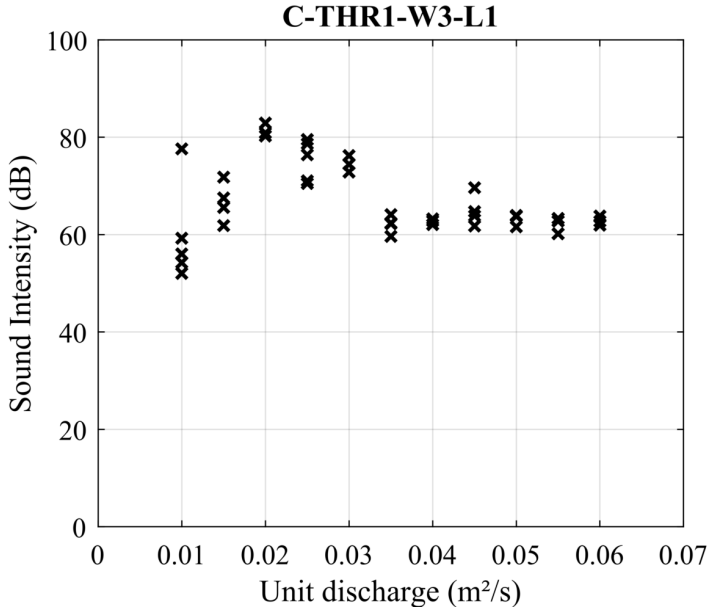

Results of sound analysis

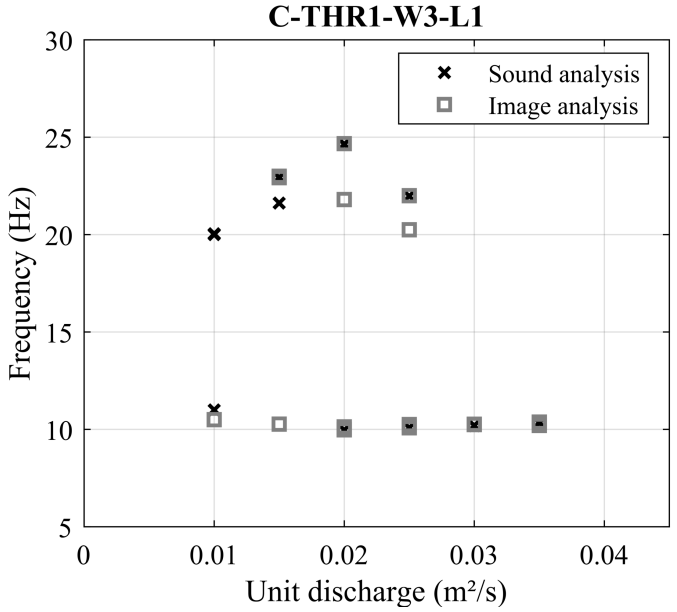

Frequencies obtained by sound and image analyses

Configuration: $C - THR1 - W3 - L2$

Abbreviation	Model	Confinement	Crest shape - R	Width W	Height L	Range of q affected by the oscillations	Extreme frequencies
$C - THR1 - W3 - L2$	1	Confined	THR - 15 cm	200 cm	250 cm	0.01 - 0.035 m^2/s	9.42;31.01 Hz

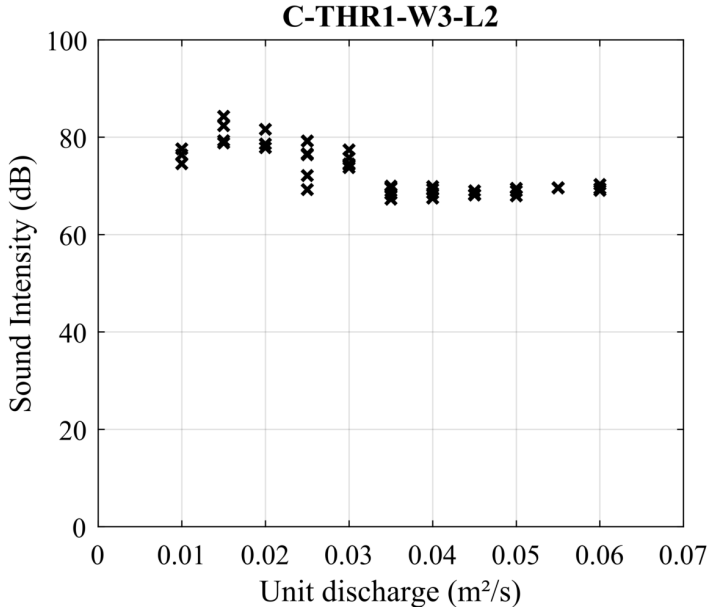

Results of sound analysis

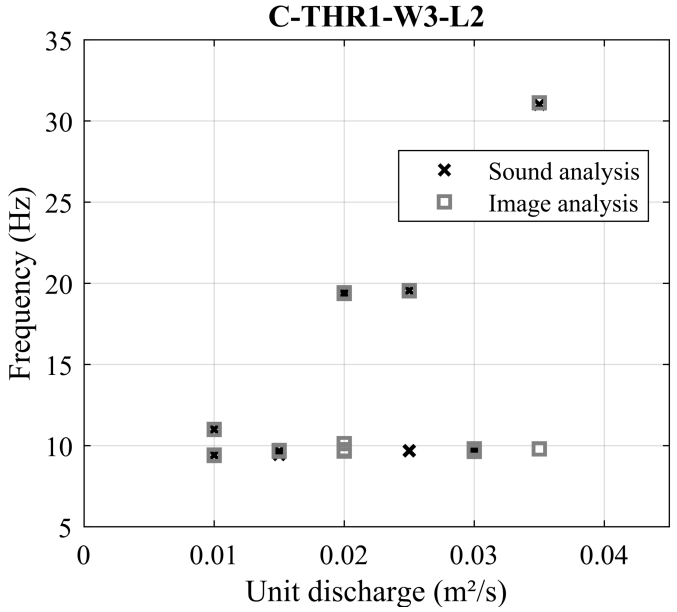

Frequencies obtained by sound and image analyses

Configuration: $C - THR1 - W3 - L3$

Abbreviation	Model	Confinement	Crest shape - R	Width W	Height L	Range of q affected by the oscillations	Extreme frequencies
$C - THR1 - W3 - L3$	1	Confined	THR - 15 cm	200 cm	200 cm	0.01 - 0.02 m^2/s	14.78;16.89 Hz

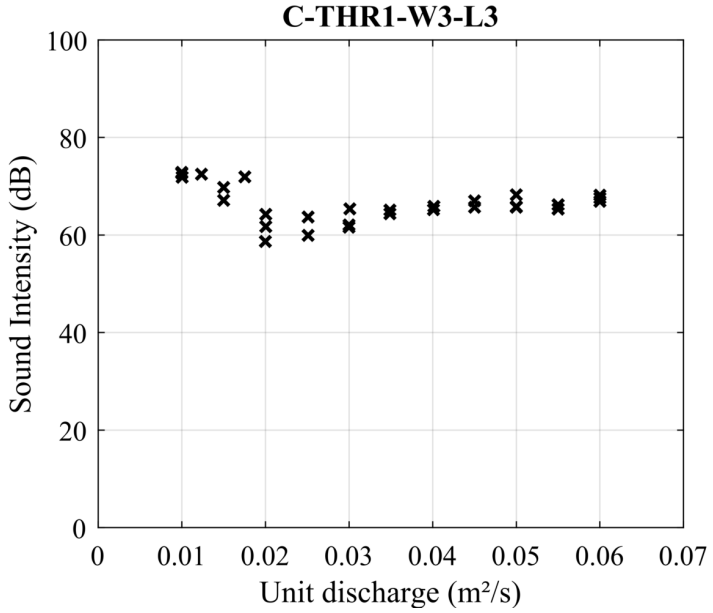

Results of sound analysis

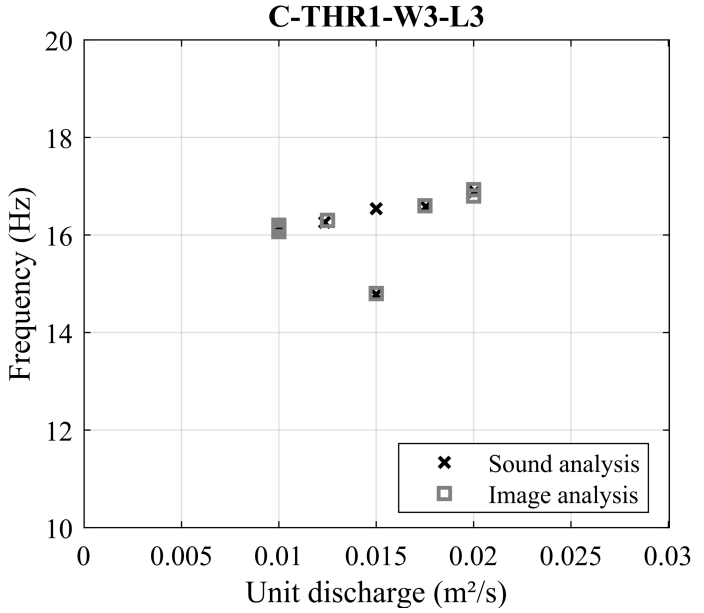

Frequencies obtained by sound and image analyses

Configuration: $C - THR1 - W3 - L4$

Abbreviation	Model	Confinement	Crest shape - R	Width W	Height L	Range of q affected by the oscillations	Extreme frequencies
$C - THR1 - W3 - L4$	1	Confined	THR - 15 cm	200 cm	150 cm	No nappe oscillation	

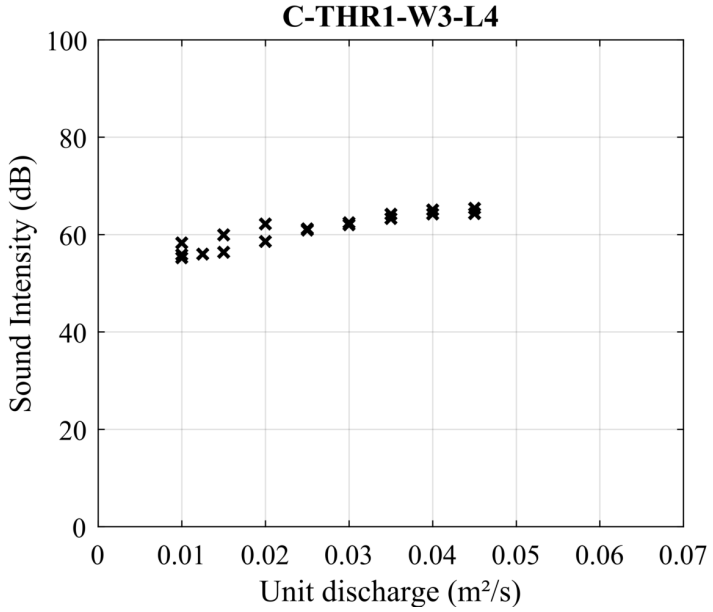

Results of sound analysis

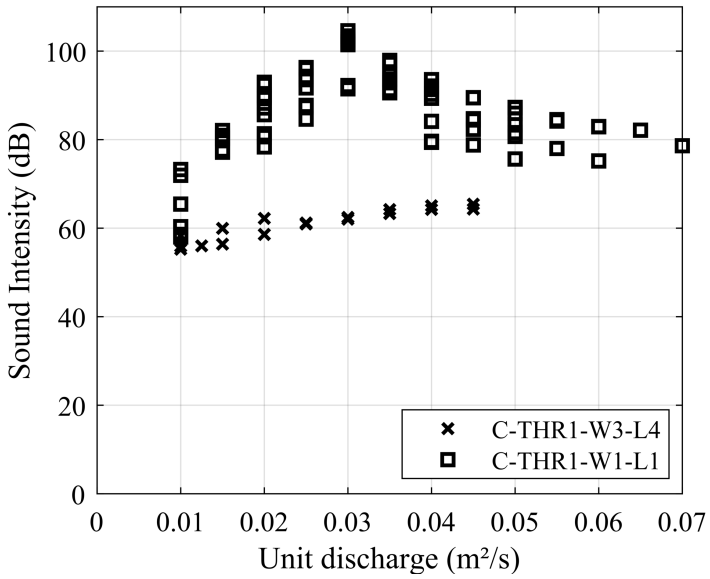

Configuration: $C - THR1 - W4 - L1$

Abbreviation	Model	Confinement	Crest shape - R	Width W	Height L	Range of q affected by the oscillations	Extreme frequencies
$C - THR1 - W4 - L1$	1	Confined	THR - 15 cm	150 cm	300 cm	0.015 - 0.03 m^2/s	16.05;24.75 Hz

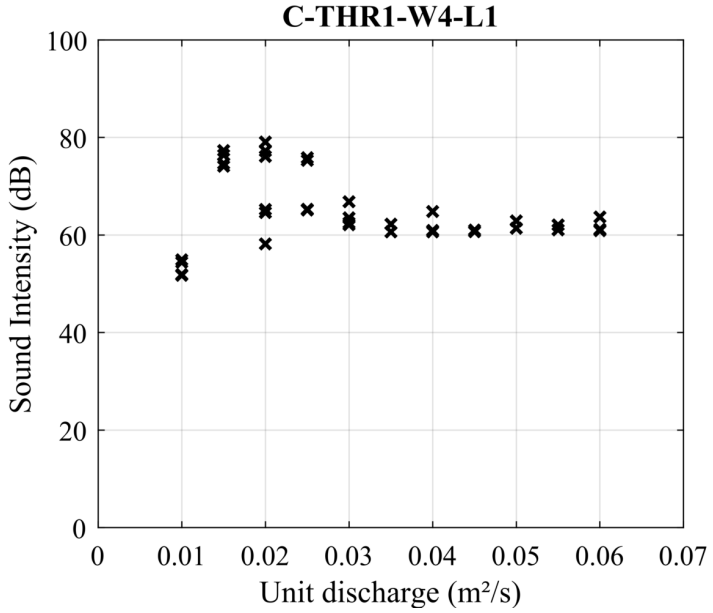

Results of sound analysis

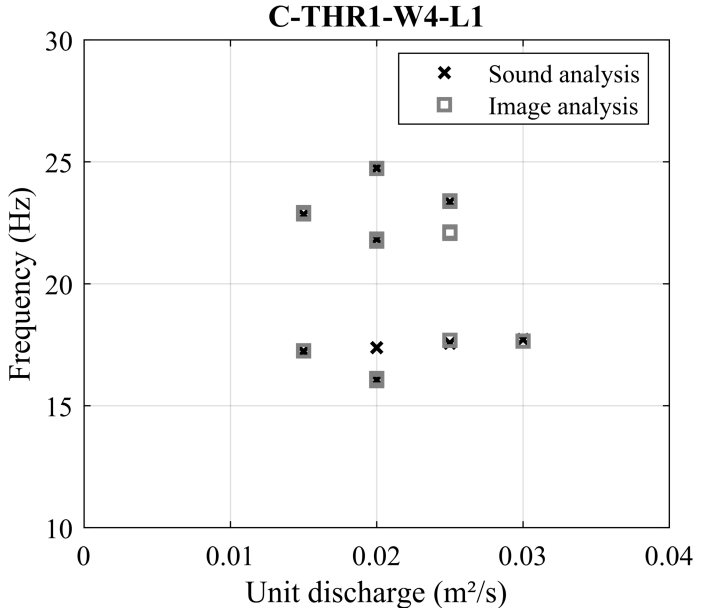

Frequencies obtained by sound and image analyses

Configuration: $C - THR1 - W4 - L2$

Abbreviation	Model	Confinement	Crest shape - R	Width W	Height L	Range of q affected by the oscillations	Extreme frequencies
$C - THR1 - W4 - L2$	1	Confined	THR - 15 cm	150 cm	250 cm	0.01 - 0.035 m^2/s	13.22;15.51 Hz

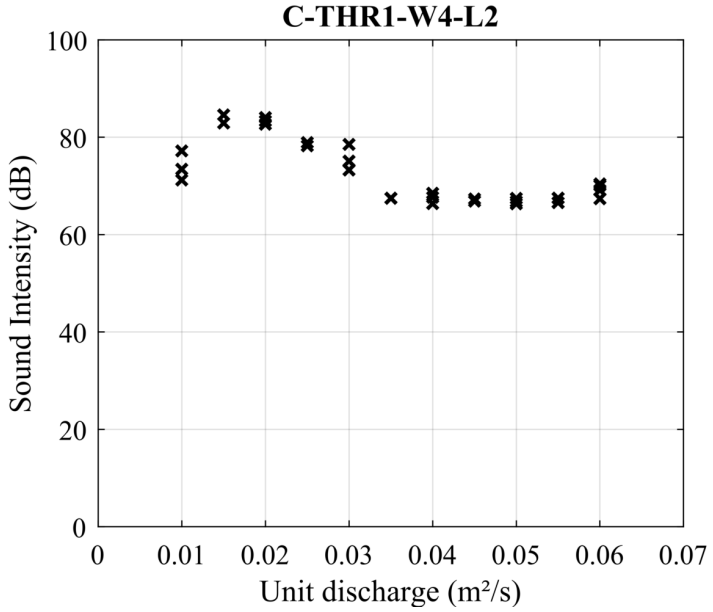

Results of sound analysis

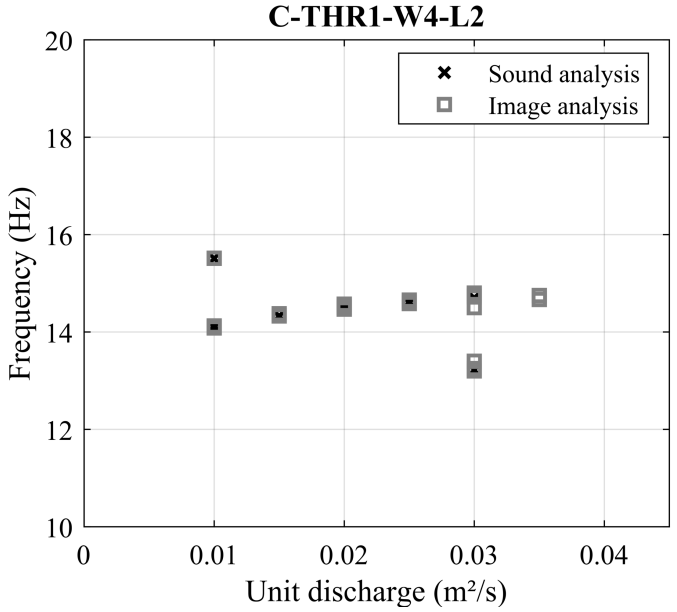

Frequencies obtained by sound and image analyses

Configuration: $C - THR1 - W4 - L3$

Abbreviation	Model	Confinement	Crest shape - R	Width W	Height L	Range of q affected by the oscillations	Extreme frequencies
$C - THR1 - W4 - L3$	1	Confined	THR - 15 cm	150 cm	200 cm	0.01 - 0.0175 m^2/s	18.11;60.54 Hz

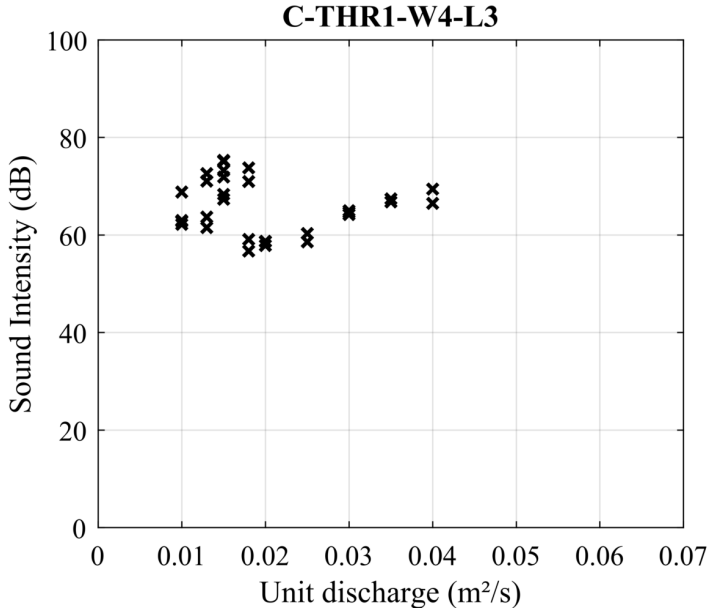

Results of sound analysis

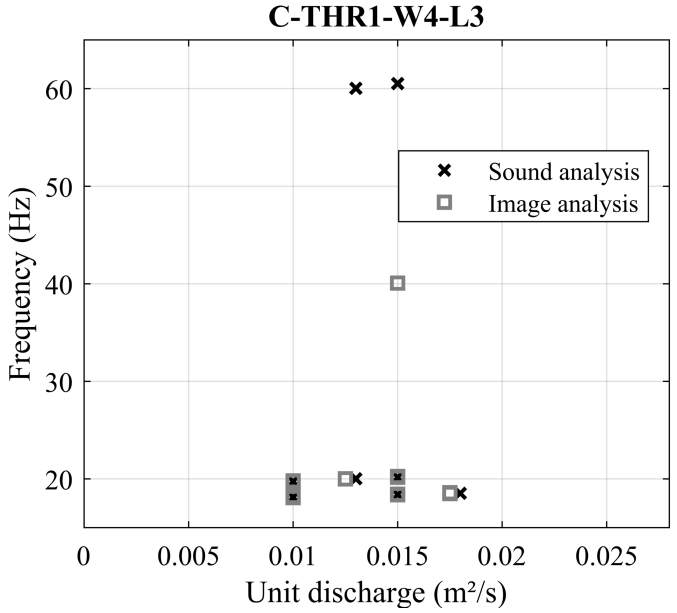

Frequencies obtained by sound and image analyses

Configuration: $C - THR1 - W4 - L4$

Abbreviation	Model	Confinement	Crest shape - R	Width W	Height L	Range of q affected by the oscillations	Extreme frequencies
$C - THR1 - W4 - L4$	1	Confined	THR - 15 cm	150 cm	150 cm	No nappe oscillation	

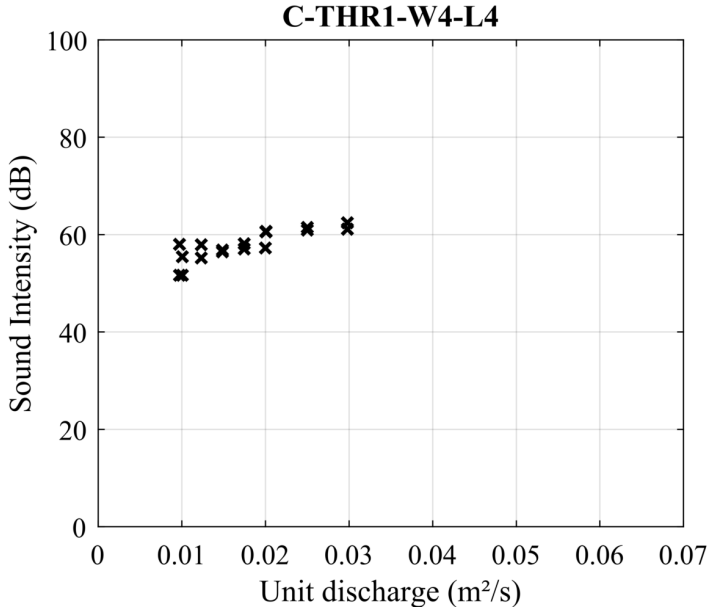

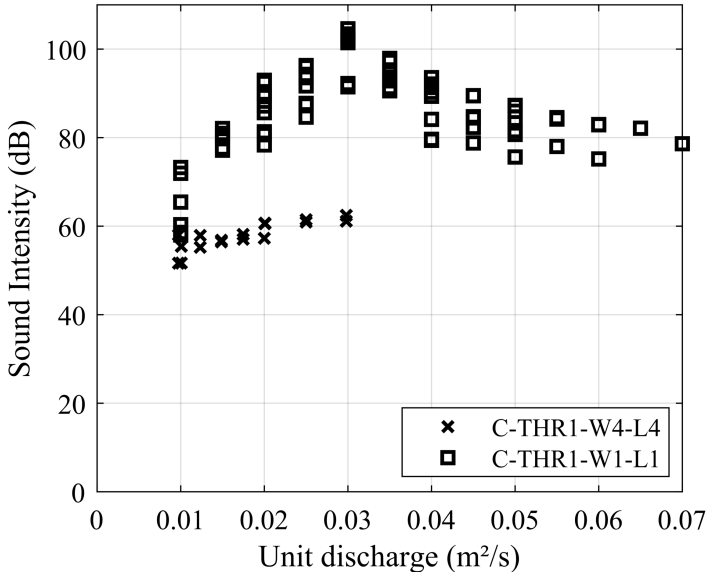

Results of sound analysis

Configuration: $C - THR1 - W6 - L1$

Abbreviation	Model	Confinement	Crest shape - R	Width W	Height L	Range of q affected by the oscillations	Extreme frequencies
$C - THR1 - W6 - L1$	1	Confined	THR - 15 cm	100 cm	300 cm	0.015 - 0.02 m^2/s	22.78;22.98 Hz

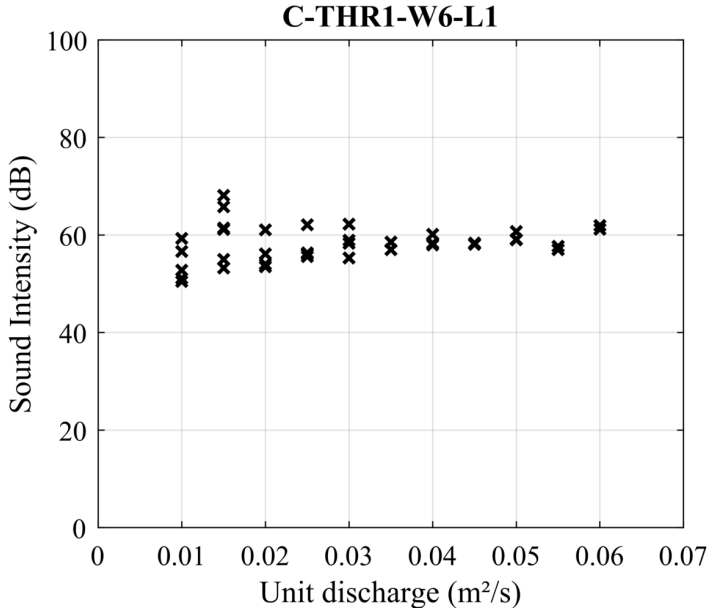

Results of sound analysis

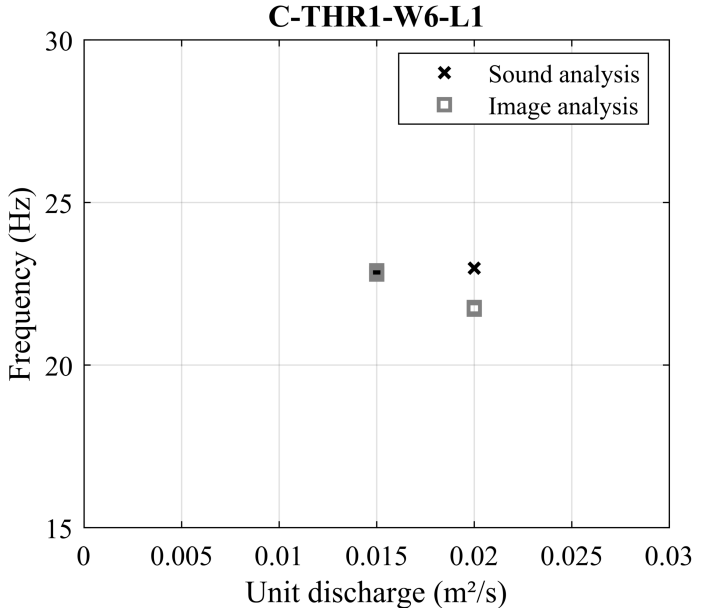

Frequencies obtained by sound and image analyses

Configuration: $C - THR1 - W6 - L2$

Abbreviation	Model	Confinement	Crest shape - R	Width W	Height L	Range of q affected by the oscillations	Extreme frequencies
$C - THR1 - W6 - L2$	1	Confined	THR - 15 cm	100 cm	250 cm	0.01 - 0.035 m^2/s	20.86;23.33 Hz

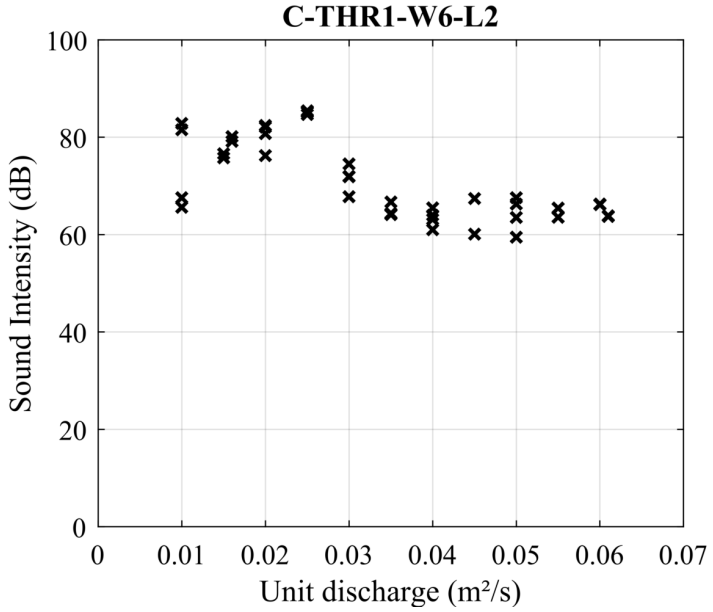

Results of sound analysis

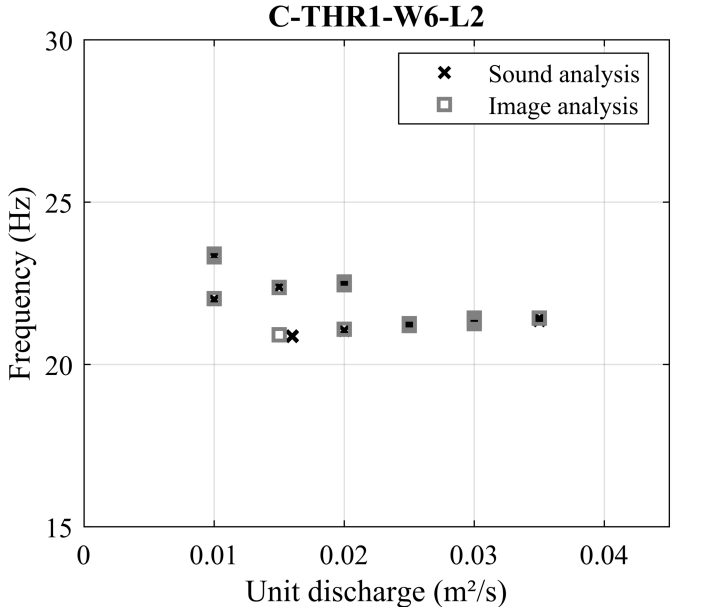

Frequencies obtained by sound and image analyses

Configuration: $C - THR1 - W6 - L3$

Abbreviation	Model	Confinement	Crest shape - R	Width W	Height L	Range of q affected by the oscillations	Extreme frequencies
$C - THR1 - W6 - L3$	1	Confined	THR - 15 cm	100 cm	200 cm	0.01 - 0.015 m^2/s	14.57;44.52 Hz

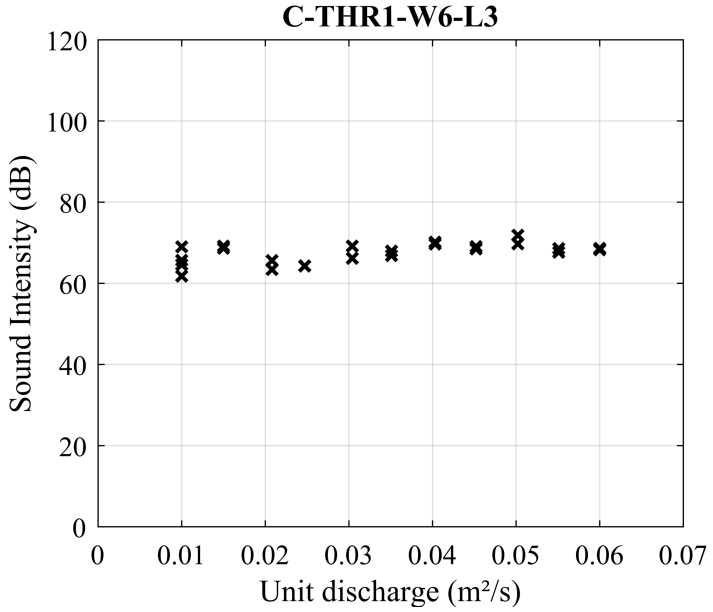

Results of sound analysis

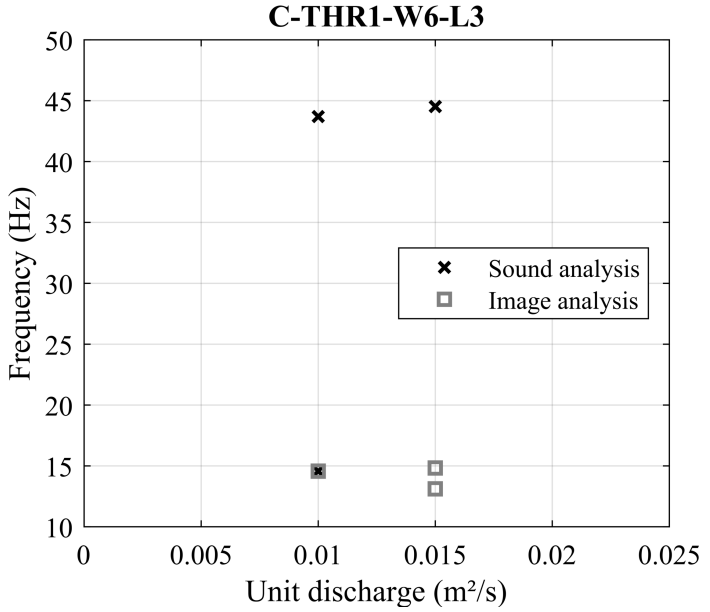

Frequencies obtained by sound and image analyses

Configuration: $C - THR1 - W6 - L4$

Abbreviation	Model	Confinement	Crest shape - R	Width W	Height L	Range of q affected by the oscillations	Extreme frequencies
$C - THR1 - W6 - L4$	1	Confined	THR - 15 cm	100 cm	150 cm	No nappe oscillation	

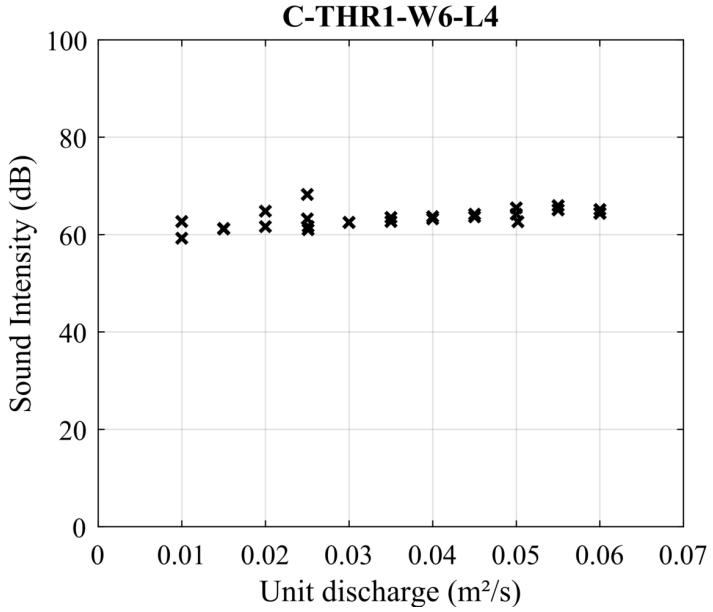

Results of sound analysis

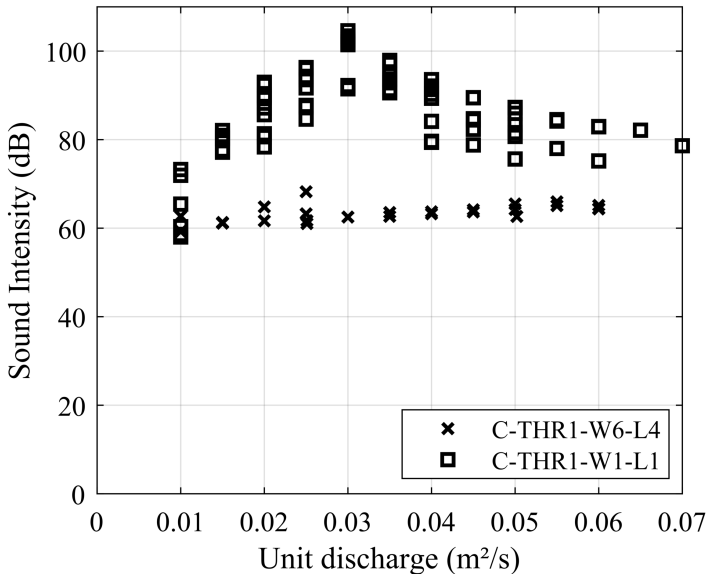

Configuration: $C - HR1 - W1 - L1$

Abbreviation	Model	Confinement	Crest shape - R	Width W	Height L	Range of q affected by the oscillations	Extreme frequencies
$C - HR1 - W1 - L1$	1	Confined	HR - 15 cm	345 cm	300 cm	No nappe oscillation	

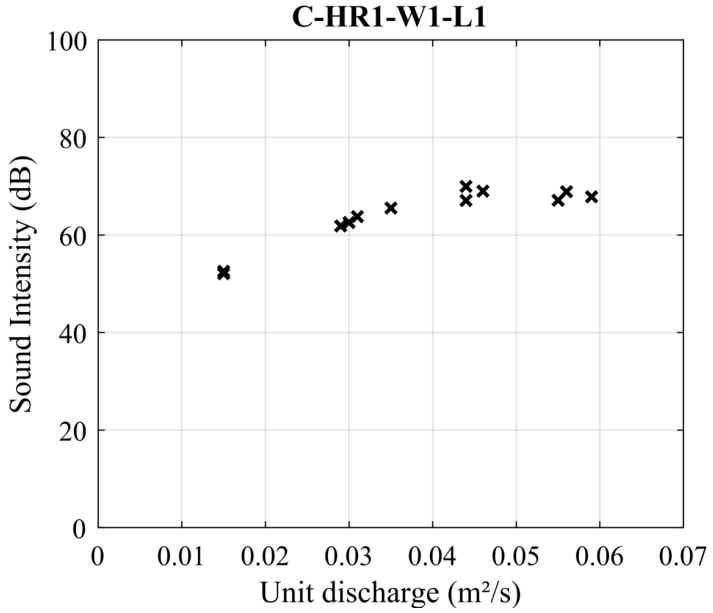

Results of sound analysis

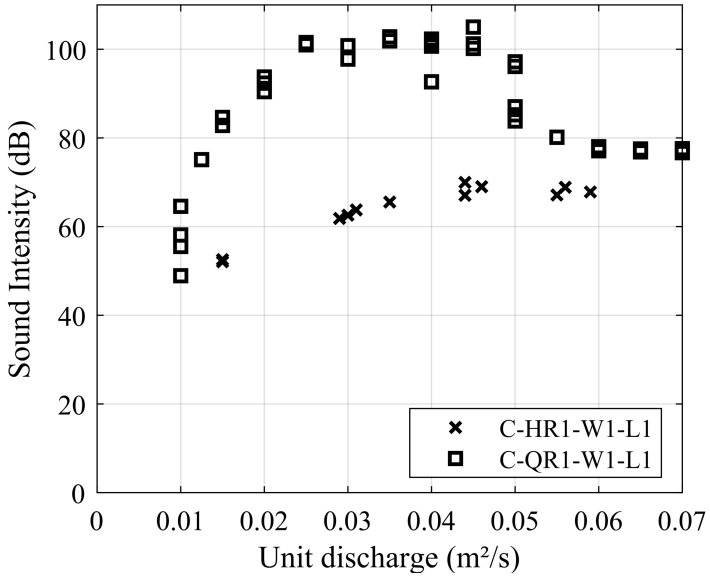

Configuration: $C - HR1 - W1 - L5$

Abbreviation	Model	Confinement	Crest shape - R	Width W	Height L	Range of q affected by the oscillations	Extreme frequencies
$C - HR1 - W1 - L5$	1	Confined	HR - 15 cm	345 cm	100 cm	0.015 - 0.045 m^2/s	13.51.2 Hz

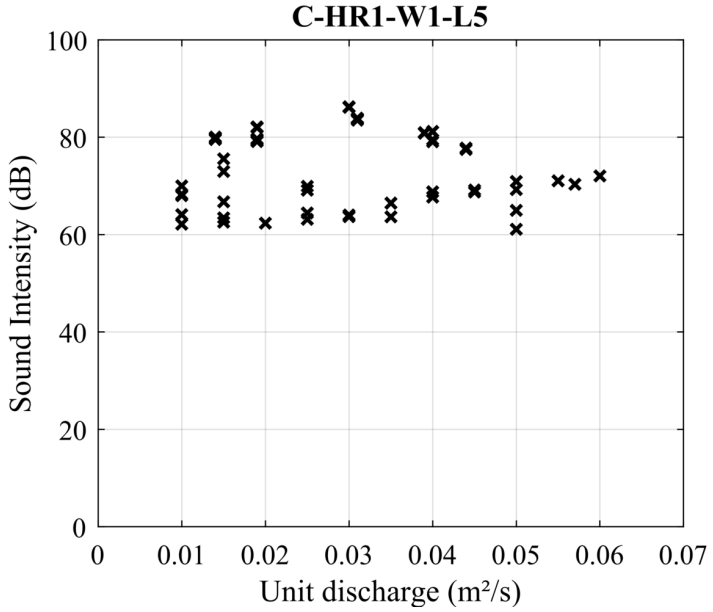

Results of sound analysis

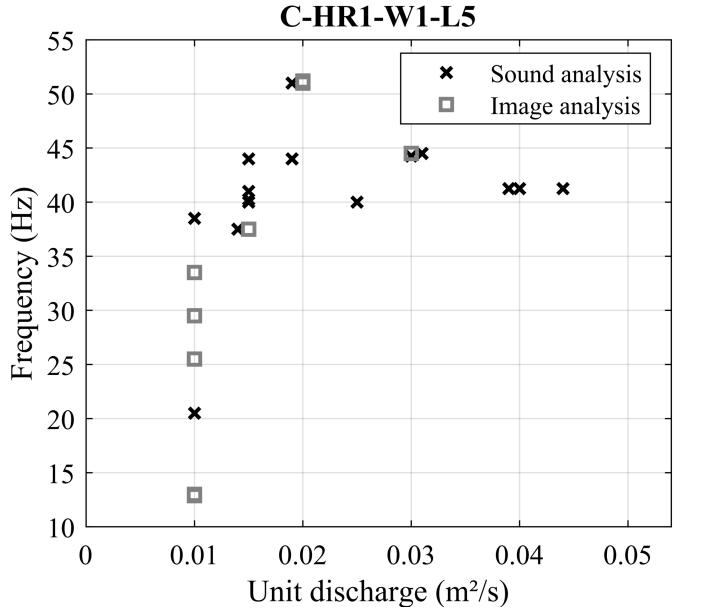

Frequencies obtained by sound and image analyses

Configuration: $C - HR1 - W1 - L5$

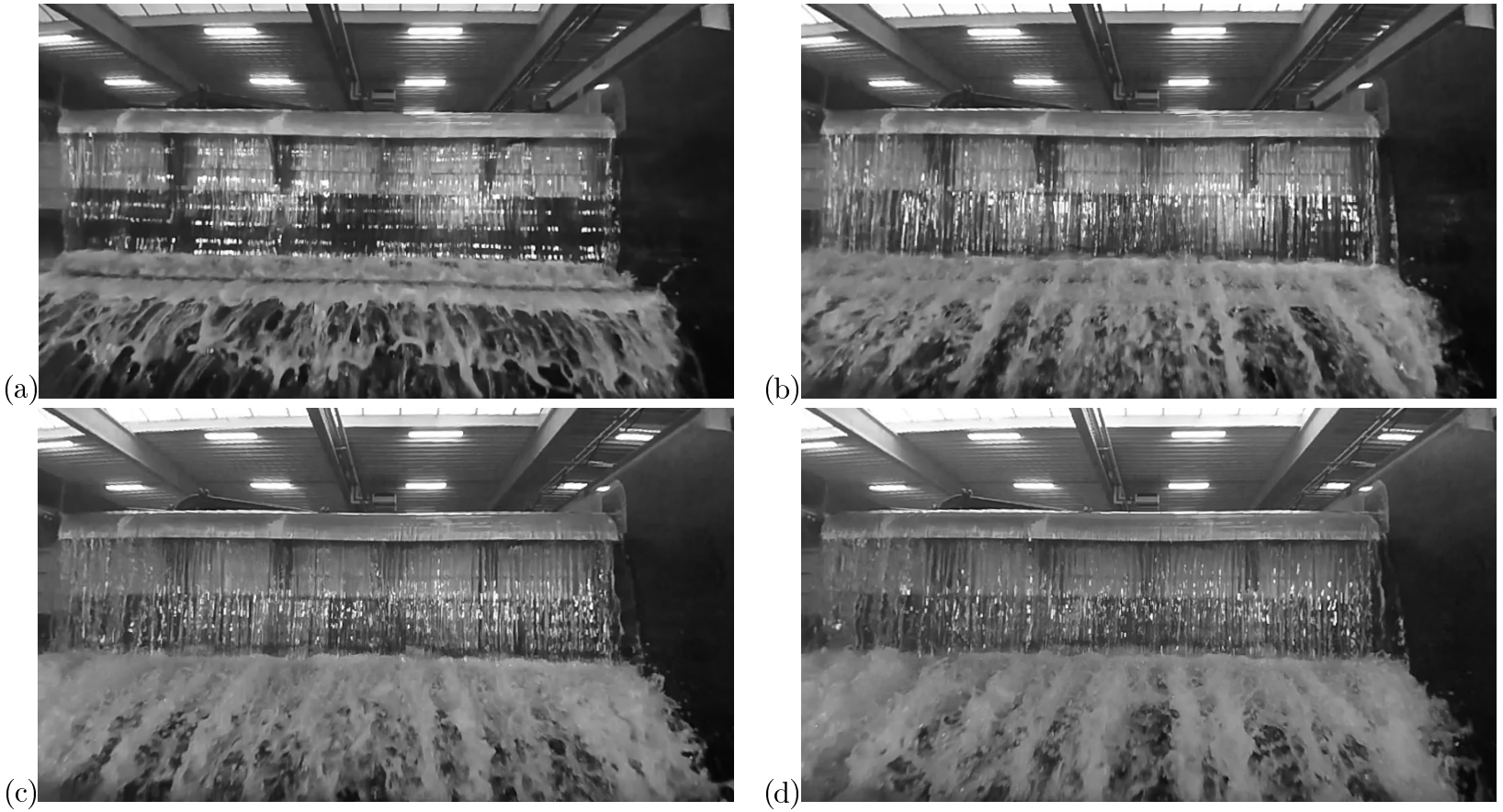

Flow characteristics : (a) $q = 0.01$ m²/s, (b) $q = 0.02$ m²/s, $q = 0.03$ m²/s and $q = 0.04$ m²/s

Configuration: $C - HR1 - W1 - L7$

Abbreviation	Model	Confinement	Crest shape - R	Width W	Height L	Range of q affected by the oscillations	Extreme frequencies
$C - HR1 - W1 - L7$	1	Confined	HR - 15 cm	345 cm	50 cm	0.01 - 0.04 m^2/s	34.25;41.25 Hz

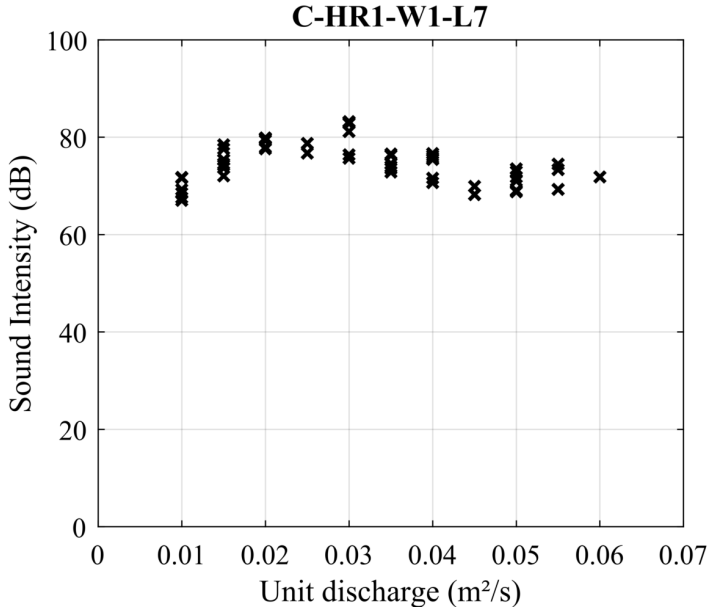

Results of sound analysis

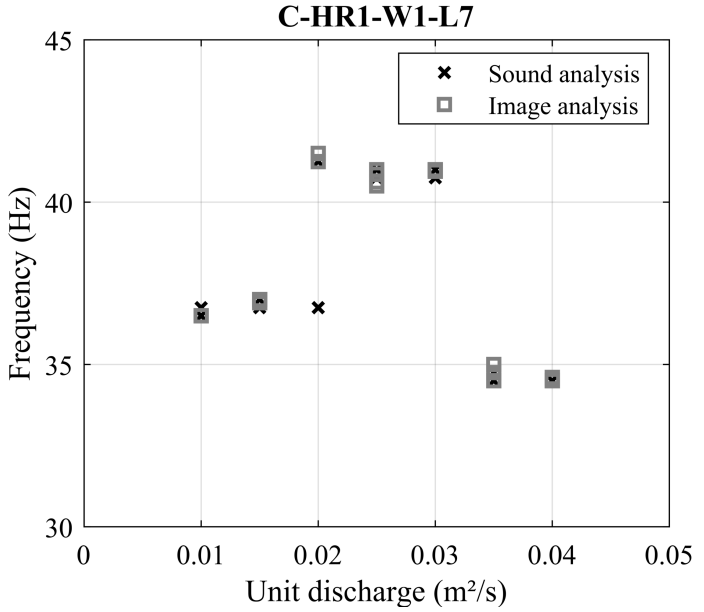

Frequencies obtained by sound and image analyses

Configuration: $UC - QR1 - W1 - L1$

Abbreviation	Model	Confinement	Crest shape - R	Width W	Height L	Range of q affected by the oscillations	Extreme frequencies
$UC - QR1 - W1 - L1$	1	Unconfined	QR - 15 cm	345 cm	300 cm	0.01 - 0.045 m^2/s	32.25;50.8 Hz

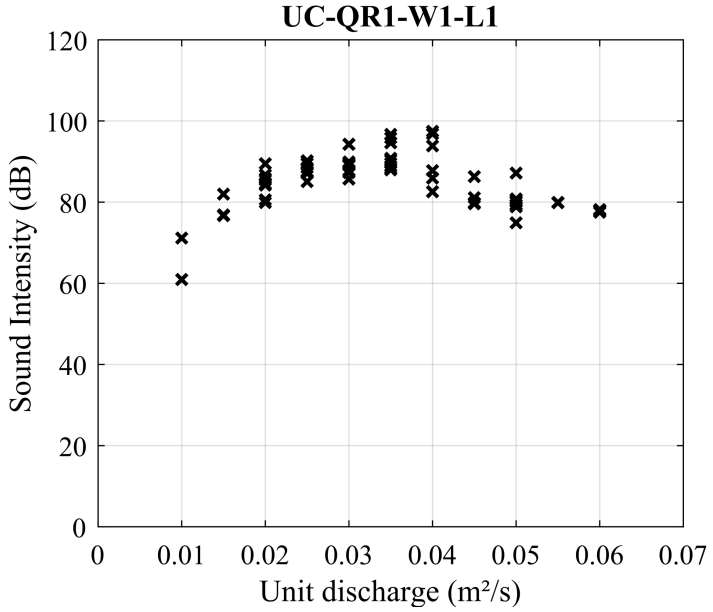

Results of sound analysis

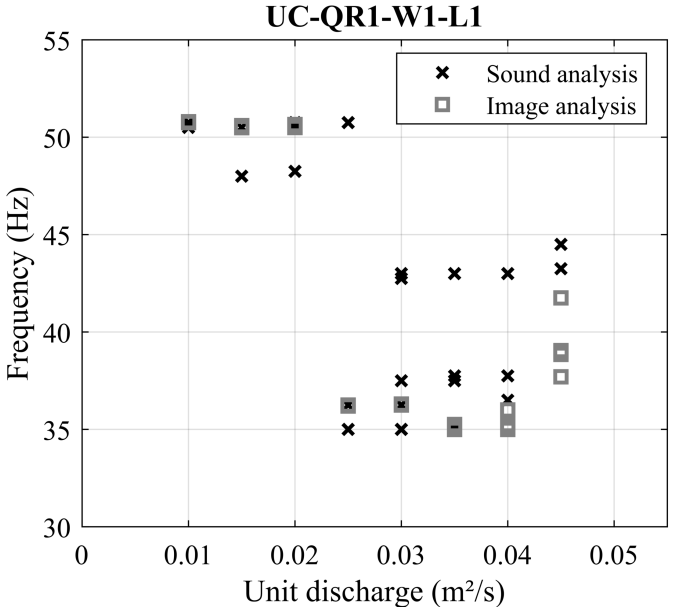

Frequencies obtained by sound and image analyses

Configuration: $UC - QR1 - W1 - L1$

(a) 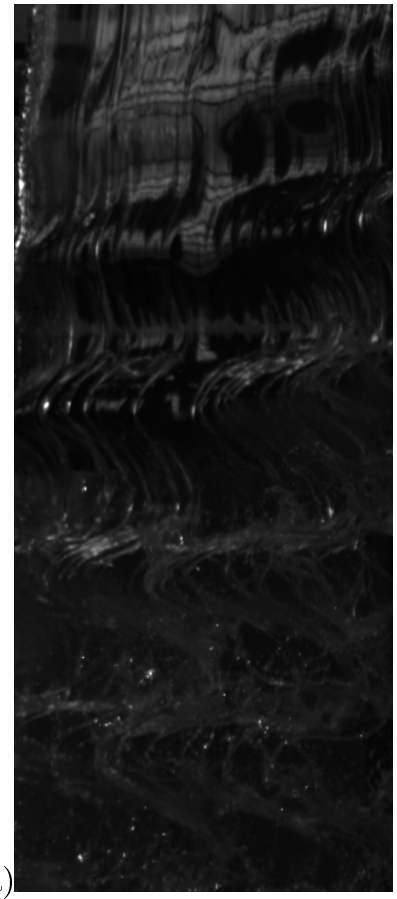 (b) 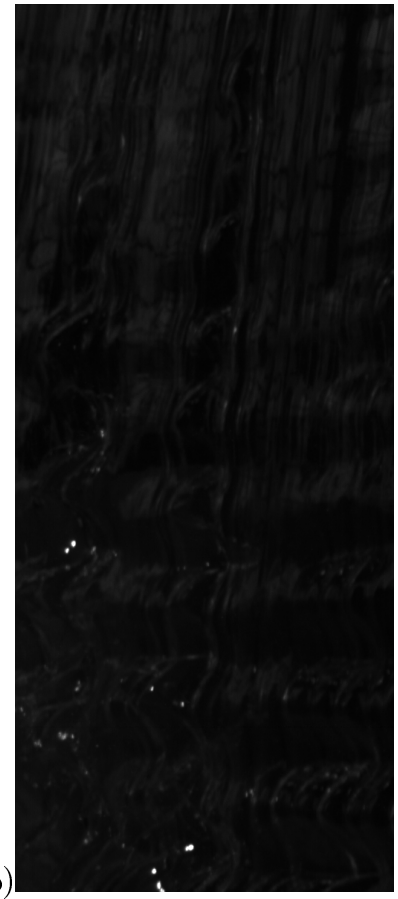 (c) 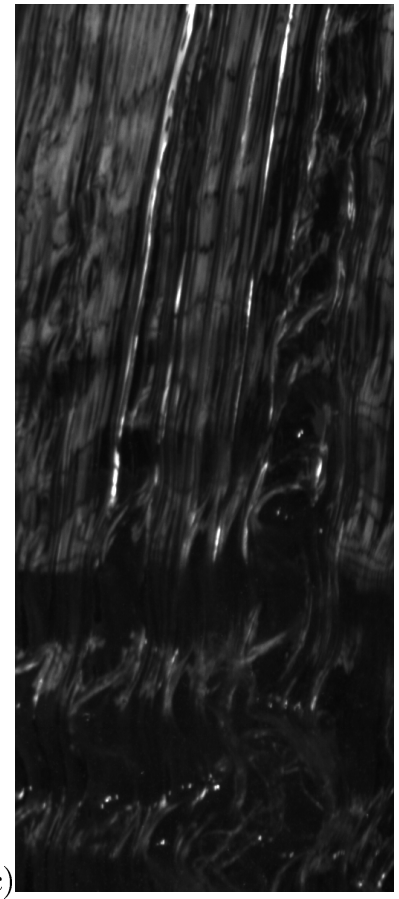

Flow characteristics : (a) $q = 0.01$ m^2/s, (b) $q = 0.02$ m^2/s and $q = 0.03$ m^2/s

Configuration: $UC - QR1 - W1 - L2$

Abbreviation	Model	Confinement	Crest shape - R	Width W	Height L	Range of q affected by the oscillations	Extreme frequencies
$UC - QR1 - W1 - L2$	1	Unconfined	QR - 15 cm	345 cm	250 cm	0.01 - 0.045 m^2/s	38.82;50.22 Hz

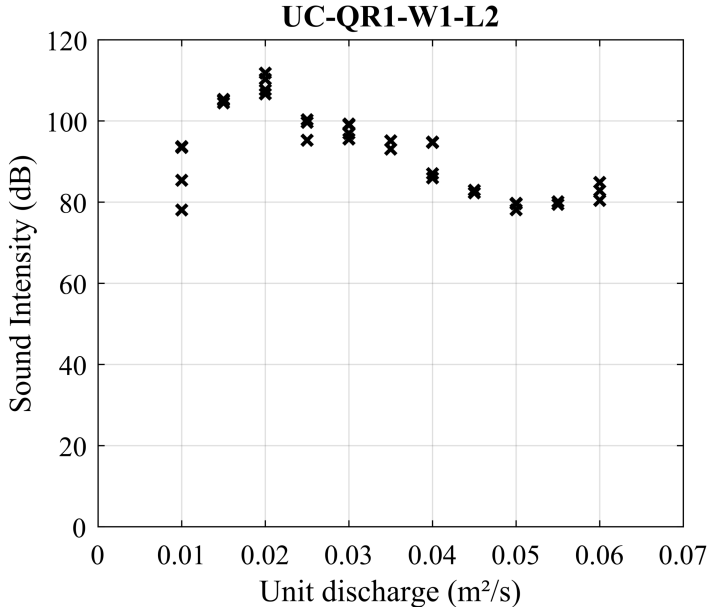

Results of sound analysis

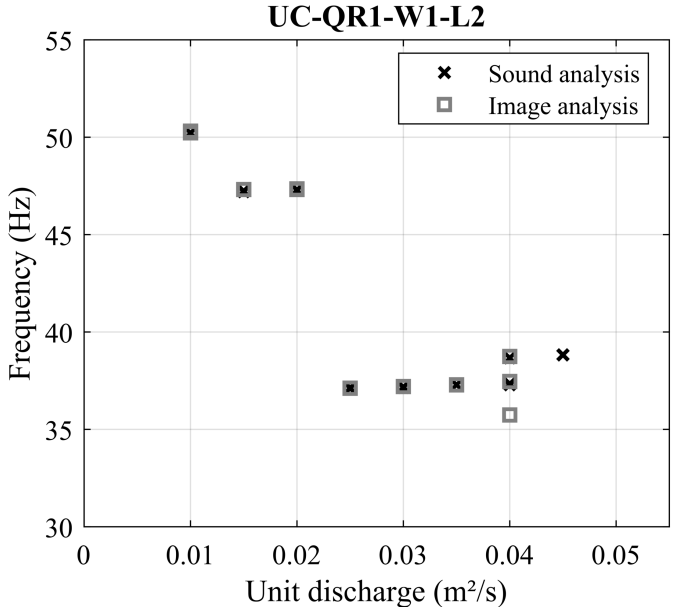

Frequencies obtained by sound and image analyses

Configuration: $UC - QR1 - W1 - L3$

Abbreviation	Model	Confinement	Crest shape - R	Width W	Height L	Range of q affected by the oscillations	Extreme frequencies
$UC - QR1 - W1 - L3$	1	Unconfined	QR - 15 cm	345 cm	200 cm	0.01 - 0.04 m^2/s	26.5;46.25 Hz

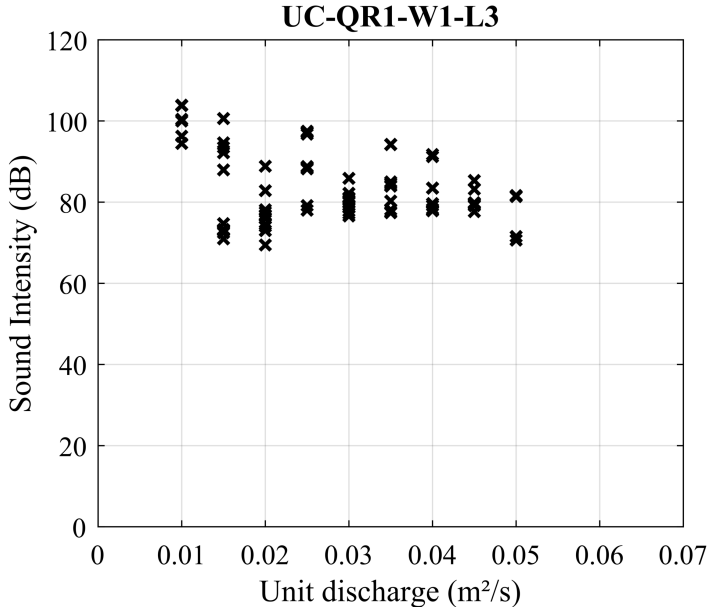

Results of sound analysis

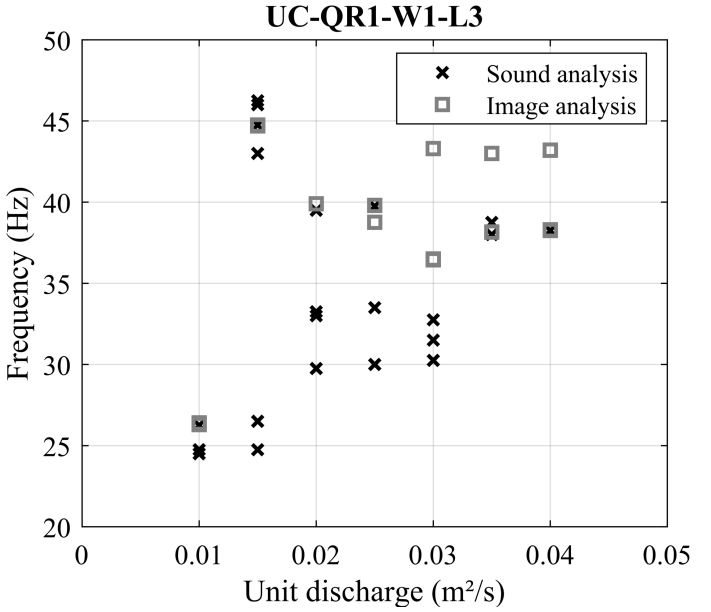

Frequencies obtained by sound and image analyses

Configuration: $UC - QR1 - W1 - L4$

Abbreviation	Model	Confinement	Crest shape - R	Width W	Height L	Range of q affected by the oscillations	Extreme frequencies
$UC - QR1 - W1 - L4$	1	Unconfined	QR - 15 cm	345 cm	150 cm	No nappe oscillation	

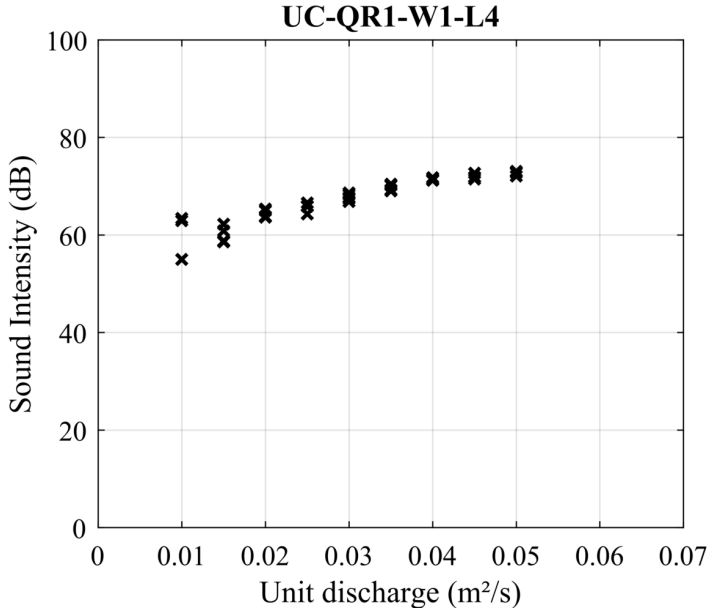

Results of sound analysis

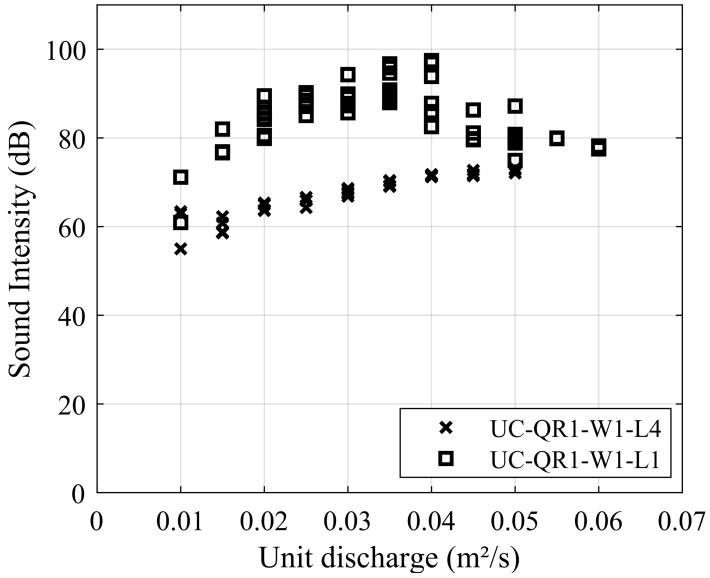

Configuration: $UC - QR1 - W1 - L5$

Abbreviation	Model	Confinement	Crest shape - R	Width W	Height L	Range of q affected by the oscillations	Extreme frequencies
$UC - QR1 - W1 - L5$	1	Unconfined	QR - 15 cm	345 cm	100 cm	No nappe oscillation	

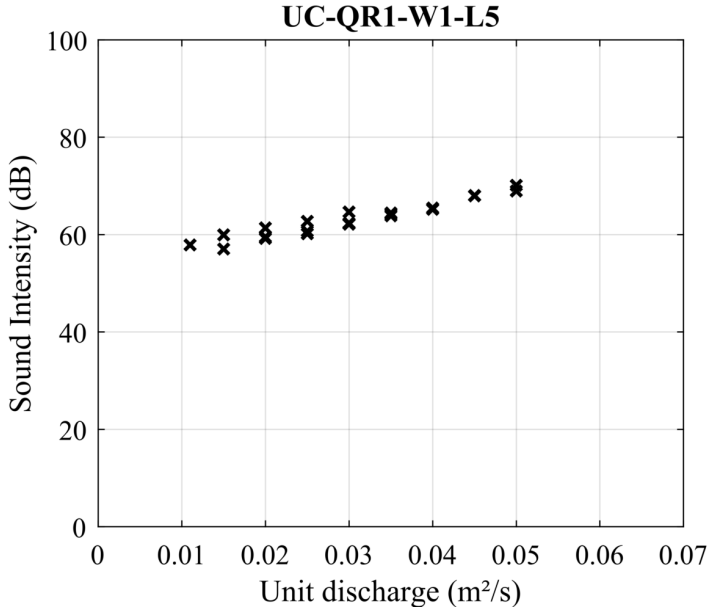

Results of sound analysis

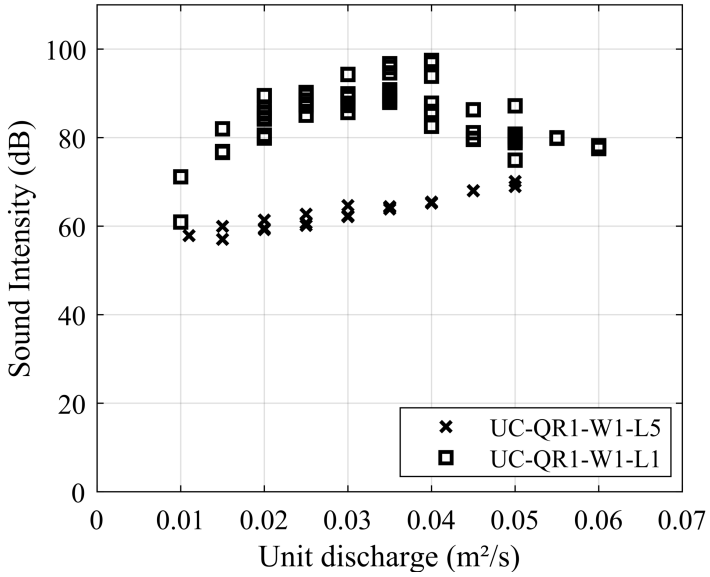

Configuration: $UC - QR1 - W1 - L7$

Abbreviation	Model	Confinement	Crest shape - R	Width W	Height L	Range of q affected by the oscillations	Extreme frequencies
$UC - QR1 - W1 - L7$	1	Unconfined	QR - 15 cm	345 cm	50 cm	No nappe oscillation	

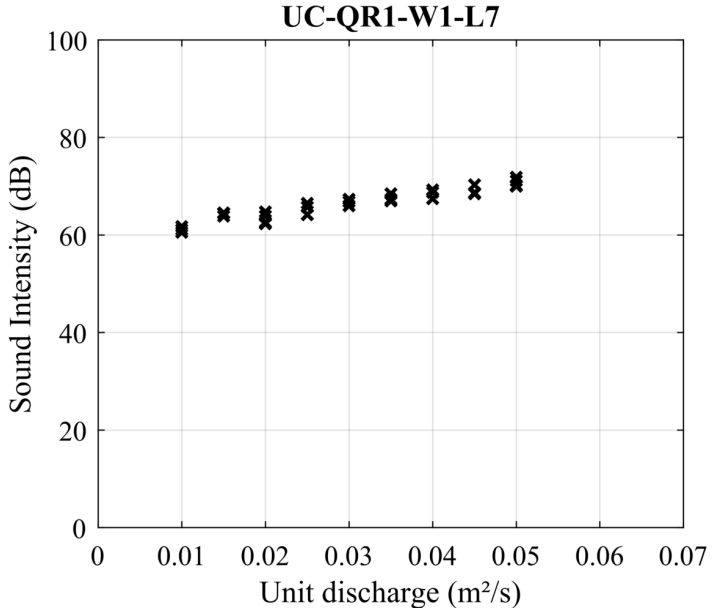

Results of sound analysis

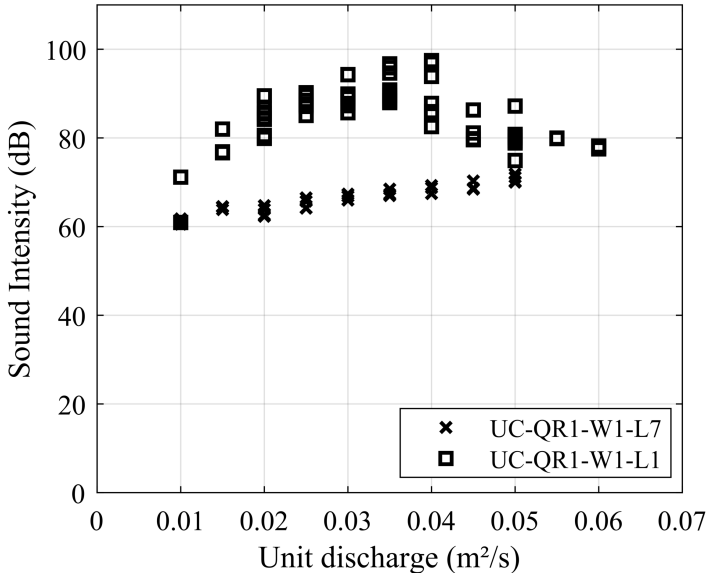

Configuration: $UC - QR1 - W2 - L1$

Abbreviation	Model	Confinement	Crest shape - R	Width W	Height L	Range of q affected by the oscillations	Extreme frequencies
$UC - QR1 - W2 - L1$	1	Unconfined	QR - 15 cm	250 cm	300 cm	0.01 - 0.04 m^2/s	43;53 Hz

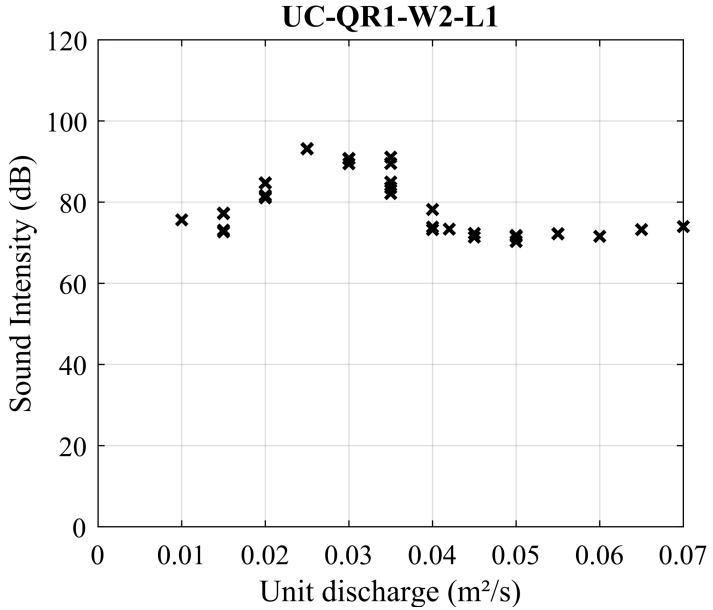

Results of sound analysis

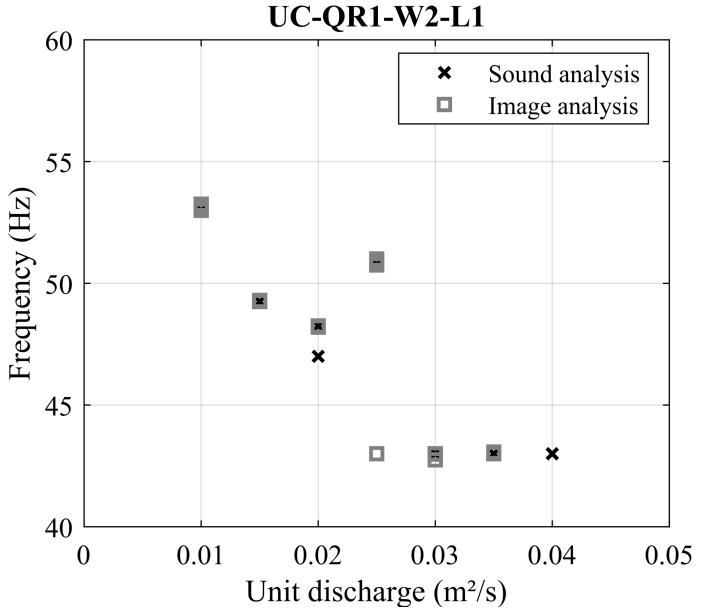

Frequencies obtained by sound and image analyses

Configuration: $UC - QR1 - W2 - L1$

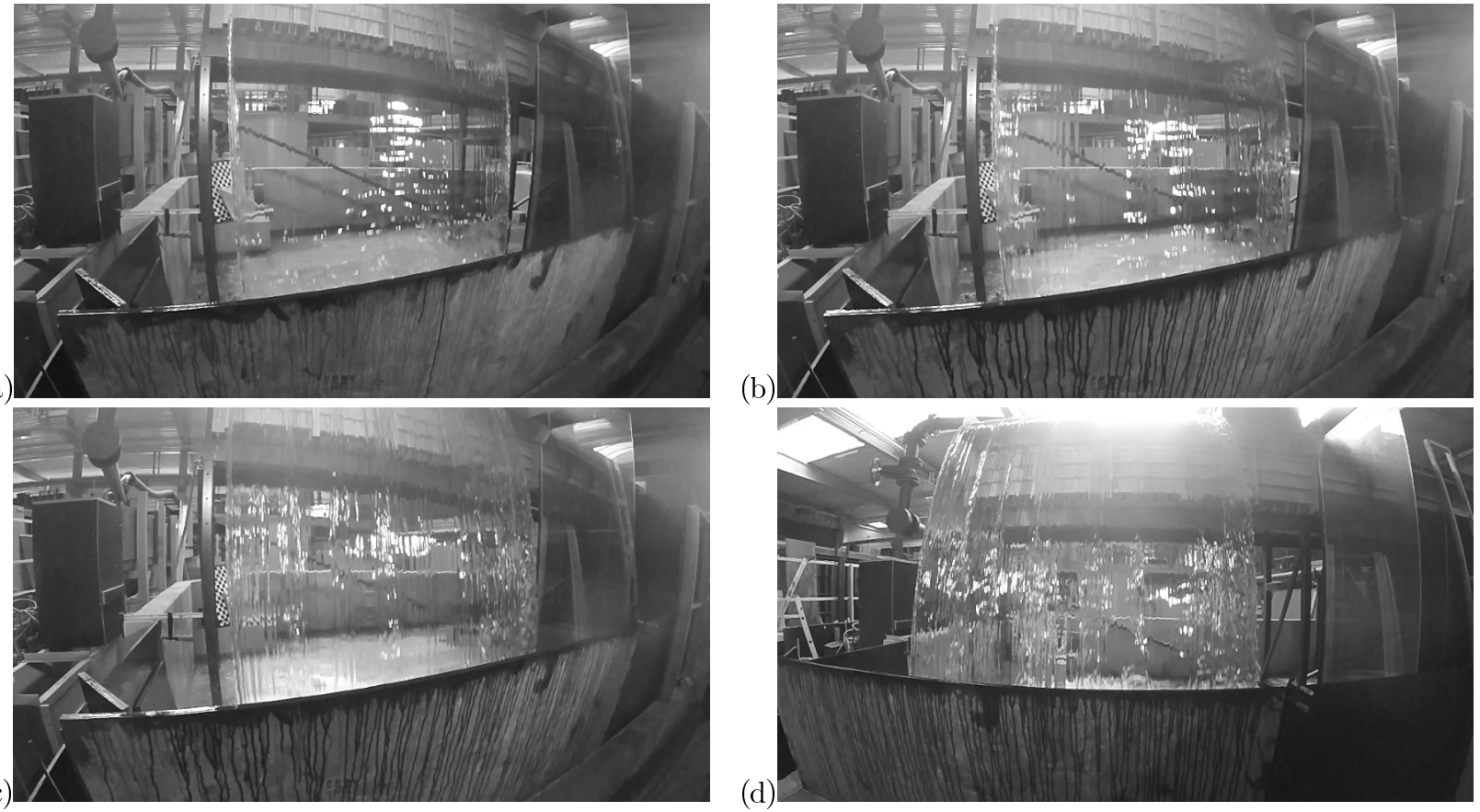

(a) (b) (c) (d)

Flow characteristics : (a) $q = 0.01$ m²/s, (b) $q = 0.02$ m²/s, $q = 0.03$ m²/s and $q = 0.04$ m²/s

Configuration: $UC - QR1 - W2 - L2$

Abbreviation	Model	Confinement	Crest shape - R	Width W	Height L	Range of q affected by the oscillations	Extreme frequencies
$UC - QR1 - W2 - L2$	1	Unconfined	QR - 15 cm	250 cm	250 cm	0.01 - 0.04 m^2/s	24.94;47.33 Hz

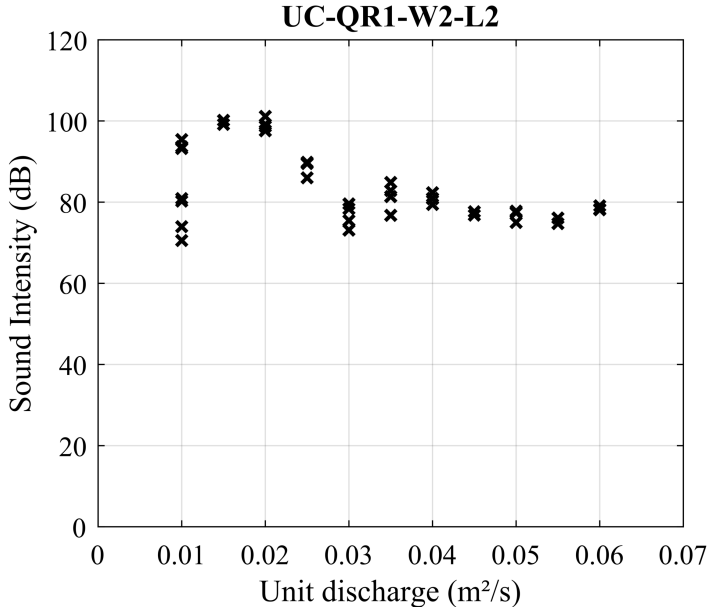

Results of sound analysis

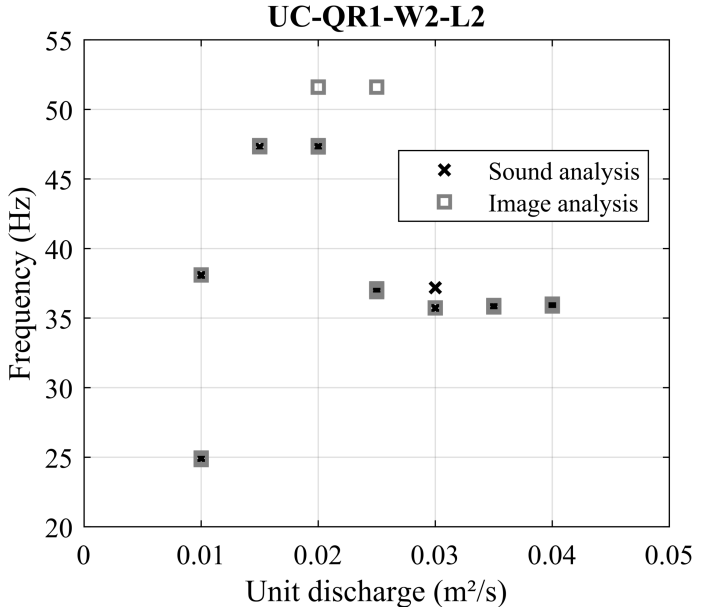

Frequencies obtained by sound and image analyses

Configuration: $UC - QR1 - W2 - L3$

Abbreviation	Model	Confinement	Crest shape - R	Width W	Height L	Range of q affected by the oscillations	Extreme frequencies
$UC - QR1 - W2 - L3$	1	Unconfined	QR - 15 cm	250 cm	200 cm	0.01 - 0.04 m^2/s	25.31;37.4 Hz

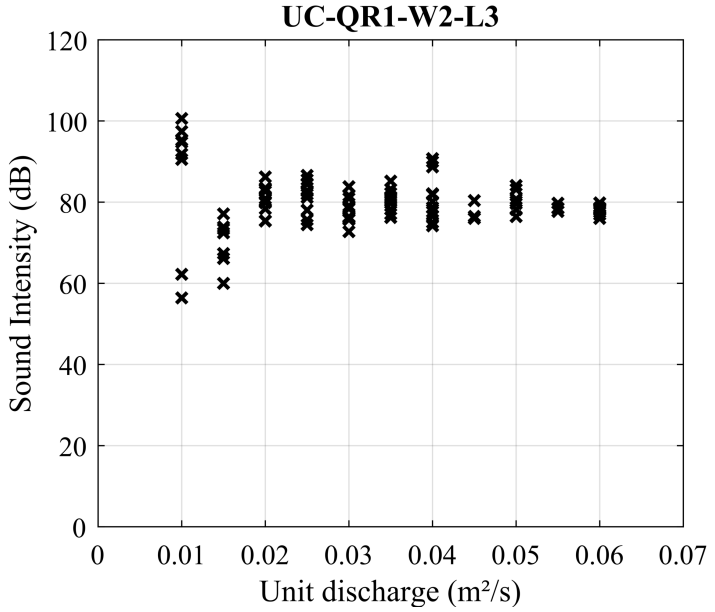

Results of sound analysis

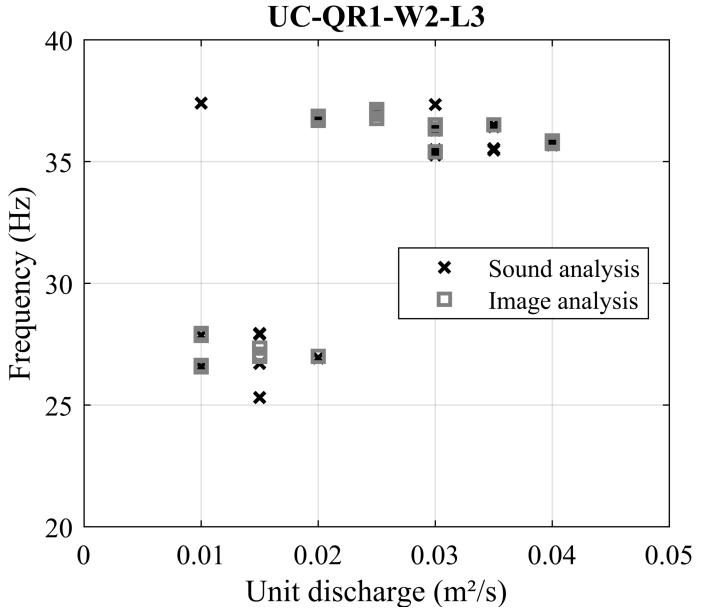

Frequencies obtained by sound and image analyses

Configuration: $UC - QR1 - W2 - L4$

Abbreviation	Model	Confinement	Crest shape - R	Width W	Height L	Range of q affected by the oscillations	Extreme frequencies
$UC - QR1 - W2 - L4$	1	Unconfined	QR - 15 cm	250 cm	150 cm	No nappe oscillation	

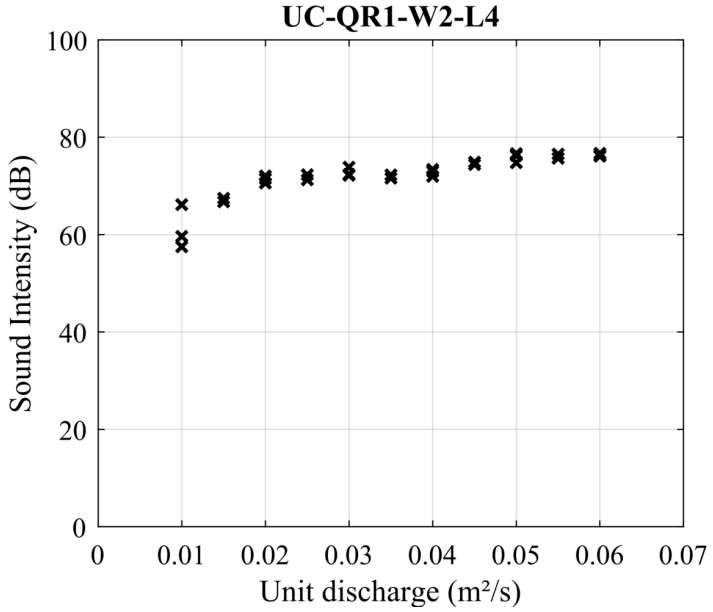

Results of sound analysis

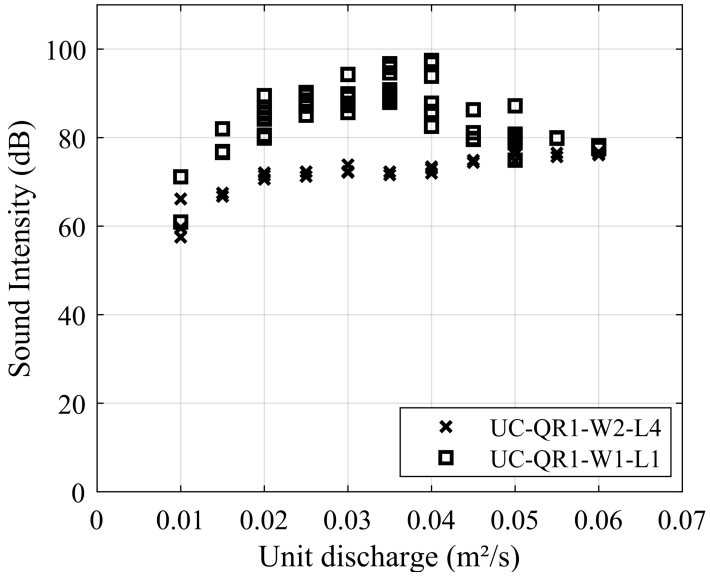

Configuration: $UC - QR1 - W2 - L7$

Abbreviation	Model	Confinement	Crest shape - R	Width W	Height L	Range of q affected by the oscillations	Extreme frequencies
$UC - QR1 - W2 - L7$	1	Unconfined	QR - 15 cm	250 cm	50 cm	No nappe oscillation	

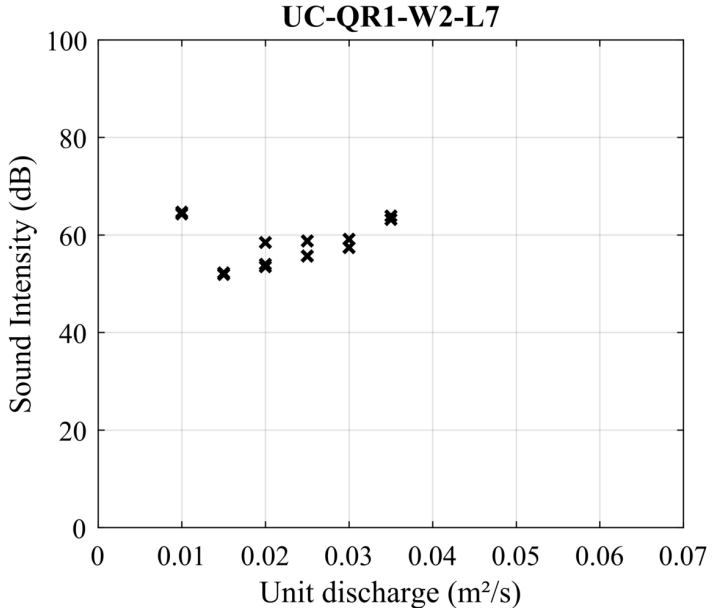

Results of sound analysis

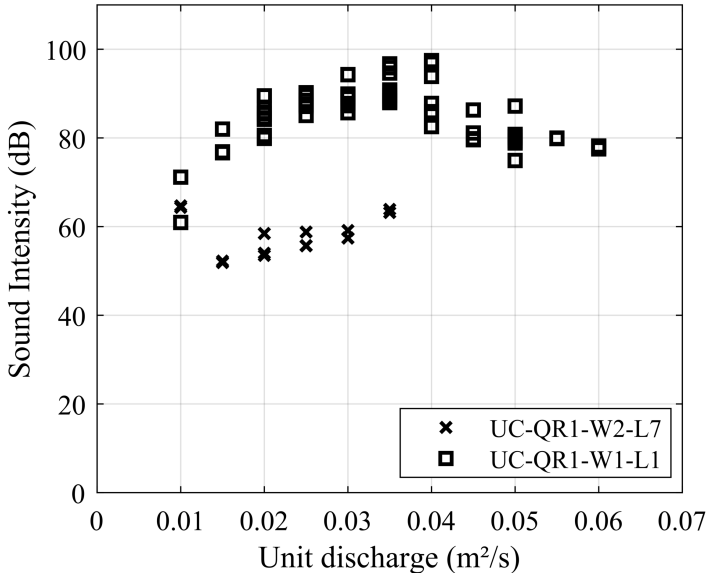

Configuration: $UC - QR1 - W3 - L3$

Abbreviation	Model	Confinement	Crest shape - R	Width W	Height L	Range of q affected by the oscillations	Extreme frequencies
$UC - QR1 - W3 - L3$	1	Unconfined	QR - 15 cm	200 cm	200 cm	0.02 - 0.025 m^2/s	34.75;35.25 Hz

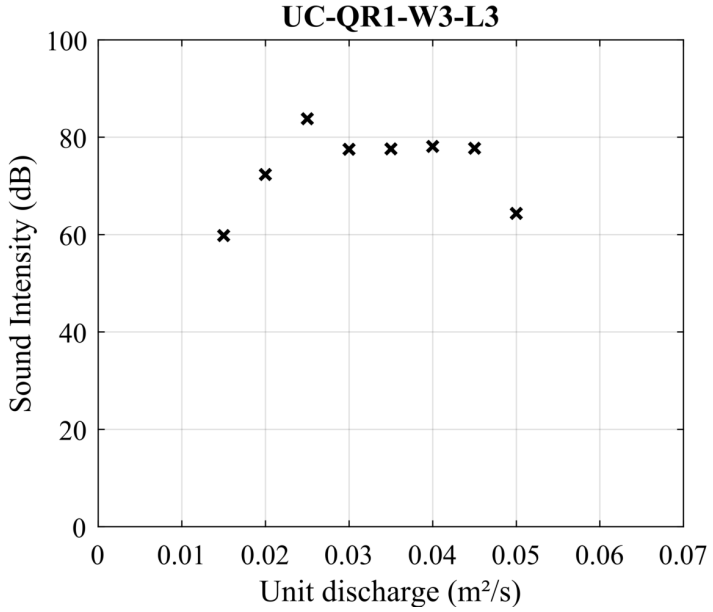

Results of sound analysis

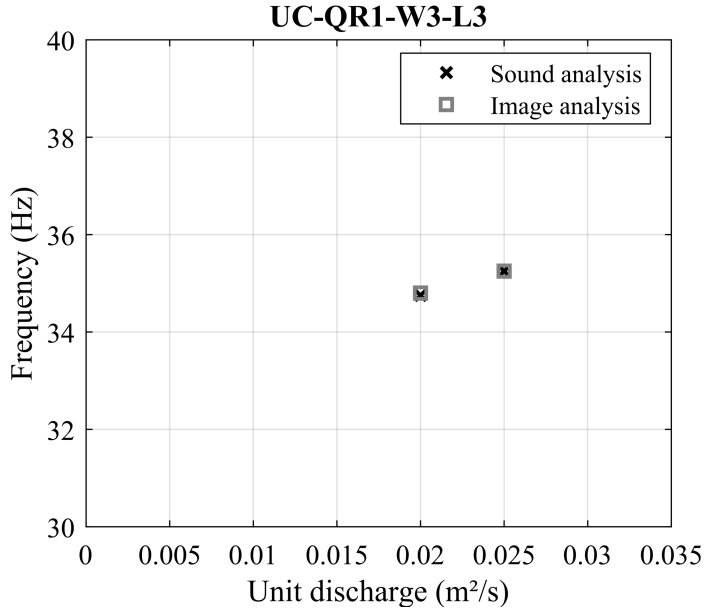

Frequencies obtained by sound and image analyses

Configuration: $UC - QR1 - W3 - L4$

Abbreviation	Model	Confinement	Crest shape - R	Width W	Height L	Range of q affected by the oscillations	Extreme frequencies
$UC - QR1 - W3 - L4$	1	Unconfined	QR - 15 cm	200 cm	150 cm	No nappe oscillation	

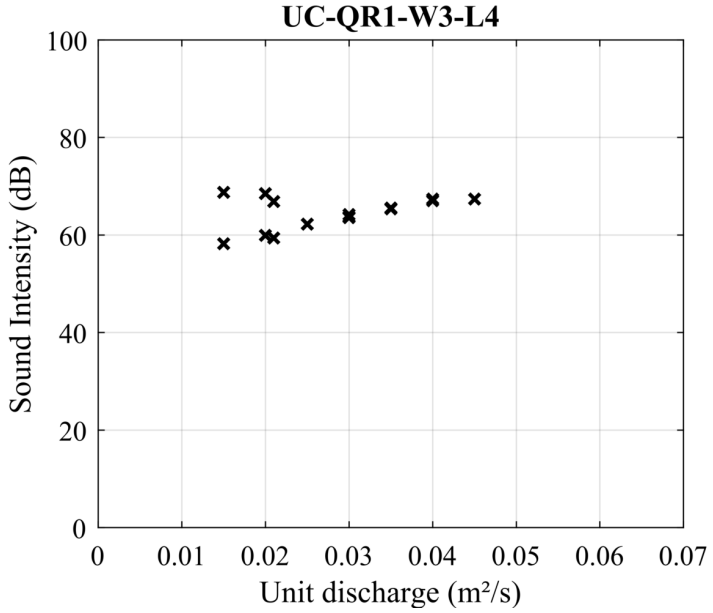

Results of sound analysis

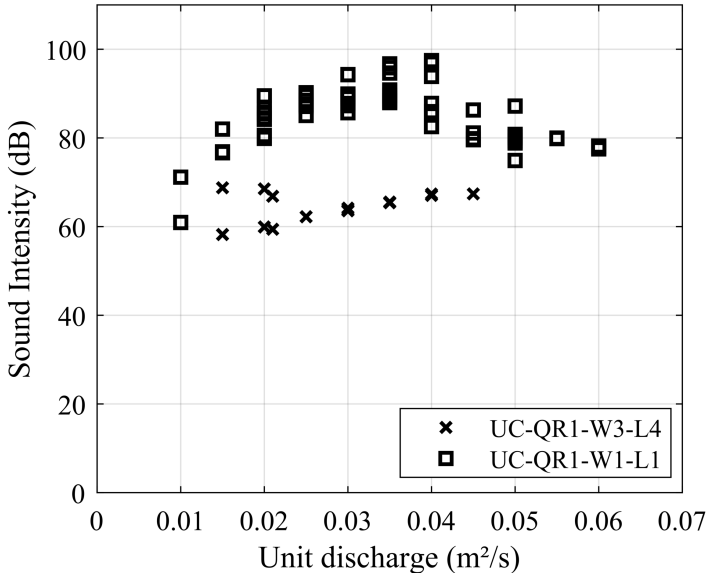

Configuration: $UC - QR1 - W3 - L5$

Abbreviation	Model	Confinement	Crest shape - R	Width W	Height L	Range of q affected by the oscillations	Extreme frequencies
$UC - QR1 - W3 - L5$	1	Unconfined	QR - 15 cm	200 cm	100 cm	No nappe oscillation	

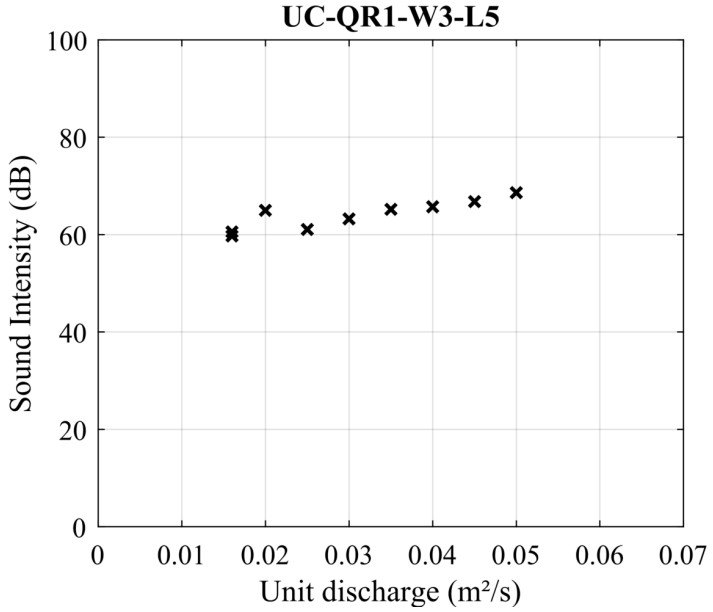

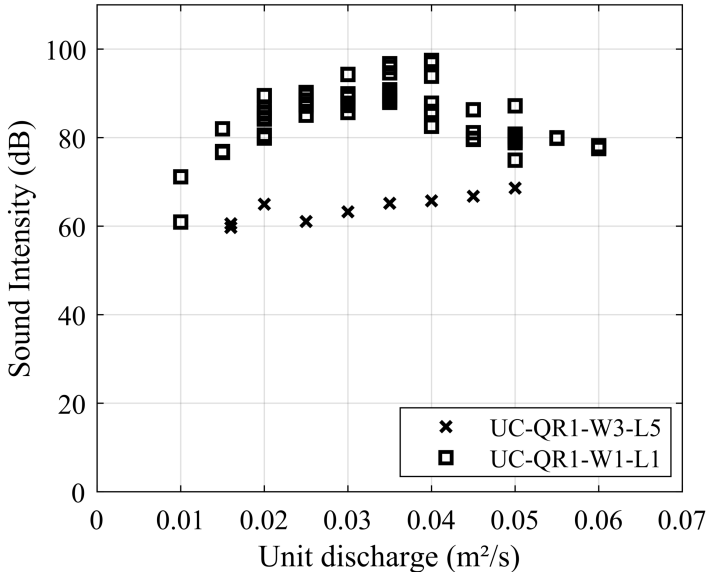

Results of sound analysis

Configuration: $UC - QR1 - W3 - L7$

Abbreviation	Model	Confinement	Crest shape - R	Width W	Height L	Range of q affected by the oscillations	Extreme frequencies
$UC - QR1 - W3 - L7$	1	Unconfined	QR - 15 cm	200 cm	50 cm	No nappe oscillation	

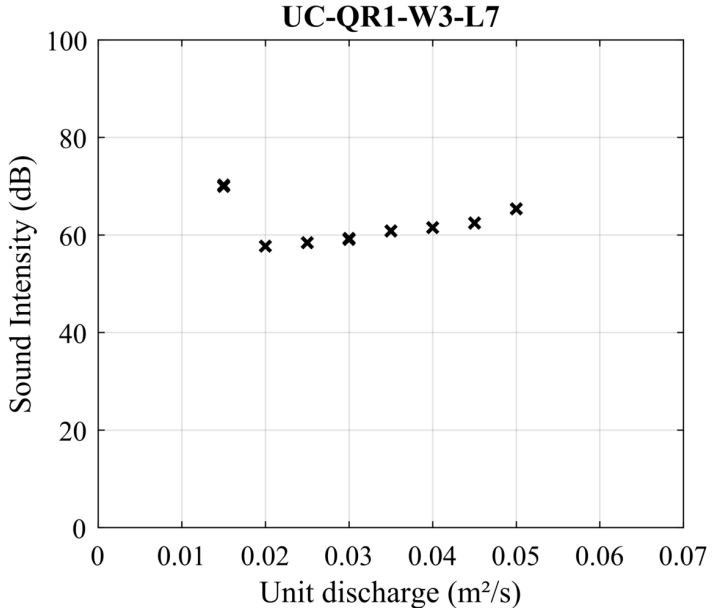

Results of sound analysis

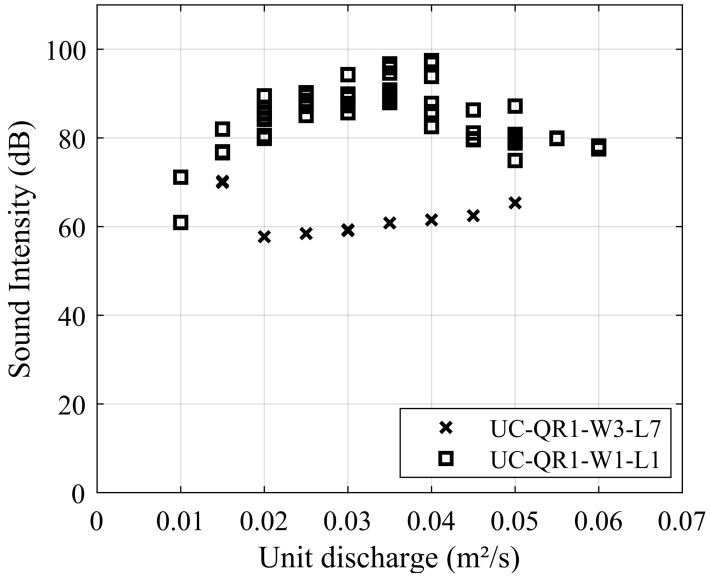

Configuration: $UC - QR1 - W4 - L1$

Abbreviation	Model	Confinement	Crest shape - R	Width W	Height L	Range of q affected by the oscillations	Extreme frequencies
$UC - QR1 - W4 - L1$	1	Unconfined	QR - 15 cm	150 cm	300 cm	0.01 - 0.025 m^2/s	48.25;54.6 Hz

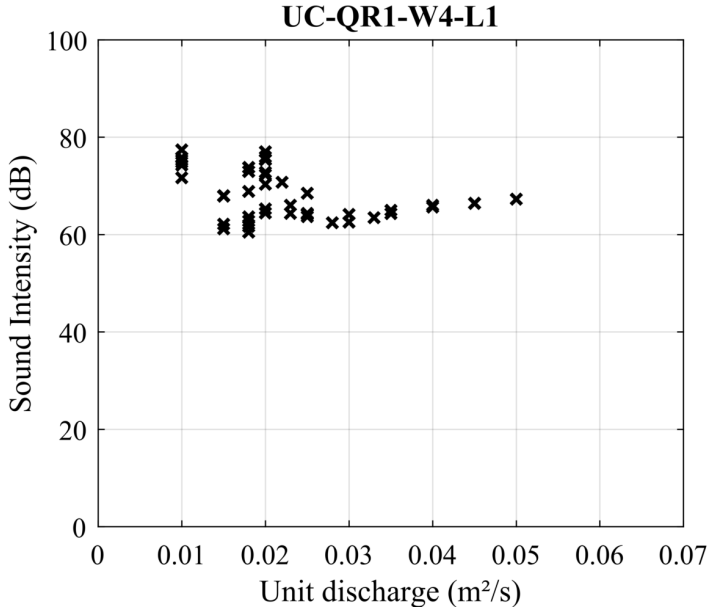

Results of sound analysis

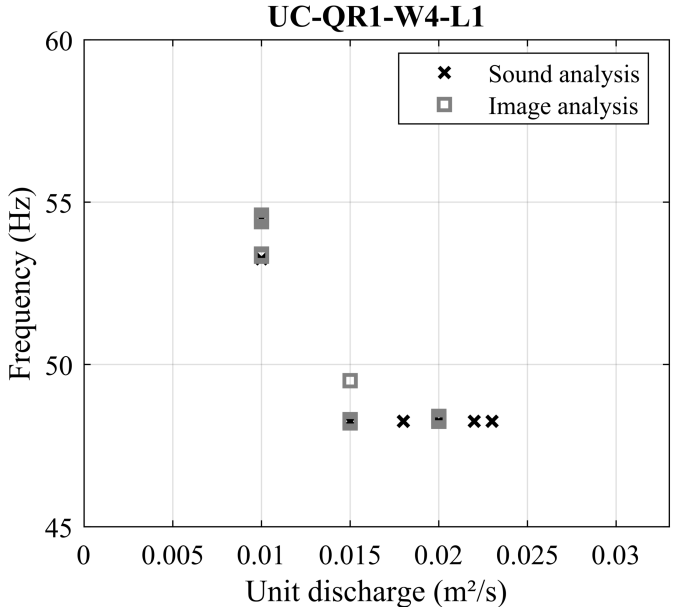

Frequencies obtained by sound and image analyses

Configuration: $UC - QR1 - W4 - L1$

(a) 

(b) 

(c) 

(d) 

Flow characteristics : (a) $q = 0.01$ m^2/s, (b) $q = 0.02$ m^2/s, $q = 0.03$ m^2/s and $q = 0.04$ m^2/s

Configuration: $UC - QR1 - W4 - L2$

Abbreviation	Model	Confinement	Crest shape - R	Width W	Height L	Range of q affected by the oscillations	Extreme frequencies
$UC - QR1 - W4 - L2$	1	Unconfined	QR - 15 cm	150 cm	250 cm	0.01 - 0.015 m^2/s	29.74;29.92 Hz

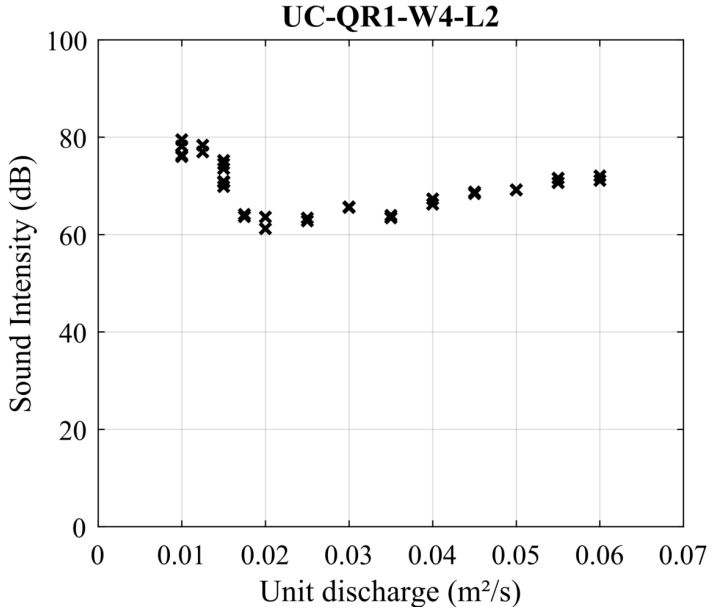

Results of sound analysis

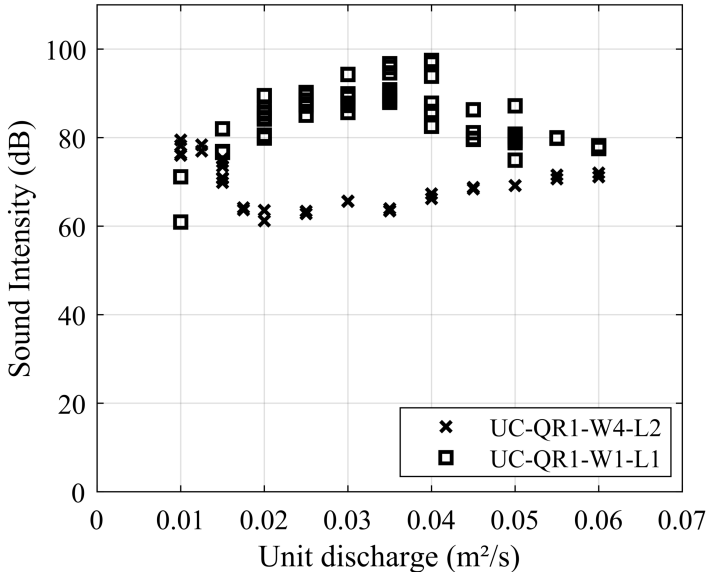

Frequencies obtained by sound and image analyses

Configuration: $UC - QR1 - W4 - L3$

Abbreviation	Model	Confinement	Crest shape - R	Width W	Height L	Range of q affected by the oscillations	Extreme frequencies
$UC - QR1 - W4 - L3$	1	Unconfined	QR - 15 cm	150 cm	200 cm	No nappe oscillation	

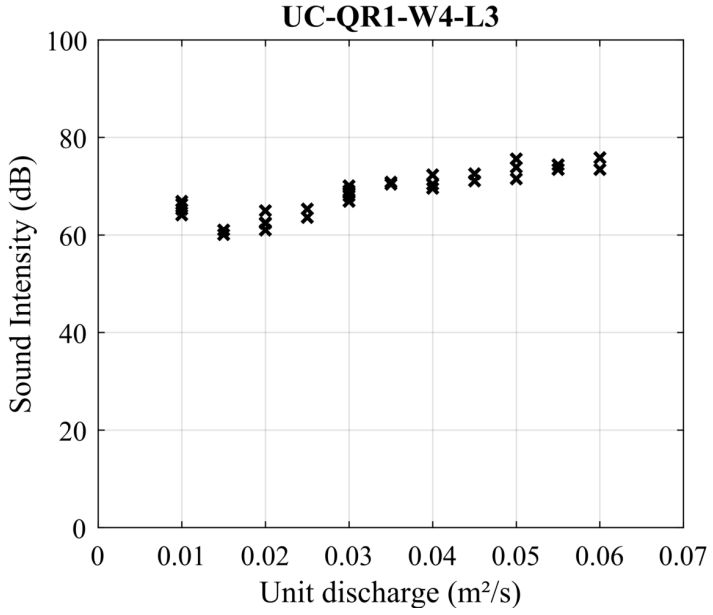

Results of sound analysis

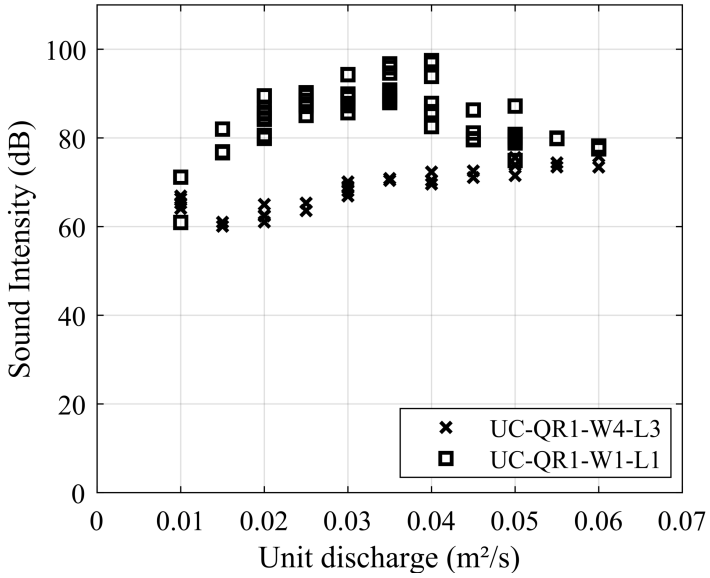

Configuration: $UC - QR1 - W6 - L1$

Abbreviation	Model	Confinement	Crest shape - R	Width W	Height L	Range of q affected by the oscillations	Extreme frequencies
$UC - QR1 - W6 - L1$	1	Unconfined	QR - 15 cm	100 cm	300 cm	No nappe oscillation	

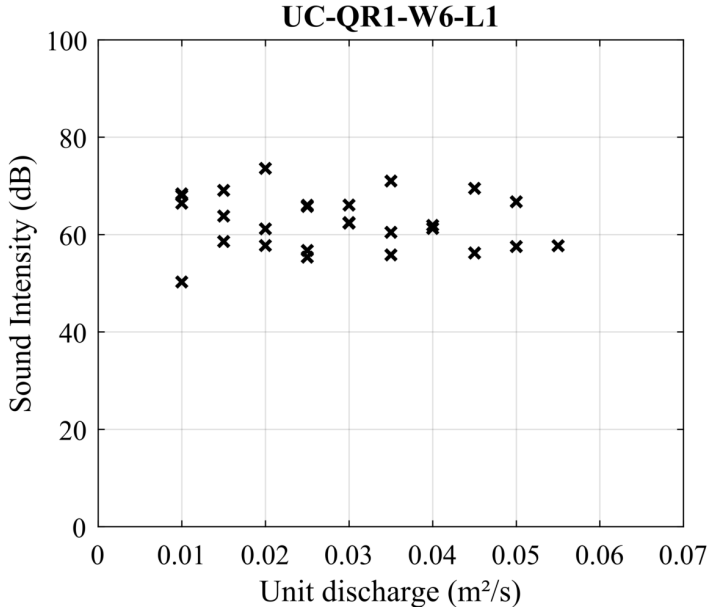

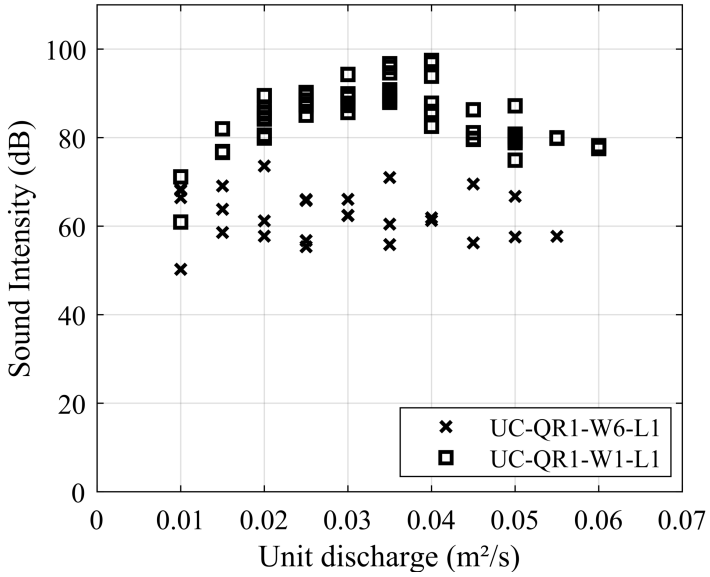

Results of sound analysis

Configuration: $C - QR2 - W5 - L5$

Abbreviation	Model	Confinement	Crest shape - R	Width W	Height L	Range of q affected by the oscillations	Extreme frequencies
$C - QR2 - W5 - L5$	2	Confined	QR - 5 cm	120 cm	100 cm	0.015 - 0.06 m^2/s	33.9;49 Hz

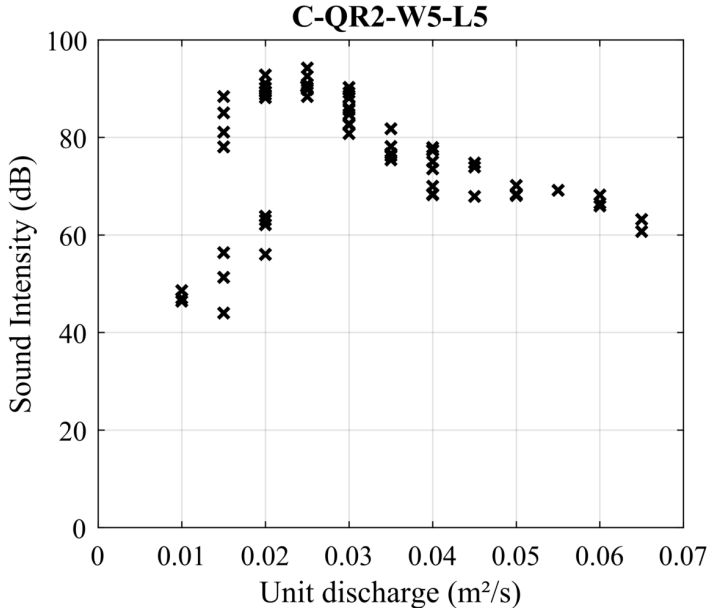

Results of sound analysis

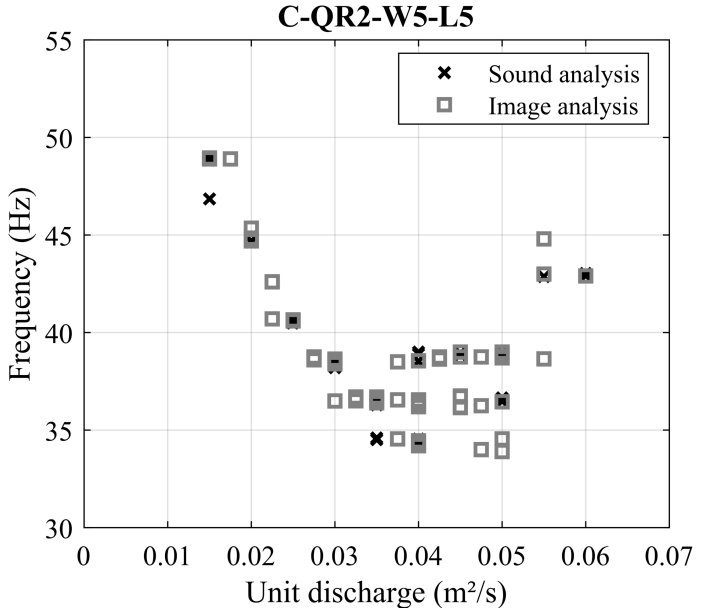

Frequencies obtained by sound and image analyses

Configuration: $C - QR2 - W5 - L5$

(a) 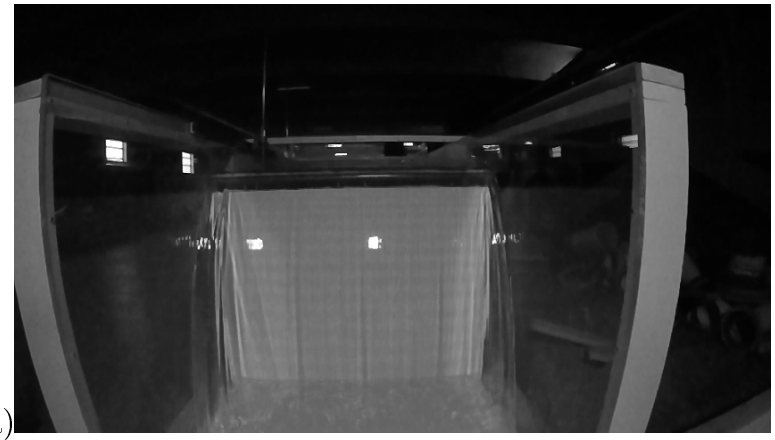

(b) 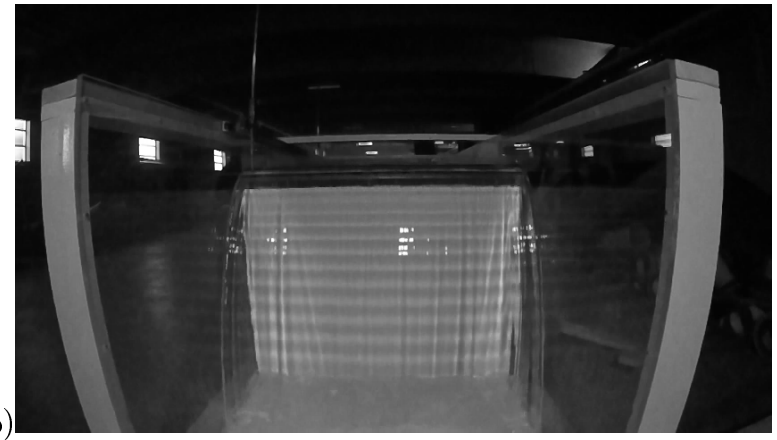

(c) 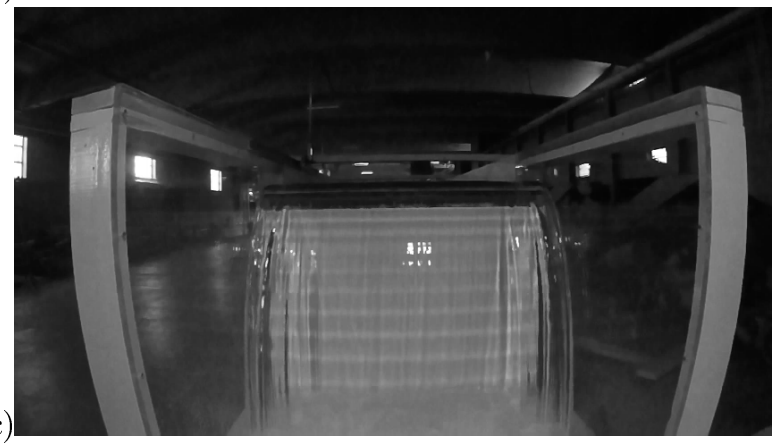

(d) 

Flow characteristics : (a) $q = 0.015$ m^2/s, (b) $q = 0.02$ m^2/s, $q = 0.03$ m^2/s and $q = 0.04$ m^2/s

Configuration: $C - QR2 - W5 - L6$

Abbreviation	Model	Confinement	Crest shape - R	Width W	Height L	Range of q affected by the oscillations	Extreme frequencies
$C - QR2 - W5 - L6$	2	Confined	QR - 5 cm	120 cm	75 cm	0.02 - 0.06 m^2/s	32.1;48.3 Hz

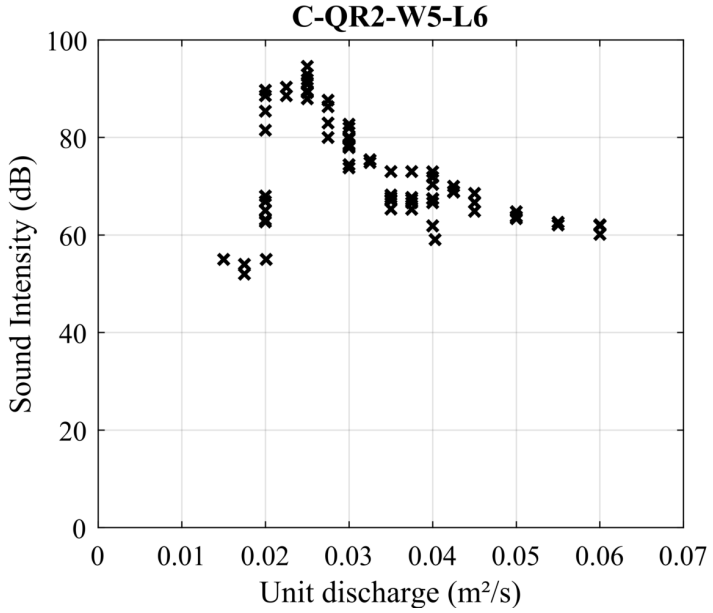

Results of sound analysis

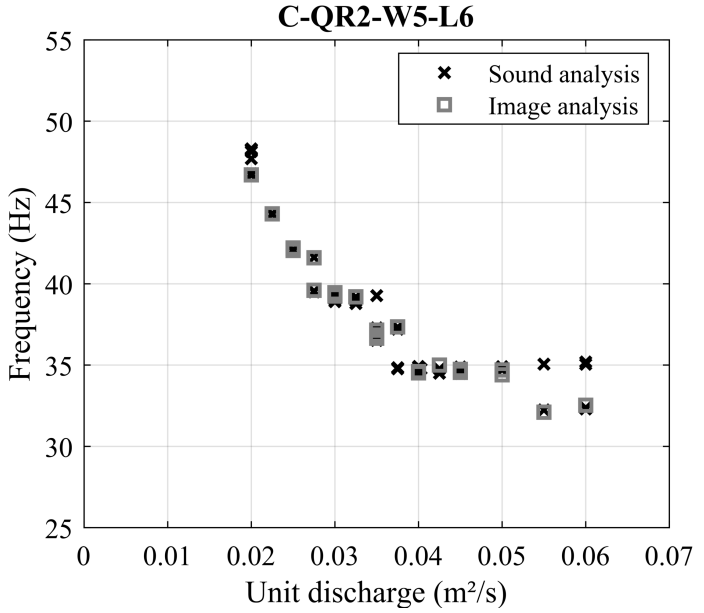

Frequencies obtained by sound and image analyses

Configuration: $C - QR2 - W5 - L6$

(a) 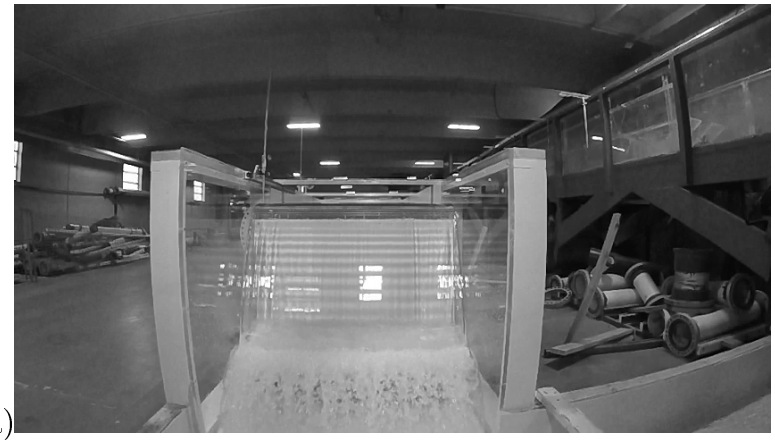

(b) 

(c) 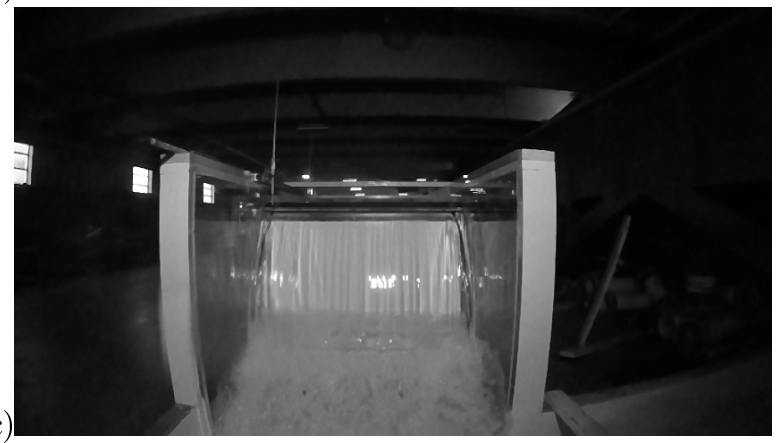

(d) 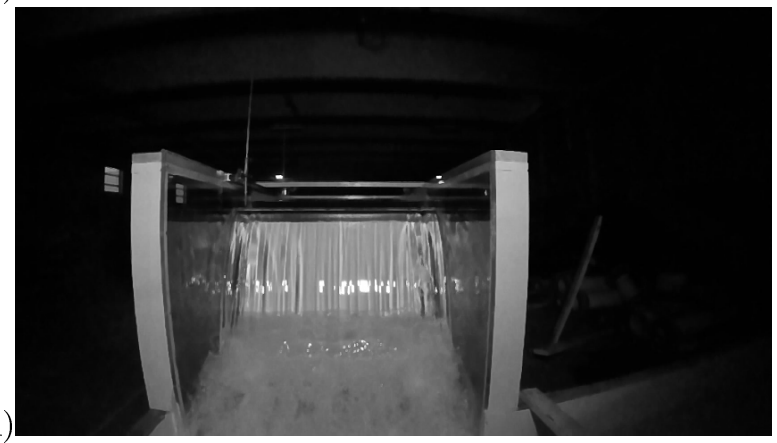

Flow characteristics : (a) $q = 0.02$ m^2/s, (b) $q = 0.03$ m^2/s, $q = 0.04$ m^2/s and $q = 0.05$ m^2/s

Configuration: $C - QR2 - W5 - L7$

Abbreviation	Model	Confinement	Crest shape - R	Width W	Height L	Range of q affected by the oscillations	Extreme frequencies
$C - QR2 - W5 - L7$	2	Confined	QR - 5 cm	120 cm	50 cm	No nappe oscillation	

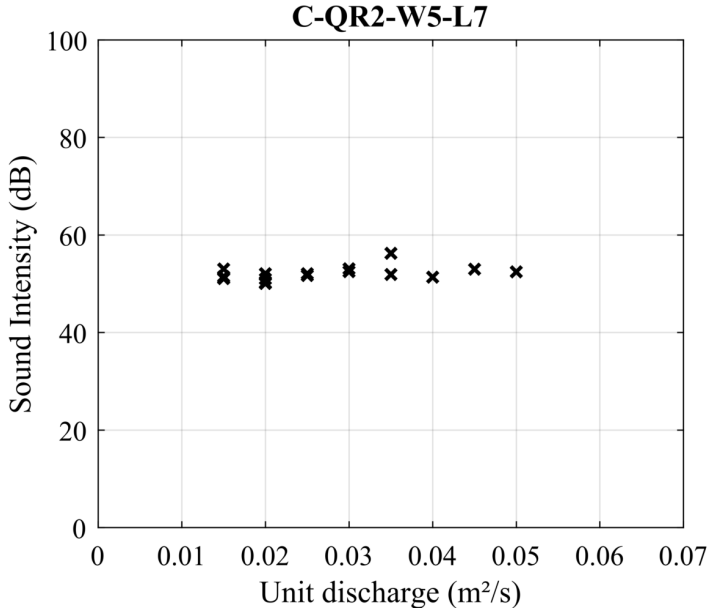

Results of sound analysis

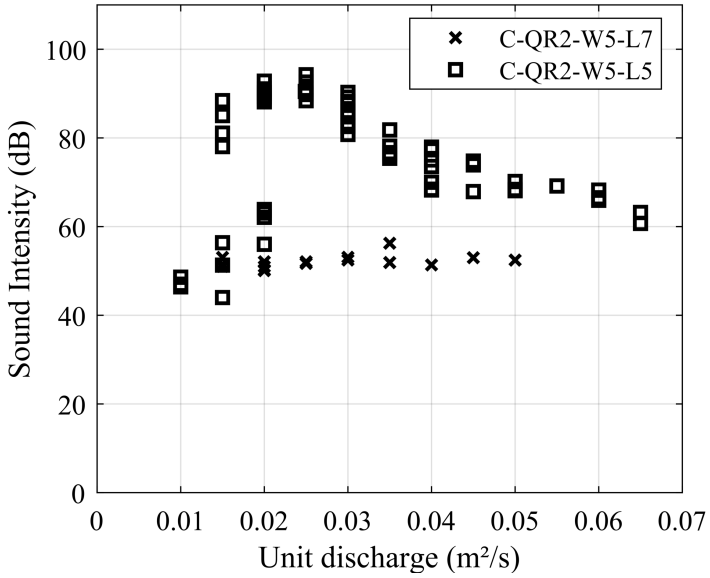

Configuration: $C - THR2 - W5 - L5$

Abbreviation	Model	Confinement	Crest shape - R	Width W	Height L	Range of q affected by the oscillations	Extreme frequencies
$C - THR2 - W5 - L5$	2	Confined	THR - 5 cm	120 cm	100 cm	0.015 - 0.05 m^2/s	37.6;58.75 Hz

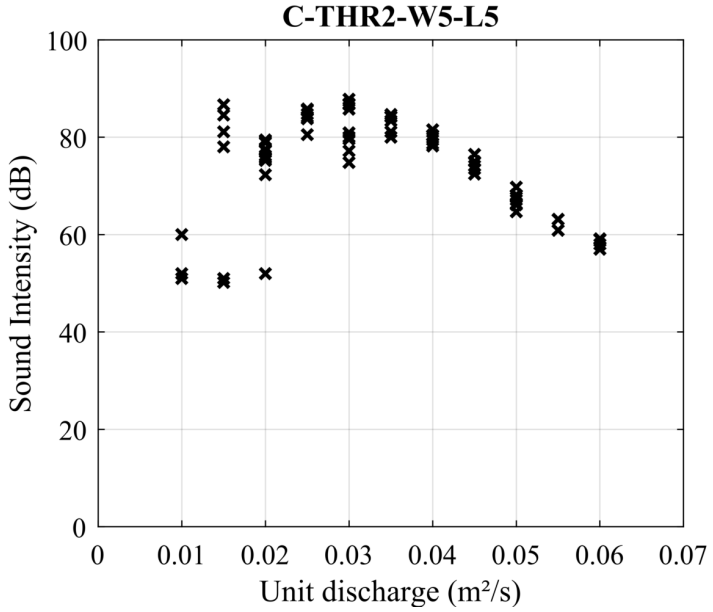

Results of sound analysis

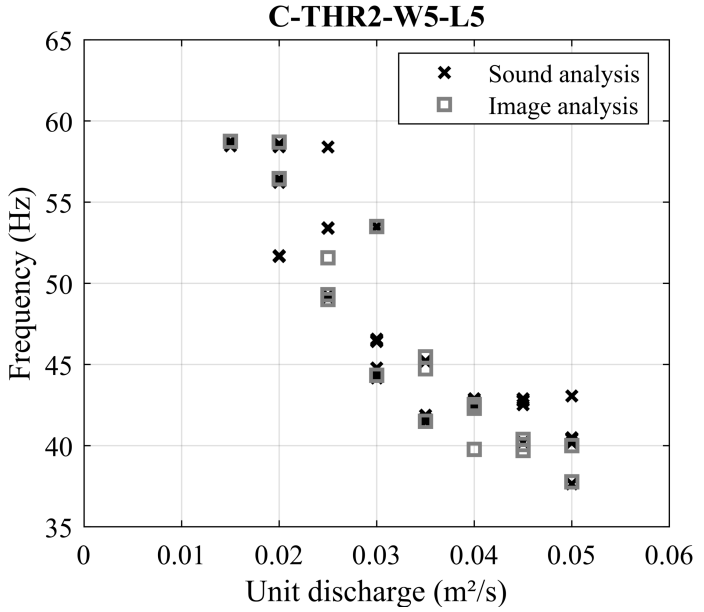

Frequencies obtained by sound and image analyses

Configuration: $C - THR2 - W5 - L5$

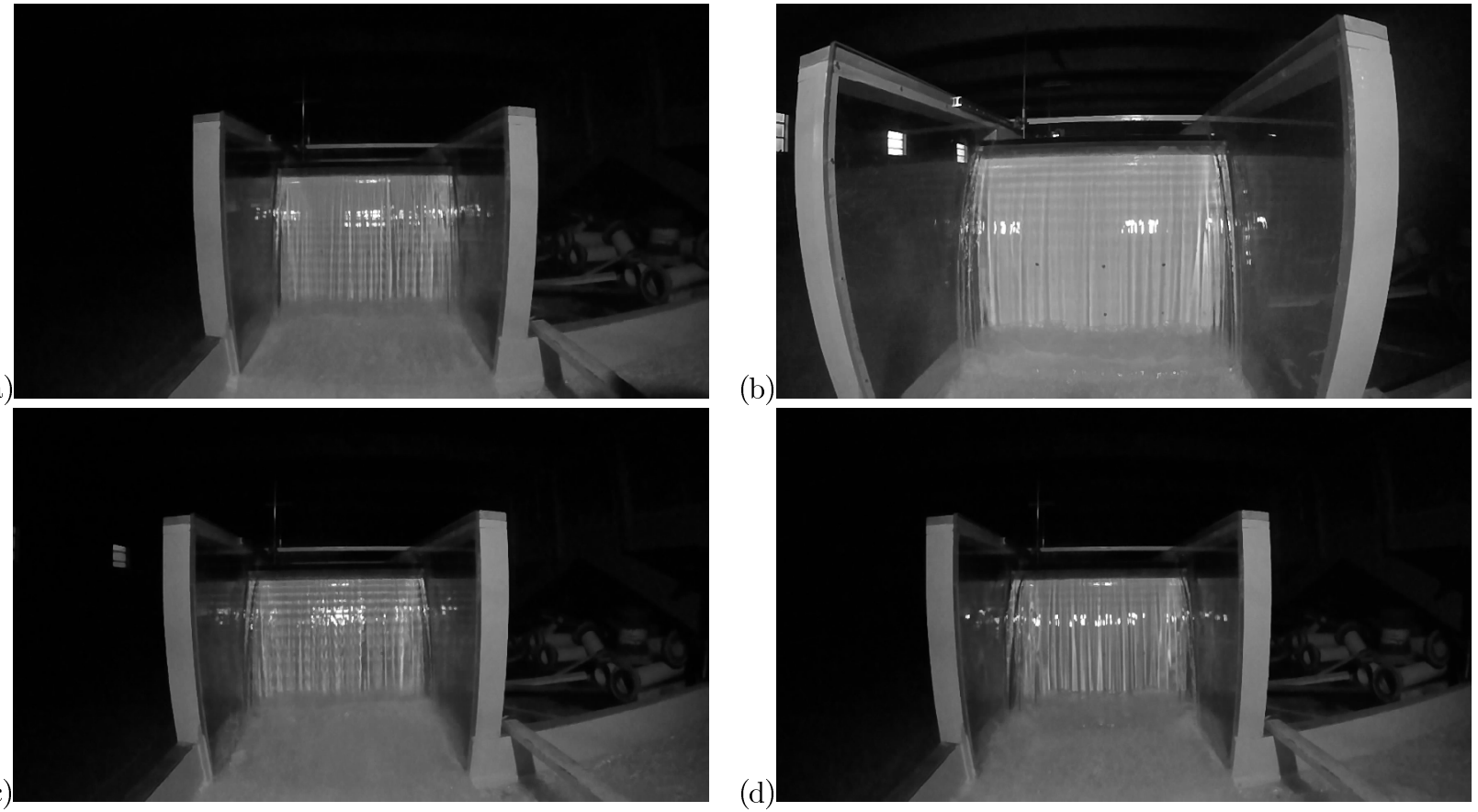

Flow characteristics : (a) $q = 0.02$ m²/s, (b) $q = 0.03$ m²/s, $q = 0.04$ m²/s and $q = 0.05$ m²/s

Configuration: $C - THR2 - W5 - L6$

Abbreviation	Model	Confinement	Crest shape - R	Width W	Height L	Range of q affected by the oscillations	Extreme frequencies
$C - THR2 - W5 - L6$	2	Confined	THR - 5 cm	120 cm	75 cm	No nappe oscillation	

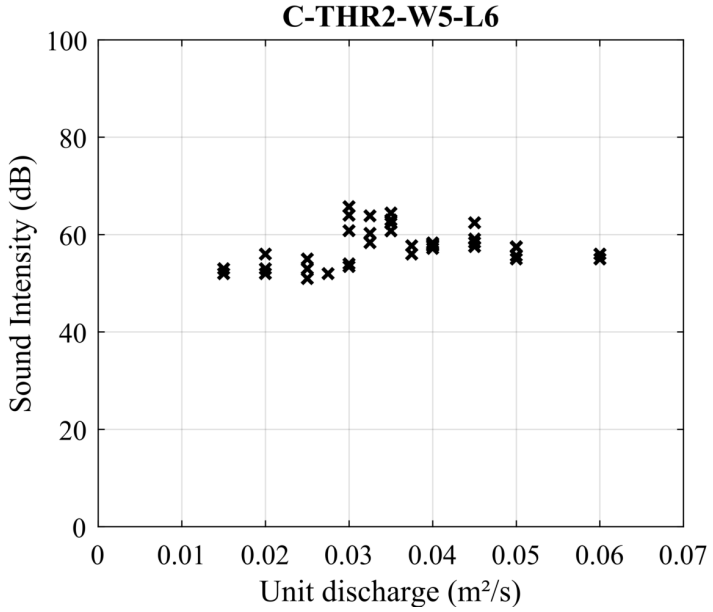

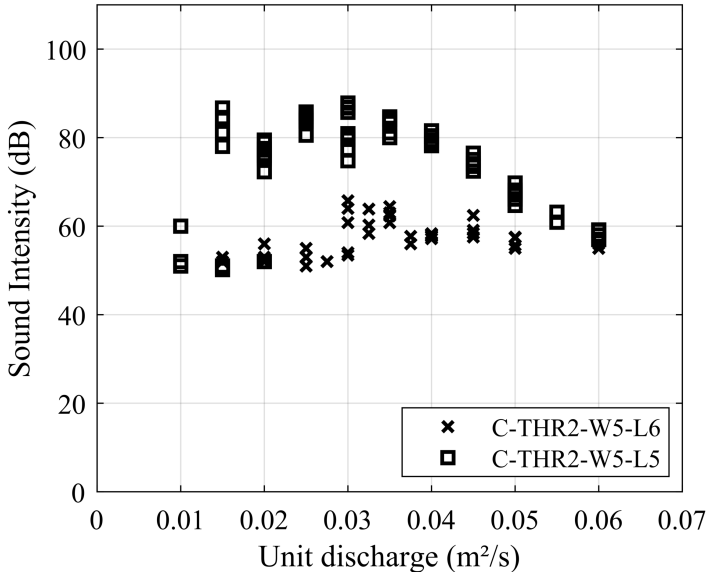

Results of sound analysis

Configuration: $C - THR2 - W5 - L7$

Abbreviation	Model	Confinement	Crest shape - R	Width W	Height L	Range of q affected by the oscillations	Extreme frequencies
$C - THR2 - W5 - L7$	2	Confined	THR - 5 cm	120 cm	50 cm	No nappe oscillation	

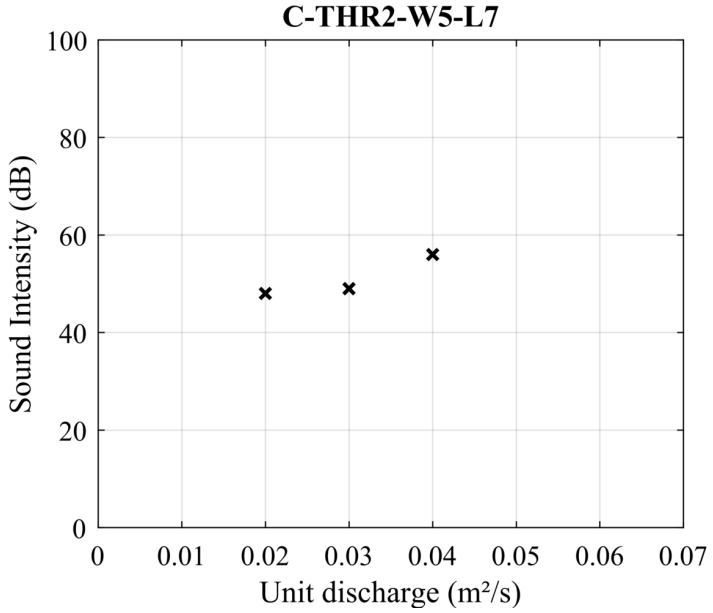

Results of sound analysis

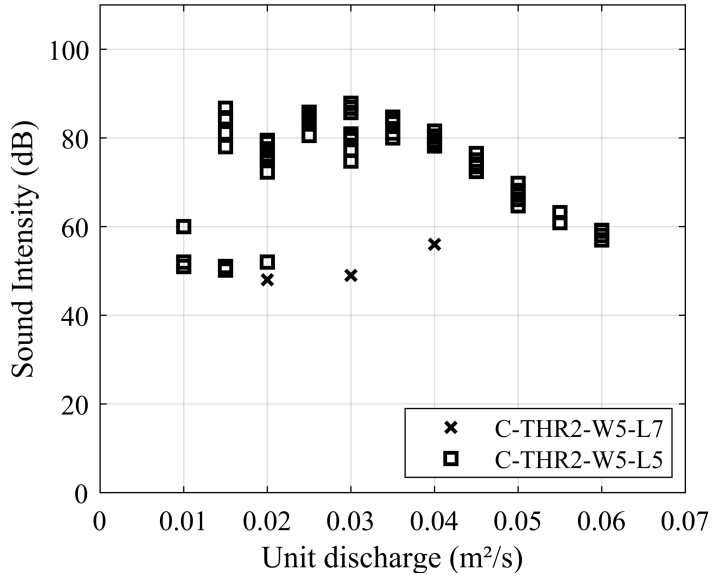

Configuration: $C - R - W5 - L5$

Abbreviation	Model	Confinement	Crest shape - R	Width W	Height L	Range of q affected by the oscillations	Extreme frequencies
$C - R - W5 - L5$	2	Confined	R	120 cm	100 cm	No nappe oscillation	

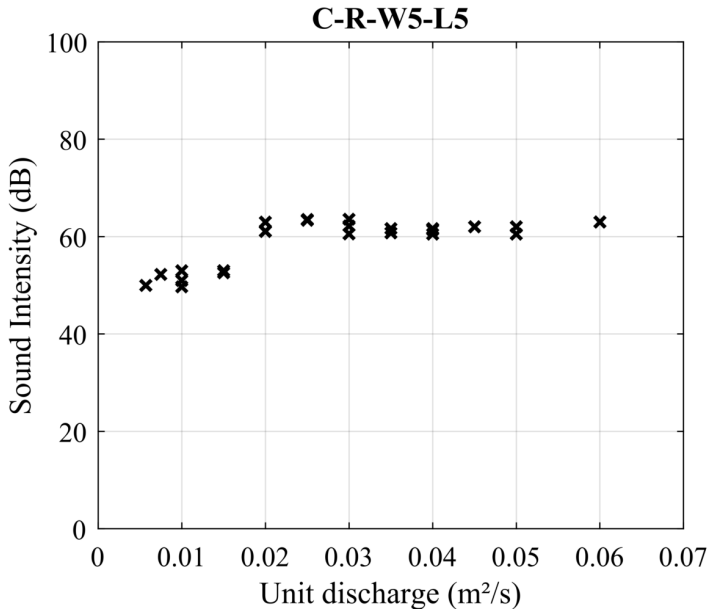

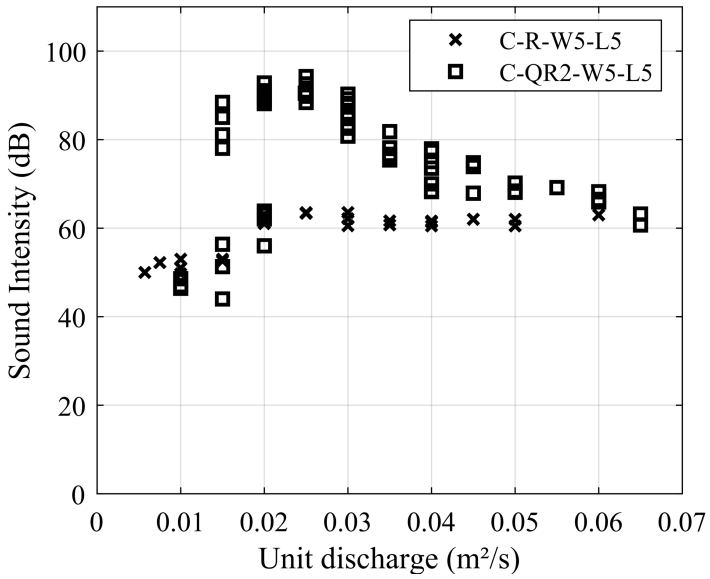

Results of sound analysis

Configuration: $C - RR - W5 - L5$

Abbreviation	Model	Confinement	Crest shape - R	Width W	Height L	Range of q affected by the oscillations	Extreme frequencies
$C - RR - W5 - L5$	2	Confined	RR	120 cm	100 cm	0.02 - 0.025 m^2/s	38.17;42.47 Hz

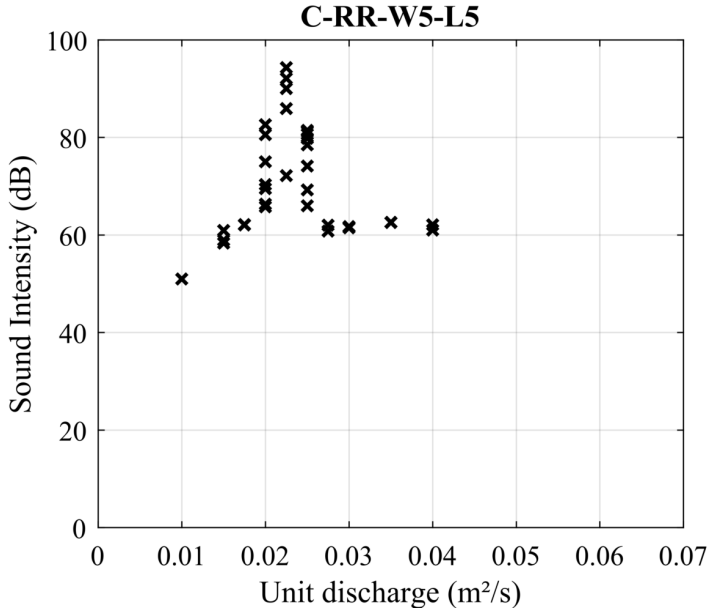

Results of sound analysis

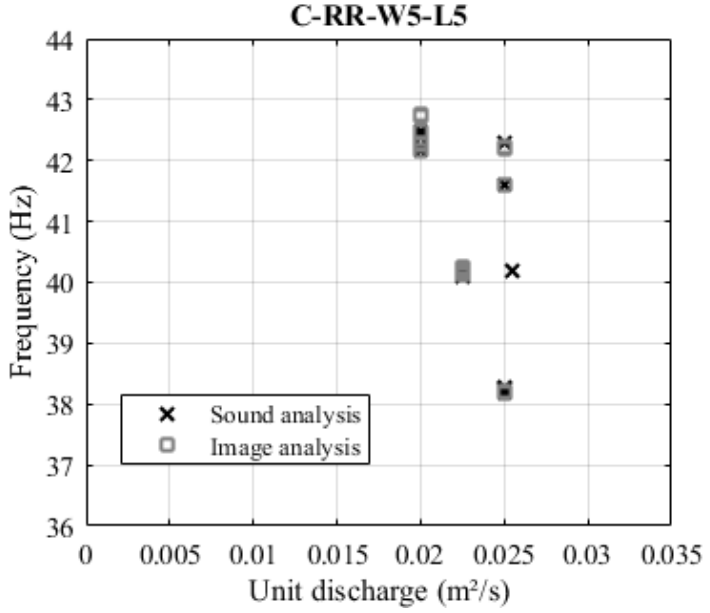

Frequencies obtained by sound and image analyses

Appendix C

Supplemental data to Section V.3.3

As reported in Chapter V, Section V.3.3, a dimensional analysis was engaged in an effort to link the geometric characteristics of a configuration to the oscillations frequencies. As a first step, the 10 independent characteristic parameters of the phenomenon, called variables in the following, have been listed in Table C.1.

In Section V.3.3, focusing on the frequency characteristics of nappe oscillations, the parameters Π_3 and Π_4 were multiplied to define a new parameter $F = \Pi_3\Pi_4 = fq/v^2$. This parameter was reported as function of the parameter Π_1. The others Π-parameters were not developed as they are not linked to the oscillations characteristics. These Π-parameters are illustrated in Fig.C.1 to Fig.C.6.

In addition, dimensionless numbers were calculated based on the water level at the crest and unit discharge (Eq.C.0.1) and are reported in Fig.C.7 to Fig.C.9.

$$\begin{aligned} Fr^* &= \Pi_4\Pi_5 = \frac{q}{\sqrt{ge^3}} \\ We^* &= \Pi_4^2\Pi_6 = \frac{\rho q^2}{\sigma e} \\ Re^* &= \Pi_4\Pi_7 = \frac{\rho q}{\mu} \end{aligned} \tag{C.0.1}$$

Table C.1: Dimensional analysis: variables and Π-parameters. Variables used for expressing the dimension of the problem are in bolt

Types	Variables	Notations	SI unit	Π-parameters
Geometry	Fall height	L	m	$\Pi_1 = L/e$
	Weir width	W	m	$\Pi_2 = W/e$
Hydraulics	**Water depth at the crest detachment**	e	**m**	-
	Characteristic fall velocity	$v = \sqrt{v_0^2 + 2gL} - v_0$	**m/s**	-
	Characteristic frequency of the oscillations	f	1/s	$\Pi_3 = fe/v$
	Unit discharge	q	$\mathrm{m^2/s}$	$\Pi_4 = q/(ve)$
	Gravitational acceleration	g	$\mathrm{m/s^2}$	$\Pi_5 = v/\sqrt{ge} = Fr$
Fluid	**Density**	ρ	$\mathbf{kg/m^3}$	-
	Surface tension	σ	$\mathrm{kg/s^2}$	$\Pi_6 = \rho v^2 e/\sigma = We$
	Dynamic viscosity	μ	kg/ms	$\Pi_7 = \rho ve/\mu = Re$

Table C.2: Extreme values of Π-parameters and other dimensionless numbers

	Extreme
$\Pi_1 = L/e$	12.72;390.09
$\Pi_2 = W/e$	20.35;438.7
$\Pi_3 = fe/v$	0.01;0.63
$\Pi_4 = q/(ve)$	0.07;0.48
$\Pi_5 = v/\sqrt{ge} = Fr$	4.9;24.9
$\Pi_6 = \rho v^2 e/\sigma = We$	$1.84 \times 10^3; 4.13 \times 10^4$
$\Pi_7 = \rho vd/\mu = Re$	$3.62 \times 10^4; 3.98 \times 10^5$
$Fr^* = \frac{q}{\sqrt{ge^3}}$	1.34;4.64
$We^* = \frac{\rho q^2}{\sigma e}$	$76; 1.33 \times 10^3$
$Re^* = \frac{\rho q}{\mu}$	$10^4; 6 \times 10^4$

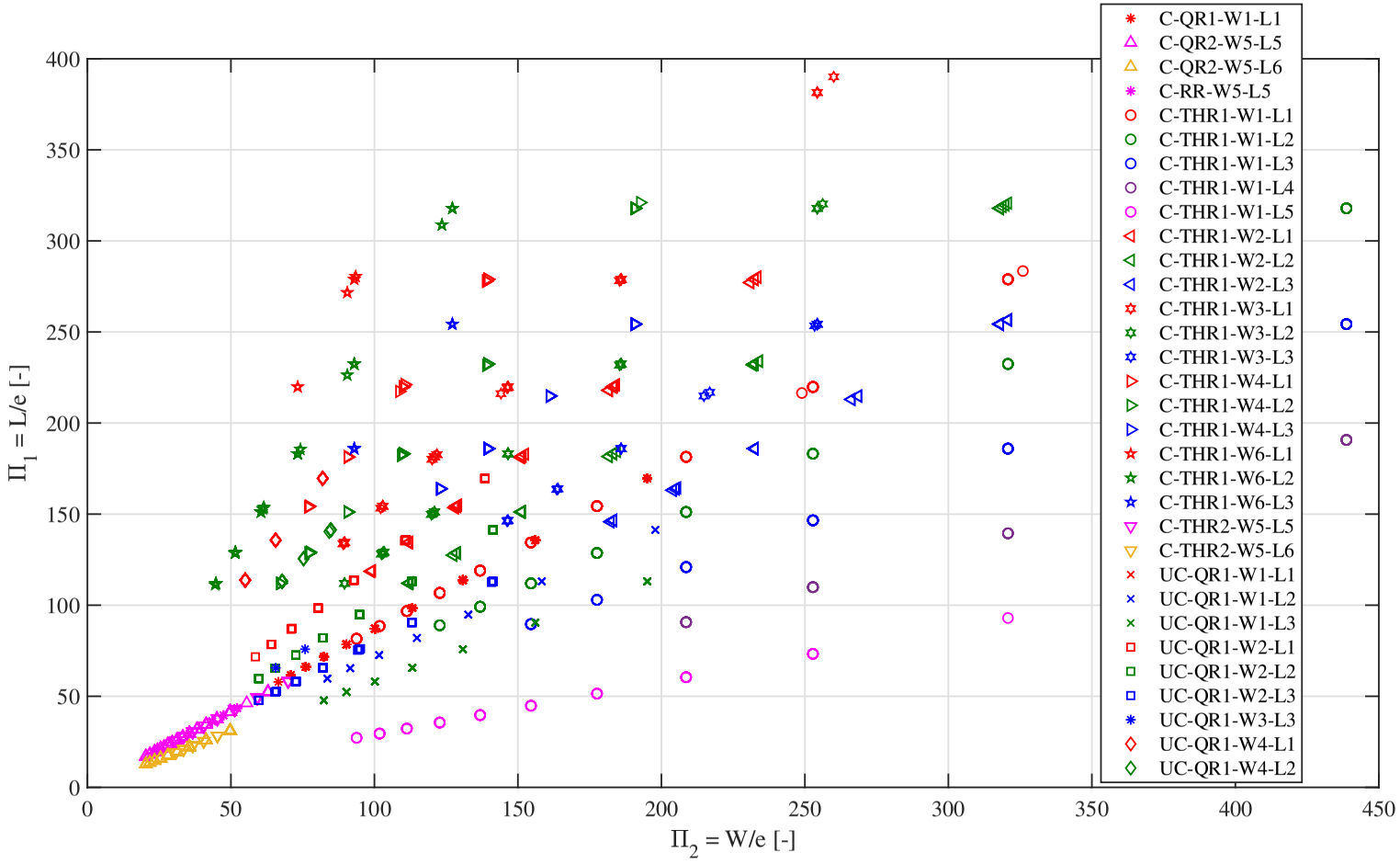

Figure C.1: $\Pi_1 - \Pi_2$

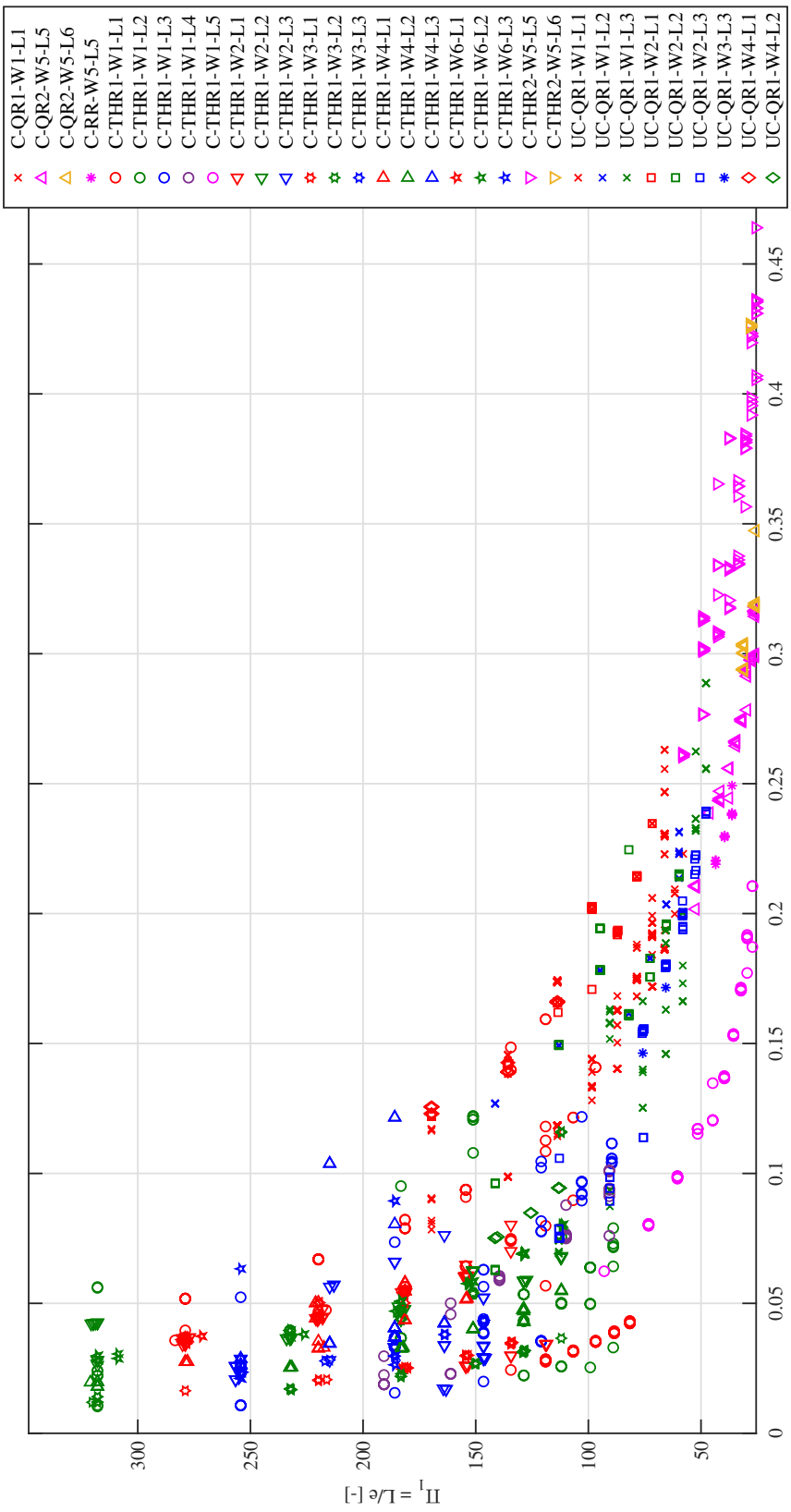

Figure C.2: $\Pi_1 - \Pi_3$

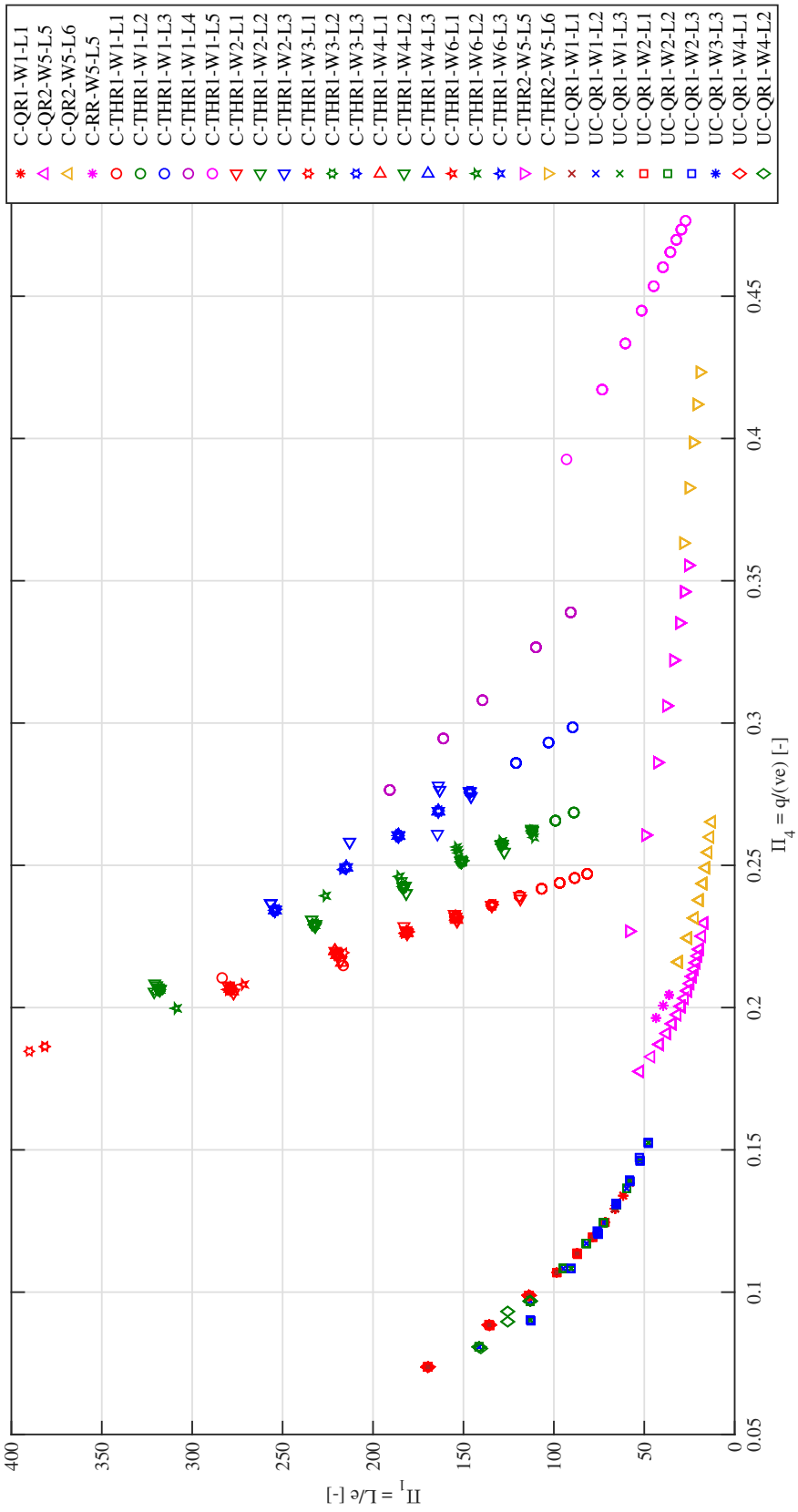

Figure C.3: $\Pi_1 - \Pi_4$

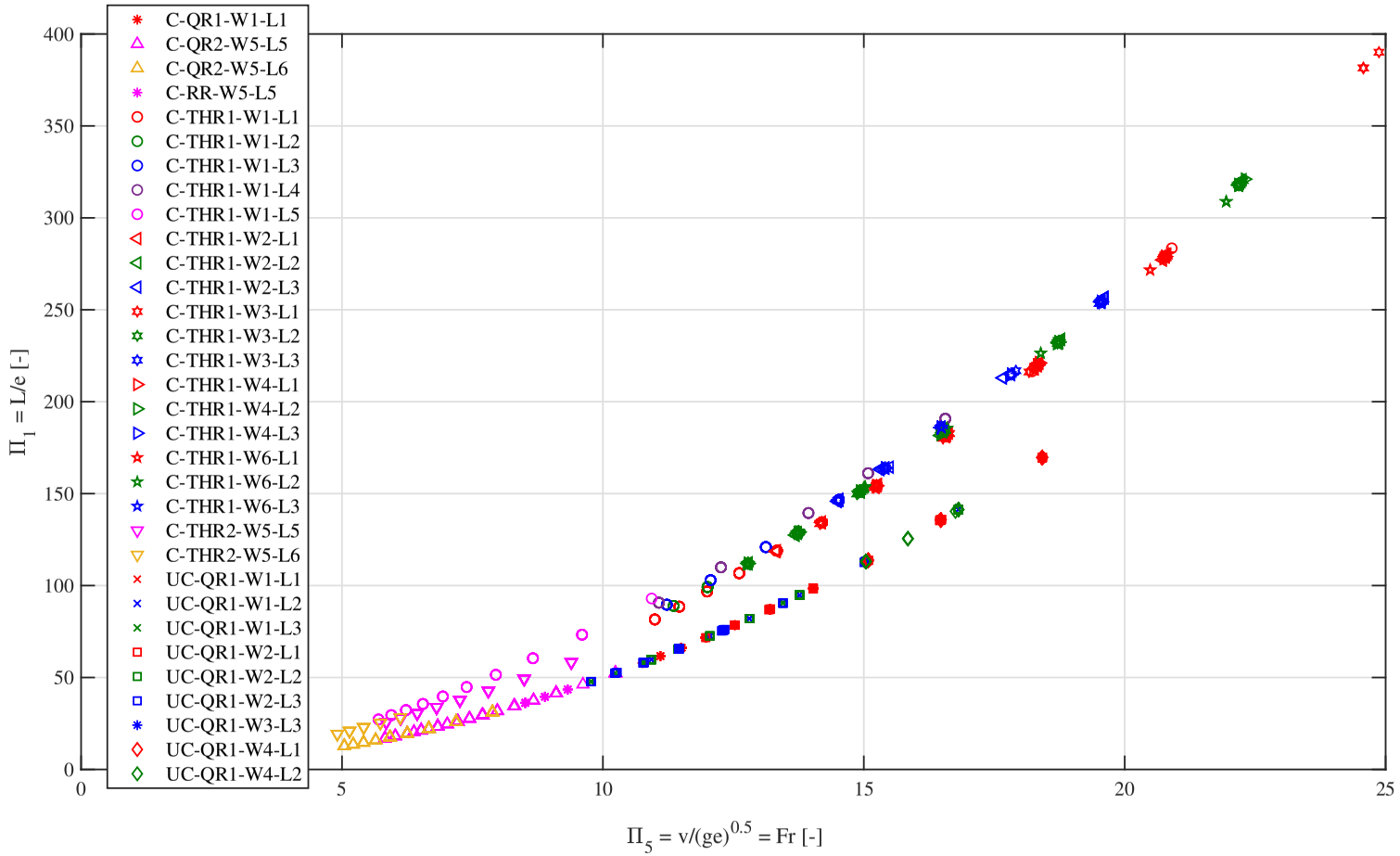

Figure C.4: $\Pi_1 - \Pi_5$

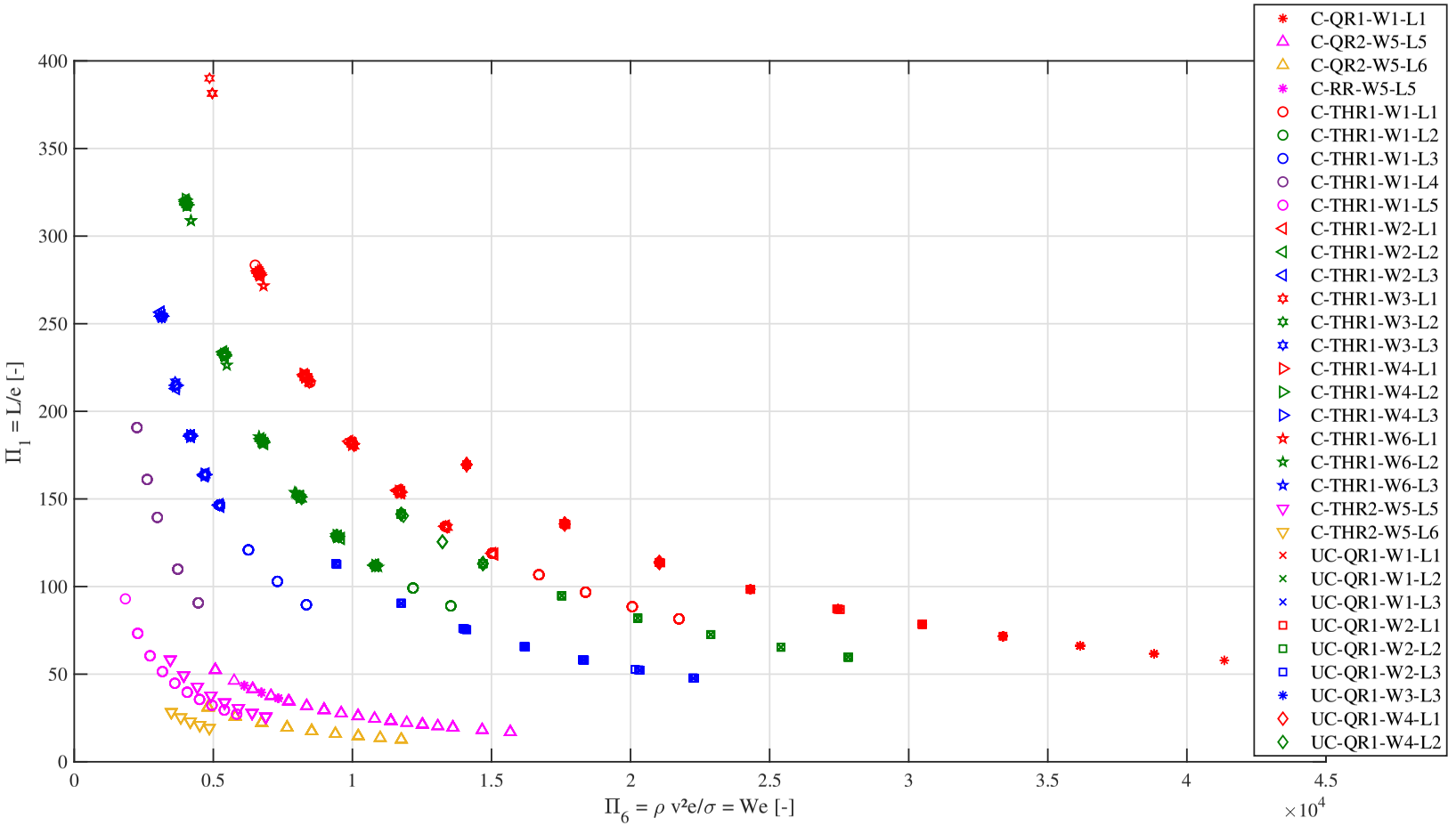

Figure C.5: $\Pi_1 - \Pi_6$

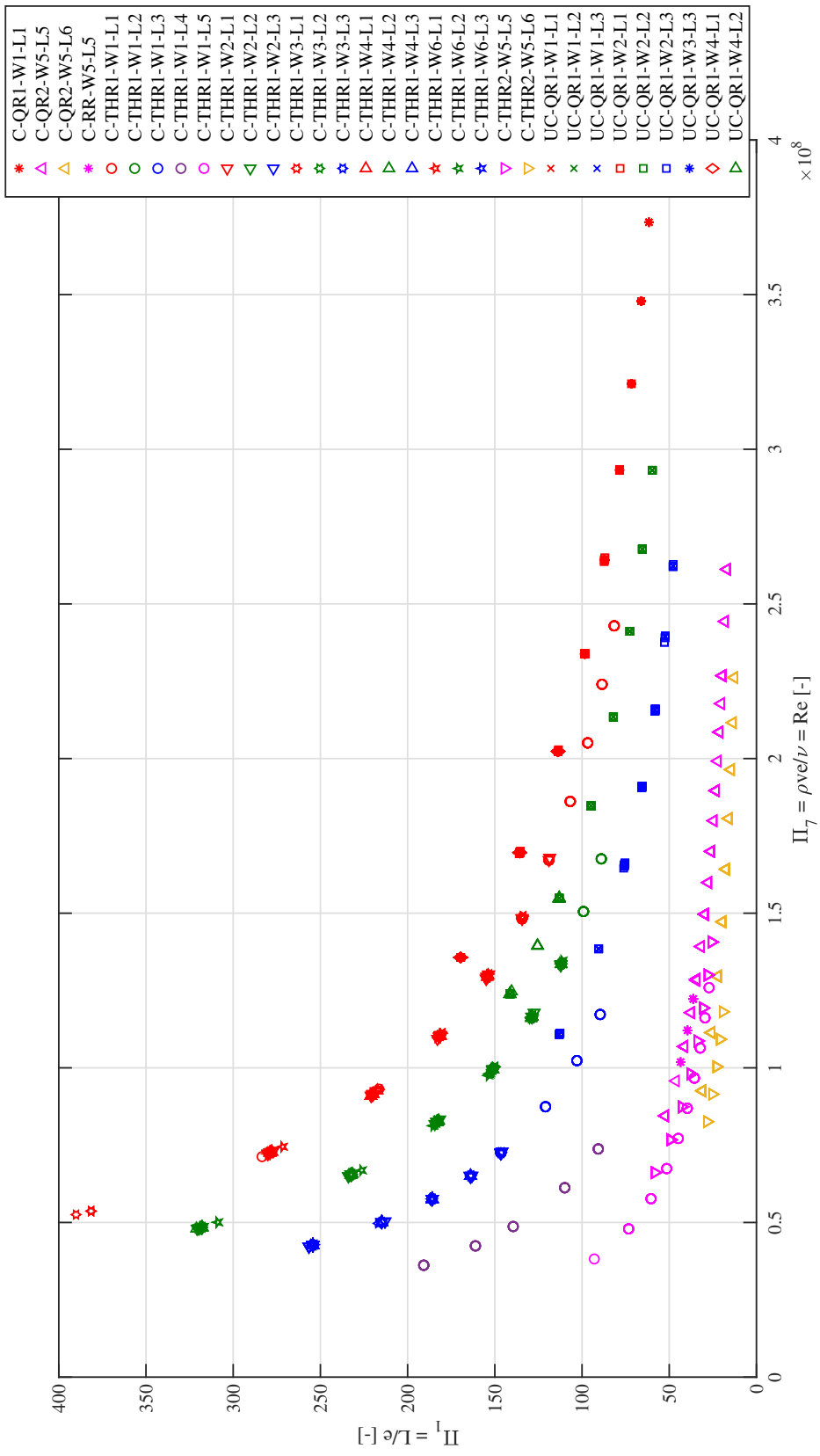

Figure C.6: $\Pi_1 - \Pi_7$

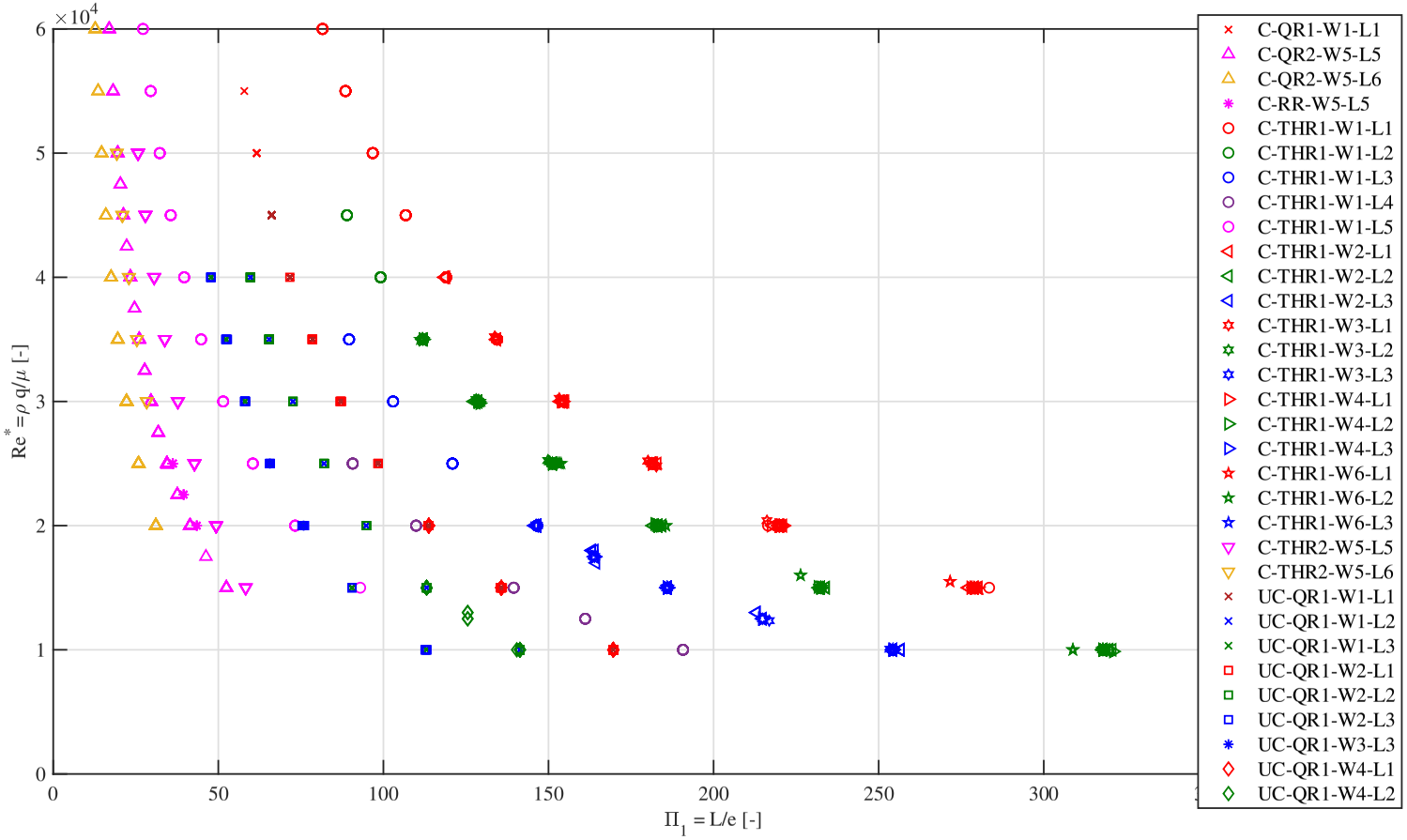

Figure C.7: $Re^* - \Pi_1$

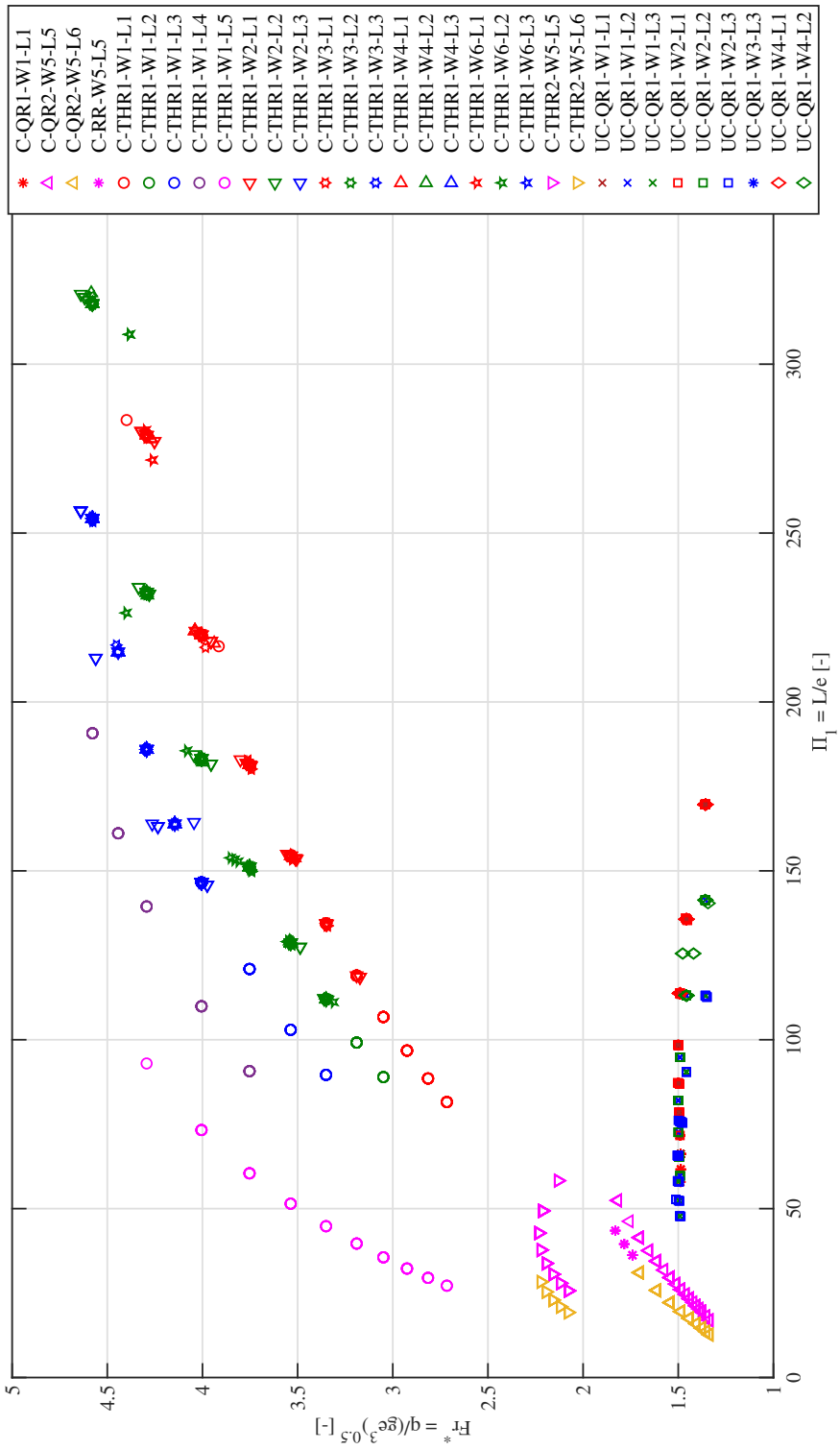

Figure C.8: $Fr^* - \Pi_1$

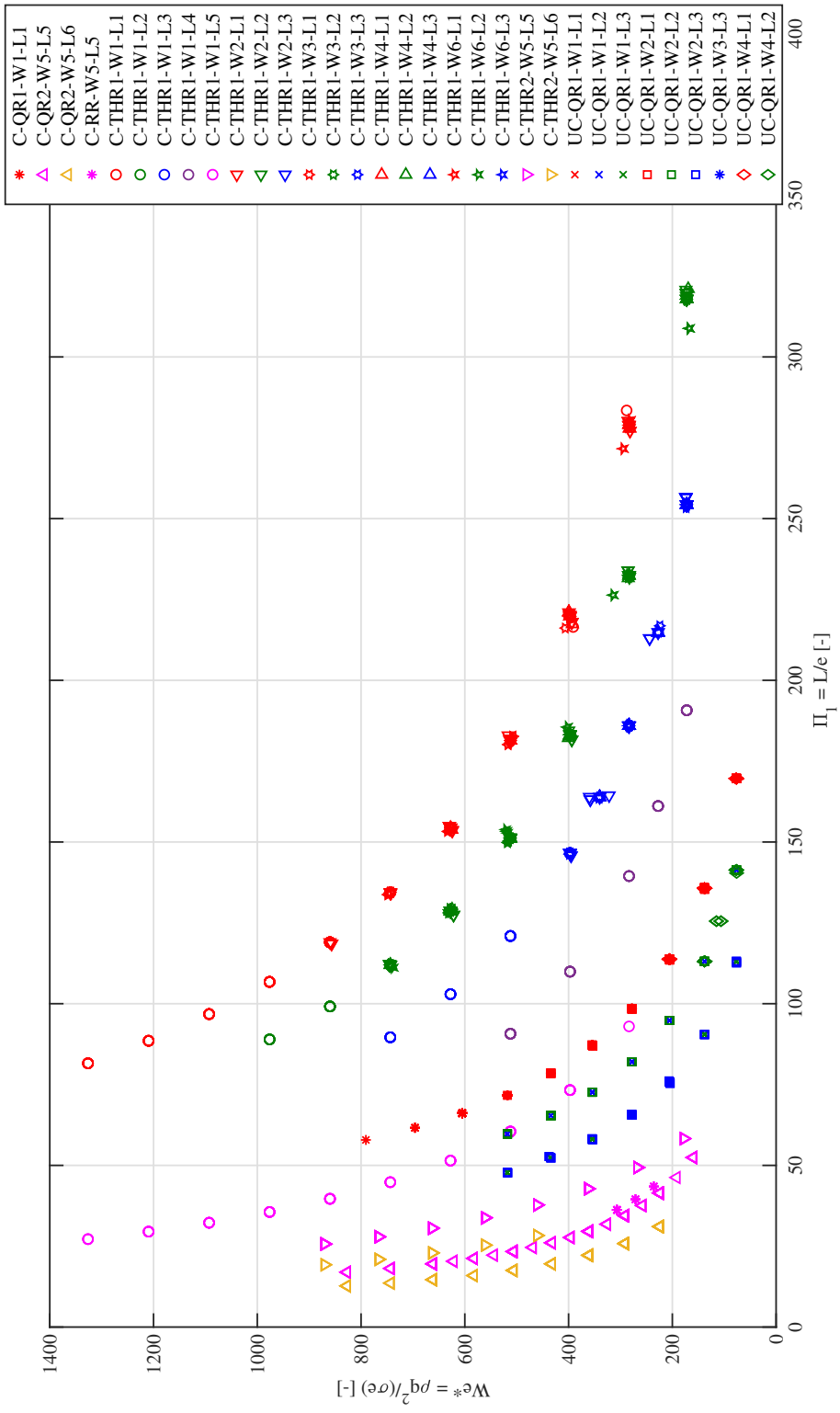

Figure C.9: $We^* - \Pi_1$